University of Alberta

Clinical applications of TCP and NTCP models: Incorporation of NTCP models into modern inverse planning optimization and investigation of the applicability of population-averaged and non-averaged TCP models for the purpose of parameter estimation

by

Colleen Gayle Schinkel

A thesis submitted to the Faculty of Graduate Studies and Research
in partial fulfillment of the requirements for the degree of

Doctor of Philosophy

in

Medical Physics

Department of Physics

Edmonton, Alberta

Fall 2007

Your file Votre référence
ISBN: 978-0-494-33056-2
Our file Notre référence
ISBN: 978-0-494-33056-2

Abstract

The clinical applicability of tumour control probability (TCP) and normal tissue complication probability (NTCP) models is investigated. A method of choosing dose-volume constraint points based on biological criteria is presented. This method requires random sampling from the functional space of all monotonically decreasing functions in the unit square. A random function generator is developed by determining and utilizing the distribution that describes the number of normalized integral dose volume histograms (DVHs) passing through a point in DVH space. Randomly simulated DVHs that result in clinically acceptable levels of complication are selected and averaged, producing a mean DVH, from which dose-volume constraints may be selected. The impact of the number of constraints to be fulfilled on the likelihood that a DVH satisfying them will result in an acceptable NTCP is also determined. A property of the integral dose-volume histogram (DVH) space is analytically investigated – a curve is constructed by connecting points belonging to step-like integral DVHs with a NTCP equal to a particular value, α. It is proven that any DVH that at least partially lies above this curve results in NTCP > α. The functional form similarity between the individual and fundamental population TCP models is investigated. Using the fact that both models can be expressed in terms of the parameters D_{50} (dose at 50% control) and γ_{50} (normalized slope at D_{50}), it is shown that they have almost identical functional form for values of $\gamma_{50} \geq 1$. The possibility of applying the individual TCP model for the case of heterogeneous irradiations is discussed. By making use of this functional similarity, the α/β (ratio of linear quadratic

radiosensitivity parameters) estimates that would be obtained by fitting each TCP model to clinical data are analytically compared. It is shown that the α/β ratio estimated from clinical dose-response data is model-dependent – a population TCP model that accounts for heterogeneity in radiosensitivity will produce a higher α/β estimate than that resulting from the individual TCP model. Finally, the impact of clinical data quality on the accuracy of estimated TCP model parameters is investigated, by means of numerical experiments with pseudo-data.

Acknowledgements

I would like to express my sincere thanks to my supervisors, and those that I worked closely with during my research. First, I would like to thank Dr. B. Gino Fallone for his support as a supervisor, and for helping to obtain funding for my work. I would also like to thank Dr. Pavel Stavrev, Dr. Nadia Stavreva and Dr. Marco Carlone for their guidance, discussions, and help.

Thanks also go out to the rest of my supervisory committee and examiners, all of whom provided excellent feedback and comments on my thesis work: Dr. Ron Sloboda, Dr. Dave Murray, Dr. Jack Tuszynski, and Dr. Colin Orton. In addition, I would like to thank Dr. Brad Warkentin and Dr. Rufus Scrimger for their contributions to my research.

I am grateful for funding from the Alberta Heritage Foundation for Medical Research, the Alberta Cancer Board, the Canadian Institutes of Health Research, and the University of Alberta.

Table of Contents

Chapter 1 Introduction and Background 1
1.1 Introduction 1
1.1.1 Radiation therapy 1
1.1.2 Radiobiology 2
1.2 Cell damage by radiation 5
1.3 The linear quadratic model 5
1.3.1 Dose rate effects and the LQ model 6
1.3.2 The relationship between the α/β ratio and dose-fractionation for external-beam treatments 7
1.3.2.1 Effect of fractionation on cell survival curves 7
1.3.2.2 Fractionation sensitivity and the α/β ratio 8
1.3.2.3 Early and late-responding tissues 10
1.4 TCP and NTCP models 11
1.4.1 TCP models 11
1.4.1.1 The individual TCP model based on Poisson statistics 11
1.4.1.2 The population TCP model 13
1.4.2 NTCP models 15
1.4.2.1 The Lyman (sigmoidal dose response) model 16
1.4.2.2 The critical volume model 17
1.5 Incorporation of radiobiological models into the treatment planning process 19
1.5.1 Inverse planning optimization by means of physical dose-volume constraints 20
1.5.2 Radiobiological optimization 22
1.5.3 Ranking of treatment plans and evaluating potential dose escalation benefits 23
1.6 Estimating the α/β ratio from clinical dose-response data 24
1.7 Thesis objectives 26
1.7.1 Incorporation of NTCP models and parameter sets into modern treatment planning systems 26
1.7.2 Analytical investigation of the effects of inter-tumour heterogeneity on parameter ratio estimates 27
1.8 Outline 28
1.9 References 29

Chapter 2 A theoretical approach to the estimation of dose-volume constraints and their impact on dose-volume histogram selection 38
2.1 Introduction 38
2.2 Background 40

2.2.1 Some definitions 40
2.2.2 NTCP models 41
2.2.2.1 The Lyman (Sigmoidal dose response) NTCP model 41
2.2.2.2 Critical volume population model 42
2.2.3 Model parameters 43
2.3 Method 43
2.3.1 Reverse mapping of NTCP onto DVH space – a theoretical approach for dose-volume constraint estimation 43
2.3.1.1 Generation of random DVHs 44
2.3.1.2 Scaling the random DVHs 44
2.3.1.3 Probability that a DVH, with a user-specified NTCP, passes through a given point in the dose-volume histogram space 47
2.3.1.4 Constraint point estimation 48
2.3.2 Reverse mapping of NTCP onto DVH space – a theoretical approach to the investigation of the radiobiological impact of a set of dose-volume constraints 49
2.4 Results 50
2.5 Discussion 59
2.5.1 Suitability of the calculated constraint points for inverse planning 60
2.5.2 Random integral DVHs and dose scaling 63
2.5.3 Comparison with other methods of dose-volume constraint determination 65
2.5.4 Physical versus radiobiological optimization 67
2.6 Conclusions 69
2.7 References 70

Chapter 3 Reverse mapping of normal tissue complication probabilities onto dose volume histogram space: The problem of randomness of the dose volume histogram sampling 76
3.1 Introduction 76
3.2 Background 77
3.3 Theory 78
3.3.1 Determining the distribution of curves passing through a point in the unit square 79
3.3.2 Constructing a generator of random functions subject to the hypergeometric distribution. A random walk generator. 84
3.4 Comparison of different generators 85
3.4.1 Random number descent (Stavrev *et al.*[1]) 85
3.4.2 Random angle - random step descent 86
3.5 Discussion and conclusions 91
3.6 References 92

Chapter 4 Analytical investigation of properties of the iso-NTCP envelope 94
4.1 Introduction 94
4.2 Proof for the Lyman model 95
4.3 Proof for the critical volume NTCP model 98
4.4 Discussion and conclusions 100
4.5 References 101

Chapter 5 Functional form comparison between the population and the individual Poisson based TCP models 103
5.1 Introduction 103
5.2 Background and method 104
5.2.1 The Poisson-based individual TCP model 105
5.2.2 The population-based TCP model 106
5.2.3 Functional form comparison between individual and population-based TCP models 107
5.3 Results 108
5.4 Discussion 111
5.5 Conclusions 114
5.6 References 115

Chapter 6 An analytic investigation into the effect of population heterogeneity on parameter ratio estimates 119
6.1 Introduction 119
6.2 Background – TCP models 122
6.2.1 The individual TCP model 122
6.2.2 The population-based TCP model 123
6.3 Functional similarity of the individual and population TCP models 124
6.4 Mapping relationships between parameter ratios for the individual and population models 125
6.4.1 Analytic relationship between individual and population radiobiological parameters 125
6.4.2 Analytic relationship between individual and population α/β in the limit of dominant heterogeneity in radiosensitivity 127
6.4.3 Analytic relationship between individual and population α/β in the limit of dominant heterogeneity in clonogen number 130
6.4.4 Results 130
6.5 Investigation of parameter estimates from the individual and population TCP models 131
6.5.1 Generation of pseudo-data 132
6.5.1.1 Using assumed radiobiological ($\overline{\alpha}$, $\overline{\ln N_0}$ σ_α) parameters 132
6.5.1.2 Using the geometric (D_{50}, γ_{50}) parameters 134
6.5.2 Method – estimating α/β from the individual and population-based TCP models 135

6.5.3 Results 137
6.5.3.1 Results using assumed radiobiological parameters 137
6.5.3.2 Results using geometric parameters 140
6.6 Discussion 141
6.7 Conclusion 145
6.8 References 145

Chapter 7 Statistical quality of clinical dose-response data required to resolve TCP model parameters 150
7.1 Introduction 150
7.2 Method 152
7.2.1 Generation of pseudo-data 152
7.2.2 Determination of parameters of best fit and their confidence intervals .. 154
7.3 Results 154
7.3.1 General results 155
7.3.2 Effect of dose range and statistics per point on 95% CI 156
7.3.3 Effect of $\gamma_{50,th}$ on 95% CI 159
7.3.4 Effect of $D_{50,th}$ on 95% CI 161
7.3.5 Effect of data location (TCP_x) on 95% CI 163
7.4 Discussion 165
7.5 Conclusions 167
7.6 References 168

Chapter 8 Summary and general discussion 170
8.1 The incorporation of NTCP models and parameters into inverse planning 170
8.2 Functional similarity of the individual and population-based TCP models 171
8.3 The effect of inter-tumour heterogeneity on parameter ratio estimates 174
8.4 Quality of available clinical dose-response data 176
8.5 References 176

Chapter 9 Conclusions and future work 179
9.1 Concluding remarks 179
9.2 Future work 180
9.3 References 183

Appendix A NTCP model parameters 184
A.1 References 184

Appendix B Determination of the number of trajectories connecting two points in DVH space 186

Appendix C Special cases for the number of trajectories connecting two points in DVH space 188

Appendix D Generation of pseudo-clinical dose-response data 190
D.1 References 191

Appendix E Determining best-fit TCP parameters and their confidence limits 192
E.1 References 193

Appendix F Fitted parameter values for pseudo-data 194

Bibliography 199

List of Tables

Table 2-1: Estimates for the clinical maximum dose range to 16 critical structures (D_{low}, D_{high}) that typically occur during the listed treatments (values based on treatments given at the Cross Cancer Institute). Also shown are values for the maximum dose range (D_5 and D_{99}) calculated according to both the Lyman and CV population models. The parameters D_5 and D_{99} are used to scale randomly-generated DVHs appropriately to calculate constraint points using the reverse mapping method. The following abbreviations are used: CNS – central nervous system; PTV – planning target volume; H&N – head and neck. 46

Table 2-2: Constraint points interpolated from the average of DVHs with a Lyman NTCP of 5 ± 0.5% for 16 organs. For each of the relative volumes shown across the top of the chart, the interpolated dose in Gy is given for each organ if this value is non-zero. The far right column in the table shows the fraction of randomly-generated DVHs, out of a total of 1×10^6, that have an NTCP of 5 ± 0.5%, $P_{NTCP=5\%}$. 51

Table 2-3: Same as Table 2-2, but calculated using the CV population NTCP model... 52

Table 2-4: This table illustrates the effect of D_{max} range on calculated constraint points. Dose-volume constraint points were calculated for lung with the random DVHs scaled according to D_{max} ranges of $D_5 - D_{99}$, D_5 – 90Gy, 60 – 65 Gy and 60 – 90Gy, using both the Lyman and CV population models. 57

Table 2-5: This table shows three quantities calculated for the end-point brain necrosis, for the given sets of constraints. Calculations were done with both the Lyman and CV population NTCP models, and for each constraint volume given, a dose value from either Table 2-2 (for the Lyman model analysis) or Table 2-3 (for the CV population model analysis) was selected (except for the Emami constraint point, for which the dose was 60 Gy). The first quantity in this table is $P_\varepsilon(NTCP = 5 \pm 0.5\%)$, which represents the probability that a DVH with $NTCP \in [4.5\%, 5.5\%]$ passes within the ε-vicinity (ε = 1%) of the chosen constraint(s). The value $P(NTCP > 5.5\%)$ is the probability that a DVH which satisfies the chosen constraint(s) has an NTCP that is greater than 5.5%. Finally, this table shows the NTCP range in which 95% of the DVHs satisfying the constraint(s) result [the 95% confidence interval (CI)]. 59

Table 5-1: Individual parameters (α' and N_0) calculated for the γ_{50} values listed and D_{50} = 50 Gy. A set of population-based parameters ($\overline{\alpha'}$, σ'), calculated for the same

values of γ_{50} and D_{50}, is also listed. The population-based parameters were calculated assuming a value of $\overline{N_0} = 10^8$ for the average number of clonogens.. 111

Table 6-1: Estimates for the population and individual α/β ratio, along with 95% confidence intervals, from the pseudo-datasets shown in Figure 6-3. Also shown are estimates and 95% CIs for the ratio $\gamma_{50,e}/\gamma_{50,b}$, calculated by means of each TCP model. Finally, Eq. (6-17) was used to calculate an estimate and 95% CI for the individual α/β ratio based on the population estimate for the same parameter. All of these quantities were calculated for the EBRT-brachytherapy dataset pairs that were generated from assumed values for the population radiobiological parameters (Sec. 6.4.1) and the theoretical population α/β ratios shown. 138

Table 6-2: This table shows the same information as for Table 6-1, but for the EBRT-brachytherapy dataset pairs illustrated in Figure 6-4. 140

Table 7-1: Values for all quantities that characterize each of five series of generated pseudo-datasets. The leftmost column gives the main varied quantity of each series, and blue cells represent the specific values chosen for the varied quantity of interest. To assess the impact of a certain quantity on the accuracy of estimated model parameters, each pseudo-dataset in the series was fit with Eq. (7-1), and the corresponding change in the 95% CI width of each parameter was assessed. 153

Table 7-2: Illustrates the effect of an increase in each quantity in the leftmost column on the width of the 95% CI for parameters obtained from fitting. Up-arrows in the rightmost column indicate an increase in the 95% CI width (and correspondingly, a decrease in the accuracy of the estimated parameters), and down-arrows indicate a decrease in the 95% CI width (i.e., an increase in the accuracy of the parameter estimates). 156

Table 7-3: 95% confidence intervals (absolute, $C_u - C_l$, and relative, %) for the parameters D_{50} and γ_{50} obtained from fits to pseudo-datasets with $n_p = 5$ and $TCP_x = 70\%$ generated from a TCP curve with $D_{50,th} = 50$ Gy and $\gamma_{50,th} = 1$. 157

Table 7-4: 95% confidence intervals (absolute, $C_u - C_l$, and relative, %) for the parameters D_{50} and γ_{50} obtained from fits to pseudo-datasets with $n_p = 5$ and $TCP_x = 70\%$ generated from a TCP curve with $D_{50,th} = 50$ Gy and $\gamma_{50,th} = 1.5$. 159

Table 7-5: 95% confidence intervals (absolute, $C_u - C_l$, and relative, %) for the parameters D_{50} and γ_{50} obtained from fits to pseudo-datasets with $n_p = 5$ and $TCP_x = 70\%$ generated from a TCP curve with $D_{50,th} = 50$ Gy and $\gamma_{50,th} = 2$. 160

Table 7-6: 95% confidence intervals (absolute, $C_u - C_l$, and relative, %) for the parameters D_{50} and γ_{50} obtained from fits to pseudo-datasets with $n_p = 5$ and $TCP_x = 70\%$ generated from TCP curves with $D_{50,th} = 30$ and 70 Gy and $\gamma_{50,th} = 1$ 162

Table 7-7: 95% confidence intervals (absolute, $C_u - C_l$, and relative, %) for the parameters D_{50} and γ_{50} obtained from fits to pseudo-datasets with $n_p = 5$ and TCP_x = 60% and 80% generated from TCP curves with $D_{50,th} = 50$ Gy and $\gamma_{50,th} = 1$. 164

Table 7-8: Non-normalized slope, $\theta_{50,th}$, corresponding to the $D_{50,th}$ and $\gamma_{50,th}$ values listed. 166

Table F-1: Fitted parameter values (D_{50}, γ_{50}) and 95% confidence intervals for the pseudo-datasets generated from a TCP curve with theoretical parameter values of $D_{50,th} = 50$ Gy and $\gamma_{50,th} = 1$. The minimum negative log likelihood value is also shown, with its 95% confidence interval, for each fitted pseudo-dataset. Each dataset consisted of a total of $n_p = 5$ points, with the first point at a dose corresponding to $TCP_x = 70\%$. 194

Table F-2: Shows the same information as does Table F-1, but in this case the data were generated from a TCP curve with theoretical parameter values of $D_{50,th} = 50$ Gy and $\gamma_{50,th} = 1.5$. Each dataset consisted of a total of $n_p = 5$ points, with the first point at a dose corresponding to $TCP_x = 70\%$. 195

Table F-3: Shows the same information as Table F-1 and Table F-2, but in this case the data were generated from a TCP curve with theoretical parameter values of $D_{50,th} =$ 50 Gy and $\gamma_{50,th} = 2$. Each dataset consisted of a total of $n_p = 5$ points, with the first point at a dose corresponding to $TCP_x = 70\%$. 196

Table F-4: Fitted parameters and 95% confidence intervals for datasets generated from TCP curves with $D_{50,th} = [30, 70]$ Gy and $\gamma_{50,th} = 1$. Each dataset consisted of a total of $n_p = 5$ points over a dose interval (ΔD) of either 10 or 20 Gy, with the first point at a dose corresponding to $TCP_x = 70\%$. 197

Table F-5: Fitted parameters and 95% confidence intervals for datasets generated from TCP curves with $D_{50,th} = 50$ Gy and $\gamma_{50,th} = 1$. Each dataset consisted of a total of n_p = 5 points over a dose range of $\Delta D = 10$ Gy, with the first point at a dose corresponding to $TCP_x = 60\%$ in one case and 80% in the other. 198

List of Figures

Figure 1-1: Cell survival curves for a non-fractionated external-beam treatment (red) and a fractionated treatment (black). In this particular example, d = 2 Gy/fr, α = 0.3, and α/β = 2. If time is allowed for all β-type damage to be repaired between fractions, each new fractional dose corresponds to 'repeating' the first part of the survival curve. This idea is represented by the dotted curve. 8

Figure 1-2: The effect of α/β on fractionation sensitivity. Survival curves are plotted for the case of no fractionation (red), d = 4 Gy/fraction (black) and d = 2 Gy/fraction (blue). Also shown is the difference, ΔD, between the total doses required to produce a given survival fraction of cells (lnS = -25) for each of the two fractionation regimes. In (a), these curves are shown for an α/β ratio of 10 Gy, and in (b), they are shown for α/β = 3 Gy. 9

Figure 1-3: Individual TCP curves with different radiosensitivity values (black), and the population TCP curve that represents an average of many such individual TCP functions 14

Figure 1-4: Optimized integral dose-volume histograms for the target (red), the spinal cord (blue) and a volume representing the cord plus a margin (green) of a head and neck treatment plan. Constraints for each volume are represented by circles of the same colours. 21

Figure 2-1: (a) and (b) – a sample of DVHs with NTCP=5±0.5% (grey dotted curves) calculated according to the Lyman NTCP model (a) and the CV population NTCP model (b) for the endpoint heart pericarditis. Also shown in each of these subplots are the average of all DVHs with NTCP = 5 ± 0.5% along with the constraint points interpolated from this curve (solid black curve with diamond points). The Emami constraints for heart are shown for comparison as circles, along with the 5% iso-NTCP envelope that passes near to the Emami points. 53

Figure 2-2: Plot of the average DVH for each of 6 NTCP intervals for the endpoint heart pericarditis. Averages were calculated based on the Lyman NTCP model (a) and the CV population model (b). From the lowest volume to the highest volume curves, the intervals are NTCP = [0%, 10%] (first solid line), [10%, 20%] (first dotted line), [20%, 30%] (dash-dotted line), [50%, 60%] (dashed line), [70%, 80%] (second solid line) and [90%, 100%] (second dotted line). 55

Figure 2-3: A subset of DVHs that have a critical volume population NTCP of 5±0.5% for the endpoint lung pneumonitis (grey dashed curves), the average of these DVHs and the interpolated constraint points (solid curve with black diamonds). Each

subplot shows these curves for a different DVH dose scaling: (a) $D_{min} - D_{max} = D_5 - D_{99}$, (b) $D_5 - 90Gy$, (c) $60 - 65Gy$ and (d) $60 - 90Gy$. In each subplot, the 5% iso-NTCP envelope is shown along with the Emami points (O) for lung pneumonitis. The NTCPs are those of the average DVHs. 56

Figure 2-4: Lyman (left) and CV population (right) NTCP probability distributions for the endpoint brain necrosis for the given sets of calculated dose-volume constraint points. A total of 2×10^6 DVHs were simulated in order to build these distributions, and of those, the ones that passed within a vicinity of $\varepsilon = 1\%$ were deemed to satisfy the constraints. Shown in each subplot are two additional quantities: the probability that a DVH which satisfies the given constraint(s) will have an NTCP that is greater than 5.5% [$P(NTCP > 5.5\%)$] and the 95% confidence intervals (CIs) for the distributions. In (a) and (b), the NTCP distributions for the Emami v = ⅓, D = 60 Gy constraint point is shown for comparison (black line)..... 58

Figure 2-5: Averaged DVH (dotted line) and dose-volume constraint estimates (diamonds) for rectum, calculated by means of the reverse mapping method. The Lyman NTCP model with the Burman parameters was used to obtain these constraint points. Shown for comparison are the averaged DVH for non-bleeders from Jackson et al.[59] (upper solid curve) and the lower limit of its 67% confidence range (lower solid curve). The Lyman NTCP of the non-bleeder DVH is given in the upper right corner of this plot. 67

Figure 3-1: Monotonically decreasing functions. Our initial assumption is that the number of functions passing through different points - for example points P and Q - should be different and should depend on the position of the point. The thick black line represents a step like trajectory from point D to point B..... 78

Figure 3-2: Plot assisting us in the determination of the number of curves from point D to point B passing through point M_k lying on the intercept PQ and also in the determination of the number of curves connecting an intermediate point T with the end point B passing through point $M'_{k'}$..... 81

Figure 3-3: Illustration of the random angle - random step descent generator..... 86

Figure 3-4: Comparison between the three different DVH generators according to the averaged DVH curves resulting in $NTCP \in [4.5; 5.5]\%$ for liver, brain, bladder and spinal cord..... 88

Figure 3-5: Comparison between the three hybrid DVH generators with initial jump simulating partial organ irradiation according to the averaged DVH curves resulting in $NTCP \in [4.5; 5.5]\%$ for liver, brain, bladder, and spinal cord..... 90

Figure 4-1: Illustration of an α-iso-NTCP envelope and two arbitrary DVH curves – one that crosses the envelope at the point (D_k, v_k) and one that is tangential to the envelope at the same point. Also shown is a step-like DVH passing through (D_k, v_k)

that corresponds to homogeneous partial organ irradiation. The NTCP of the step-like DVH should be equal to α, while the NTCP for both arbitrary DVHs should be greater than α. 96

Figure 5-1: Individual (solid) and population-averaged (dotted) TCP curves for D_{50} = 50 Gy and the γ_{50} values shown in each sub-plot. 109

Figure 5-2: The ratio of the area difference, $\Delta A = A_{TCPpop} - A_{TCPind}$, between the two TCP curves, to the total area under the population TCP curve (A_{TCPpop}), plotted for the values of γ_{50} used to generate the curves shown in Figure 5-1. 110

Figure 6-1: (a) – (d) Individual TCP curve (dotted) and population TCP curve for the limit of dominant heterogeneity in radiosensitivity (solid) – Eq. (6-6) – with parameter values D_{50} = 50Gy and the γ_{50}'s shown in each sub-plot. (e) – (h) Individual TCP curve (dotted) and population TCP curve for the limit of dominant heterogeneity in clonogen number (dashed) – Eq. (6-9) – for the same geometric parameter values as (a) – (d). 126

Figure 6-2: The α/β ratio estimated from clinical dose-response data by means of the individual TCP model as a function of the same ratio estimated by means of the population TCP model for the case of dominant heterogeneity in radiosensitivity. Equation (6-17) defines the relationship between the individual and population-based estimates for α/β, and is plotted here for a value of d = 2 Gy/fraction for each of the $\gamma_{50,e}/\gamma_{50,b}$ values shown. For the case of $\gamma_{50,e}/\gamma_{50,b}$ = 1, Eq. (6-17) gives a straight line; that is, the estimate for α/β from the individual model is identical to that from the population model. As $\gamma_{50,e}/\gamma_{50,b}$ increases, a given population α/β maps to a smaller individual α/β. 131

Figure 6-3: Pseudo-data generated from theoretical brachytherapy and EBRT dose-response curves. The theoretical population-based TCP curve from which the points were generated is also shown (solid line), along with the individual TCP curve that corresponds to the same γ_{50} and D_{50} values (dotted line). The value of $\overline{\alpha}$ was assumed to be equal to 0.3, σ_α was assumed to be equal to 0.14, and the D_{50} for the brachytherapy curve was taken to be 84.9 Gy. Pseudo-data and the assumed TCP curves for permanent implant brachytherapy are shown in (a), (b) shows the pseudo-data and curves for $\overline{\alpha}/\overline{\beta}$ = 3 Gy, and (c) corresponds to $\overline{\alpha}/\overline{\beta}$ = 10 Gy. 134

Figure 6-4: Pseudo-data generated from theoretical population TCP curves (solid line). In each case, the individual TCP curve corresponding to the same D_{50} and γ_{50} values is also shown. (a) shows the pseudo-data corresponding to a theoretical brachytherapy curve with $D_{50,b}$ = 84.3 Gy and $\gamma_{50,b}$ = 1.35. (b), (c) and (d) show the pseudo-data corresponding to theoretical EBRT curves with $D_{50,e}$ = 69.5 and $\gamma_{50,e}/\gamma_{50,b}$ ratios of 1.05, 1.15 and 1.50, respectively 136

Figure 6-5: (a) Plot of the best-fit value of α/β as estimated from the individual TCP model vs. the best-fit value of $\overline{\alpha}/\overline{\beta}$ from the population TCP model for the pseudo-datasets generated from assumed radiobiological population parameters. The diamond point corresponds to the pseudo-data for a theoretical $\overline{\alpha}/\overline{\beta}$ of 3 Gy, and the circular point corresponds to the pseudo-data for a theoretical $\overline{\alpha}/\overline{\beta}$ of 10 Gy (Figure 6-3). The 95% confidence intervals for the individual and population-based α/β ratios are also shown. The solid line represents the relationship given by Eq. (6-17) for the best-fit value of $\gamma_{50,e}/\gamma_{50,b}$ as estimated from the population TCP model for the $\left(\overline{\alpha}/\overline{\beta}\right)_{th}$ = 3 Gy data – 1.50 (Table 6-1). The dotted line represents Eq. (6-17) for the best-fit normalized slope ratio corresponding to the $\left(\overline{\alpha}/\overline{\beta}\right)_{th}$ = 10 Gy data ($\gamma_{50,e}/\gamma_{50,b}$ = 1.23, Table 6-1). (b) This plot shows the same data as (a), for the pseudo-data generated from theoretical TCP curves with assumed values for the geometric parameters D_{50} and γ_{50}. The solid line represents the relationship given by Eq. (6-17) for $(\gamma_{50,e}/\gamma_{50,b})_{th}$ = 1.05, the dashed line corresponds to $(\gamma_{50,e}/\gamma_{50,b})_{th}$ = 1.15, and the dotted line corresponds to to $(\gamma_{50,e}/\gamma_{50,b})_{th}$ = 1.50. The triangle point represents the best-fit α/β ratios and 95% confidence intervals from the individual and population-based models for the dataset generated assuming $(\gamma_{50,e}/\gamma_{50,b})_{th}$ = 1.05, the circular point corresponds to $(\gamma_{50,e}/\gamma_{50,b})_{th}$ = 1.15, and the square point corresponds to $(\gamma_{50,e}/\gamma_{50,b})_{th}$ = 1.50. 139

Figure 7-1: Pseudo-datasets with n_p = 5 points over a dose interval of ΔD = 10 Gy generated from a population-averaged TCP curve with $D_{50,th}$ = 50 Gy and $\gamma_{50,th}$ = 1. Each dataset was generated assuming a different number of patients per point (N); the selected values of N are shown in each sub-plot. The error bars represent the 68% CI for each point, and were calculated assuming binomial statistics. 155

Figure 7-2: The relative 95% CI for D_{50} (a) and γ_{50} (b) from Table 7-3 plotted as a function of the number of patients per point (N) on a log-log scale for the three dose intervals 10, 20 and 30 Gy. 158

Figure 7-3: The relative 95% CI for D_{50} (◇) and γ_{50} (□) as a function of dose range, ΔD, corresponding to the pseudo-datasets with TCP_x = 70%, N = 1000, $D_{50,th}$ = 50 Gy and $\gamma_{50,th}$ = 1 158

Figure 7-4: The relative 95% CIs for the parameters D_{50} (a) and γ_{50} (b) plotted as a function of the number of patients per point (N) on a log-log scale for three theoretical normalized slope values – $\gamma_{50,th}$ = 1, 1.5 and 2. The estimated parameters correspond to datasets where n_p = 5, TCP_x = 70%, ΔD = 10 Gy, and $D_{50,th}$ = 50 Gy. 160

Figure 7-5: The relative 95% CI for D_{50} (◇) and γ_{50} (□) as a function of the assumed normalized slope, $\gamma_{50,th}$, corresponding to the pseudo-datasets with n_p = 5, TCP_x = 70%, N = 1000, $D_{50,th}$ = 50 Gy and ΔD = 10 Gy. 161

Figure 7-6: The relative 95% CIs for the parameters D_{50} (a) and γ_{50} (b) plotted as a function of the number of patients per point (N) on a log-log scale for three theoretical D_{50} values – $D_{50,th}$ = 30, 50 and 70 Gy. The estimated parameters correspond to datasets where n_p = 5, TCP_x = 70%, ΔD = 10 Gy, and $\gamma_{50,th}$ = 1..... 162

Figure 7-7: The relative 95% CI for D_{50} (◇) and γ_{50} (□) as a function of the assumed dose at 50% control, $D_{50,th}$, corresponding to the pseudo-datasets with TCP_x = 70%, N = 1000, $\gamma_{50,th}$ = 1 and ΔD = 10 Gy..... 163

Figure 7-8: The relative 95% CIs for the parameters D_{50} (a) and γ_{50} (b) plotted as a function of the number of patients per point (N) on a log-log scale for three TCP_x values – 60%, 70% and 80%. The estimated parameters correspond to datasets generated from a curve with $D_{50,th}$ = 50 Gy and $\gamma_{50,th}$ = 1 where n_p = 5 and ΔD = 10 Gy..... 164

Figure 7-9: The relative 95% CI for D_{50} (◇) and γ_{50} (□) as a function of TCP_x, corresponding to the pseudo-datasets with $D_{50,th}$ = 50 Gy, $\gamma_{50,th}$ = 1, N = 1000, and ΔD = 10 Gy..... 165

Figure C-1: Consideration of the special cases when the random walk created by the generator may leave the unit square..... 189

List of Abbreviations

2D	Two-dimensional
3DCRT	Three-dimensional image-based conformal radiotherapy
CT	computed tomography
CV	Critical volume (NTCP model)
DNA	Deoxyribonucleic acid
dDVH	differential dose-volume histogram
DVH	dose-volume histogram
EBRT	External-beam radiation therapy
EUD	Equivalent uniform dose
FSU	Functional sub-unit
GMD	Generalized mean dose
GTV	Gross tumour volume
iDVH	integral dose-volume histogram
IMRT	Intensity-modulated radiation therapy
LQ	Linear quadratic (cell survival model)
MLC	Multi-leaf collimator
NTCP	Normal tissue complication probability
OAR	Organ at risk
PDF	Probability distribution function
RTOG	Radiation Therapy Oncology Group

PTV	Planning target volume
SDR	Sigmoidal dose-response (NTCP model)
TCP	Tumour control probability

List of Symbols

D	Radiation dose [Gy].
$S(D)$, $P_S(D)$	Represents the fraction of cells that survive irradiation to dose D.
α	Represents lethal (non-repairable) damage in a cell that results from a single radiation interaction.
β	Represents sub-lethal (repairable) damage in a cell that results from two separate radiation interactions.
μ	Repair constant for sub-lethal lesions.
$G(\mu,T)$	Lea-Catcheside dose-protraction factor – describes repair of sub-lethal lesions that occurs for low dose rates. T represents total irradiation time.
d	(Constant) dose per fraction in a fractionated radiation treatment.
N_S	Mean number of tumour cells that survive a treatment in which a total dose, D, is delivered.
N_0	Total (initial) number of clonogens in a tumour before a radiation treatment. This is an individual TCP model parameter.
λ	Cell repopulation, or growth-rate, constant.
T	Total treatment time in the individual or population TCP model expressions.
$\lambda' = \lambda T/n$	Cell repopulation constant scaled by the number of days per fraction (T = total treatment time in days, n = total number of fractions in treatment).
α'	For constant dose per fraction, d, this parameter is a combination of radiosensitivity and repopulation parameters – $\alpha' = \alpha + \beta d + \lambda'/d$ (this is a parameter of the individual TCP model).
$\overline{\alpha'}$	Average of α' over a population of patients – $\overline{\alpha'} = \overline{\alpha} + \overline{\beta} d + \overline{\lambda'}/d$ (this is a parameter of the population-averaged TCP model).
$\overline{\alpha}$	Average of α over a population of patients.

$\overline{\beta}$	Average of β over a population of patients.
$\overline{\lambda'}$	Average of λ' over a population of patients.
σ'	Parameter (of the population-averaged TCP model) that represents the inter-tumour heterogeneity in $\alpha' - (\sigma')^2 = \sigma_\alpha{}^2 + \sigma_\beta{}^2 d^2 + \frac{(\sigma_{\lambda'})^2}{d^2}$.
σ_α	Standard deviation of the parameter α. Represents the amount of inter-tumour heterogeneity in α among a patient population.
σ_β	Standard deviation of the parameter β. Represents the amount of inter-tumour heterogeneity in β among a patient population.
$\sigma_{\lambda'}$	Standard deviation of the parameter λ'. Represents the amount of inter-tumour heterogeneity in λ' among a patient population.
$\overline{\ln N_0}$	Average log clonogen number of a population of patients (population-averaged TCP model parameter).
Γ	Euler's gamma constant (approximate value is 0.577).
$\sigma_{\ln N_0}$	Parameter that represents inter-tumour heterogeneity in $\ln N_0$ (population-averaged TCP model parameter).
D_{50}	Dose at 50% control (for TCP models) or 50% complication rate and whole-organ irradiation (for the Lyman NTCP model).
γ_{50}	Normalized slope at D_{50} (TCP model parameter).
θ_{50}	Non-normalized slope at D_{50}.
D_f	Dose at an arbitrary tumour control level of f, where $0 \leq f \leq 1$.
γ_f	Normalized slope at D_f.
(v, D)	A relative volume-dose point of a DVH.
$\Phi(x)$	Probit function.
m	Parameter that describes the slope of a normal tissue dose-response curve in the Lyman model.

a	Volume parameter for EUD in the Lyman model.
M_{FSU}	Number of FSUs that must be destroyed in order for a complication to occur in an organ.
N_{FSU}	Total number of FSUs that comprise an organ.
μ_{cr}	The relative critical volume (individual CV NTCP model) or population-averaged relative critical volume (population CV NTCP model).
$\overline{\mu}_d$	The relative mean damaged volume (CV NTCP model).
$\sigma_{\mu d}$	Standard deviation of $\overline{\mu}_d$ (individual CV NTCP model).
$P_{FSU}(D)$	Probability of damaging a FSU when it is irradiated to a (uniform) dose of D (CV NTCP model).
D_{50}^{FSU}	FSU dose at 50% control for $P_{FSU}(D)$ (CV NTCP model).
γ_{50}^{FSU}	FSU normalized slope for $P_{FSU}(D)$ (CV NTCP model).
N_c	Number of cells in a FSU (for the CV NTCP model).
α_c	Radiosensitivity of a cell in a FSU.
$\sigma_{\mu cr}$	Standard deviation of relative critical volume in the population CV NTCP model.
n	(1) Number of fractions in a standard external-beam treatment. (2) Observed number of 'successes' in the binomial or Poisson distribution formula.
p	In the Poisson or binomial distribution expressions, p is the probability of a 'success'.
N	(1) The total number of 'trials' in the Poisson or binomial distribution expressions. (2) The number of patients per point in a generated pseudo-dataset.
α/β	This ratio determines a tissue's sensitivity to fractionation. It is typically low (~3) for late-responding tissues and high (~10) for early-responding tissues.
λ/α	A parameter ratio that represents the amount of dose per day that is needed to combat tumour growth.

$\overline{\alpha'}/\sigma'$	A parameter ratio that represents the relative heterogeneity among a patient population.
$V_{int}(D)$	Volume that is irradiated to at least a dose, D, in an integral DVH.
Θ	Heaviside step function.
$D(\vec{r})$	Dose distribution in a structure of interest.
ε	Radius of a circle surrounding a dose-volume constraint point, through which a DVH must pass in order for it to satisfy the constraint.
$D_{\max,k}$	Maximum dose point for a DVH defined as DVH_k.
N_{DVH}	Total number of DVHs generated by means of the reverse mapping method.
n_k	A uniform randomly-generated number, used to assign a maximum dose value to a DVH generated during the reverse mapping process.
D_5, D_{99}	Doses that give a NTCP of 5 and 99%, respectively, assuming uniform whole-organ irradiation. These quantities are used for the reverse mapping process.
D_{low}, D_{high}	Typical clinical lower and upper limits, respectively, for maximum organ dose.
$P(D, v \mid ...)$	DVH point probability. The probability that a DVH, with a user-specified NTCP range, passes through a given point in the dose-volume histogram space.
$V_{mean}(D_i)$	The relative volume of the average DVH at the dose point D_i. This quantity is used during the reverse mapping process.
n_{DVH}	The total number of DVHs with NTCP = 5 ± 0.5%. Used during the reverse mapping process.
$P_{NTCP=5\%}$	The fraction of DVHs, generated by means of the reverse mapping method, with NTCP = 5 ± 0.5%.
$P(_{NTCP>5.5\%})$	The probability that a DVH which satisfies a set of constraints leads to an unacceptable NTCP of greater than 5.5%.

$P_\varepsilon(...)$	The probability that a DVH with $NTCP \in [4.5, 5.5]\%$ passes within the ε-vicinity of the chosen constraint(s).
(D_k, v_k)	Point on the α-iso-NTCP envelope in integral DVH space.
$\Delta A / A_{TCP_{pop}}$	Normalized difference between the areas under the individual and population-averaged TCP curves.
$\gamma_{50,e}/\gamma_{50,b}$	Ratio of normalized slope parameters corresponding to the TCP curves that represent an external-beam treatment and a low-dose brachytherapy treatment for a given tumour type.
TCP_x	TCP level that is characteristic of a point in a generated pseudo-clinical tumour dose-response dataset.
D_x	Dose point corresponding to TCP_x.
ΔD	Dose interval corresponding to a generated pseudo-dataset. This quantity represents the dose range in which the individual points fall.
n_p	Total number of points that comprise a generated pseudo-dataset.
C_u, C_l	Upper and lower 95% confidence limits for a fitted parameter.

Chapter 1 Introduction and Background

1.1 Introduction

1.1.1 Radiation therapy

The most common types of radiation used for the treatment of cancer are photons and electrons, delivered via external-beam linear accelerators or administered by placing radioactive sources right at the treatment site (brachytherapy). While these forms of cancer therapy are an effective means of tumour control, it is inevitable that some healthy tissues will be irradiated when dose is delivered to the tumour.

The probability of controlling a tumour as a function of delivered radiation dose is defined as the tumour control probability (TCP). When plotted in dose-TCP space, this curve is sigmoidal. Similarly, the probability that a certain dose will lead to a complication in a normal tissue or organ is known as the normal tissue complication probability (NTCP). The NTCP is also a sigmoidal function of dose. The goal of radiation therapy is to maximize TCP while minimizing NTCP. Currently, this is accomplished by keeping the normal tissue dose low in comparison to the dose delivered

to the tumour, and through dose fractionation techniques. Dose distributions are optimized through the use of three-dimensional treatment planning and highly conformal delivery techniques, such as intensity modulated radiation therapy (IMRT). It is generally accepted that the complication rate should ideally be around 5% or less. Of course, for some treated sites it is possible to achieve even lower complication rates, while for others it is not possible to get as low as 5%. The value of 5% is somewhat arbitrarily quoted as a reasonably low complication rate in the clinic, however.

Other factors besides dose distribution can influence TCP and NTCP. Fundamentally, the dose-response function for an organ (or tumour) is dependant on the effect of ionizing radiation on biological tissues.

1.1.2 Radiobiology

The field of radiobiological modeling involves the investigation of the impact of ionizing radiation on cell survival, and the quantification of the dose-response of cells, organs, and tumours in the form of models.

This branch of science is reasonably well-understood at the cellular level. Considerable progress has been made in regards to research involving the deposition of energy in a cell by ionizing radiation and the consequential cellular damage and/or reproductive death. Also, through laboratory experiments, the in-vitro response of cells to radiation has been quantified and modeled. *In vitro* cell survival parameters are thus reasonably well-known. Investigations continue to be carried out in the field of radiobiology to further our understanding of the mechanisms involved in the response of cells to ionizing radiation, and also to ultimately take this knowledge and apply it clinically.

Within the past couple of decades, there has been considerable research activity involving the application of radiobiological principles to clinical radiation therapy. In this vein, attempts have been made to collect dose-response data for both normal tissues and tumours, and then to apply radiobiological dose-response models to such data. Once model parameters have been estimated in this way, they could conceivably be used to

predict the effects of different treatments regimes (different dose distributions, fractionation regimes, or total dose delivered, for example) on NTCP and TCP. TCP and NTCP models could potentially be used for the purpose of ranking different treatment plans, or they could be incorporated into the treatment planning process itself (for example, they could be used for inverse planning optimization). A few researchers have assumed that the *in vivo* radiobiological parameters and parameter ratios can be extracted from model fits to clinical dose-response data. It is hoped that the results of such parameter estimations could be applied clinically (for example, radiosensitivity parameter estimates for tumour and normal tissue may be used to determine optimal dose delivery patterns, that is, fractionation regimes).

The incorporation of radiobiological models and principles in the radiation therapy process in this way could ultimately lead to treatments with improved outcome, and research in this area is currently being carried out with this as a goal. However, this particular branch of research is still relatively new, and hence there are some difficulties associated with the field.

For one thing, the clinical dose-response datasets that are currently available for both tumours and normal tissues are generally sparse, and subject to considerable uncertainty. Tumour dose-response data tend to cover only a narrow range in the high-probability end of the curve. In contrast, normal tissue dose-response data normally covers only a narrow range in the low-probability end of the curve. In addition, the existing dose-response datasets are not generally based on a large number of samples (for example, in dose escalation trials, generally less than ~100 patients are treated to a given prescription dose), which increases the uncertainty associated with a given dataset. A number of different TCP and NTCP models have been proposed, ranging from purely phenomenological to being derived on the basis of radiobiological principles, and they all tend to describe existing clinical dose-response data equally well. That is, the quality of such data is not high enough to distinguish one model from another.

Clinical dose-response data are population-averaged and include the effects of inter-tumour heterogeneity. On the other hand, data from synergistic/inbred animal experiments, in which inter-individual heterogeneity is negligible, are capable of distinguishing between different individual dose-response models. For example, the data

of Fischer and Moulder[1] were obtained from animal experiments in which tumour size was carefully monitored. This dataset also contained enough points to fully sample the entire dose-response curve. Stavreva *et al.*[2] fit this dataset with different individual TCP models, and found that the Zaider-Minerbo[3] model, which takes cell repopulation into account, best fit the data. Unfortunately, the existing clinical datasets are not nearly as detailed, and represent a significant amount of inter-tumour heterogeneity.

While the effect of ionizing radiation on an *in vitro* sample of cells is well-understood and the radiobiological parameters well-determined, considerably less is known about the *in vivo* situation. The *in vivo* environment is much more complicated than the *in vitro* one, and is difficult to reproduce for the purpose of laboratory experiments. Therefore, *in vivo* radiobiological parameters are theoretically determined from dose-response data by means of TCP and NTCP models. When the effects of intra- and inter- tumour/organ heterogeneity are taken into account, it may not be possible to estimate *in vivo* parameters directly from dose-response data in the first place.

These difficulties have thus far delayed the widespread use of radiobiological principles in a clinical setting. However, it is still useful to carry out investigations related to clinical radiobiology. The dose-response data that are currently available may have some use in treatment planning, and for the relative ranking of treatment plans. Even if this proves not to be the case, methods that are developed using such data may be used in a clinical setting once better clinical data do become available. Also, while it may not currently be possible to determine individual *in vivo* radiobiological parameters accurately, this may not be true for parameter ratios.

The next few sections of this chapter outline the field of radiobiology, starting from the effects of radiation at a cellular level, and the modeling of cell survival. The main TCP and NTCP models are described, as well as their use in treatment planning and in parameter estimation. The objectives of this thesis are then outlined, followed by a brief description of the contents of each following chapter.

1.2 Cell damage by radiation

When a group of cells is exposed to ionizing radiation, the latter can interact either directly or indirectly with DNA to eventually lead to damage and potentially reproductive death. With a direct interaction, the radiation causes an ionization event on the DNA itself. With an indirect interaction, it ionizes a nearby water molecule to produce highly reactive species (such as the hydroxyl radical – OH•). The reactive species then interact with DNA and causes damage.

The relationship between the surviving fraction of a population of irradiated cells and the radiation dose delivered to the cells is described by the cell survival curve. A number of cell survival models have been developed to describe this curve, but the most widely used one is the linear quadratic (LQ) model, originally derived by Chadwick and Leenhouts.[4]

1.3 The linear quadratic model

In the original derivation by Chadwick and Leenhouts, a single DNA double-strand break was assumed to be the type of damage that eventually leads to the loss of a cell's reproductive capability. A double-strand break could result from one of two possible events:

(i) One radiation event breaks both DNA strands.

(ii) Two separate radiation events cause two single-strand breaks, which then combine to produce one double-strand break if they occur close enough in time and space.

According to the LQ model, the cell survival curve is given by:

$$S(D) = \exp\left[-\left(\alpha D + \beta D^2\right)\right], \tag{1-1}$$

where, in the Chadwick and Leenhouts interpretation, α [Gy^{-1}] represents double strand breaks caused by a single radiation event, and β [Gy^{-2}] represents double strand breaks caused by the interaction of two single strand breaks from two different radiation events. The parameters α and β describe a cell's radiosensitivity.

Since the original derivation of the LQ model by Chadwick and Leenhouts, it has been determined that the existence of a single DNA double-strand break does not necessarily lead to reproductive death of a cell. The current theory is that the number of chromosomal aberrations, which consist of clusters of double-strand breaks, correlates with cell survival when cells are irradiated.[5] This observation does not change the form of the LQ model given by Eq. (1-1), but it does lead to a different interpretation of linear (α-type) and quadratic (β-type) damage. The α-type damage is now interpreted as the formation of complex chromosomal aberrations caused by one radiation event, while the β-type damage now represents the formation of complex chromosomal aberrations through the interaction of DNA double-strand breaks caused by separate radiation events.

Alternatively, the α and β terms of the LQ model may be interpreted as lethal lesions, and sub-lethal lesions, respectively. This interpretation relates to the ability of cells to repair different types of damage. Lethal lesions are those that are completely non-repairable, while sub-lethal lesions could potentially either interact with each other to lead to a lethal lesion, or they could be repaired by the cell.

1.3.1 Dose rate effects and the LQ model

The number of lethal lesions produced depends on dose rate. The lower the dose rate, the higher the chances that sub-lethal lesions are repaired. The effect of dose-rate on cell survival curves has been observed experimentally,[6] and the complete form of the LQ model explicitly includes this effect:

$$S = \exp\left[-\left(\alpha D + G(\mu, T)\beta D^2\right)\right]. \tag{1-2}$$

The repair constant for sub-lethal lesions is given by the parameter μ, and T [s] is the time of irradiation (which depends on dose rate). The function $G(\mu,T)$ is known as the Lea-Catcheside dose-protraction factor, originally presented by Lea.[7] It ranges from 0 at very low dose rates (all sub-lethal lesions are repaired before they can interact to form lethal lesions), to 1 at very high dose rates (all sub-lethal lesions interact to form lethal lesions). For the case of constant dose rate and exponential repair with repair constant μ [s^{-1}], this function is given by the expression:[7]

(1-3) $$G(\mu,T)=\frac{2}{\mu T}\left[1-\frac{1}{\mu T}\left(1-e^{-\mu T}\right)\right].$$

Following either the method proposed by Lea[7] to derive this function, or that of Kellerer and Rossi,[8] a dose-protraction factor may be derived for situations where the dose rate is not constant (for example, an exponentially-decaying dose rate, such as the one that would occur for brachytherapy treatments).

1.3.2 The relationship between the α/β ratio and dose-fractionation for external-beam treatments

1.3.2.1 Effect of fractionation on cell survival curves

For a typical external-beam radiation therapy (EBRT) treatment, the total prescribed dose is delivered in a number of smaller daily fractions, usually around 2 Gy each. For non-fractionated dose delivery, the natural logarithm of the LQ survival curve is given by:

(1-4) $$\ln S=-\left(\alpha D+\beta D^2\right),$$

and a plot of ln$S$ vs. dose, D, is parabolic as shown by the red curve in Figure 1-1. Now suppose a total dose, D, is delivered in n equal fractions of dose d, with enough time between irradiations to allow complete repair to occur. In this case, we have:

(1-5) $$S=\left[e^{-\left(\alpha d+\beta d^2\right)}\right]^n \Rightarrow \ln S=-\left(\alpha n d+\beta n d^2\right).$$

Substituting $D = nd$ in Eq. (1-5), we arrive at the following survival curve for a fractionated treatment:

(1-6) $$\ln S=-(\alpha+\beta d)D=-\alpha D\left(1+\frac{d}{\alpha/\beta}\right).$$

When Eq. (1-6) is plotted as ln$S$ vs. D, the result is a straight line and, in comparison to a non-fractionated treatment [Eq. (1-4)], the same total dose, D, will result in less cell killing. A smaller dose per fraction results in a larger survival fraction for a given total

dose, D. The difference between fractionated and non-fractionated treatments is illustrated in Figure 1-1, for $\alpha/\beta = 2$ Gy, $\alpha = 0.3$, and $d = 2$ Gy/fr.

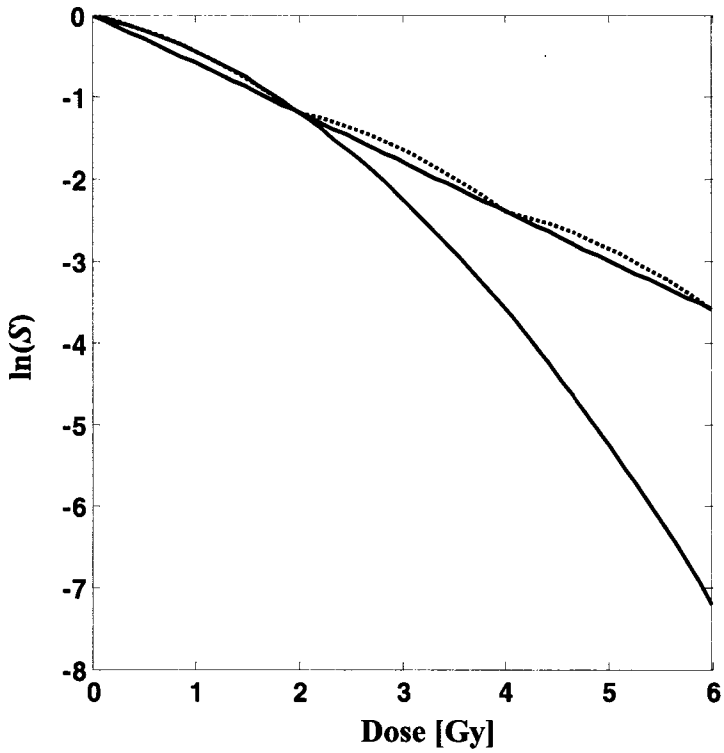

Figure 1-1: Cell survival curves for a non-fractionated external-beam treatment (red) and a fractionated treatment (black). In this particular example, $d = 2$ Gy/fr, $\alpha = 0.3$, and $\alpha/\beta = 2$. If time is allowed for all β-type damage to be repaired between fractions, each new fractional dose corresponds to 'repeating' the first part of the survival curve. This idea is represented by the dotted curve.

1.3.2.2 Fractionation sensitivity and the α/β ratio

The α/β ratio [Gy] describes the amount of curvature of a cell survival curve. A large α/β ratio implies that the interaction of sub-lethal lesions plays only a minor role in cell killing relative to direct cell-killing through α-type damage. The opposite is true for tissues with a low α/β ratio – the interaction of sub-lethal lesions to produce lethal damage dominates cell kill. In the latter case, repair should also have a greater role in cell survival.

The sensitivity of a group of cells to the dose per fraction, d is determined by the α/β ratio, and this concept is illustrated in Figure 1-2. In Figure 1-2(a), three survival curves are plotted for the case of $\alpha/\beta = 10$ Gy and $\alpha = 0.3$. The red dotted curve

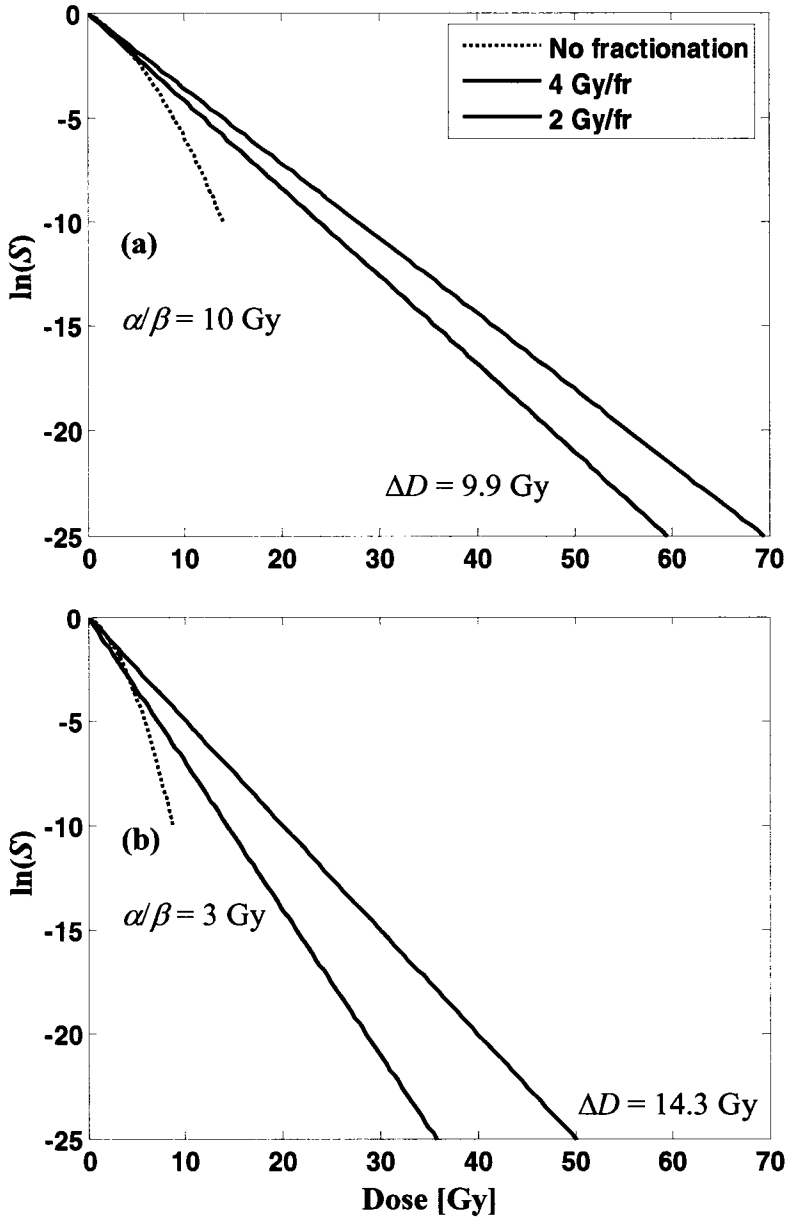

Figure 1-2: The effect of α/β on fractionation sensitivity. Survival curves are plotted for the case of no fractionation (red), d = 4 Gy/fraction (black) and d = 2 Gy/fraction (blue). Also shown is the difference, ΔD, between the total doses required to produce a given survival fraction of cells ($\ln S$ = -25) for each of the two fractionation regimes. In (a), these curves are shown for an α/β ratio of 10 Gy, and in (b), they are shown for α/β = 3 Gy.

corresponds to the case of no fractionation. The black curve describes cell survival fraction for a dose per fraction of 4 Gy, and the blue curve describes cell survival fraction for d = 2 Gy/fraction. The dose difference, ΔD, between the two fractionated treatment curves at an iso-effect of $\ln S$ = -25 is also shown; for α/β = 10 Gy, this quantity amounts to ΔD = 9.9 Gy.

Similar curves are shown in Figure 1-2(b), but in this case the α/β ratio was set equal to 3 Gy. For this example, the dose difference to produce the same iso-effect of $\ln S$ = -25 for the two different fractionation regimes is ΔD = 14.3 Gy. Tissues with a lower α/β ratio thus exhibit an increased sensitivity to sparing by dose fractionation.

1.3.2.3 Early and late-responding tissues

The effects of radiation on normal tissues can be characterized according to the time it takes for them to manifest. Early effects result from the immediate depletion of parenchymal and/or stem cells (the former are cells that directly perform a tissue's function and the latter are those that proliferate to produce new parenchymal cells). Late effects result from the depletion of stromal cells (which support the function of parenchymal cells). The time at which the effects of radiation become apparent has been observed to depend on the rate of proliferation of the cells that comprise a tissue. Early-responding tissues tend to be composed of cells that proliferate rapidly; while late-responding tissues regenerate at a significantly slower rate. A given organ can exhibit both early and late effects following irradiation, depending on its composition.

It has been observed experimentally that late-responding tissues are more sensitive to changes in fractionation size than early-responding tissues.[9,10] This observation may be explained by considering the cell survival curves, and the α/β ratios, of late and early-responding tissues. Fowler[11] published a paper in 1983 that reported measured α/β ratios for a variety of late and early-responding tissues. The early-responding tissues tended to have higher α/β ratios (~10 Gy) than did the late-responding tissues (~3 Gy).

The majority of tumours can be considered early-responding tissues – they proliferate rapidly, and have relatively high α/β ratios. Thus, by delivering the prescribed dose for a radiation treatment in a number of daily fractions, the surrounding, late-responding normal tissues are allowed time for repair of sub-lethal lesions. For the case where the tumour being treated has a higher α/β ratio than the surrounding normal tissues, fractionated treatments with d = 2 Gy/fr should facilitate maximum TCP with minimum NTCP. This value for d was arrived at based on clinical experience, and is consistent with the α/β ratio description.

The α/β ratio is a fairly important quantity, as the difference between α/β for the treated tumour and that of the surrounding normal tissues is an important factor in determining an optimum fractionation regime.

1.4 TCP and NTCP models

While cell survival models are adequate for describing the results of lab experiments in which a number of cells are irradiated *in vitro*, more complex models are required to describe tumour control probability and normal tissue complication probability. In this section, the TCP and NTCP models referred to throughout the rest of this thesis are summarized.

1.4.1 TCP models

1.4.1.1 The individual TCP model based on Poisson statistics

The Poisson distribution,

(1-7) $$f(n,\nu)=\frac{\nu^n}{n!}e^{-\nu},$$

is a special case of the binomial distribution,

(1-8) $$f(n;N,p)=\frac{N!}{n!(N-n)!}p^n(1-p)^{N-n}.$$

The binomial distribution gives the probability of observing a total of n successes out of N trials, where the probability of one success is p. The Poisson distribution may be applied when the number of trials, N, is very large, while the probability of one success, p, is very small. In Eq. (1-7), the mean (or expected) number of successes is given by ν (= Np) and n still corresponds to the number of observed successes.

The individual TCP model is derived under the assumption that tumour control is achieved only by killing all tumour clonogens.[12] Let the total number of clonogens in a tumour be equal to N_0, and the probability of one clonogen surviving irradiation be equal to $P_S(D)$, the cell survival fraction after a dose, D. In this case, we can assume that N_0 is large, $P_S(D)$ is small, and the product $\nu = N_0P_S(D)$ is finite. The probability of no surviving clonogens [$n = 0$ in Eq. (1-7)] after a tumour receives a dose, D (i.e., the TCP), under the assumption of Poisson statistics, is given by:

(1-9) $$TCP_{ind} = e^{-N_0P_S(D)},$$

Adding in a simple description for clonogen repopulation[13] that takes place over the time of the treatment, T, the expression becomes:

(1-10) $$TCP_{ind} = e^{-N_0P_S(D)\exp(\lambda T)},$$

where λ [s^{-1}] is the growth-rate constant.

Now assume that the treatment consists of n fractions of equal dose, d ($nd = D$), over time T, and that there is sufficient time between fractions for full repair of damage to occur. The cell survival fraction, $P_S(D)$, is assumed to be well-represented by the linear quadratic formula [Eq. (1-1)]. In this case, Eq. (1-10) becomes:

(1-11) $$\begin{aligned} TCP_{ind} &= \exp[-N_0\exp(-\alpha D-\beta dD)\exp(\lambda T)] \\ &= \exp[-N_0\exp(-(\alpha+\beta d)D+\lambda T)] \end{aligned}.$$

For a constant dose per fraction, the growth constant can be scaled by the number of days per fraction, $\lambda' = \lambda T/n$. Under these assumptions, the individual TCP model can be written as:

(1-12) $$TCP_{ind} = \exp[-N_0\exp(-\alpha' D)] = \exp\left[-N_0\exp\left(-\left(\alpha+\beta d-\frac{\lambda'}{d}\right)D\right)\right],$$

where α and β are the linear quadratic radiosensitivity parameters.

The validity of the Poisson TCP model was questioned by Tucker and Travis,[14] and others[3,15-18] who explored the non-Poisson nature of TCP. Under certain conditions, however, it has also been shown[15,19] that the distribution of the number of clonogen cells remaining at the end of a treatment is well-approximated by the Poisson distribution. In view of these results, and also because of the relative complexity of the non-Poisson TCP models, the individual TCP function that is derived on the basis of Poisson statistics is often used for clinical radiobiology purposes.

1.4.1.2 The population TCP model[20]

For tumours as well as for normal tissues, the dose-response exhibited by a clinical series is a population-based, rather than an individual, response. The inter-tumour heterogeneity within a clinical dataset leads to a dose-response curve that is flattened relative to the individual dose-response curve. An illustration of this concept is shown in Figure 1-3. The black TCP curves correspond to individual tumours with different radiosensitivity parameters, α'. The average of a number of these curves over a population distribution of radiosensitivity parameters gives the population TCP curve shown in blue.

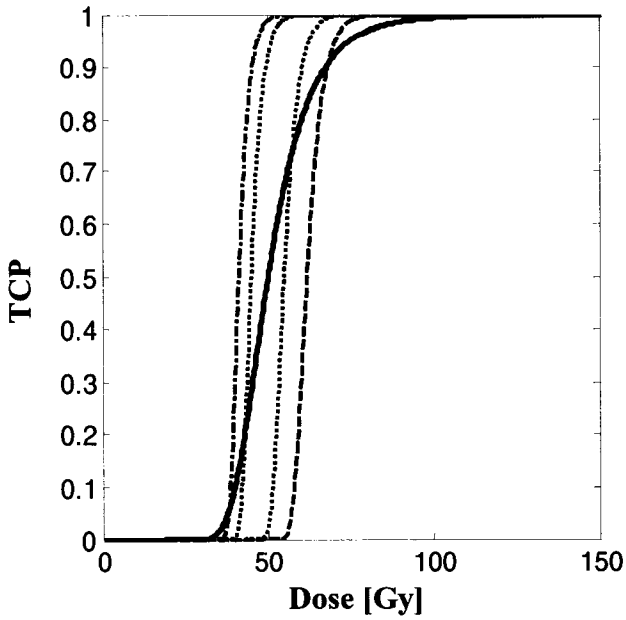

Figure 1-3: Individual TCP curves with different radiosensitivity values (black), and the population TCP curve that represents an average of many such individual TCP functions.

A population-based TCP model may be derived from an individual TCP model by averaging Eq. (1-12) over distributions for α' and N_0. Carlone *et al.*[20] derived a fundamental form of the population TCP model in this way by making use of the following assumptions:

- There is no correlation between any of the parameters for an individual. Thus, the multidimensional probability distribution function (PDF) for all parameters can be represented as the product of the PDF for each individual parameter.
- Assume a lognormal PDF for N_0, and a Gaussian PDF for α'.
- Assume that heterogeneity in the radiosensitivity parameter α' is much larger than that in the log of initial clonogen number, $\ln N_0$.

Under these assumptions, the population TCP model is given by:[20]

$$TCP_{pop} = \frac{1}{2} erfc\left[\sqrt{\pi}\gamma_{50}\left(\frac{D_{50}}{D} - 1\right)\right], \tag{1-13}$$

where

(1-14) $$\gamma_{50} = \frac{1}{\sqrt{2\pi}} \frac{\overline{\alpha'}}{\sigma'}$$

and

(1-15) $$D_{50} = \frac{\Gamma + \overline{\ln N_0}}{\overline{\alpha'}}.$$

The parameters $\overline{\alpha'}$ and $\overline{\ln N_0}$ represent population averages of the corresponding individual parameters, where

(1-16) $$\overline{\alpha'} = \overline{\alpha} + \overline{\beta} d - \frac{\overline{\lambda'}}{d}.$$

The heterogeneity in $\overline{\alpha'}$ is σ', and is given by:

(1-17) $$(\sigma')^2 = \sigma_\alpha{}^2 + \sigma_\beta{}^2 d^2 + \frac{(\sigma_{\lambda'})^2}{d^2}.$$

A similar expression may be derived for the limit where heterogeneity in clonogen number dominates.

1.4.2 NTCP models

For the TCP models presented above, it was assumed that the entire tumour is irradiated to a uniform dose, *D*. While this is not a bad approximation for tumours treated by means of a standard EBRT technique, this is not the case for irradiated organs at risk. Normal tissues are generally irradiated heterogeneously during radiation treatments. Thus, NTCP models must take nonuniform dose distributions into account. In addition to the heterogeneous irradiation patterns, many organs exhibit volume effects – some organs will exhibit very few complications if the irradiated volume remains small, even if that part of the organ receives a relatively high dose. NTCP models must also take these volume effects into account.

1.4.2.1 The Lyman[21] (sigmoidal dose response) model

This is a phenomenological model that describes normal tissue dose-response using the following function:

$$NTCP = \Phi\left(\frac{EUD - D_{50}}{mD_{50}}\right), \tag{1-18}$$

where Φ is the probit function,

$$\Phi(x) = \frac{1}{\sqrt{2\pi}}\int_{-\infty}^{x}\exp\left(\frac{-t^2}{2}\right)dt = \frac{1}{2}\left[1 + erf\left(\frac{x}{\sqrt{2}}\right)\right], \tag{1-19}$$

and $x = (EUD - D_{50})/mD_{50}$.

EUD is the equivalent uniform dose,[22] which is defined as the uniform organ dose that would produce the same effect as the given heterogeneous dose distribution, as specified by a differential dose-volume histogram (dDVH) defined by the points $\{D_j, v_j\}$. The dDVH describes the distribution of dose in an organ at risk or a target volume. Dose is binned, and each dose bin contains the fraction of the total volume that receives a dose within the range of the dose bin. The EUD or generalized mean dose GMD, which in this case is chosen to represent the EUD, is calculated from the dDVH as follows:[23-25]

$$EUD = GMD = \left(\sum_j v_j D_j^{1/a}\right)^a. \tag{1-20}$$

There are three parameters that determine the response of normal tissues to radiation according to the Lyman model: m, a and D_{50}. The dose-volume dependence of a tissue is determined by the parameter a, m is related to the slope of the dose-response curve, and D_{50} is the (whole-organ) dose that gives a 50% complication rate and thus determines the position of the response curve. The Lyman model is a population model – D_{50} is assumed to be normally distributed among a population of patients, with standard deviation mD_{50}.

1.4.2.2 The critical volume model[26-28]

The derivation of the critical volume NTCP model is based on biological considerations, unlike the Lyman model. Withers *et al.*[29] introduced the idea that organs are composed of a collection of functional subunits (FSUs) that carry out an organ's function. In this description, an organ is able to function as long as a certain number of its FSUs are viable. In other words, the organ has a number of redundant FSUs, all of which must be destroyed for its function to be compromised – this collection of FSUs is referred to as the *functional reserve*. Organs that require all of their FSUs to function (i.e., those that have a functional reserve of zero) are referred to as serial organs; an example is the spinal cord. Organs that have a functional reserve consisting of two or more FSUs are referred to as parallel.

The critical volume model expresses this description mathematically. It is derived based on the following assumptions:

- Normal tissue is composed of FSUs.
- The distribution of organ function among its FSUs is homogeneous. That is, each FSU has an identical role in carrying out organ function, regardless of its location within the organ.
- An FSU is destroyed if all cells within it are destroyed.
- The radiation response of each cell within an FSU is independent of the response of other cells.
- The radiation response of each FSU is statistically independent.
- A normal-tissue complication occurs if a certain number, M_{FSU}, out of a total of N_{FSU} FSUs are destroyed, or equivalently, if a certain fraction of the FSUs, μ_{cr}, is destroyed (where $\mu_{cr} = M_{FSU}/N_{FSU}$). The parameter μ_{cr} is called the relative critical volume. For parallel organs, M_{FSU} is some number greater than one. The critical volume model may also be applied to serial organs[28] with $M_{FSU} = 1$. This special case is referred to as the critical element model. The discussion in this section will be limited to the critical volume model.

1.4.2.2.1 Individual critical volume model

For an individual, the critical volume NTCP is given by the expression:

$$NTCP_{ind} = \Phi\left[\frac{\sqrt{N_{FSU}}(\bar{\mu}_d - \mu_{cr})}{\sigma_{\mu d}}\right], \tag{1-21}$$

where N_{FSU} is the total number of FSUs that comprise the organ, μ_{cr} is the critical relative volume, $\bar{\mu}_d$ is the relative mean damaged volume,

$$\bar{\mu}_d = \sum_j v_j P_{FSU}(D_j), \tag{1-22}$$

and $\sigma_{\mu d}$ is the standard deviation of $\bar{\mu}_d$,

$$\sigma_{\mu d} = \sqrt{\sum_j v_j P_{FSU}(D_j)(1 - P_{FSU}(D_j))}. \tag{1-23}$$

The points v_j and D_j represent a differential DVH. $P_{FSU}(D_j)$ is the probability of damaging a functional subunit when it is irradiated to dose D_j. Here, it is assumed that the damage to an FSU is described by a probit function parameterized using position and normalized slope parameters – D_{50}^{FSU} and γ_{50}^{FSU},

$$P_{FSU}(D_j) = \Phi\left(\sqrt{2\pi}\gamma_{50}^{FSU} \ln\frac{D_j}{D_{50}^{FSU}}\right). \tag{1-24}$$

1.4.2.2.2 Population critical volume model

Clinical data describe a normal tissue dose-response that is averaged over a population of individuals. A more appropriate model that is applicable to realistic dose-response data can be derived by averaging the individual critical volume model over a population (as was done for the population TCP model), and thus taking inter-patient variability into consideration. Further assumptions made to arrive at a population critical volume model are:

- The individual model can be approximated as a step function:

(1-25) $$NTCP_{ind} = \begin{cases} 0 & \bar{\mu}_d < \mu_{cr} \\ 1 & \bar{\mu}_d \geq \mu_{cr} \end{cases}.$$

- Inter-patient variability is dominated by variation in relative critical volume, μ_{cr}, and thus any other sources of heterogeneity can be neglected.
- Values for μ_{cr} are log-log normally distributed in the population (because this parameter is bounded by [0,1]) with $-\ln(-\ln \mu_{cr})$ having a standard deviation of $\sigma \approx -\sigma_{\mu cr} / \mu_{cr} \ln \mu_{cr}$.

The population critical volume model, under these assumptions, is:

(1-26) $$NTCP_{pop} = \Phi\left(\frac{-\ln(-\ln \bar{\mu}_d) + \ln(-\ln \mu_{cr})}{\sigma}\right),$$

where μ_{cr} in the above expression now represents the average relative critical volume for a population.

1.5 Incorporation of radiobiological models into the treatment planning process

An essential part of radiation therapy is treatment planning. This process begins with the delineation of target volume(s) along with organs at risk (OARs) based on patient images (e.g., a computed tomography (CT) dataset). Beam energies, sizes, and locations are then determined and a dose distribution calculated. Through this process, a treatment that should result in the delivery of the prescribed dose to the tumour is designed by ensuring coverage of the planning target volume (PTV). The PTV includes the visible tumour (gross tumour volume – GTV), any microscopic disease that may be present (clinical target volume – CTV), and a margin that takes into account patient movement, positioning errors, and mechanical and dosimetric uncertainties. Normally the treatment plan is designed so that the PTV will be irradiated as uniformly as possible; under-dosed areas may lead to failure to achieve tumour control. At the same time, the dose to the surrounding OARs is minimized.

Modern advances in imaging, computer technology, and radiation delivery techniques have allowed for the development of three-dimensional image-based conformal radiotherapy (3DCRT). This is accomplished through the use of 3-dimensional treatment planning systems and beam-shaping devices such as a multi-leaf collimator (MLC). The treatment plans for 3DCRT can be produced by means of forward or inverse planning.

In forward planning, the planner defines all beam parameters (directions, weights, blocks, wedges, etc.) and the field shapes (selected to conform to the PTV). Dose is then calculated and evaluated, and adjustments to the beam parameters are made until a satisfactory dose distribution is produced. With inverse planning, the number of beams and their directions are selected. The desired dose distribution is chosen by defining a number of constraints (for example, limits placed on the maximum OAR dose or the minimum PTV dose), and then a computer algorithm is used to optimize beam parameters to obtain a dose distribution that follows the specified constraints as closely as possible.[30] This is the treatment planning process that is most often used to produce plans for intensity-modulated radiation therapy (IMRT). With IMRT, highly conformal dose distributions are delivered by varying the intensity across each beam's field (the nonuniform beam intensity is accomplished by varying the MLC leaf positions during a treatment). The varying intensity of each IMRT beam is represented by different beamlet weights in a treatment planning system, and it is these weights that are optimized through the inverse planning process.

1.5.1 Inverse planning optimization by means of physical dose-volume constraints

Modern treatment planning systems handle inverse planning optimization by means of physical dose-volume constraints. Central to this process is the specification of an objective, or cost, function. This function represents the 'goodness' of a treatment plan, and its numerical value is calculated from a weighted average of the differences between the delivered and prescribed doses in every volume of interest delineated in the

treatment plan.[30] The objective function is minimized until the DVHs for the target and relevant normal tissues come as close as possible to satisfying each dose-volume constraint for the treatment. An example of the integral DVHs for an optimized head and neck plan (created using a sample dataset and the Pinnacle treatment planning system) is shown in Figure 1-4, along with the specified dose-volume constraints. The constraint

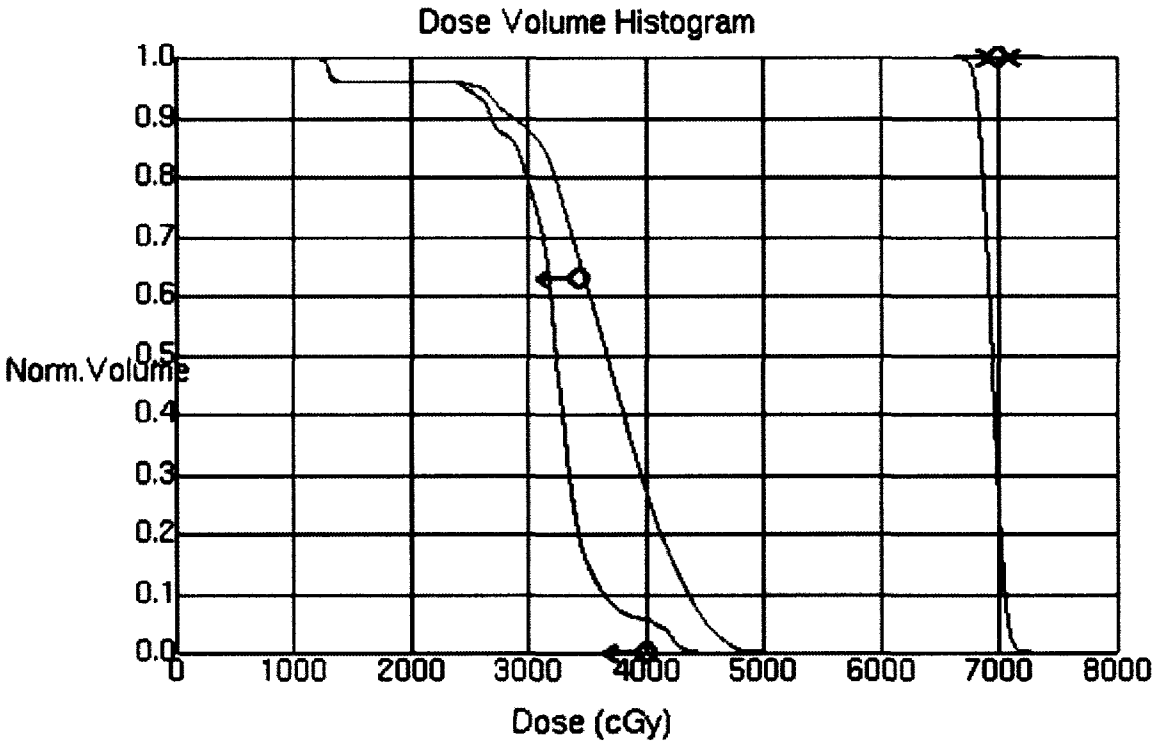

Figure 1-4: Optimized integral dose-volume histograms for the target (red), the spinal cord (blue) and a volume representing the cord plus a margin (green) of a head and neck treatment plan. Constraints for each volume are represented by circles of the same colours.

for the target (red) was to deliver the prescription dose of 70 Gy uniformly to 100% of the target volume. A constraint was also defined for the spinal cord (blue) – the maximum dose to this volume should not exceed 40 Gy. Finally, a constraint was defined for the volume representing the cord plus a margin (green) – no more than 63% of the organ is to receive a dose that exceeds 34.5 Gy.

Physical dose-volume constraint points for normal tissues are usually selected based on clinical experience.

1.5.2 Radiobiological optimization

The goal of treatment planning is to minimize NTCP while maximizing TCP, so the use of objective functions that are based directly on biological models promises a more direct approach than optimization by physical dose-volume constraints. A number of authors have published papers on inverse planning based on biological optimization.[31-41]

Pure biological optimization (maximizing TCP for the target and minimizing NTCP for the outlined critical structures) turns out to be problematic in practice. For typical treatment plans, not all critical structures are outlined; only those that are in close enough proximity to the treated site that they are at risk of receiving a significant dose. Ideal tumour control is achieved when the TCP function is equal to 1, and this maximum is only reached when the tumour dose is infinitely large [see Eq. (1-13), for example]. Thus, in an attempt to maximize TCP, the inverse planning algorithm delivers very large doses to the tumour, through the normal tissues that were not outlined for optimization purposes. This phenomenon is demonstrated in Fig. 3 of de Meerleer *et al.*,[36] and is discussed in Stavrev *et al.*[40]

Because of this difficulty associated with pure biological optimization, a hybrid physico-biological approach has been suggested.[35,36,40] For this type of inverse planning optimization, physical dose-volume constraints are set for the tumour, and NTCP is minimized for each of the critical structures. Another approach that has been explored is optimization based on EUD [Eq. (1-20)].[22,42-45] In this case, constraints are specified directly for the EUDs of the target and normal tissues. Use of the EUD, similarly to the use of NTCP, takes inhomogeneous dose distributions into account, eliminating the need for multiple dose-volume constraints for normal tissues.

Despite the advances made in the area of biological optimization, clinical inverse planning is currently still based on physical dose-volume constraints. Optimization based

on biological objectives is generally discouraged, based on the unknown predictive power of the available models.[46,47] The main contributor to this problem is the incomplete and scarce nature of the available clinical data.

1.5.3 Ranking of treatment plans and evaluating potential dose escalation benefits

The advent of 3DCRT has made it possible to increase the prescribed target dose for some tumour sites, and this has led to a number of clinical trials investigating the potential benefits of dose escalation (e.g. prostate[48-52] and lung[53,54]).

TCP and NTCP models can theoretically be used for radiation therapy (RT) plan ranking. This follows from the probabilistic nature of cell kill by radiation and also from the fact that we are dealing with a population of patients – hence only the probability of a given response could be estimated. Currently, worldwide, the process of plan ranking relies more on the experience of radiation oncologists than on radiobiological criteria expressed in mathematical forms. Unfortunately, TCP and NTCP models currently have limited use in treatment plan ranking, although a number of software tools have been developed for this purpose.[55-58] The usual reasoning of those who are opposed to the application of TCP/NTCP models in the evaluation and ranking of clinical treatment plans is that the actual predictive power of these models is unknown, due to the scarcity and relatively poor quality of the available clinical dose-response data.

On the other hand, models based on the LQ theory for cellular response and the notion that TCP is equal to the probability of zero clonogen survivors (introduced by Munro and Gilbert[12]) have been shown[2,13,59] to describe dose-response data well. For the purposes of plan ranking, as shown by Stanescu *et al.*,[60] there is no need to know the exact parameter values. If, for each parameter value, we have TCP(plan1)>TCP(plan2), then the second plan is inferior to first one. This notion could be easily generalized for NTCP and for a combined TCP/NTCP plan ranking cost function. Nowadays, we have sufficient information indicating that the TCP/NTCP models at our disposal adequately

describe the existing data. Thus, only a general knowledge of TCP/NTCP models is necessary for the purpose of plan ranking.

1.6 Estimating the α/β ratio from clinical dose-response data

While TCP curves with fitted parameters may be useful for treatment plan ranking and evaluating dose escalation benefits, it is generally not possible to obtain estimates for radiobiological parameters from fits of either the individual or the population TCP model to clinical dose-response data. If the individual model is fit to a clinical (i.e., a population-averaged) dose-response dataset, the estimates for the parameters α' and $\ln N_0$ turn out to be unrealistically low.[61,62] For the population TCP model, it is generally not possible to obtain unique radiobiological parameter estimates, due to the fact that many different combinations of parameters fit the data equally well.

However, it has been postulated that the same difficulties involved in determining individual radiobiological parameters may not apply to parameter ratios, such as α/β. As previously mentioned, the α/β ratio is a clinically-important quantity, as it determines the effect of dose per fraction on the tumour and normal tissue responses. This quantity has been estimated for cell lines from a variety of tumours and normal tissues using linear quadratic theory.[11] Yet, it is only relatively recently that attempts have been made to estimate the α/β ratio for tumours by means of TCP models and clinical dose-response data.

One of the most influential papers along these lines was published by Brenner and Hall[63] in 1999. In this work, the authors noted that the cell proliferation rate for prostate cancer is quite slow in comparison to other cancers. Because cell proliferation rate correlates with the α/β ratio, the authors proposed that α/β for prostate cancer is most likely low, as is the case for late-responding normal tissues. Thus, prostate cancer should respond to fractionation in a similar way as do late-responding normal tissues, which would mean that the differential response of tumour and normal tissue would disappear. In this case, then, the sparing of normal tissues by reducing dose per fraction becomes less important, assuming the total dose delivered is adjusted to take into account fraction

size. In principle, a hypofractionated treatment (i.e., a larger dose per fraction with a reduced total delivered dose) for this site should be equally effective as the standard treatment involving 2 Gy per fraction. Such a treatment regime would be more efficient, and beneficial to the patient, as fewer hospital visits would be required.

As a supporting argument to the hypothesis of a lower prostate α/β ratio, Brenner and Hall estimated this quantity by means of the individual Poisson-based TCP model. To do so, they fit two different dose-response datasets for prostate cancer, each with different fractionation regimes. One dataset was for an external-beam radiation therapy (EBRT) dose escalation trial, with the standard dose per fraction of 2 Gy.[64] The other dataset corresponded to brachytherapy treatment by permanent implantation of ^{125}I seeds.[65] Since the dose rate for the latter treatment is very low, one may assume that all sub-lethal lesions are repaired, and that the dose-protraction factor in Eq. (1-2) is equal to zero. It can also be assumed for this particular cancer that repopulation is negligible. Thus, if the individual TCP model [Eq. (1-12)] is fit to the brachytherapy dataset, estimates for α and $\ln N_0$ may be obtained. If the same model is fit to the EBRT dataset, the parameters $\alpha' = \alpha + \beta d$ and $\ln N_0$ may be estimated. The α/β ratio may then be estimated from the formula:[66]

$$\frac{\alpha}{\beta} = \frac{\alpha d}{\alpha' - \alpha}. \tag{1-27}$$

From the estimates for α and α', Brenner and Hall deduced that the α/β ratio for prostate cancer is 1.5 Gy [0.8, 2.2].

The Brenner and Hall paper initiated a significant amount of literature activity related to the determination of α/β for prostate cancer. Fowler[67] conducted a similar analysis as did Brenner and Hall, using a more extensive dataset, and likewise arrived at a low value for α/β. Others[68-73] also took an interest in estimating α/β by means of TCP models and clinical data, and the collective evidence of a low α/β ratio has led to the initiation of a number of clinical hypofractionation trials for this treatment site,[74-78] including one at our own institution.

Estimating the α/β ratio by means of the individual TCP model requires the assumption that parameter ratios are insensitive to the presence of inter-tumour heterogeneity. Very few investigations on the influence of inter-tumour heterogeneity on

parameter ratio estimates have been carried out. Dubray and Thames[79] conducted numerical experiments in which the effect of heterogeneity in clonogen number on parameter ratio estimates was studied, and found to have very little influence on the estimated parameter ratio value. Less detailed experiments were conducted for other forms of inter-tumour heterogeneity. Carlone *et al.*[66] investigated the difference between prostate α/β estimates obtained using a population and an individual TCP model. To do so, they utilized clinical dose-response data for two EBRT dose escalation trials[64,80] and one ^{125}I dose-response dataset.[65] It was found that α/β estimates from the population TCP model had much larger confidence intervals than the estimates from the individual TCP model. The clinical dose-response datasets were of too poor a quality to determine whether or not a difference in the best-fit individual and population α/β estimates exists – the 95% confidence interval from the population α/β estimates overlapped with those of the individual estimates.

1.7 Thesis objectives

Although limitations to the application of radiobiological theory to clinically-relevant problems exist, clinical radiobiology is an important field and has the potential to lead to advances in radiation therapy. This thesis investigates two different applications of TCP/NTCP models to clinically-relevant problems. The first involves the incorporation of models into the treatment planning process, and the second involves the estimation of clinically-relevant parameter ratios from TCP models.

1.7.1 Incorporation of NTCP models and parameter sets into modern treatment planning systems

As previously mentioned, current treatment planning systems do not utilize biological optimization for inverse planning, due to the lack of a sufficient amount of clinical dose-response data to describe NTCP. However, in some institutions, physical

dose-volume constraints are chosen based on existing dose-response data. That is, the 'raw' dose-response data points are applied directly as physical constraints for normal tissues. This approach is problematic, and will always lead to higher NTCPs than desired, as will be explained in further chapters.

The first main objective of this thesis is to develop a method that allows one to calculate physical dose-volume constraint points for normal tissues based on existing NTCP models and parameter sets. These constraint points have radiobiological significance, and may be used by the currently-available treatment planning systems for inverse planning optimization. It is also shown that, while the calculated constraint points are capable of producing dose distributions that lead to sufficiently low NTCP, the application of physical constraint points for inverse planning also excludes a number of DVHs that lead to viable NTCP values.

1.7.2 Analytical investigation of the effects of inter-tumour heterogeneity on parameter ratio estimates

Very few studies have been undertaken thus far to determine whether the α/β ratio estimated from an individual TCP model is different from that estimated from a population model, yet the majority of works in which this ratio is estimated by means of TCP models and clinical dose-response data involve the assumption that inter-patient heterogeneity does not influence parameter ratios.

The second main objective of this thesis is to determine whether this assumption is, in fact, reasonable. Specifically, the difference between the α/β estimate that would be obtained from the individual TCP model and from the population TCP model will be analytically investigated. Two cases will be considered – the case where heterogeneity in clonogen number is the dominant form within a clinical dose-response dataset, and the case where heterogeneity in radiosensitivity dominates. All analytic results will be tested through numerical simulations involving pseudo-data.

1.8 Outline

Chapter 2 outlines a method for calculating physical dose-volume constraints for the purpose of inverse planning optimization, based on existing NTCP models and parameter sets. This method is called reverse mapping of NTCP into DVH space. Constraint points are calculated for several organs, using two different NTCP models and parameter sets based on the same dose-response data. The ability of physical dose-volume constraint points to limit NTCP in OARs is also investigated theoretically, by means of the reverse mapping method. This chapter was published[81] in *Medical Physics* in 2006. In Chapter 3, the proper theory of DVH generation is presented. Probability distributions are derived that describe the density of random DVH curves passing through a given point in DVH space, and these distributions are used to develop a random DVH generator. The DVH generator is then compared with two other, simpler ones. A version of Chapter 3 was published[82] in *Medical Physics* in 2006. In Chapter 2, a curve in DVH space was defined that we refer to as the iso-NTCP envelope. It was numerically observed to have the property that any DVH which is tangential to or crosses this curve will have an NTCP greater than or equal to the one used to construct the curve. Chapter 4 presents the theoretical proof of this property, for three different NTCP models. A version of this chapter has been published[83] in *Radiology & Oncology* in 2007 and previously[84] in *Medical Physics* as an AAPM (American Association of Physicists in Medicine) abstract.

In Chapter 5, the functional forms of the individual and population-averaged TCP models are compared. It is determined that each model is functionally similar – if they are both fit to the same clinical dose-response dataset, nearly identical estimates for the geometric parameters γ_{50} and D_{50} would be obtained. The conceptual inadequacy of applying the individual model to a population-averaged dataset is discussed. Also, the possibility of applying a modified version of the individual TCP model to a population of heterogeneously-irradiated tumours is discussed, for the purposes of estimating geometric parameters. A version of this chapter was published[85] in *Radiology & Oncology* in 2007, and has previously[86] been published in *Medical Physics* as an AAPM abstract.

In Chapter 6, the functional similarity between the individual and population-averaged TCP models is used to derive analytic relationships between the α/β ratio estimates that would be obtained from both models if they are fit to the same clinical dataset. It is shown that, when heterogeneity in radiosensitivity is the dominant form among a patient population, the individual and population TCP models will lead to different α/β estimates. A version of this chapter has been accepted for publication by the *International Journal of Radiation Oncology Biology Physics*, and is currently in press.[87]

In Chapter 7, numerical simulations with pseudo-data are conducted to estimate the statistics that would be required of a 'typical' clinical dose-response dataset if it were to be used for estimating the parameters D_{50} and γ_{50} from the population TCP model. Specifically, the number of patients for each dose point in a dose escalation trial that is required to lead to reasonable 95% confidence intervals for the fitted parameters is estimated.

In Chapter 8, conclusions are presented, and potential areas of future work are discussed.

1.9 References

1. J. J. Fischer and J. E. Moulder, "The steepness of the dose-response curve in radiation therapy. Theoretical considerations and experimental results," Radiology **117**, 179-184 (1975).

2. N. Stavreva, P. Stavrev, B. Warkentin, and B. G. Fallone, "Investigating the effect of cell repopulation on the tumor response to fractionated external radiotherapy," Med Phys **30**, 735-742 (2003).

3. M. Zaider and G. N. Minerbo, "Tumour control probability: a formulation applicable to any temporal protocol of dose delivery," Phys Med Biol **45**, 279-293 (2000).

4. K. H. Chadwick and H. P. Leenhouts, "A molecular theory of cell survival," Phys Med Biol **18**, 78-87 (1973).

5. M. N. Cornforth and J. S. Bedford, "A quantitative comparison of potentially lethal damage repair and the rejoining of interphase chromosome breaks in low passage normal human fibroblasts," Radiat Res **111**, 385-405 (1987).

6. J. S. Bedford and J. B. Mitchell, "Dose-rate effects in synchronous mammalian cells in culture," Radiat Res **54**, 316-327 (1973).

7. D. E. Lea, "Actions of Radiations on Living Cells," University Press, Cambridge (1946).

8. A. M. Kellerer and H. H. Rossi, "The theory of dual radiation action," Current Topics in Radiation Research Quarterly **8**, 85-158 (1972).

9. H. D. Thames, Jr., L. J. Peters, H. R. Withers, and G. H. Fletcher, "Accelerated fractionation vs hyperfractionation: rationales for several treatments per day," Int J Radiat Oncol Biol Phys **9**, 127-138 (1983).

10. H. D. Thames, Jr., H. R. Withers, L. J. Peters, and G. H. Fletcher, "Changes in early and late radiation responses with altered dose fractionation: implications for dose-survival relationships," Int J Radiat Oncol Biol Phys **8**, 219-226 (1982).

11. J. F. Fowler, "Dose response curves for organ function or cell survival," Br J Radiol **56**, 497-500 (1983).

12. T. R. Munro and C. W. Gilbert, "The relation between tumour lethal doses and the radiosensitivity of tumour cells," Br J Radiol **34**, 246-251 (1961).

13. P. Stavrev, M. Weldon, B. Warkentin, N. Stavreva, and B. G. Fallone, "Radiation damage, repopulation and cell recovery analysis of in vitro tumour cell megacolony culture data using a non-Poissonian cell repopulation TCP model," Phys Med Biol **50**, 3053-3061 (2005).

14. S. L. Tucker and E. L. Travis, "Comments on a time-dependent version of the linear-quadratic model," Radiother Oncol **18**, 155-163 (1990).

15. L. G. Hanin, M. Zaider, and A. Y. Yakovlev, "Distribution of the number of clonogens surviving fractionated radiotherapy: a long-standing problem revisited," Int J Radiat Biol **77**, 205-213 (2001).

16. W. S. Kendal, "A closed-form description of tumour control with fractionated radiotherapy and repopulation," Int J Radiat Biol **73**, 207-210 (1998).

17. A. Yakovlev, "Comments on the distribution of clonogens in irradiated tumors," Radiat Res **134**, 117-122 (1993).

18. M. Zaider, M. J. Zelefsky, L. G. Hanin, A. D. Tsodikov, A. Y. Yakovlev, and S. A. Leibel, "A survival model for fractionated radiotherapy with an application to prostate cancer," Phys Med Biol **46**, 2745-2758 (2001).

19. L. G. Hanin, "A stochastic model of tumor response to fractionated radiation: limit theorems and rate of convergence," Math Biosci **191**, 1-17 (2004).

20. M. Carlone, B. Warkentin, P. Stavrev, and B. G. Fallone, "Fundamental form of the population TCP model in the limit of large heterogeneity," Med. Phys. **33**, 1634-1642 (2006).

21. J. T. Lyman, "Complication probability as assessed from dose-volume histograms," Radiat Res Suppl **8**, S13-19 (1985).

22. A. Niemierko, "Reporting and analyzing dose distributions: a concept of equivalent uniform dose," Med Phys **24**, 103-110. (1997).

23. A. Niemierko, "A generalized concept of Equivalent Uniform Dose", presented at the 41th AAPM Annual Meeting, Nashville, (1999).

24. A. Niemierko and M. Goitein, "Calculation of normal tissue complication probability and dose-volume histogram reduction schemes for tissues with a critical element architecture," Radiother Oncol **20**, 166-176 (1991).

25. P. Stavrev, D. Hristov, and E. Sham, "IMRT Inverse Treatment Planning Optimization Based on Physical Constraints and Biological Objectives", presented at the 47th Annual General Meeting of the Canadian Organization of Medical Physicists (COMP), Kelowna, BC, Canada, (2001).

26. A. Jackson, G. J. Kutcher, and E. D. Yorke, "Probability of radiation-induced complications for normal tissues with parallel architecture subject to non-uniform irradiation," Med Phys **20**, 613-625 (1993).

27. A. Niemierko and M. Goitein, "Modeling of normal tissue response to radiation: the critical volume model," Int J Radiat Oncol Biol Phys **25**, 135-145 (1993).

28. P. Stavrev, N. Stavreva, A. Niemierko, and M. Goitein, "Generalization of a model of tissue response to radiation based on the idea of functional subunits and binomial statistics," Phys Med Biol **46**, 1501-1518 (2001).

29. H. R. Withers, J. M. Taylor, and B. Maciejewski, "Treatment volume and tissue tolerance," Int J Radiat Oncol Biol Phys **14**, 751-759 (1988).

30. Memorial Sloan-Kettering Cancer Center, "*A Practical Guide to Intensity-Modulated Radiation Therapy*", (Medical Physics Publishing, Madison, Wisconsin, 2003).

31. A. Brahme, "Optimized radiation therapy based on radiobiological objectives," Semin Radiat Oncol **9**, 35-47. (1999).

32. A. Brahme, "Development of radiation therapy optimization," Acta Oncol **39**, 579-595 (2000).

33. A. Brahme, "Individualizing cancer treatment: biological optimization models in treatment planning and delivery," Int J Radiat Oncol Biol Phys **49**, 327-337. (2001).

34. W. R. De Gersem, S. Derycke, C. O. Colle, C. De Wagter, and W. J. De Neve, "Inhomogeneous target-dose distributions: a dimension more for optimization?," Int J Radiat Oncol Biol Phys **44**, 461-468 (1999).

35. W. R. De Gersem, S. Derycke, C. De Wagter, and W. C. De Neve, "Optimization of beam weights in conformal radiotherapy planning of stage III non-small cell lung cancer: effects on therapeutic ratio," Int J Radiat Oncol Biol Phys **47**, 255-260 (2000).

36. G. O. De Meerleer, L. A. Vakaet, W. R. De Gersem, C. De Wagter, B. De Naeyer, and W. De Neve, "Radiotherapy of prostate cancer with or without intensity modulated beams: a planning comparison," Int J Radiat Oncol Biol Phys **47**, 639-648 (2000).

37. P. Kallman, A. Agren, and A. Brahme, "Tumour and normal tissue responses to fractionated non-uniform dose delivery," Int J Radiat Biol **62**, 249-262 (1992).

38. J. Lof, B. K. Lind, and A. Brahme, "An adaptive control algorithm for optimization of intensity modulated radiotherapy considering uncertainties in beam profiles, patient set-up and internal organ motion," Phys Med Biol **43**, 1605-1628. (1998).

39. A. Niemierko, "Random search algorithm (RONSC) for optimization of radiation therapy with both physical and biological end points and constraints," Int J Radiat Oncol Biol Phys **23**, 89-98 (1992).

40. P. Stavrev, D. Hristov, B. Warkentin, E. Sham, N. Stavreva, and B. G. Fallone, "Inverse treatment planning by physically constrained minimization of a biological objective function," Med Phys **30**, 2948-2958 (2003).

41. X. H. Wang, R. Mohan, A. Jackson, S. A. Leibel, Z. Fuks, and C. C. Ling, "Optimization of intensity-modulated 3D conformal treatment plans based on biological indices," Radiother Oncol **37**, 140-152. (1995).

42. O. Chapet, E. Thomas, M. L. Kessler, B. A. Fraass, and R. K. Ten Haken, "Esophagus sparing with IMRT in lung tumor irradiation: an EUD-based optimization technique," Int J Radiat Oncol Biol Phys **63**, 179-187 (2005).

43. A. Olafsson, R. Jeraj, and S. J. Wright, "Optimization of intensity-modulated radiation therapy with biological objectives," Phys Med Biol **50**, 5357-5379 (2005).

44. Q. Wu, D. Djajaputra, Y. Wu, J. Zhou, H. H. Liu, and R. Mohan, "Intensity-modulated radiotherapy optimization with gEUD-guided dose-volume objectives," Phys Med Biol **48**, 279-291 (2003).

45. X. Zhang, H. Liu, X. Wang, L. Dong, Q. Wu, and R. Mohan, "Speed and convergence properties of gradient algorithms for optimization of IMRT," Med Phys **31**, 1141-1152 (2004).

46. V. Moiseenko, J. Battista, and J. Van Dyk, "Normal tissue complication probabilities: dependence on choice of biological model and dose-volume histogram reduction scheme," Int J Radiat Oncol Biol Phys **46**, 983-993 (2000).

47. M. Zaider and H. I. Amols, "Practical considerations in using calculated healthy-tissue complication probabilities for treatment-plan optimization," Int J Radiat Oncol Biol Phys **44**, 439-447 (1999).

48. D. Brabbins, A. Martinez, D. Yan, D. Lockman, M. Wallace, G. Gustafson, P. Chen, F. Vicini, and J. Wong, "A dose-escalation trial with the adaptive radiotherapy process as a delivery system in localized prostate cancer: analysis of chronic toxicity," Int J Radiat Oncol Biol Phys **61**, 400-408 (2005).

49. R. Cheung, S. L. Tucker, A. K. Lee, R. de Crevoisier, L. Dong, A. Kamat, L. Pisters, and D. Kuban, "Dose-response characteristics of low- and intermediate-risk prostate cancer treated with external beam radiotherapy," Int J Radiat Oncol Biol Phys **61**, 993-1002 (2005).

50. R. Jacob, A. L. Hanlon, E. M. Horwitz, B. Movsas, R. G. Uzzo, and A. Pollack, "Role of prostate dose escalation in patients with greater than 15% risk of pelvic lymph node involvement," Int J Radiat Oncol Biol Phys **61**, 695-701 (2005).

51. C. Vargas, D. Yan, L. L. Kestin, D. Krauss, D. M. Lockman, D. S. Brabbins, and A. A. Martinez, "Phase II dose escalation study of image-guided adaptive radiotherapy for prostate cancer: use of dose-volume constraints to achieve rectal isotoxicity," Int J Radiat Oncol Biol Phys **63**, 141-149 (2005).

52. M. J. Zelefsky, D. A. Kuban, L. B. Levy, L. Potters, D. C. Beyer, J. C. Blasko, B. J. Moran, J. P. Ciezki, A. L. Zietman, T. M. Pisansky, M. Elshaikh, and E. M. Horwitz, "Multi-institutional analysis of long-term outcome for stages T1-T2

prostate cancer treated with permanent seed implantation," Int J Radiat Oncol Biol Phys **67**, 327-333 (2007).

53. J. S. Belderbos, W. D. Heemsbergen, K. De Jaeger, P. Baas, and J. V. Lebesque, "Final results of a Phase I/II dose escalation trial in non-small-cell lung cancer using three-dimensional conformal radiotherapy," Int J Radiat Oncol Biol Phys **66**, 126-134 (2006).

54. J. Bradley, M. V. Graham, K. Winter, J. A. Purdy, R. Komaki, W. H. Roa, J. K. Ryu, W. Bosch, and B. Emami, "Toxicity and outcome results of RTOG 9311: a phase I-II dose-escalation study using three-dimensional conformal radiotherapy in patients with inoperable non-small-cell lung carcinoma," Int J Radiat Oncol Biol Phys **61**, 318-328 (2005).

55. I. El Naqa, G. Suneja, P. E. Lindsay, A. J. Hope, J. R. Alaly, M. Vicic, J. D. Bradley, A. Apte, and J. O. Deasy, "Dose response explorer: an integrated open-source tool for exploring and modelling radiotherapy dose-volume outcome relationships," Phys Med Biol **51**, 5719-5735 (2006).

56. O. Gayou, D. S. Parda, and M. Miften, "EUCLID: an outcome analysis tool for high-dimensional clinical studies," Phys Med Biol **52**, 1705-1719 (2007).

57. B. Sanchez-Nieto and A. E. Nahum, "BIOPLAN: software for the biological evaluation of radiotherapy treatment plans," Med Dosim **25**, 71-76 (2000).

58. B. Warkentin, P. Stavrev, N. Stavreva, C. Field, and B. G. Fallone, "A TCP-NTCP estimation module using DVHs and known radiobiological models and parameter sets," J Appl Clin Med Phys **5**, 50-63 (2004).

59. N. A. Stavreva, B. Warkentin, P. V. Stavrev, and B. G. Fallone, "Investigating the effect of clonogen resensitization on the tumor response to fractionated external radiotherapy," Med Phys **32**, 720-725 (2005).

60. T. Stanescu, J. Hans-Sonke, P. Stavrev, and B. G. Fallone, "3T MR-based treatment planning for radiotherapy of brain lesions," Radiol Oncol **40**, 125-132 (2006).

61. D. J. Brenner, "Dose, volume, and tumor-control predictions in radiotherapy," Int J Radiat Oncol Biol Phys **26**, 171-179 (1993).

62. A. Dasu, I. Toma-Dasu, and J. F. Fowler, "Should single or distributed parameters be used to explain the steepness of tumour control probability curves?," Phys Med Biol **48**, 387-397 (2003).

63. D. J. Brenner and E. J. Hall, "Fractionation and protraction for radiotherapy of prostate carcinoma," Int J Radiat Oncol Biol Phys **43**, 1095-1101 (1999).

64. G. E. Hanks, T. E. Schultheiss, A. L. Hanlon, M. Hunt, W. R. Lee, B. E. Epstein, and L. R. Coia, "Optimization of conformal radiation treatment of prostate cancer: report of a dose escalation study," Int J Radiat Oncol Biol Phys **37**, 543-550 (1997).

65. R. G. Stock, N. N. Stone, A. Tabert, C. Lannuzzi, and J. K. DeWyngaert, "A dose-response study for I-125 prostate implants," Int J Radiat Oncol Biol Phys **41**, 101-108 (1998).

66. M. Carlone, D. Wilkins, B. Nyiri, and P. Raaphorst, "Comparison of alpha/beta estimates from homogeneous (individual) and heterogeneous (population) tumor control models for early stage prostate cancer," Med Phys **30**, 2832-2848 (2003).

67. J. Fowler, R. Chappell, and M. Ritter, "Is alpha/beta for prostate tumors really low?," Int J Radiat Oncol Biol Phys **50**, 1021-1031 (2001).

68. H. B. Kal and M. P. Van Gellekom, "How low is the alpha/beta ratio for prostate cancer?," Int J Radiat Oncol Biol Phys **57**, 1116-1121 (2003).

69. C. R. King and J. F. Fowler, "A simple analytic derivation suggests that prostate cancer alpha/beta ratio is low," Int J Radiat Oncol Biol Phys **51**, 213-214 (2001).

70. C. R. King and C. S. Mayo, "Is the prostrate alpha/beta ratio of 1.5 from Brenner & Hall a modeling artifact," Int J Radiat Oncol Biol Phys **47**, 536-539 (2000).

71. A. E. Nahum, B. Movsas, E. M. Horwitz, C. C. Stobbe, and J. D. Chapman, "Incorporating clinical measurements of hypoxia into tumor local control modeling of prostate cancer: implications for the alpha/beta ratio," Int J Radiat Oncol Biol Phys **57**, 391-401 (2003).

72. J. Z. Wang, M. Guerrero, and X. A. Li, "How low is the alpha/beta ratio for prostate cancer?," Int J Radiat Oncol Biol Phys **55**, 194-203 (2003).

73. J. Z. Wang, X. A. Li, C. X. Yu, and S. J. DiBiase, "The low alpha/beta ratio for prostate cancer: what does the clinical outcome of HDR brachytherapy tell us?," Int J Radiat Oncol Biol Phys **57**, 1101-1108 (2003).

74. G. S. Higgins, D. B. McLaren, G. R. Kerr, T. Elliott, and G. C. Howard, "Outcome analysis of 300 prostate cancer patients treated with neoadjuvant androgen deprivation and hypofractionated radiotherapy," Int J Radiat Oncol Biol Phys **65**, 982-989 (2006).

75. P. A. Kupelian, V. V. Thakkar, D. Khuntia, C. A. Reddy, E. A. Klein, and A. Mahadevan, "Hypofractionated intensity-modulated radiotherapy (70 gy at 2.5 Gy

per fraction) for localized prostate cancer: long-term outcomes," Int J Radiat Oncol Biol Phys **63**, 1463-1468 (2005).

76. J. E. Livsey, R. A. Cowan, J. P. Wylie, R. Swindell, G. Read, V. S. Khoo, and J. P. Logue, "Hypofractionated conformal radiotherapy in carcinoma of the prostate: five-year outcome analysis," Int J Radiat Oncol Biol Phys **57**, 1254-1259 (2003).

77. A. Pollack, A. L. Hanlon, E. M. Horwitz, S. J. Feigenberg, A. A. Konski, B. Movsas, R. E. Greenberg, R. G. Uzzo, C. M. Ma, S. W. McNeeley, M. K. Buyyounouski, and R. A. Price, Jr., "Dosimetry and preliminary acute toxicity in the first 100 men treated for prostate cancer on a randomized hypofractionation dose escalation trial," Int J Radiat Oncol Biol Phys **64**, 518-526 (2006).

78. E. E. Yeoh, R. H. Holloway, R. J. Fraser, R. J. Botten, A. C. Di Matteo, J. Butters, S. Weerasinghe, and P. Abeysinghe, "Hypofractionated versus conventionally fractionated radiation therapy for prostate carcinoma: Updated results of a phase III randomized trial," Int J Radiat Oncol Biol Phys **66**, 1072-1083 (2006).

79. B. M. Dubray and H. D. Thames, "The clinical significance of ratios of radiobiological parameters," Int J Radiat Oncol Biol Phys **35**, 1099-1111 (1996).

80. W. H. Pinover, A. L. Hanlon, E. M. Horwitz, and G. E. Hanks, "Defining the appropriate radiation dose for pretreatment PSA < or = 10 ng/mL prostate cancer," Int J Radiat Oncol Biol Phys **47**, 649-654 (2000).

81. C. Schinkel, P. Stavrev, N. Stavreva, and B. G. Fallone, "A theoretical approach to the problem of dose-volume constraint estimation and their impact on the dose-volume histogram selection," Med. Phys. **33**, 3444-3459 (2006).

82. K. Markov, C. Schinkel, P. Stavrev, N. Stavreva, M. Weldon, and B. G. Fallone, "Reverse mapping of normal tissue complication probabilities onto dose volume histogram space: the problem of randomness of the dose volume histogram sampling," Med. Phys. **33**, 3435-3443 (2006).

83. P. Stavrev, C. Schinkel, N. Stavreva, K. Markov, and B. G. Fallone, "Analytical investigation of properties of the iso-NTCP envelope," Radiol Oncol **41**, 41-47 (2007).

84. P. Stavrev, C. Schinkel, N. Stavreva, K. Markov, and B. G. Fallone, "SU-FF-T-370: Properties of the Iso-NTCP Envelope (AAPM 48th Annual Meeting, Orlando, FL, July 30 - Aug 3)," Med Phys **33**, 2131 (2006).

85. C. Schinkel, N. Stavreva, P. Stavrev, M. Carlone, and B. G. Fallone, "Functional form comparison between the population and the individual Poisson based TCP models," Radiol Oncol **41**, 90-98 (2007).

86. C. Schinkel, N. Stavreva, M. Carlone, P. Stavrev, and B. G. Fallone, "On the equivalence of the population and individual TCP models (AAPM 48th Annual Meeting, Orlando, FL, July 30 - Aug 3)," Med Phys **33**, 2125 (2006).

87. C. Schinkel, M. Carlone, B. Warkentin, and B. G. Fallone, "An analytic investigation into the effect of population heterogeneity on parameter ratio estimates," Int J Radiat Oncol Biol Phys **in press** (2007).

Chapter 2 A theoretical approach to the estimation of dose-volume constraints and their impact on dose-volume histogram selection

A version of this chapter was published as:

C. Schinkel, P. Stavrev, N. Stavreva, and B. G. Fallone, "A theoretical approach to the problem of dose-volume constraint estimation and their impact on the dose-volume histogram selection," Med. Phys. **33**, 3444 – 3459 (2006)

2.1 Introduction

The most advanced treatment planning systems to date make use of inverse planning software in order to produce plans that will deliver a high dose to the target while minimizing dose, and thus normal tissue complication probability (NTCP), to the surrounding structures. This is accomplished through the specification of physical dose-volume objectives and constraints, and there are often multiple constraints selected for a given organ at risk. These constraints are often selected based on clinical experience. However, in many institutions, they are chosen based on the dose-response values published by Emami *et al.*[1] This work is the first and remains the largest compilation of dose-response data to date. It contains estimates of doses that lead to 5 and 50% complication probability for partial volume irradiation of a variety of organs. Tolerance doses are given for relative irradiated volumes of ⅓, ⅔, and 1. It is assumed that, in each case, a homogeneous dose is delivered to the given relative volume while the rest of the organ receives no dose. Thus, any dose-response data from Emami *et al.* are equivalent to single-step dose-volume histograms (DVHs). During the majority of treatments, the

organs at risk are irradiated heterogeneously as opposed to homogeneously. Therefore, using any of the Emami 5% complication rate dose-volume points, or combinations of them, as constraints would likely fail to produce a treatment plan that would yield the desired NTCP of 5% or less.

To avoid the difficulties that could result from using raw clinical dose-response data (such as the Emami *et al.* estimates) directly as constraints, one might consider using biological, rather than physical, inverse planning optimization.[2-6] That is, specify a constraint NTCP value for each organ at risk instead of a physical dose-volume point. Then the dose to the organ would be limited based on NTCP models and parameters reflecting clinical dose-volume characteristics of different tissues. Inverse planning can, in principle, use NTCP constraints directly. For example, an intensity modulated radiation therapy (IMRT) plan can vary the beamlet weights to satisfy both the physical and radiobiological constraints simultaneously.[2-4,6] Although biological optimization is not a new concept,[7,8] it is not currently available as an option for inverse planning on commercially available treatment planning systems. The main reason why biological constraints are not routinely used for inverse planning is the lack of a sufficient amount of clinical dose-response data on which to base NTCP model parameter estimates.[9-11] Misinterpretation of model formalism and assumptions also contributes to this problem. Due to the incompleteness of the clinical dose-response data available currently, biological optimization for inverse planning is generally discouraged.[10,11] This is a puzzling fact, considering that almost three decades have passed since the introduction of the concept. The work of Emami *et al.* unfortunately did not provoke an appropriate data gathering "rush," which would have led to the creation of sufficiently large data sets. Different researchers have started analyzing small data sets of real clinical data, and alternative sets of parameter estimates for different NTCP models have been reported.[12-27] Some of the reports, though, use data obtained under different conditions (tumour radio-sensitizing,[13-15] surgical or non-surgical intrusion,[28] dose-volume versus dose-wall histograms,[29-31] etc.). Therefore, care should be taken that the application of these parameter estimates be consistent with the conditions under which they were derived.[32]

The purpose of applying physical dose-volume constraints is to produce a plan that results in a low complication probability, and the problem remains that the Emami

dose-volume points are sometimes used as constraint points. In this chapter, we present a method that enables the calculation of physical dose-volume constraints that are based on NTCP models for the purpose of inverse planning optimization. Specifically, we apply a Monte Carlo method of reverse NTCP mapping[33] to calculate dose-volume constraints for 16 organs for which parameter value information is available.[34,35] The method makes use of the random DVH generator introduced in Chapter 3 and our companion work.[36] The NTCP for each randomly generated DVH is estimated by application of the Lyman[32,37] and the critical volume NTCP models.[38-42] The investigation of the impact of these two well-known NTCP models on dose-volume constraint estimation is the second purpose of this study. Dose-volume constraint points are calculated by interpolating from the average of all DVHs with NTCP = 5 ± 0.5%. It is shown that these points have the potential to increase the probability that the inversely planned treatment will lead to an acceptably low NTCP for the organs at risk.

2.2 Background

We give some definitions and a short discussion of the models and parameters necessary for the understanding of our present study.

2.2.1 Some definitions

Integral dose-volume histogram: defines the volume V_{int}, which is irradiated to at least a dose D:

$$V_{\text{int}}(D) = \int_{\textit{Structure Of Interest}} \Theta[D(\vec{r}) - D]\, d^3\vec{r}\,, \tag{2-1}$$

where Θ is the Heaviside step function and $D(\vec{r})$ is the dose distribution in the structure of interest.[43] From the definition of an integral DVH it is clear that any monotonically decreasing function in the region [0,1] × [0,1] could represent a normalized integral DVH.

Iso-NTCP envelope: The curve $v(D)$ defined by the relationship NTCP(D, v) = α, where D is the dose of partial homogeneous irradiation of the relative volume v will be called an α-iso-NTCP envelope.

The α-iso-NTCP envelope has a very interesting property: If a DVH is tangential to or crosses the envelope, so that a part of the DVH curve happens to be above it, the NTCP in which this DVH results is higher than α.

ε dose-volume constraint vicinity: Consider an integral dose-volume histogram, DVH_k, with dose-volume points (D, v) and a maximum dose of $D_{\max,k}$ at $v = 0$. If, for a particular dose-volume constraint point $\{v_i, D_i\}$ ($i = 1, \ldots, n_c$), the following condition is met:

$$\min \sqrt{(v - v_i)^2 + \left(\frac{D - D_i}{D_{\max,k}}\right)^2} \leq \varepsilon, \tag{2-2}$$

then this DVH belongs to the ε-vicinity of the given constraint and is said to satisfy the *ε-criterion.* This definition selects functions that are crossing a circle of radius ε around a constraint point.

2.2.2 NTCP models

2.2.2.1 The Lyman (Sigmoidal dose response) NTCP model

he Sigmoidal dose response (SDR) model, first introduced by Lyman,[37] describes the dose-response of normal tissues as follows:

$$NTCP = \Phi\left(\frac{EUD - D_{50}}{mD_{50}}\right), \tag{2-3}$$

where Φ is the probit function

$$\Phi(x) = \frac{1}{\sqrt{2\pi}} \int_{-\infty}^{x} \exp\left(\frac{-t^2}{2}\right) dt = \frac{1}{2}\left[1 + erf\left(\frac{x}{\sqrt{2}}\right)\right] \tag{2-4}$$

and $x = (EUD - D_{50})/mD_{50}$.

The equivalent uniform dose (EUD)[44] is defined as the uniform organ dose that would produce the same effect as the given heterogeneous dose distribution, as specified by a differential dose-volume histogram (dDVH) defined by the points $\{D_j, v_j\}$. The EUD or generalized mean dose (GMD), which in this case is chosen to represent the EUD, is calculated from the dDVH as follows:[45-47]

$$EUD = GMD = \left(\sum_j v_j D_j^{1/a} \right)^a . \tag{2-5}$$

There are three parameters that determine the response of normal tissues to radiation according to the Lyman model: m, a, and D_{50}. The dose-volume dependence of a tissue is determined by the parameter a, m gives the slope of the dose-response curve, and D_{50} is the dose that gives a 50% complication rate and thus determines the position of the response curve.

2.2.2.2 Critical volume population model

The critical volume (CV) model[38,39,41] is based on the idea that organs are composed of functional subunits (FSUs) and that a complication occurs when a certain number of these FSUs are destroyed. The response of different tissues is determined by the application of binomial statistics. Here we use the CV population NTCP model,[35,42,48] which takes into account inter-patient variability in normal tissue response and describes dose-volume response averaged over a population of individuals:

$$NTCP_{pop} \approx \Phi\left(\frac{-\ln(-\ln \bar{\mu}_d) + \ln(-\ln \mu_{cr})}{-\sigma_{\mu_{cr}} / \mu_{cr} \ln \mu_{cr}} \right), \tag{2-6}$$

where

$$\bar{\mu}_d = \sum_j v_j \Phi\left(\sqrt{2\pi} \gamma_{50}^{FSU} \ln\left(D_j / D_{50}^{FSU} \right) \right). \tag{2-7}$$

For the CV population model, it is assumed that the interpatient variability is limited to the parameter μ_{cr} (the mean critical relative volume). The parameters for this model

include the mean critical volume μ_{cr}, the population variation in this parameter $\sigma_{\mu_{cr}}$, the position of the FSU dose response D_{50}^{FSU}, and the slope of the FSU dose response γ_{50}^{FSU}.

2.2.3 Model parameters

For the calculations in this chapter, we use the CV population model parameters from Stavrev *et al.*[35] These authors estimated parameters that are based on the dose-response estimates of Emami *et al.*[1] for each of 16 types of normal tissue (see Table 2-1). For the SDR model proposed by Lyman, we use parameters derived by Burman *et al.*[34] that are also based on the Emami *et al.*[1] data. Burman *et al.*[34] provided SDR parameter estimates for 27 organs in total (a list of these organs is given in Burman *et al.*). For this work, our database consists of 16 organs for which both SDR and CV population NTCP model parameters exist.

2.3 Method

2.3.1 Reverse mapping of NTCP onto DVH space – a theoretical approach for dose-volume constraint estimation

In general, the reverse mapping method is carried out as follows:

i. Generate monotonically decreasing dose-volume histogram functions.

ii. Calculate the NTCPs corresponding to these dose-volume histogram functions.

iii. Identify DVH functions resulting in NTCP values falling in a user-specified NTCP interval. Plot all these DVHs.

iv. From *iii*, calculate the probability (frequency) of a DVH, within a user-specified NTCP interval, to pass through a given point in the dose-volume histogram space.

v. From *iv*, calculate the averaged and the most probable DVHs. These two curves may each serve as a source of dose-volume constraint points, for the process of inverse treatment planning by physical objective functions.

2.3.1.1 Generation of random DVHs

The first step of the reverse mapping process involves the generation of N_{DVH} random integral DVH curves that decrease monotonically from a relative volume of 1 and a relative dose of 0 to (0,1). The proper theory of DVH generation is presented in Chapter 3 and Markov *et al.*[36] In that chapter it is theoretically determined that the distribution of the number of monotonically decreasing functions passing through a point in the dose-volume histogram space follows the hypergeometric distribution, which is given in Sec. 3.3.1. The generator that we use in this simulation is based on the random walk theory and simulates in a random fashion trajectories corresponding to monotonically decreasing functions (finite series) situated in the unit square [0,1] × [1,0] subject to the hyper-geometric distribution.

2.3.1.2 Scaling the random DVHs

To calculate NTCP, the relative dose values of the integral DVHs must first be scaled to absolute doses. That is, we must multiply the relative dose points of each randomly generated integral dose-volume histogram by a maximum dose value appropriate to each organ of interest. The maximum dose of the k^{th} randomly generated DVH, DVH_k (where $k = 1, \ldots, N_{DVH}$) is designated as $D_{\max,k}$ and is calculated using the expression:

(2-8) $$D_{\max,k} = D_5 + n_k(D_{99} - D_5),$$

where n_k is a uniform randomly generated number (between 0 and 1). We have chosen the uniform distribution for n_k because there is no reason to believe that the possible maximum doses should have any other distribution. The dose values D_5 and D_{99} are those that give a NTCP of 5 and 99%, respectively, assuming uniform whole-organ irradiation, and are thus different for each of the 16 organs. The reason for the choice of D_5 and D_{99} will be explained below. Two sets of D_5 and D_{99} values were calculated: one based on the CV population model and one based on the Lyman model. Table 2-1 shows a list of all 16 organs along with the calculated D_5 and D_{99} values. Examples of typical

clinical D_{max} ranges, along with the treatments associated with those values, are shown for comparison. It should be emphasized that the clinical values for the minimal and maximal doses do not necessarily correspond to NTCPs of 5 and 99%. Instead, the clinical values for these parameters indicate the observed range of maximum organ dose during actual treatments. To avoid confusion, we will hereafter refer to these clinical values as D_{low} and D_{high}. Note that the upper and lower limits of clinical organ dose (Table 2-1) are sometimes extreme in comparison to the calculated limits (for example, an organ may have a typical clinical D_{low} of 0). Clinical maximum organ dose for a given treatment depends on factors such as where the planning target volume (PTV) is located in relation to the normal tissue of interest and the maximum dose prescribed to the PTV. Organs that have a clinical D_{low} value of zero (Table 2-1) reflect the fact that for the type of treatment listed, they may not be within the radiation field at all (the esophagus, for example). On the other hand, there are some normal tissues that have a good chance of receiving a significant dose during treatment of a tumour in their vicinity (the lung, for example, will always receive a relatively high maximum dose during lung tumour treatments).

For the purpose of customization and to avoid biasing between the results for different organs, we have chosen to use the calculated D_5 and D_{99} to define the range of D_{max} instead of the clinical values. The minimum value of D_5 was chosen arbitrarily to eliminate the generation of DVHs with unrealistically low NTCP. Also, in half of the organs (Table 2-1), the clinical D_{low} values are relatively close to D_5. Ideally, we would like to generate a decent number of low-NTCP DVHs to choose the constraints from, because our ultimate goal is to generate constraint points that will have a good chance of producing a clinically acceptable NTCP. We realize that, for some sites, the range of maximum delivered dose may be significantly different than $D_5 - D_{99}$. This case is also investigated here, namely the impact of D_{max} range on the dose-volume constraint estimation.

In addition, part of this work involves grouping the randomly generated DVHs into intervals according to the resulting NTCP values from each of the two different models, and then calculating the averaged DVH for each NTCP interval (intervals are 0 –

Table 2-1: Estimates for the clinical maximum dose range to 16 critical structures (D_{low}, D_{high}) that typically occur during the listed treatments (values based on treatments given at the Cross Cancer Institute). Also shown are values for the maximum dose range (D_5 and D_{99}) calculated according to both the Lyman and CV population models. The parameters D_5 and D_{99} are used to scale randomly-generated DVHs appropriately to calculate constraint points using the reverse mapping method. The following abbreviations are used: CNS – central nervous system; PTV – planning target volume; H&N – head and neck.

Organ	Treatment Type	Clinical		Lyman		CV Pop.	
		D_{low} (Gy)	D_{high} (Gy)	D_5 (Gy)	D_{99} (Gy)	D_5 (Gy)	D_{99} (Gy)
Lung	Radical lung treatment (60 Gy to PTV)	60	65	17.3	34.8	18.7	46.5
Liver	Abdomen - eg stomach cancer (45 Gy to PTV)	30	50	30.1	54.0	30.2	52.0
Brain	CNS - eg Glioblastoma (60 Gy to PTV)	60	65	45.2	80.9	45.8	85.1
Heart	Radical lung treatment (60 Gy to PTV)	0	60	40.1	59.2	40.6	61.0
Kidney	—	—	—	23.4	34.5	22.8	40.0
Esophagus	Radical lung treatment (60 Gy to PTV)	0	65	55.7	85.4	56.2	82.4
Stomach	Abdomen - eg stomach cancer (45 Gy to PTV)	40	55	50.0	86.2	53.0	80.7
Brachial plexus	Radical lung treatment (60 Gy to PTV)	0	50	60.2	95.9	60.6	87.4
Bladder	Prostate (74 Gy to PTV)	70	76	65.5	100.5	65.8	98.3
Mandible	H&N (70 Gy to PTV)	50	75	60.2	88.7	60.8	83.5
Brain stem	CNS - eg Glioblastoma (60 Gy to PTV)	0	55	50.0	86.2	49.6	87.1
Larynx	H&N (70 Gy to PTV)	55	75	70.1	94.0	70.6	91.1
Small intestine	Abdomen - eg stomach cancer (45 Gy to PTV)	40	55	40.5	75.5	41.2	71.7
Colon	Abdomen - eg stomach cancer (45 Gy to PTV)	40	55	45.1	69.1	45.6	66.6
Spinal cord	H&N (70 Gy to PTV)	40	50	47.4	93.6	46.7	86.1
Skin	Breast (50 Gy to PTV)	30	60	56.2	89.5	54.2	88.9

10, ..., 90 – 100%). In order to explore the DVH space properly and produce the averages corresponding to different NTCP ranges, we require a sufficient number of the DVHs to yield the corresponding NTCPs. While the clinical D_{low} and D_{high} are encountered more readily during radiation treatments than the calculated values, they may result in a bias of the distribution of all possible NTCPs for a critical structure. That is, some NTCP ranges may contain only a small sample of DVHs. To avoid this potential problem and to ensure that there will be a large enough number of DVHs in each NTCP interval, we chose to use the calculated values of D_5 and D_{99} to define the range of D_{max}.

2.3.1.3 Probability that a DVH, with a user-specified NTCP, passes through a given point in the dose-volume histogram space

Following the method outlined in Sections 2.3.1.1 and 2.3.1.2, N_{DVH} integral DVH curves have now been generated for a given organ at risk. We proceed by evaluating the NTCP of each integral DVH. To do this, a differential DVH is calculated from each of the N_{DVH} integral ones and then used, along with the SDR and CV population models with appropriate parameter values, to evaluate the NTCPs.

The ratio of the number of DVHs resulting in a user-specified NTCP range $[a,b]$ that pass through a given point in the dose-volume space (D, v) to the number of all generated DVHs passing through this point:

$$P\left(D,v \mid DVH_{NTCP\in[a,b]} : \{D,v\} \in DVH\right) = \frac{N_{\{D,v\}\in DVH_{NTCP\in[a,b]}}}{N_{\text{all } DVHs \text{ through } \{D,v\}}}, \tag{2-9}$$

may serve as an estimate of the probability that a DVH, with a user-specified NTCP range, passes through a given point in the dose-volume histogram space. Hereafter this quantity will be referred to as "DVH point probability." The DVH point probability defined in Eq. (2-9) depends on both the DVH generation algorithm and the dose scaling, $D_{\max,k}$.

Currently, an acceptable level of normal tissue complication is around 5% or less for radiation treatments. A NTCP range of [4.5%, 5.5%] was selected to represent clinically-acceptable DVHs in our calculation of the DVH point probability. For some treatment sites, it is possible to achieve a lower NTCP than the chosen range and for others, it is not possible to get as low as NTCP = 5.5%. The range of 5 ± 0.5% was selected to illustrate the reverse mapping method. To use this method for treatment planning, the NTCP range should be chosen to best reflect what is achievable for the site of interest. The DVH point probability was calculated for a given organ at risk from the N_{DVH} DVHs generated by means of Sections 2.3.1.1 and 2.3.1.2. From the randomly generated DVHs, those resulting in a NTCP in the range [4.5%, 5.5%] were selected. The dose-volume space was split in square bins and Eq. (2-9) was evaluated at each bin.

2.3.1.4 Constraint point estimation

For the purpose of inverse planning, constraint points are selected for nearby organs to limit dose (and correspondingly NTCP) to these structures while allowing delivery of the treatment dose to the PTV. We propose the radiobiological constraint points be estimated from the integral DVH that is the average of all integral DVHs resulting in a NTCP in the range [4.5%, 5.5%]. This curve could be estimated from the DVH point probability defined by Eq. (2-9) or calculated directly from the generated DVHs that have a NTCP in the corresponding range. We use the latter method to determine the average DVH. Specifically, the relative volume of the average DVH at the dose point D_i is calculated using the formula

$$V_{mean}(D_i) = \frac{1}{n_{DVH}} \sum_{j=1}^{n_{DVH}} V_j(D_i), \tag{2-10}$$

where n_{DVH} is the total number of DVHs with NTCP = 5 ± 0.5%. The average DVH (calculated as shown) and the weighted average DVH (calculated from the probability distribution) are one and the same function. Indeed, upon checking, we found that the average DVH coincides with the weighted average DVH within statistical error. Because larger statistics are required for the accurate determination of the probability distributions, and hence the weighted averages, we have chosen to use the arithmetic mean DVH calculated according to the above formula.

An additional and alternative source of dose-volume constraints may be found in the most probable integral DVH, which could be directly calculated from the DVH point probability, Eq. (2-9). However, for the organs at risk investigated here, we will use the average DVH to estimate a set of dose-volume constraint points at relative volumes of 0.1, 0.2, ..., 0.9. The average and the most probable DVHs are the two most characteristic quantities of the 2-dimensional distribution of DVHs that result in the desired NTCP and are both potential sources for constraint points.

Initially there are no indications that the DVH averaged from those resulting in NTCP = [4.5%, 5.5%] should be an object of the same kind, that is, resulting in the same

NTCP range. However, it is easily seen that this averaged DVH is also a monotonic function – a sum of monotonic functions is a monotonic function.

Average DVHs are also calculated for other NTCP ranges (0–10, 10–20 ...90–100%) to indicate where the DVHs with higher NTCP values may be located. NTCPs of these average curves are calculated to verify whether the average DVH has a NTCP that is within the corresponding range.

For completeness, the 67% confidence limits of the average of all DVHs with a NTCP of 5 ± 0.5% are calculated from the DVH point probability.

2.3.2 Reverse mapping of NTCP onto DVH space – a theoretical approach to the investigation of the radiobiological impact of a set of dose-volume constraints

The use of dose-volume constraints in the process of inverse treatment planning does not necessarily lead to low complication probability of the organs at risk. We believe that the reliability of a certain set of dose-volume constraints can be revealed by considering the following problems:

Problem 1: What is the probability distribution of the NTCPs corresponding to the DVHs belonging to a certain ε-vicinity of a given set of dose-volume constraints?

Problem 2: What is the 95% most probable interval of NTCP values corresponding to the DVHs belonging to a certain ε-vicinity of a given set of dose-volume constraints?

Problem 3: What is the probability that a DVH, belonging to a certain ε-vicinity of a given set of dose-volume constraints, will result in a particular NTCP value, for instance NTCP > 5.5% or a NTCP belonging to a given interval of values?

Problem 4: What is the probability that a DVH resulting in a NTCP belonging to a given interval of values belongs to the ε-vicinity of a given set of dose-volume constraints?

The following algorithm, based on the reverse mapping method, was implemented in order to obtain the solutions of problems 1 – 4:

i. Generate monotonically decreasing dose-volume histogram functions (2.3.1.1).

ii. Calculate the NTCPs corresponding to these dose-volume histogram functions.

iii. Count the number of DVHs resulting in NTCPs belonging to a certain interval $[a,b]$ of NTCP values - $N_{curves\ with\ NTCP\in[a,b]}$.

iv. Choose a set of dose-volume constraints.

v. For each generated DVH, determine whether it belongs to the ε-vicinity of the chosen set of dose-volume constraints. If it does, save the corresponding NTCP value.

vi. Use the saved NTCP values to build the distribution sought in problem 1.

vii. Based on this distribution calculate the quantity sought in problem 2.

viii. For the DVHs belonging to the ε-vicinity of the chosen set of dose-volume constraints, count the number of those resulting in NTCPs belonging to the interval $[a,b]$, $N_{curves\in\varepsilon-vicinity\ with\ NTCP\in[a,b]}$.

ix. Calculate the probability sought in problem 3 according to the following ratio:

$$\frac{N_{curves\in\varepsilon-vicinity\ with\ NTCP\in[a,b]}}{N_{curves\in\varepsilon-vicinity}}$$

x. Calculate the probability sought in problem 4 according to the following ratio:

$$\frac{N_{curves\in\varepsilon-vicinity\ with\ NTCP\in[a,b]}}{N_{curves\ with\ NTCP\in[a,b]}}$$

For the calculations in the above algorithm we used the ε-vicinity definition presented in Sec. 2.2.1.

2.4 Results

Table 2-2 lists the dose-volume constraints (in Gy) for each of 16 organs, calculated by interpolating from the average of all DVHs resulting in a NTCP of 5 ± 0.5% according to the Lyman NTCP model at the relative volumes of 0.1, 0.2, ..., 0.9. Table 2-3 gives the dose-volume constraints for the same organs, calculated according to the CV population NTCP model. For all organs and for both NTCP models, the first few

high-volume constraint points are characterized by negligibly small doses (close to zero). A total of 1×10^6 integral DVHs were simulated for each organ to calculate these constraint points. The fraction of these simulated DVHs that resulted in NTCP = 5 ± 0.5%, $P_{NTCP=5\%}$, is shown in the last column of Table 2-2 and Table 2-3. As it is impractical to include figures for all 16 organs listed in Table 2-2 and Table 2-3, the endpoint of heart pericarditis was selected for illustration purposes. In Figure 2-1(a) and (b), a sample of the family of nearly iso-NTCP randomly-generated DVH curves that result in $NTCP \in [4.5\%, 5.5\%]$ are shown for both chosen models. The average, along

Table 2-2: Constraint points interpolated from the average of DVHs with a Lyman NTCP of 5 ± 0.5% for 16 organs. For each of the relative volumes shown across the top of the chart, the interpolated dose in Gy is given for each organ if this value is non-zero. The far right column in the table shows the fraction of randomly-generated DVHs, out of a total of 1×10^6, that have an NTCP of 5 ± 0.5%, $P_{NTCP=5\%}$.

Organ/Volume	0.1	0.2	0.3	0.4	0.5	0.6	0.7	0.8	0.9	$P_{NTCP=5\%}$
Lung	27.9	25.0	22.7	20.9	19.2	17.5	14.3	—	—	1.4%
Liver	40.9	36.6	33.6	31.0	27.2	18.7	—	—	—	2.2%
Brain	58.7	52.5	48.1	43.8	35.1	10.9	—	—	—	2.6%
Heart	51.0	47.8	45.3	43.1	41.1	38.3	31.8	—	—	1.0%
Kidney	30.8	29.0	27.7	26.5	25.4	24.3	23.0	19.7	—	0.5%
Esophagus	58.6	54.6	47.7	35.5	—	—	—	—	—	2.9%
Stomach	58.8	53.4	48.9	40.2	21.4	—	—	—	—	3.0%
Brachial plexus	61.0	56.6	48.9	36.2	—	—	—	—	—	2.7%
Bladder	86.9	81.2	76.8	72.9	69.3	65.6	58.2	—	—	0.8%
Mandible	64.2	59.9	53.1	40.7	6.3	—	—	—	—	2.9%
Brain stem	59.5	53.9	49.6	41.9	25.3	—	—	—	—	2.9%
Larynx	79.2	74.2	70.5	65.0	55.1	35.2	—	—	—	1.9%
Small intestine	47.5	42.9	38.8	30.6	7.4	—	—	—	—	3.1%
Colon	54.2	49.6	46.3	42.3	34.5	16.5	—	—	—	2.3%
Spinal cord	49.2	45.8	39.7	29.1	—	—	—	—	—	2.9%
Skin	62.2	57.4	51.7	40.5	13.2	—	—	—	—	3.0%

Table 2-3: Same as Table 2-2, but calculated using the CV population NTCP model.

Organ/Volume	0.1	0.2	0.3	0.4	0.5	0.6	0.7	0.8	0.9	$P_{NTCP=5\%}$
Lung	33.3	28.6	25.1	22.3	19.8	16.1	—	—	—	1.7%
Liver	41.7	37.7	34.7	32.3	29.8	25.0	9.0	—	—	1.5%
Brain	55.5	49.5	44.9	36.1	15.8	—	—	—	—	3.3%
Heart	51.7	47.9	45.2	42.9	40.5	36.2	23.2	—	—	1.2%
Kidney	33.3	30.4	28.2	26.3	24.6	22.7	19.0	—	—	1.0%
Esophagus	58.3	53.9	45.8	31.6	—	—	—	—	—	3.8%
Stomach	55.4	51.1	43.3	29.5	—	—	—	—	—	3.8%
Brachial plexus	59.6	54.4	46.5	33.7	—	—	—	—	—	4.6%
Bladder	84.9	79.4	75.1	71.4	67.9	—	—	—	—	1.0%
Mandible	63.0	58.1	49.4	35.0	—	—	—	—	—	4.5%
Brain stem	60.5	54.2	49.5	41.6	25.2	—	—	—	—	3.3%
Larynx	79.0	74.5	71.2	66.4	58.3	43.1	—	—	—	1.9%
Small intestine	47.9	43.3	39.0	30.5	9.2	···	—	—	—	3.3%
Colon	54.2	50.0	46.9	43.4	36.7	23.3	—	—	—	2.1%
Spinal cord	48.0	44.0	36.7	23.7	—	—	—	—	—	4.4%
Skin	60.2	55.1	48.5	36.1	—	—	—	—	—	4.0%

with the proposed constraint points calculated as discussed in Section 2.3, are also shown in Figure 2-1(a) and (b). The averaged DVHs result in NTCP values of 4.98 ± 0.02% for the Lyman and 4.98 ± 0.02% for the CV population model. Finally, the Emami[1] constraint points (each of these lead to NTCP = 5% assuming uniform, partial organ irradiation) and the 5% iso-NTCP envelopes for both NTCP models are also plotted for comparison in Figure 2-1(a) and (b). The property of the envelope stated in the definition (Sec. 2.2.1) is clearly illustrated in both plots; namely, no DVH with NTCP $\leq$ 5% crosses the envelope. It should be noted that a DVH passing through a combination of constraints from the envelope has a NTCP higher than 5%.

As defined in Sec. 2.3.1.3, we call the probability of a DVH, with a user-specified NTCP, passing through a given point in the dose-volume histogram space the DVH point probability. The DVH point probabilities were used to estimate the 67% confidence limits for DVHs resulting in NTCP = 5 ± 0.5%. Figure 2-1(c) and (d) present an example of what these probabilities look like. The averaged DVH together with the 67% confidence

limits for the end point heart-pericarditis are also shown. Both the DVH point probabilities and the confidence limits indicate more spread of the DVHs with NTCP = 5 ± 0.5% in the low dose regions; while in the high dose regions, the majority of DVHs pass through or near the average.

The calculated most probable DVHs for both NTCP models are plotted in Figure 2-1(e) and (f). The NTCP values corresponding to the most probable DVH curves are 5.7 ± 0.1% for the Lyman model and 5.1 ± 0.1% for the CV population model.

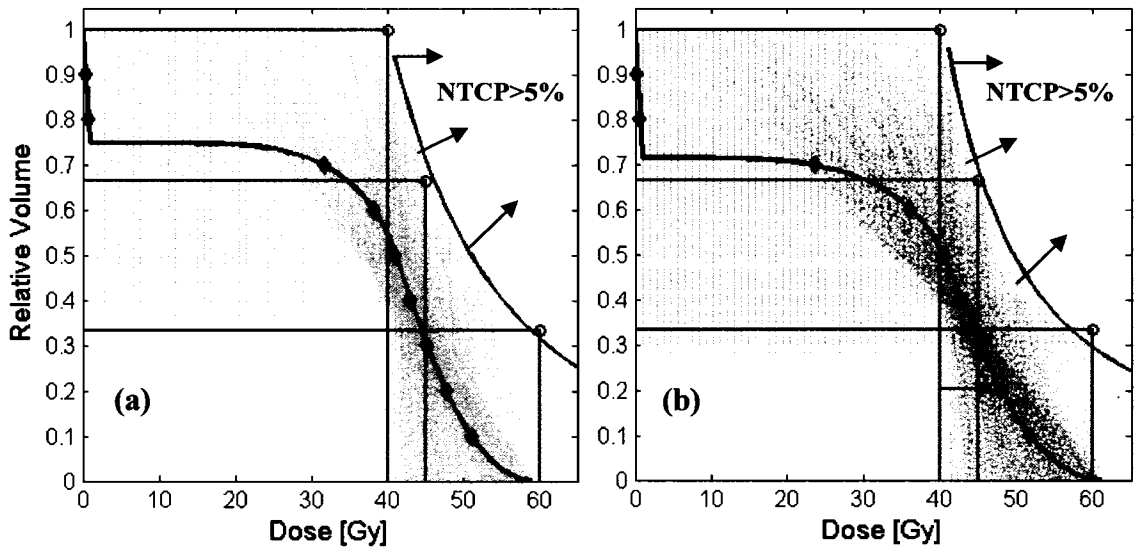

Figure 2-1: (a) and (b) – a sample of DVHs with NTCP=5±0.5% (grey dotted curves) calculated according to the Lyman NTCP model (a) and the CV population NTCP model (b) for the endpoint heart pericarditis. Also shown in each of these subplots are the average of all DVHs with NTCP = 5 ± 0.5% along with the constraint points interpolated from this curve (solid black curve with diamond points). The Emami constraints for heart are shown for comparison as circles, along with the 5% iso-NTCP envelope that passes near to the Emami points.

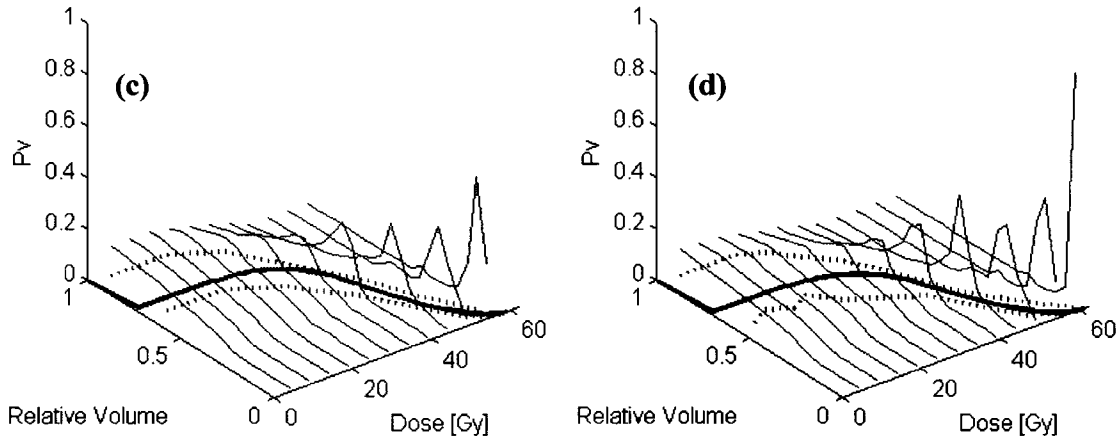

Figure 2-1 (c) and (d) – Show the DVH point-probabilities (curves in the *zy* plane) for heart calculated using the Lyman model (c) and the CV population model (d). The average of DVHs with NTCP = 5 ± 0.5% is shown (dark curve in *xy* plane) for comparison, along with the 67% confidence limits (dashed curves in *xy* plane) that were calculated by means of the DVH point-probabilities.

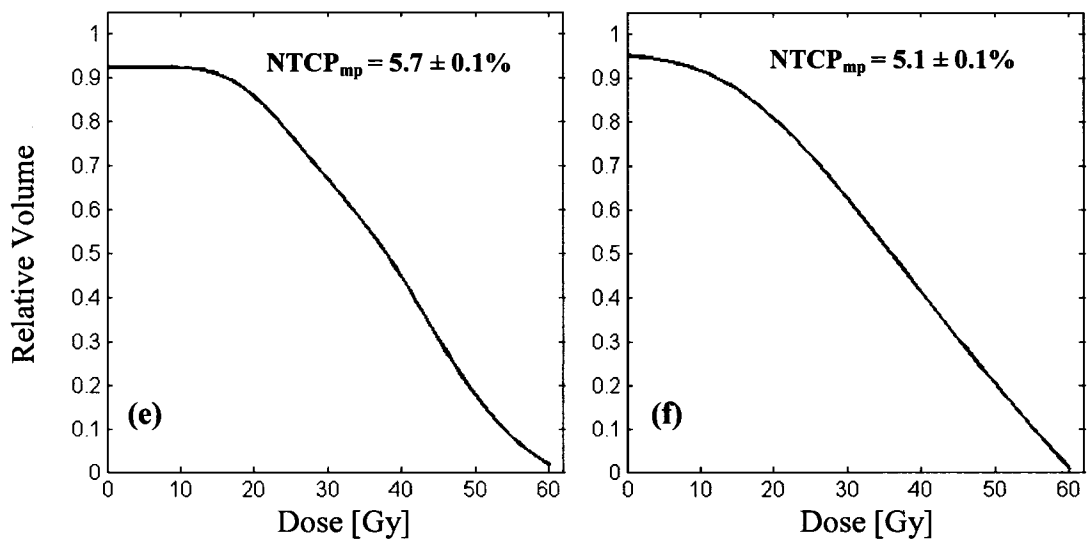

Figure 2-1 (e) and (f) – The most probable DVH curves for heart, calculated from the DVH point-probabilities in (c) and (d). The Lyman model was used for (e), and the Lyman NTCP of the most probable DVH is shown in the upper right corner. For (f), the CV population model results are shown, along with the CV population NTCP for this curve.

In Figure 2-2, for the same end-point, heart pericarditis, the average DVHs are shown for six different intervals of NTCP values: 0–10, 10–20, 20–30, 50–60, 70–80, and 90–100%. Figure 2-2(a) shows the average DVHs calculated based on the Lyman NTCP model, and Figure 2-2(b) shows the average DVHs calculated based on the CV population model.

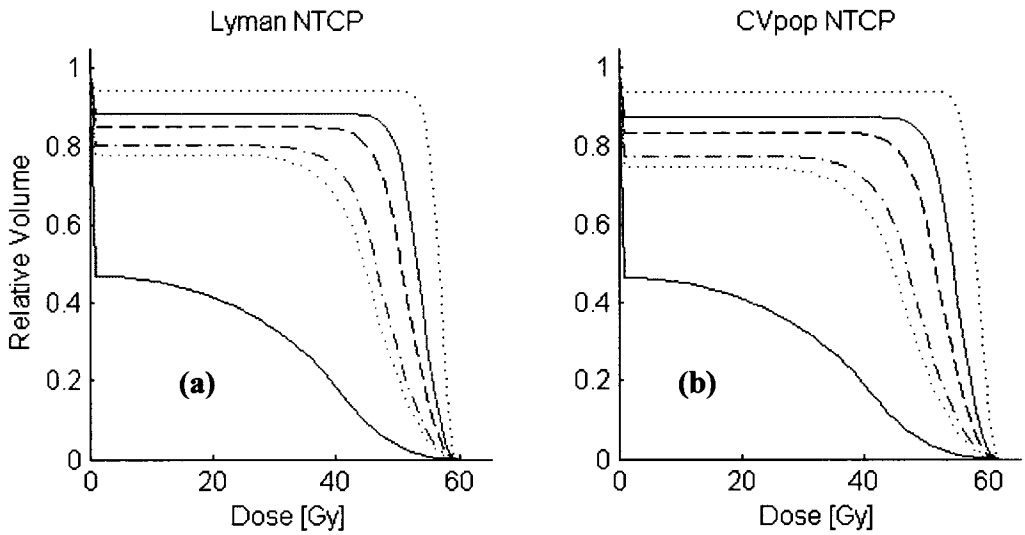

Figure 2-2: Plot of the average DVH for each of 6 NTCP intervals for the endpoint heart pericarditis. Averages were calculated based on the Lyman NTCP model (a) and the CV population model (b). From the lowest volume to the highest volume curves, the intervals are NTCP = [0%, 10%] (first solid line), [10%, 20%] (first dotted line), [20%, 30%] (dash-dotted line), [50%, 60%] (dashed line), [70%, 80%] (second solid line) and [90%, 100%] (second dotted line).

Out of the 16 organs investigated in this chapter, the lung is unique in that the clinical D_{high} value of 65 Gy is significantly larger than the D_{99} estimated using either of the NTCP models (Table 2-1). In some clinics, there are dose escalation protocols for lung tumours that can get as high as 90 Gy.[49] In order to demonstrate the impact of the $D_{\max}$ range on the dose-volume constraint estimation, we use the lung and the CV population model as an example (Figure 2-3). The average DVHs and the constraint points are calculated for the following ranges of $D_{\max}$ values [Eq. (2-8)]: $D_{\max,k} = D_5 + n_k(D_{99} - D_5)$ shown in Figure 2-3(a); $D_{\max,k} = D_5 + n_k(90\text{Gy} - D_5)$ shown in Figure 2-3(b); $D_{\max,k} = 60\text{Gy} + n_k(65\text{Gy} - 60\text{Gy})$ shown Figure 2-3(c) – this

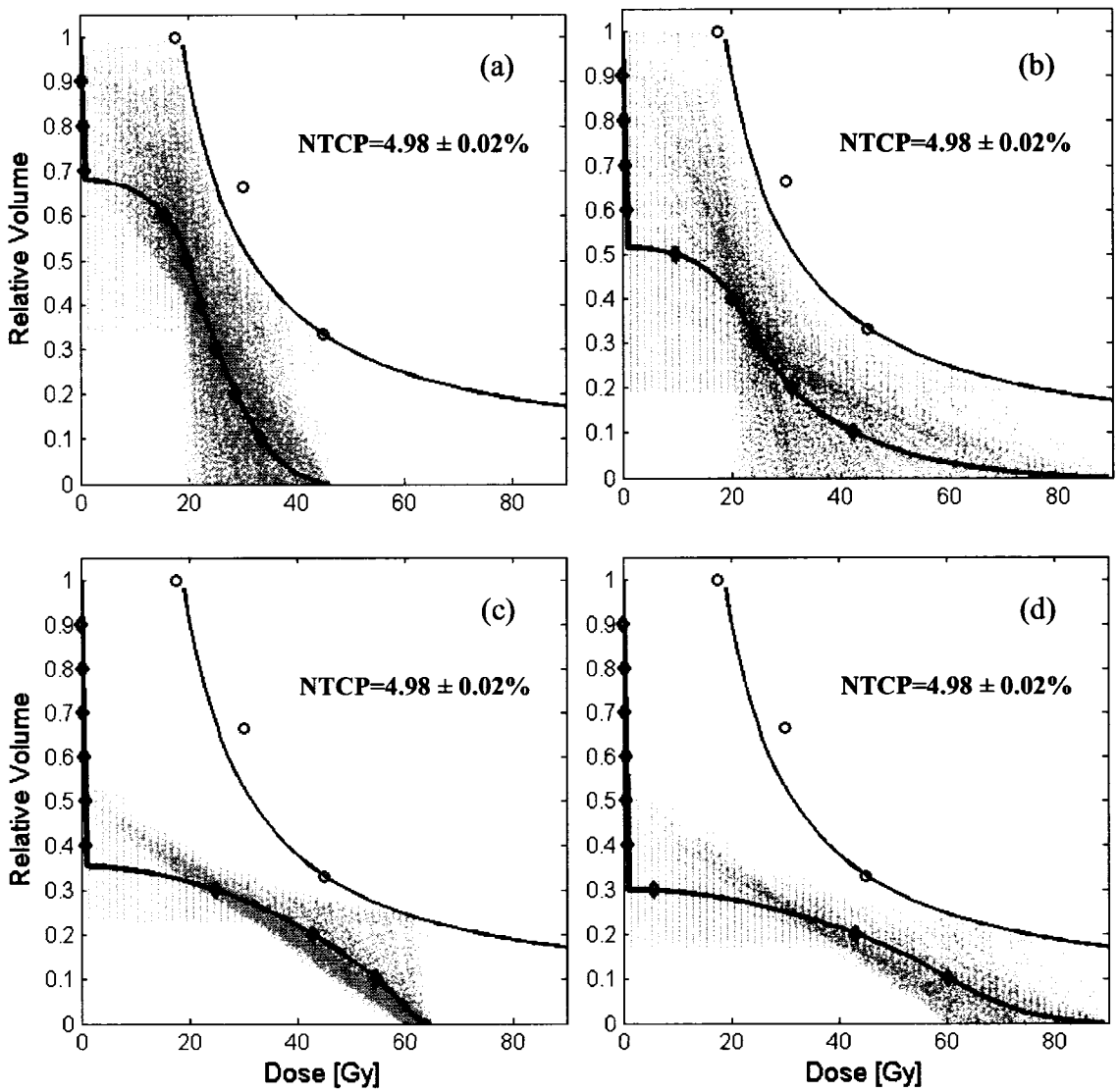

Figure 2-3: A subset of DVHs that have a critical volume population NTCP of 5±0.5% for the endpoint lung pneumonitis (grey dashed curves), the average of these DVHs and the interpolated constraint points (solid curve with black diamonds). Each subplot shows these curves for a different DVH dose scaling: (a) $D_{min} - D_{max} = D_5 - D_{99}$, (b) $D_5 - 90Gy$, (c) 60 – 65Gy and (d) 60 – 90Gy. In each subplot, the 5% iso-NTCP envelope is shown along with the Emami points (○) for lung pneumonitis. The NTCPs are those of the average DVHs.

corresponds to the sample clinical maximum dose range given in Table 2-1; and $D_{\max,k} = 60\text{Gy} + n_k(90\text{Gy} - 60\text{Gy})$ shown in Figure 2-3(d). The iso-NTCP envelope and the Emami constraint points are presented as well. NTCP values for each averaged DVH are shown on the corresponding subplots. The calculations were done using both NTCP models and the estimated constraint points are presented in Table 2-4 for comparison.

Table 2-4: This table illustrates the effect of $D_{\max}$ range on calculated constraint points. Dose-volume constraint points were calculated for lung with the random DVHs scaled according to $D_{\max}$ ranges of $D_5 - D_{99}$, $D_5 - 90\text{Gy}$, 60 – 65 Gy and 60 – 90Gy, using both the Lyman and CV population models.

	Lyman constraint dose				CV Pop. constraint dose			
Volume	D_5–D_{99}	D_5–90Gy	60–65Gy	60–90Gy	D_5–D_{99}	D_5–90Gy	60–65Gy	60–90Gy
0.1	27.9	40.8	54.3	59.3	33.3	42.6	54.8	60.4
0.2	24.9	30.0	41.9	40.8	28.6	31.4	43.0	43.2
0.3	22.7	23.8	22.6	—	25.1	25.0	25.1	6.0
0.4	20.9	19.1	—	—	22.3	20.1	—	—
0.5	19.2	10.6	—	—	19.8	10.0	—	—
0.6	17.5	—	—	—	16.1	—	—	—
0.7	14.3	—	—	—	—	—	—	—
0.8	—	—	—	—	—	—	—	—
0.9	—	—	—	—	—	—	—	—

Figure 2-4 presents the probability distributions of the NTCPs corresponding to the DVH curves belonging to a certain ε-vicinity (ε = 1%) for several sets of dose-volume constraints. Again, both NTCP models discussed in this chapter were used. In Figure 2-4, the Lyman model results are presented on the left while the CV population model results are presented on the right. The end point of brain necrosis was chosen for this investigation. The following sets of dose-volume constraints were selected and used to calculate the corresponding distributions: (D, v) = (48.1 Gy, 0.3) in Figure 2-4(a); (D ,v) = (44.9 Gy, 0.3) in Figure 2-4(b); the pair (D_1, v_1) = (52.5 Gy, 0.2), (D_2, v_2) = (48.1 Gy, 0.3) in Figure 2-4(c); the pair (D_1, v_1) = (49.5 Gy, 0.2), (D_2, v_2) = (44.9 Gy, 0.3) in Figure 2-4(d); the set (D_1, v_1) = (58.7 Gy, 0.1), (D_2, v_2) = (48.1 Gy, 0.3), (D_3, v_3) =(43.8 Gy, 0.4) in Figure 2-4(e); and the set (D_1, v_1) = (55.5 Gy, 0.1), (D_2, v_2) = (44.9 Gy, 0.3), (D_3, v_3) =

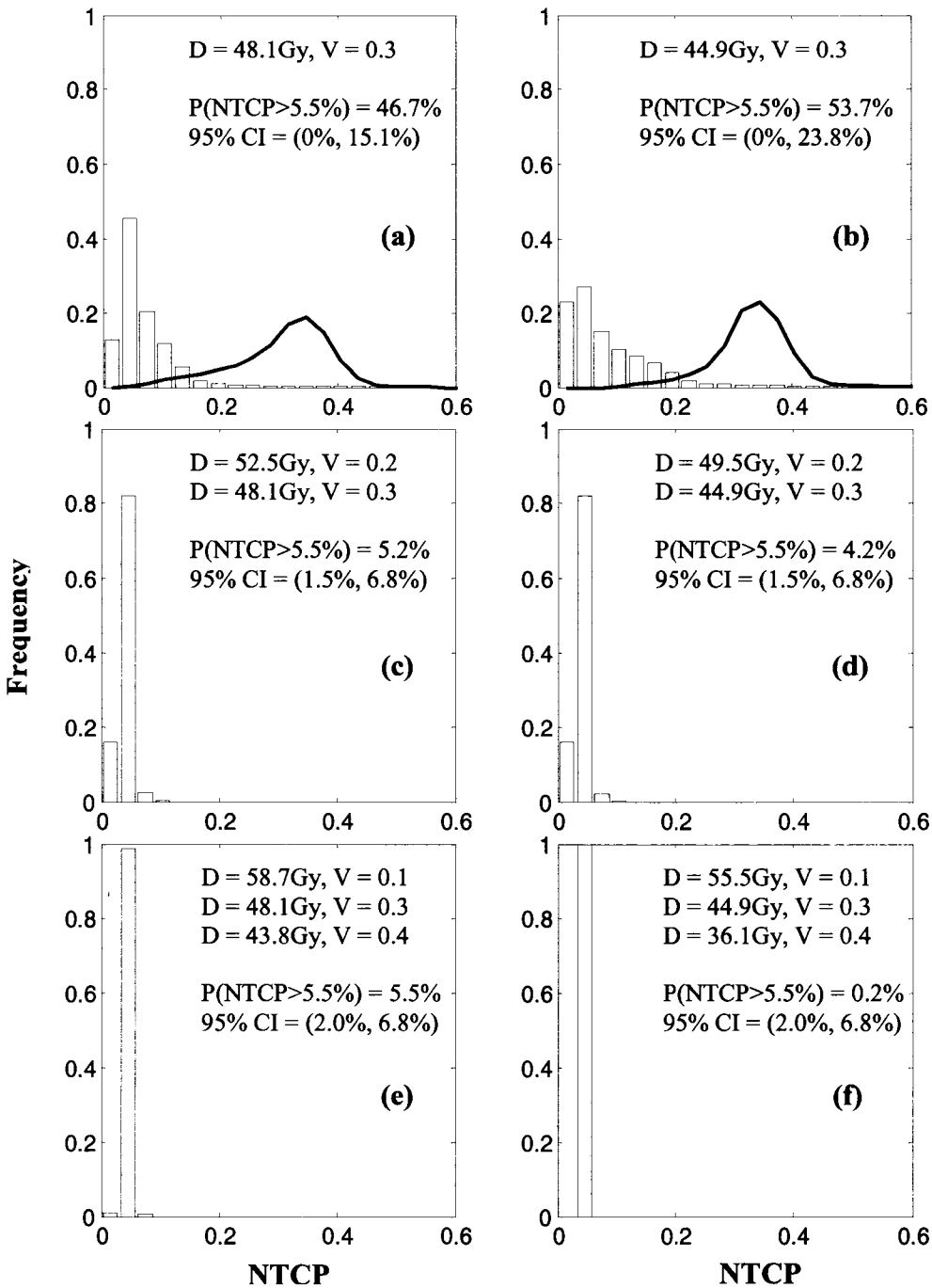

Figure 2-4: Lyman (left) and CV population (right) NTCP probability distributions for the endpoint brain necrosis for the given sets of calculated dose-volume constraint points. A total of 2×10^6 DVHs were simulated in order to build these distributions, and of those, the ones that passed within a vicinity of $\varepsilon = 1\%$ were deemed to satisfy the constraints. Shown in each subplot are two additional quantities: the probability that a DVH which satisfies the given constraint(s) will have an NTCP that is greater than 5.5% [$P(NTCP > 5.5\%)$] and the 95% confidence intervals (CIs) for the distributions. In (a) and (b), the NTCP distributions for the Emami $v = \frac{1}{3}$, $D = 60$ Gy constraint point is shown for comparison (black line).

(36.1 Gy, 0.4) in Figure 2-4(f). The probability of observing a value of NTCP > 5.5% for the DVHs belonging to a certain ε-vicinity is calculated for each set of dose-volume constraints and is given in the corresponding subplots together with the 95% NTCP most probable interval. In Figure 2-4(a) and (b), NTCP probability distributions for the $v = 1/3$, $D = 60$ Gy Emami point are shown (black line) along with those for the $v = 0.3$ calculated points. The above values together with the probability that a DVH resulting in a NTCP = $5 \pm 0.5\%$ will belong to the ε-vicinity of the chosen sets of dose-volume constraints are presented in Table 2-5.

Table 2-5: This table shows three quantities calculated for the end-point brain necrosis, for the given sets of constraints. Calculations were done with both the Lyman and CV population NTCP models, and for each constraint volume given, a dose value from either Table 2-2 (for the Lyman model analysis) or Table 2-3 (for the CV population model analysis) was selected (except for the Emami constraint point, for which the dose was 60 Gy). The first quantity in this table is $P_{\varepsilon}(NTCP = 5 \pm 0.5\%)$, which represents the probability that a DVH with $NTCP \in [4.5\%, 5.5\%]$ passes within the ε-vicinity ($\varepsilon = 1\%$) of the chosen constraint(s). The value $P(NTCP > 5.5\%)$ is the probability that a DVH which satisfies the chosen constraint(s) has an NTCP that is greater than 5.5%. Finally, this table shows the NTCP range in which 95% of the DVHs satisfying the constraint(s) result [the 95% confidence interval (CI)].

	P_{ε}(NTCP = 5 ± 0.5%)		P(NTCP > 5.5%)		95% CI	
Constraint Volume(s)	**Lyman**	**CV Pop.**	**Lyman**	**CV Pop.**	**Lyman**	**CV Pop.**
Emami $v = 1/3$, $D = 60$Gy	0.004%	0.0%	100.0%	100.0%	11.7 - 43.7%	18.0 - 44.7%
0.3	18.2%	8.0%	46.7%	53.7%	0.0 - 15.1%	0.0 - 23.8%
0.2, 0.3	3.9%	1.5%	5.2%	4.2%	1.5 - 6.8%	1.5 - 6.8%
0.1, 0.3, 0.4	1.6%	0.1%	5.5%	0.2%	2.0 - 6.8%	2.0 - 6.8%

2.5 Discussion

The theoretical approach of reverse NTCP mapping onto DVH space described above was used to estimate dose-volume constraints for the needs of inverse treatment

planning and to provide a basis for comparison between the physical and biological radiation therapy optimization.

2.5.1 Suitability of the calculated constraint points for inverse planning

In Sec. 2.3.1, we proposed that physical dose-volume constraints may be estimated from the curve that represents the average of all DVHs with an NTCP of 5 ± 0.5%. For these constraint points to be "reasonable," the NTCP of the average DVH should also fall within the same interval. However, not all DVHs resulting in a certain NTCP are suitable for choosing constraint points. An example is a step like DVH corresponding to partial organ homogeneous irradiation resulting in the desired NTCP (such as the Emami DVHs). Our investigations show that the averaged DVH indeed results in a NTCP that is within the above range of values for both the Lyman and the CV population NTCP models. This holds true for all of the investigated organs and the different intervals in which the maximum dose for the simulated DVHs was selected. An example of this can be seen in Figure 2-1 and Figure 2-4. These figures also indicate that, in general, the region of DVHs with NTCP ~5% is more spread out at low doses and more concentrated at high doses. In Sec. 2.3.1, we mentioned that a potential alternate source for dose-volume constraint points is the most probable DVH. This curve almost coincides with the average DVH in the low-volume region; thus, the difference in the NTCPs of the two curves is due mainly to the differences in the high-volume, low-dose region. However, while the average of the DVHs resulting in NTCP = 5 ± 0.5% is also an object of the same kind, this condition is not always satisfied for the most probable DVH (Figure 2-1). Thus, we have placed more emphasis on the average DVH as a source for dose-volume constraints.

The dose-volume constraint points estimated here and presented in Table 2-2 and Table 2-3 only reflect the data presented in the Emami *et al.* work through the mathematical forms of the NTCP models derived on the basis of some biological observations or assumptions about the tissue response to irradiation.[37-40,42,50] About the data presented in the Emami *et al.* work the authors are aware that "The Emami estimates

are not, in any sense of the word, primary data. Rather, they are a distillation from the literature of whatever information could be gleaned, combined with the clinical impressions of experienced radiation oncologists."[35] On the other hand they are widely cited and used in the clinical practice together with the Lyman model with parameter estimates of Burman *et al.* This is why we turned to these parameter estimates to illustrate the application of the reverse mapping method to the problem of dose-volume constraint estimation. This also gave us the opportunity to compare, through the results obtained, two different NTCP models, when the values of their parameters are derived from the same source. It should be pointed out, however, that this method is not confined to the NTCP models or parameter values used in this chapter. Constraint points may be calculated according to the method outlined in Sec. 2.3.1 using a completely different NTCP model and/or parameter set if one desires. The use of a different parameter set could potentially have an impact on the constraint calculation, but such a comparison is beyond the scope of this chapter. One way to estimate the impact of a different, for example, more recent, parameter set is to calculate the 5% iso-NTCP envelope based on the new parameter set and observe its deviation from the envelope calculated from the previous set. For example, the iso-NTCP envelope of the Dawson *et al.*[13] liver parameters for the Lyman model is shifted considerably to the right in comparison to the Emami parameters for this organ (e.g., see the 10% iso-NTCP envelopes in Fig. 1 of their work). The corresponding impact of using the Dawson parameters in place of the Emami ones for constraint point estimation could thus be considerable. If more accurate parameter estimates are available, these should be used for the dose-volume constraint estimation.

It may seem that the model predictions deduced from the Emami *et al.* tolerances are assumed to be more reliable than the original estimates. However, if the model accurately reflects the nature of the phenomenon, the model predictions are as reliable as the data used to derive the model parameters. The use of a model broadens our capability to predict the outcome in cases that have not yet been investigated by means of an experiment.

We would like to point out that care has to be exercised in the interpretation of the iso-NTCP envelope depicted in Figure 2-1(a) and (b) or Figure 2-3. It is misleading to

assume that any curve in the region to the left of the 5% iso-NTCP envelope will result in an acceptable NTCP of about 5%. We can only say that there is a chance that a DVH lying in this region may result in an acceptable NTCP of around 5%, while we can say with absolute certainty that if a DVH crosses or is tangential to the 5% iso-NTCP envelope, it will definitely result in a NTCP higher than 5%. It is important to point out that the Emami points lie on or near the 5% iso-effect envelope. Therefore, it must be obvious that any DVH curve passing through any Emami point will with certainty result in an NTCP $\gtrsim$ 5%. Indeed, the 95% confidence intervals of the NTCP values corresponding to the DVHs passing through an ε-vicinity of the ⅓ volume Emami point for the brain, for instance, are [11.7%, 43.7%] for the Lyman model and [18.0%, 44.7%] for the CV population model. These confidence intervals are considerably larger than the ones – [0.0%, 15.1%] for the Lyman model and [0.0%, 23.8%] for the CV population model – characteristic of the 0.3 volume constraint point calculated according to the proposed algorithm (Table 2-2 and Table 2-3). More importantly, the lower limit of the confidence intervals for the Emami points is $\gtrsim$ 5% indicating, as stated above, that the achievable values of the NTCP will always be larger than 5%. The same calculations were done for the ⅓ and ⅔ volume Emami points and for the generated dose-volume constraint points shown in Table 2-2 and Table 2-3 for several other randomly selected organs, namely – lung, liver and bladder. In all cases, the result is the same: the lower limit of the 95% confidence intervals for observing a NTCP value for any DVH curve passing through or near an Emami point is larger than 5%; while it is always near to 0% for the generated dose-volume constraint points. Also, the NTCP confidence intervals of the generated constraint points are always narrower than the confidence intervals of the Emami points. This means that the outcome in terms of NTCP values is predictable to a higher extent in the case where the dose-volume constraints are chosen according to the proposed algorithm.

Therefore, we consider the generated dose-volume constraint points more suitable for clinical application than the Emami data points if used as dose-volume constraints.

Note that, although the constraint points derived from the two NTCP models display the same general trends (Table 2-2 and Table 2-3), there are differences in the

doses obtained for the different relative volumes. In addition, the estimates using the CV population model result in fewer constraint points with nonzero dose values for some organs than those using the Lyman model.

For all organs, the average of DVHs with a NTCP of 0 – 10% has the lowest relative volume at each dose and represents a relatively small partial volume irradiation of the critical structure (see the example for heart pericarditis – Figure 2-2). As the NTCP interval increases, the relative volumes of the curves become larger, and the average DVHs tend to 'flatten out.' The average of DVHs with a NTCP of 90 – 100% generally corresponds to a relatively uniform irradiation of a significant portion of the organ, at a relatively high dose. The NTCPs of the average DVHs shown in Figure 2-2 are consistent with the NTCP intervals used to calculate these average curves.

2.5.2 Random integral DVHs and dose scaling

The reverse mapping method of constraint point estimation relies heavily upon the generation of random DVHs and also the scaling of the dose axis to absolute values. The dependence of the average DVH on the generation algorithm is illustrated and discussed in Chapter 3 and Markov *et al.*[36] The set of clinically achievable DVHs is an undefined one, due to the fact that the treatment strategies and the available radiation treatment techniques realizing these strategies change considerably through the years. Hence, it is difficult, if not impossible, to describe the set of clinically realizable DVHs mathematically. However, the set of clinically realized DVHs is a subset of the set of all monotonically decreasing functions. The DVHs that were generated in this chapter include those that are characteristic of a portion of the organ at risk receiving no irradiation. Clinically, exact partial organ irradiation cannot be achieved as there will always be some dose deposition due to scatter. However, modern IMRT techniques and delivery systems, such as tomotherapy,[51,52] allow for dose distributions that come very close to fully sparing a portion of an organ at risk. These modern techniques expand the set of the clinically possible DVHs (making it a dynamic concept), because they expand the number of solutions through which the dose field could be delivered to the tumour.

For example, some of the integral DVHs shown in the works of Coselmon *et al.*,[53] Horton *et al.*,[54] Hanks *et al.*[55] and Wang *et al.*[56] exhibit an initial drop in relative volume around a dose of zero, indicating that a portion of these organs is almost entirely spared. In fact, the slope of this drop-off looks very similar to the one observed in the average DVHs presented in this chapter. Therefore, the random DVHs used here to estimate physical dose-volume constraint points are not impossible to achieve clinically.

There are cases that exist where the constraint points interpolated from the average DVH may not be suitable for inverse planning. For example, if the organ at risk (OAR) is sufficiently close to the target, its achievable DVH may be above the average on the high-dose side. Our experience shows that in the process of inverse planning, the OAR DVH moves "down" rather than "up," that is, the average vector of the shift, in the process of an iterative search of the solution, points toward the (0, 0) point of the DVH space. Hence the algorithm would try to go as close as possible to the dose-volume constraints "from above," although they will not be reached. A better solution might be found if a physico-biological optimization is performed; but if the achievable OAR DVH is above the average DVH as a consequence of the specifics of the individual geometry, this would present a problem for the physical inverse treatment planning no matter what the dose-volume constraints are. The OAR NTCP will remain high, irrespective of the choice of the constraint points, because it is fundamentally determined by the higher doses.

In Sec. 2.3.1.2, we observed that for some organs, the clinical range of possible maximum dose values is significantly different from the calculated D_5 and D_{99} values based on the NTCP models. An interesting result concerning the calculated D_{99} values is that depending on the model used – Lyman or CV population – the calculated D_{99} for some organs differs significantly for both models (Table 2-1). Clinical dose values exhibit varying degrees of disparity depending on factors such as the position of the target relative to the organ at risk and the prescribed target dose. Although we have opted to use the calculated D_5 and D_{99} values for dose-volume constraint estimation, with the purpose of unification, we did carry out an investigation of how the different dose ranges, to which the maximum dose could belong, would affect the values of the dose-volume constraint estimates.

The nonuniqueness of the estimated dose-volume constraints is clearly demonstrated in Figure 2-3 and in Table 2-4. These results suggest that knowledge of the range in which the maximum doses are going to be is extremely important for the determination of appropriate dose-volume constraints via the reverse mapping method. Figure 2-3 unambiguously shows that the averaged DVH results in a NTCP of the same range as the DVHs from which it is calculated, regardless of the D_{max} range. In each of the four cases illustrated, the NTCP of the averaged DVH was 4.98 ± 0.02%. It is interesting to note that the obtained averaged DVHs shown in Figure 2-3(b) and (c) resemble the averaged DVHs reported by Tsougos *et al.*[28] In their work, the occurrence of radiation pneumonitis was studied in a group of 150 patients treated for breast cancer. Their averaged DVHs suggest a trend favouring the partial organ nonirradiation similar to our results presented in Figure 2-3. As noted above, the maximum dose range will depend on the treatment site and the treatment strategy. Hence, we recommend a recalculation of the dose-volume constraints if the maximum dose range differs considerably from the one used here.

The maximum dose range of $D_5 - D_{99}$ and the NTCP range of 4.5 – 5.5% were chosen for this work to illustrate the reverse mapping constraint point estimation for a number of organs, but one is by no means limited to these parameter values. Different NTCP levels and maximum dose ranges may be selected to take into account clinical variables such as tumour size and location with respect to the organs at risk, beam arrangement, and anatomic structure. In each case, the constraint points could be recalculated for the desired NTCP and D_{max} range using the reverse mapping method.

2.5.3 Comparison with other methods of dose-volume constraint determination

Another approach to the problem of dose-volume constraints determination is described in Hartford *et al.*,[57] Huang *et al.*,[58] Jackson *et al.*[59] and Pollack *et al.*[60] It consists of classifying the clinically realized DVHs for the responders and the nonresponders for a given complication end point. However, the two DVH regions

corresponding to the two groups of responders and nonresponders obtained by this method, unfortunately, overlap considerably.[28,57,59] This effect could be due to the fact that statistics of even several hundred patients is insufficient to allow the proper determination and differentiation of the two regions in the DVH space. Indeed, due to the probabilistic nature of the tissue-dose response, a given clinical DVH may produce a responder but it may also result in a nonresponder. In addition, DVHs do not convey any information about the spatial distribution of dose. Hence, a clinically acceptable dose distribution and an unacceptable one may result in DVHs that are practically identical.

In order to compare the results from the reverse mapping method with those reported by Jackson *et al.*,[59] we calculated the dose-volume constraints for the rectum based on the Burman parameter estimates for the Lyman model. This organ was not included in the main investigation because there were no sufficient data for the extraction of parameter estimates for the CV population model.[35] Figure 2-5 shows our dose-volume constraint estimates (diamond points on the dashed line) together with the averaged DVH for nonbleeders (top solid curve) and the lower limit of its 67% confidence range (lower solid curve) obtained by Jackson *et al.*, for the patients treated to a maximum dose of 70.2 Gy. The Lyman NTCP of the Jackson *et al.* nonbleeder DVH was calculated to be 5.43% and is also shown in Figure 2-5; while the Lyman NTCP of the averaged DVH is only slightly lower – 4.99 ± 0.02%. Both NTCPs are within the acceptable interval of [4.5%, 5.5%] and thus the small difference is not very important. For the region of relative volumes less than 40%, the results from the reverse mapping method almost coincide with Jackson *et al.* observations. Because these two curves almost coincide in the high-dose region, it stands to reason that the differing low-dose regions are the cause of the observed small difference in NTCP. It is important to note that dose-volume constraints with lower relative volumes are the ones narrowing the area in the DVH space corresponding to sufficiently low complication probabilities. In other words, if points with higher relative volumes are used as constraints, there is a higher probability of allowing DVHs with unacceptable NTCP values, as the NTCP distributions widen when the relative volume increases. A similar result was reported by Hartford *et al.*[57] (Fig. 1 of their work) and it is also well illustrated in Figure 2-4.

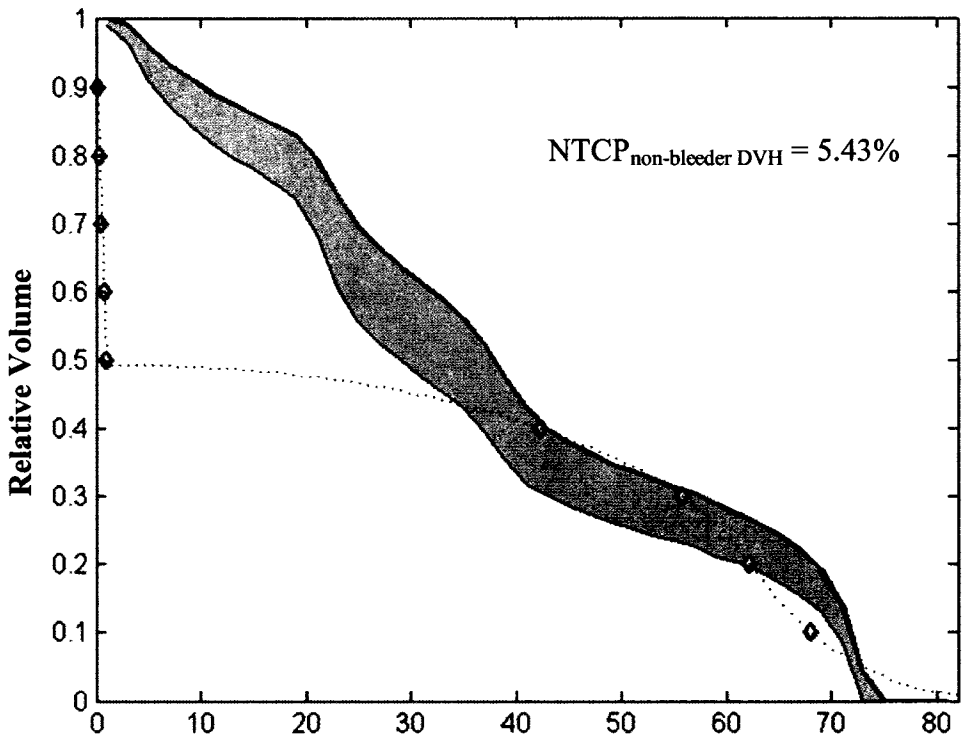

Figure 2-5: Averaged DVH (dotted line) and dose-volume constraint estimates (diamonds) for rectum, calculated by means of the reverse mapping method. The Lyman NTCP model with the Burman parameters was used to obtain these constraint points. Shown for comparison are the averaged DVH for non-bleeders from Jackson *et al.*[59] (upper solid curve) and the lower limit of its 67% confidence range (lower solid curve). The Lyman NTCP of the non-bleeder DVH is given in the upper right corner of this plot.

Thus, based on the results of this study and the ones reported by Hartford *et al.*[57] we recommend that the dose-volume constraint points be chosen among those corresponding to sufficiently low relative volumes and high doses (in the case of rectum 0.4 or less).

2.5.4 Physical versus radiobiological optimization

The selection of a given set of dose-volume constraints in the process of treatment planning presumes that these constraints will result in an appropriate restriction of the

dose, which in turn ensures an acceptable level of the complication probability for the organ at risk. The proposed reverse mapping method (Sec. 2.3.2) presents a theoretical way to investigate the radiobiological impact of a set of dose-volume constraints. Figure 2-4(a) and (b) clearly show that the distributions of the NTCP values, for the end-point brain necrosis, produced by DVHs satisfying just one dose-volume constraint are sufficiently wide and include DVHs leading to unacceptably high complication probabilities. The corresponding 95% confidence intervals given in Table 2-5 confirm the above inference. It is also seen that almost half of the DVHs passing through the ε-vicinity of the chosen constraint point result in NTCP values higher than 5.5%. The choice of more than one dose-volume constraint considerably narrows the NTCP distributions (problem 1, Sec. 2.3.2), as demonstrated in Figure 2-4(b), (c), (d), and (f). The corresponding 95% confidence intervals, when two or three dose-volume constraints are used, suggest that the DVHs satisfying these constraints result in NTCP values that are confined to a reasonably small interval of clinically acceptable complication probabilities. The fraction of DVHs leading to more than 5.5% NTCP [$P(NTCP > 5.5\%)$ – Table 2-5] is also considerably reduced compared to the case when only one constraint is used. It should be reiterated that the NTCP distributions generally become wider with the increase of the relative volume value of the lower dose-volume constraint.

The introduction of every other dose-volume constraint (first column of Table 2-5) considerably lowers the number of DVHs with $NTCP \in [4.5\%, 5.5\%]$, thus shrinking the area of the set of solutions. The investigations that were carried out for several other organs show similar trends. It was also confirmed that the use of two or three dose-volume constraints could ensure the selection of DVHs resulting in clinically acceptable complication rates. We can therefore conclude that the reverse mapping method allows us to demonstrate that the radiation treatment optimization based on physical objective functions can sufficiently restrict the dose to the organs at risk resulting in low enough NTCP values through the employment of several appropriate dose-volume constraints.

However, a comparison with the results reported in Stavrev *et al.*[6] shows that a treatment plan leading to NTCP levels of around 1% for all organs at risk (in the treatment of lungs excluding the lung in which the tumour was situated) can be clinically

achieved when the hybrid physicobiological optimization of the radiation treatment is employed where minimization of the NTCP values is sought. At the same time, the pure physical approach to optimization is self-restrictive due to the preassignment of acceptable NTCP levels, thus leaving out possible better solutions to the problem. The exclusion of clinically acceptable DVHs that occurs as a result of the imposition of physical dose-volume constraints can be seen in the $P_\varepsilon(NTCP = 5 \pm 0.5\%)$ values that are presented in Table 2-5. $P_\varepsilon(NTCP = 5 \pm 0.5\%)$ is the quantity that is described in problem 4 of Sec. 2.3.2; it represents the probability that a DVH with a NTCP in the interval [4.5%, 5.5%] satisfies a given set of constraints according to the ε-criterion. For the v = 0.3 calculated constraint point, for instance, this probability is just 18.2% for the Lyman model and has an even lower value of 8.0% for the CV population model. As more constraint points are added, the chance that a viable solution is eliminated increases, in other words, $P_\varepsilon(NTCP = 5 \pm 0.5\%)$ lowers considerably. The application of any physical dose-volume constraints – not just those that were estimated in this chapter – will exclude a number of DVHs with acceptable NTCP. The hybrid optimization method presented in Stavrev *et al.*[6] appears to be superior to pure physical optimization due to the fact that this method would not eliminate clinically desirable solutions.

2.6 Conclusions

In this study, we developed a theoretical method to estimate dose-volume constraint points based on radiobiological models for the needs of inverse treatment planning. This method presents a general guidance to the problem of dose-volume constraint estimation. Sample constraint points estimated by the use of two different NTCP models – the Lyman and the CV population model – were calculated. An interesting result is that the calculations done with both NTCP models, especially for low relative volume points, produce similar constraint points. Model parameters for both models were based on the dose-response estimates in the Emami *et al.*[1] report.

The average of a set or subset of DVHs resulting in NTCP values belonging to a given range, <DVH>, results in a NTCP that falls within the same range of values. The dose-volume constraint points from this average DVH are not unique – they depend on the range of values in which the maximum dose is allowed to vary. In order to achieve adequate functioning of the constraint points, they must be chosen among those corresponding to sufficiently low relative volumes (approximately less than 0.5). Similar results were obtained by Hartford *et al.*[57]

The use of two or three appropriately chosen low-volume constraint points can shrink the NTCP interval associated with the DVHs that pass sufficiently close to these constraints to a clinically acceptable range. If we seek DVHs with NTCP = α, then the constraint points should lie at a sufficient distance below the α-iso-NTCP envelope. This renders the Emami points inadequate as dose-volume constraints if the goal is a dose distribution resulting in ~ 5% NTCP.

2.7 References

1. B. Emami, J. Lyman, A. Brown, L. Coia, M. Goitein, J. E. Munzenrider, B. Shank, L. J. Solin, and M. Wesson, "Tolerance of normal tissue to therapeutic irradiation," Int J Radiat Oncol Biol Phys **21**, 109-122 (1991).

2. W. R. De Gersem, S. Derycke, C. O. Colle, C. De Wagter, and W. J. De Neve, "Inhomogeneous target-dose distributions: a dimension more for optimization?," Int J Radiat Oncol Biol Phys **44**, 461-468 (1999).

3. W. R. De Gersem, S. Derycke, C. De Wagter, and W. C. De Neve, "Optimization of beam weights in conformal radiotherapy planning of stage III non-small cell lung cancer: effects on therapeutic ratio," Int J Radiat Oncol Biol Phys **47**, 255-260 (2000).

4. G. O. De Meerleer, L. A. Vakaet, W. R. De Gersem, C. De Wagter, B. De Naeyer, and W. De Neve, "Radiotherapy of prostate cancer with or without intensity modulated beams: a planning comparison," Int J Radiat Oncol Biol Phys **47**, 639-648 (2000).

5. A. Niemierko, M. Urie, and M. Goitein, "Optimization of 3D radiation therapy with both physical and biological end points and constraints," Int J Radiat Oncol Biol Phys **23**, 99-108 (1992).

6. P. Stavrev, D. Hristov, B. Warkentin, E. Sham, N. Stavreva, and B. G. Fallone, "Inverse treatment planning by physically constrained minimization of a biological objective function," Med Phys **30**, 2948-2958 (2003).

7. A. Dritschilo, J. T. Chaffey, W. D. Bloomer, and A. Marck, "The complication probability factor: a method for selection of radiation treatment plans," Br J Radiol **51**, 370-374 (1978).

8. A. B. Wolbarst, E. S. Sternick, B. H. Curran, and A. Dritschilo, "Optimized radiotherapy treatment planning using the complication probability factor (CPF)," Int J Radiat Oncol Biol Phys **6**, 723-728 (1980).

9. L. Cozzi, F. M. Buffa, and A. Fogliata, "Comparative analysis of dose volume histogram reduction algorithms for normal tissue complication probability calculations," Acta Oncol **39**, 165-171 (2000).

10. V. Moiseenko, J. Battista, and J. Van Dyk, "Normal tissue complication probabilities: dependence on choice of biological model and dose-volume histogram reduction scheme," Int J Radiat Oncol Biol Phys **46**, 983-993 (2000).

11. M. Zaider and H. I. Amols, "Practical considerations in using calculated healthy-tissue complication probabilities for treatment-plan optimization," Int J Radiat Oncol Biol Phys **44**, 439-447 (1999).

12. J. C. Cheng, J. K. Wu, C. M. Huang, H. S. Liu, D. Y. Huang, S. H. Cheng, S. Y. Tsai, J. J. Jian, Y. M. Lin, T. I. Cheng, C. F. Horng, and A. T. Huang, "Radiation-induced liver disease after three-dimensional conformal radiotherapy for patients with hepatocellular carcinoma: dosimetric analysis and implication," Int J Radiat Oncol Biol Phys **54**, 156-162 (2002).

13. L. A. Dawson, D. Normolle, J. M. Balter, C. J. McGinn, T. S. Lawrence, and R. K. Ten Haken, "Analysis of radiation-induced liver disease using the Lyman NTCP model," Int J Radiat Oncol Biol Phys **53**, 810-821 (2002).

14. L. A. Dawson and R. K. Ten Haken, "Partial volume tolerance of the liver to radiation," Semin Radiat Oncol **15**, 279-283 (2005).

15. L. A. Dawson, R. K. Ten Haken, and T. S. Lawrence, "Partial irradiation of the liver," Semin Radiat Oncol **11**, 240-246 (2001).

16. A. Eisbruch, J. A. Ship, H. M. Kim, and R. K. Ten Haken, "Partial irradiation of the parotid gland," Semin Radiat Oncol **11**, 234-239 (2001).

17. G. Gagliardi, I. Lax, and L. E. Rutqvist, "Partial irradiation of the heart," Semin Radiat Oncol **11**, 224-233 (2001).

18. A. Jackson, "Partial irradiation of the rectum," Semin Radiat Oncol **11**, 215-223 (2001).

19. S. L. Kwa, J. V. Lebesque, J. C. Theuws, L. B. Marks, M. T. Munley, G. Bentel, D. Oetzel, U. Spahn, M. V. Graham, R. E. Drzymala, J. A. Purdy, A. S. Lichter, M. K. Martel, and R. K. Ten Haken, "Radiation pneumonitis as a function of mean lung dose: an analysis of pooled data of 540 patients," Int J Radiat Oncol Biol Phys **42**, 1-9 (1998).

20. S. Levegrun, L. Ton, and J. Debus, "Partial irradiation of the brain," Semin Radiat Oncol **11**, 259-267 (2001).

21. M. K. Martel, W. M. Sahijdak, R. K. Ten Haken, M. L. Kessler, and A. T. Turrisi, "Fraction size and dose parameters related to the incidence of pericardial effusions," Int J Radiat Oncol Biol Phys **40**, 155-161 (1998).

22. V. Moiseenko, T. Craig, A. Bezjak, and J. Van Dyk, "Dose-volume analysis of lung complications in the radiation treatment of malignant thymoma: a retrospective review," Radiother Oncol **67**, 265-274 (2003).

23. T. E. Schultheiss, "The controversies and pitfalls in modeling normal tissue radiation injury/damage," Semin Radiat Oncol **11**, 210-214 (2001).

24. Y. Seppenwoolde and J. V. Lebesque, "Partial irradiation of the lung," Semin Radiat Oncol **11**, 247-258 (2001).

25. Y. Seppenwoolde, J. V. Lebesque, K. de Jaeger, J. S. Belderbos, L. J. Boersma, C. Schilstra, G. T. Henning, J. A. Hayman, M. K. Martel, and R. K. Ten Haken, "Comparing different NTCP models that predict the incidence of radiation pneumonitis. Normal tissue complication probability," Int J Radiat Oncol Biol Phys **55**, 724-735 (2003).

26. E. L. Travis, "Organizational response of normal tissues to irradiation," Semin Radiat Oncol **11**, 184-196 (2001).

27. E. D. Yorke, "Modeling the effects of inhomogeneous dose distributions in normal tissues," Semin Radiat Oncol **11**, 197-209 (2001).

28. I. Tsougos, P. Mavroidis, J. Rajala, K. Theodorou, R. Jarvenpaa, M. A. Pitkanen, K. Holli, A. T. Ojala, B. K. Lind, S. Hyodynmaa, and C. Kappas, "Evaluation of dose-response models and parameters predicting radiation induced pneumonitis

using clinical data from breast cancer radiotherapy," Phys Med Biol **50**, 3535-3554 (2005).

29. J. D. Fenwick, V. S. Khoo, A. E. Nahum, B. Sanchez-Nieto, and D. P. Dearnaley, "Correlations between dose-surface histograms and the incidence of long-term rectal bleeding following conformal or conventional radiotherapy treatment of prostate cancer," Int J Radiat Oncol Biol Phys **49**, 473-480 (2001).

30. J. V. Lebesque, A. M. Bruce, A. P. Kroes, A. Touw, R. T. Shouman, and M. van Herk, "Variation in volumes, dose-volume histograms, and estimated normal tissue complication probabilities of rectum and bladder during conformal radiotherapy of T3 prostate cancer," Int J Radiat Oncol Biol Phys **33**, 1109-1119 (1995).

31. J. Y. Ting, X. Wu, J. A. Fiedler, C. Yang, M. L. Watzich, and A. Markoe, "Dose-volume histograms for bladder and rectum," Int J Radiat Oncol Biol Phys **38**, 1105-1111 (1997).

32. N. Stavreva, P. Stavrev, B. Warkentin, and B. G. Fallone, "Derivation of the expressions for gamma50 and D50 for different individual TCP and NTCP models," Phys Med Biol **47**, 3591-3604 (2002).

33. N. Stavreva, P. Stavrev, B. Warkentin, and B. G. Fallone, "Investigating the effect of cell repopulation on the tumor response to fractionated external radiotherapy," Med Phys **30**, 735-742 (2003).

34. C. Burman, G. J. Kutcher, B. Emami, and M. Goitein, "Fitting of normal tissue tolerance data to an analytic function," Int J Radiat Oncol Biol Phys **21**, 123-135 (1991).

35. P. Stavrev, N. Stavreva, A. Niemierko, and M. Goitein, "The Application of Biological Models to Clinical Data," *Phys Medica* **XVII**, 71-82 (2001).

36. K. Markov, C. Schinkel, P. Stavrev, N. Stavreva, M. Weldon, and B. G. Fallone, "Reverse mapping of normal tissue complication probabilities onto dose volume histogram space: the problem of randomness of the dose volume histogram sampling," Med. Phys. **33**, 3435-3443 (2006).

37. J. T. Lyman, "Complication probability as assessed from dose-volume histograms," Radiat Res Suppl **8**, S13-19 (1985).

38. A. Jackson, G. J. Kutcher, and E. D. Yorke, "Probability of radiation-induced complications for normal tissues with parallel architecture subject to non-uniform irradiation," Med Phys **20**, 613-625 (1993).

39. A. Niemierko and M. Goitein, "Modeling of normal tissue response to radiation: the critical volume model," Int J Radiat Oncol Biol Phys **25**, 135-145 (1993).

40. D. R. Olsen, "The tissue volume effect: a reliability model", presented at the Proc. 9th Annual ESTRO Meeting, (1990).

41. D. R. Olsen, B. K. Kambestad, and D. T. Kristoffersen, "Calculation of radiation induced complication probabilities for brain, liver and kidney, and the use of a reliability model to estimate critical volume fractions," Br J Radiol **67**, 1218-1225 (1994).

42. P. Stavrev, N. Stavreva, A. Niemierko, and M. Goitein, "Generalization of a model of tissue response to radiation based on the idea of functional subunits and binomial statistics.," Phys Med Biol **46**, 1501-1518 (2001).

43. D. Hristov, P. Stavrev, E. Sham, and B. G. Fallone, "On the implementation of dose-volume objectives in gradient algorithms for inverse treatment planning," Med Phys **29**, 848-856 (2002).

44. A. Niemierko, "Reporting and analyzing dose distributions: a concept of equivalent uniform dose," Med Phys **24**, 103-110. (1997).

45. A. Niemierko, "A generalized concept of Equivalent Uniform Dose", presented at the 41th AAPM Annual Meeting, Nashville, (1999).

46. A. Niemierko and M. Goitein, "Calculation of normal tissue complication probability and dose-volume histogram reduction schemes for tissues with a critical element architecture," Radiother Oncol **20**, 166-176 (1991).

47. P. Stavrev, D. Hristov, and E. Sham, "IMRT Inverse Treatment Planing Optimization Based on Physical Constraints and Biological Objectives", presented at the 47nd Annual General Meeting of the Canadian Organization of Medical Physicists (COMP),, Kelowna, BC, Canada, (2001).

48. A. Jackson, R. K. Ten Haken, J. M. Robertson, M. L. Kessler, G. J. Kutcher, and T. S. Lawrence, "Analysis of clinical complication data for radiation hepatitis using a parallel architecture model," Int J Radiat Oncol Biol Phys **31**, 883-891 (1995).

49. E. D. Yorke, A. Jackson, K. E. Rosenzweig, L. Braban, S. A. Leibel, and C. C. Ling, "Correlation of dosimetric factors and radiation pneumonitis for non-small-cell lung cancer patients in a recently completed dose escalation study," Int J Radiat Oncol Biol Phys **63**, 672-682 (2005).

50. H. R. Withers, J. M. Taylor, and B. Maciejewski, "The hazard of accelerated tumor clonogen repopulation during radiotherapy," Acta Oncol **27**, 131-146 (1988).

51. T. R. Mackie, J. Balog, K. Ruchala, D. Shepard, S. Aldridge, E. Fitchard, P. Reckwerdt, G. Olivera, T. McNutt, and M. Mehta, "Tomotherapy," Semin Radiat Oncol **9**, 108-117 (1999).

52. T. R. Mackie, T. Holmes, S. Swerdloff, P. Reckwerdt, J. O. Deasy, J. Yang, B. Paliwal, and T. Kinsella, "Tomotherapy: a new concept for the delivery of dynamic conformal radiotherapy," Med Phys **20**, 1709-1719 (1993).

53. M. M. Coselmon, J. M. Moran, J. D. Radawski, and B. A. Fraass, "Improving IMRT delivery efficiency using intensity limits during inverse planning," Med Phys **32**, 1234-1245 (2005).

54. J. K. Horton, J. S. Halle, S. X. Chang, and C. I. Sartor, "Comparison of three concomitant boost techniques for early-stage breast cancer," Int J Radiat Oncol Biol Phys **64**, 168-175 (2006).

55. G. E. Hanks, T. E. Schultheiss, A. L. Hanlon, M. Hunt, W. R. Lee, B. E. Epstein, and L. R. Coia, "Optimization of conformal radiation treatment of prostate cancer: report of a dose escalation study," Int J Radiat Oncol Biol Phys **37**, 543-550 (1997).

56. X. Wang, X. Zhang, L. Dong, H. Liu, Q. Wu, and R. Mohan, "Development of methods for beam angle optimization for IMRT using an accelerated exhaustive search strategy," Int J Radiat Oncol Biol Phys **60**, 1325-1337 (2004).

57. A. C. Hartford, A. Niemierko, J. A. Adams, M. M. Urie, and W. U. Shipley, "Conformal irradiation of the prostate: estimating long-term rectal bleeding risk using dose-volume histograms," Int J Radiat Oncol Biol Phys **36**, 721-730 (1996).

58. E. H. Huang, A. Pollack, L. Levy, G. Starkschall, L. Dong, I. Rosen, and D. A. Kuban, "Late rectal toxicity: dose-volume effects of conformal radiotherapy for prostate cancer," Int J Radiat Oncol Biol Phys **54**, 1314-1321 (2002).

59. A. Jackson, M. W. Skwarchuk, M. J. Zelefsky, D. M. Cowen, E. S. Venkatraman, S. Levegrun, C. M. Burman, G. J. Kutcher, Z. Fuks, S. A. Liebel, and C. C. Ling, "Late rectal bleeding after conformal radiotherapy of prostate cancer. II. Volume effects and dose-volume histograms," Int J Radiat Oncol Biol Phys **49**, 685-698 (2001).

60. A. Pollack, G. K. Zagars, and V. S. Kavadi, "Prostate specific antigen doubling time and disease relapse after radiotherapy for prostate cancer," Cancer **74**, 670-678 (1994).

Chapter 3 Reverse mapping of normal tissue complication probabilities onto dose volume histogram space: The problem of randomness of the dose volume histogram sampling

A version of this chapter was published as:

K. Markov, C. Schinkel, P. Stavrev, N. Stavreva, M. Weldon, B. G. Fallone, "Reverse mapping of normal tissue complication probabilities onto dose volume histogram space: the problem of randomness of the dose volume histogram sampling," Med. Phys. **33**, 3435-3443, 2006.

3.1 Introduction

We recently introduced the concept of reverse mapping of normal tissue complication probability (NTCP) onto the space of the dose volume histogram (DVH).[1] This method allows the investigation of DVH space with respect to the NTCPs for a given organ and a corresponding NTCP model. In this manner, one can investigate the probability that a DVH resulting in a given NTCP value would pass in the vicinity of a certain point within the DVH space. More practically, an average DVH curve can be calculated from a set of simulated DVHs individually resulting in $\mathrm{NTCP} \in [4.5; 5.5]\%$. The points from this average DVH curve can then be used as dose-volume constraints for inverse treatment planning.

One very important issue in the problem of reverse mapping of NTCP onto DVH space is that of the generation of DVH curves. It is necessary to determine a proper simulation algorithm, which will ensure that the generated DVHs are sampled from the correct distribution. Thus, the less probable DVHs will appear in the sampling process

less often, while the more probable ones will appear more often. In this chapter, we present the mathematical theory to determine the type of distribution to which is subject the number of normalized integral DVHs passing through a point in DVH space. Based on this theory, a two-dimensional (2D) random function generator is developed. This generator produces monotonically decreasing functions based on the theory of random walk, and can be used to simulate random normalized integral DVHs. Such a generator is essential to calculate physical dose-volume constraint points by the method of reverse mapping of NTCP onto DVH space. In the previous chapter and in Schinkel *et al.*[2], we calculated dose-volume constraints using the reverse mapping method for the needs of inverse treatment planning.

3.2 Background

In this study, we use normalized DVHs, where the dose delivered to different relative sub-volumes of the organ is normalized to the maximum dose delivered and is measured as a percent dose in terms of the maximum. It is clear, then, that any monotonically decreasing function in the region [1,0] × [0,1] could represent a normalized integral DVH (Figure 3-1). Several Monte Carlo procedures can be used to simulate monotonically decreasing functions by creating finite series. We propose in this chapter a Monte Carlo procedure which we call a "random walk" DVH generator. Two procedures that are simpler than the one proposed here have been used for DVH generation elsewhere:

(1) Random number descent[1] and

(2) Random angle - random step descent[3]

They will be described in detail further below, and compared to the appropriate random walk DVH generator, whose theory we present here.

3.3 *Theory*

Let us consider, for instance, the set of all continuous monotonically decreasing functions in the unit square [1,0] × [0,1]. These functions completely fill up the unit square. Our initial assumption is that the density of functions passing through different points – for example, points *P* and *Q* in Figure 3-1 – should be different and should depend on the position of the point. It is not simple to express this notion mathematically. The power of a set in the set theory will produce equal powers for each set of continuous monotonically decreasing functions passing through any point within the unit square and

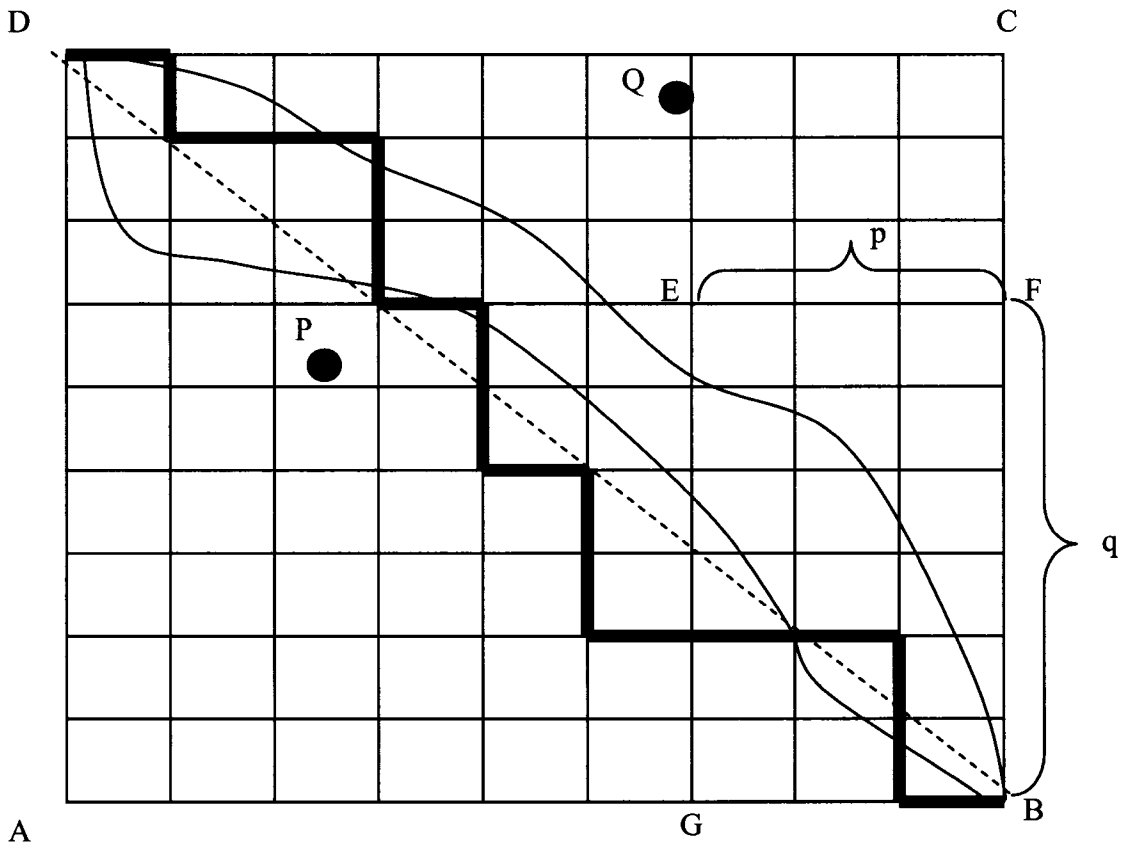

Figure 3-1: Monotonically decreasing functions. Our initial assumption is that the number of functions passing through different points - for example points *P* and *Q* - should be different and should depend on the position of the point. The thick black line represents a step like trajectory from point *D* to point *B*.

thus would give an inaccurate estimate in this case. Alternatively, one can define a certain measure in the space of continuous monotonically decreasing functions in the interval [0,1]. We opted to simplify the operation by considering the discrete version of the problem.

3.3.1 Determining the distribution of curves passing through a point in the unit square

The unit square *ABCD*, which encompasses the region of the functions of interest, can be divided through a net of vertical and horizontal lines into a finite number of small squares. Then, the curves representing the functions of interest will be portrayed through steplike trajectories from point *D* to point *B* that pass only through points from the dividing net. An example of such a trajectory is shown in Figure 3-1.

The discrete version of the problem defined in this way determines a *finite* number of trajectories connecting any two points in a monotonically decreasing fashion. Indeed, the number of steplike trajectories connecting, for instance, points *E* and *B* in Figure 3-1 depends only on the size *p* and *q* of the rectangle *EFBG*. This fact will enable us to count the number of steplike trajectories passing through different points. By dividing this number by the total number of trajectories connecting points *D* and *B* (which is the total number of possible DVHs) we will determine the distribution of DVHs depending on the position of the point.

We can construct each trajectory from point *D* to point *B* through randomly choosing points of passage which lie on a series of vertical intercepts (intercepts parallel to the *Y* axes) (Figure 3-1). However, due to such a choice of the intercepts, the trajectories become degenerate, i.e., a function may pass through more than one point on the intercept. Therefore, the sum of the trajectories passing through all points of an intercept will be greater than the total number of trajectories from point *D* to point *B*. In order to avoid the double counting of trajectories, a different choice of intercepts will be made. We will consider intercepts perpendicular to the diagonal *DB*. This choice of intercepts determines the construction of trajectories that are unique. A proof of this statement will be given below [Eq. (3-3)].

The further consideration of the problem will be facilitated if we translate and rotate the coordinate system at 45° as shown in Figure 3-2 so that the X axis of the new system coincides with DB and the Y axis is parallel to the intercepts. The coordinates of point D in the new coordinate system are (0, 0). The coordinates of point B are (0, $2N$) where N is the number of horizontal/vertical lines of the dividing net. The trajectories from point D to point B represent a well known mathematical process – random walk with a step of +1 or -1. A step of +1 is a step forward which increases both the x and y coordinates with +1. A step of -1 is a step downward, which increases the x coordinate with +1 but decreases the y coordinate with -1. Examples of a step forward (+1) and a step downward (-1) are shown in Figure 3-2. It is shown in Appendix B (see also Feller[4]) that the number of trajectories connecting point D with point E, for instance, with coordinates $E_x = m$ and $E_y = r$ is

$$N_{D(0,0),E(m,r)} = \binom{m}{(m+r)/2} = \binom{m}{(m-r)/2} = \binom{m}{(m \pm r)/2}. \tag{3-1}$$

The last equality is written for compactness. It should also be pointed out that because each step changes both coordinates with 1, the coordinates of all points from the dividing net in the square $ABCD$ are either both odd or both even numbers, independent of the number of steps via which each point is reached from point D.

In Appendix B it is also shown that the number of trajectories connecting two points depends only on the difference between their coordinates. For instance, the number of trajectories from point E_1 with coordinates (x_1, y_1) to point E_2 with coordinates (x_2, y_2) equals the number of trajectories between point (0, 0) and point $(\underbrace{x_2 - x_1}_{m}, \underbrace{y_2 - y_1}_{r})$, i.e.,

$$N_{E_1(x_1,y_1),E_2(x_2,y_2)} = \binom{x_2 - x_1}{((x_2 - x_1) \pm (y_2 - y_1))/2} = \binom{m}{(m \pm r)/2}. \tag{3-2}$$

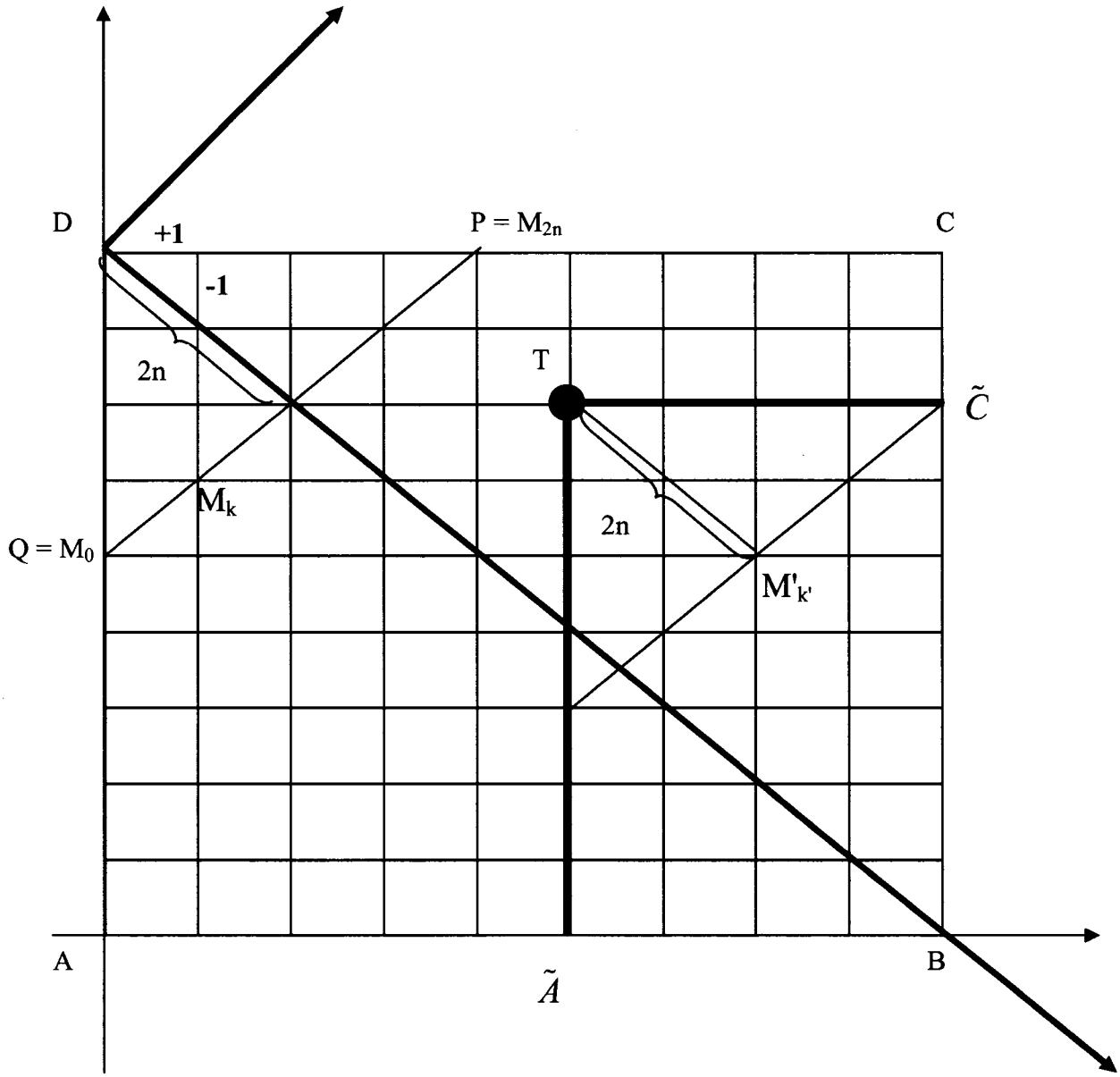

Figure 3-2: Plot assisting us in the determination of the number of curves from point D to point B passing through point M_k lying on the intercept PQ and also in the determination of the number of curves connecting an intermediate point T with the end point B passing through point $M'_{k'}$.

Let us consider now the intercept PQ as shown in Figure 3-2. We will consider points M_k from it that coincide with points from the dividing net and therefore are reachable from point D via the steplike trajectories discussed above. The number of these points is $2n+1$ ($k = 0, \ldots, 2n$) where n determines the position of the intercept along the X axis, $2n$ being the x coordinate of all points lying on it. The simulated density of curves passing through different points does not depend on the values of N and n, only the resolution of the picture depends on them. Therefore, the values of N and n are a matter of choice depending on the researcher, the desired resolution, and computational time. In this work we have chosen $N = 300$ and $n = 10$, based on these considerations. We have also tried other values of N and n and have noticed no significant difference in the results. Due to the obvious symmetry of the problem the y coordinate of point P is also $2n$, $P(2n, 2n)$ and the y coordinate of point Q is $(-2n)$, $Q(2n, -2n)$. Point M_k has coordinates $(2n, -2n+2k)$.

Based on Eqs. (3-1) and (3-2), we can calculate the number of trajectories from point D to point M_k, N_{D,M_k}, and also from point M_k to point B, $N_{M_k,B}$. The product $N_{D,M_k}.N_{M_k,B}$ gives the number of curves from point D to point B passing through point M_k. Since the set $Q, \ldots, M_k \ldots, P$ is the full set of points of the intercept PQ coinciding with points from the dividing net and because the trajectories through these points are unique due to the choice of the intercept, we expect that the sum $\sum_{k=0}^{2n} N_{D,M_k}.N_{M_k,B}$ should be equal to the total number of curves connecting points D and B, $N_{D,B}$:

$$N_{D,B} = \sum_{k=0}^{2n} N_{D,M_k}.N_{M_k,B} \Rightarrow \binom{2N}{N} = \sum_{k=0}^{2n} \binom{2n}{k}\binom{2N-2n}{N-k}. \tag{3-3}$$

Indeed, according to the well-known identity of Wandermond[5] the right-hand equation is fulfilled. Thus, we have proven the uniqueness of the trajectories passing through the chosen intercept. This uniqueness secures the simulation of trajectories with the correct density, which is the aim of this chapter.

The ratio $\binom{2n}{k}\binom{2N-2n}{N-k}\Big/\binom{2N}{N}$ gives the density of curves through point M_k or the probability that a curve passes through this point for each k=0, 1, 2, ..., $2n$. This probability happens to be the hypergeometric distribution. Naturally, each intercept is characterized by its own hypergeometric distribution depending on the value of n, i.e., depending on the position of the intercept along the x axis.

As will be shown below, it is necessary to determine the distribution of curves connecting intermediate points in the plane of square $ABCD$ with the end point B.

We will consider a set of intercepts lying at distance $2n$ from each other along the x axis as shown in Figure 3-2. Now we consider, for instance, a point T lying on the K^{th} intercept and having coordinates ($2nK$, $2R$). K and R determine the positions of the intercept and the point. The values of K and R are not chosen in the direct sense; they are the coordinates of the randomly realized point of passage at a certain step of the procedure of constructing the random curve. We have to examine only curves connecting point T and point B that lie in rectangle $\tilde{A}T\tilde{C}B$ (Figure 3-2) since only these curves are monotonically decreasing. We construct the intercept $P'Q'$ lying at distance $2n$ from point T and therefore having $2n$ + 1 points coinciding with points from the dividing net. Then, analogous to Eq. (3-3), we have:

$$N_{T,B}=\sum_{k'=0}^{2n}N_{T,M'_{k'}}.N_{M'_{k'},B}=\binom{2N-2nK}{N-nK+R}=\sum_{k'=0}^{2n}\binom{2n}{k'}\binom{2N-2nK-2n}{N-nK+R-k'} \tag{3-4}$$

where $M'_{k'}$ is a point from the intercept $P'Q'$ with coordinates ($2nK$+$2n$, $2R$-$2n$+$2k'$), (k' = 0, 1, ..., $2n$). This expression is only slightly modified in comparison to Eq. (3-3). The corresponding density of curves passing through point $M'_{k'}$ from the intermediate point T to point B is given by the ratio $\binom{2n}{k'}\binom{2N-2nK-2n}{N-nK+R-k'}\Big/\binom{2N-2nK}{N-nK+R}$.

3.3.2 Constructing a generator of random functions subject to the hypergeometric distribution. A random walk generator.

Each curve connecting points D and B is constructed via the generation of a number of points through which this curve passes. These points lie on intercepts positioned at equal distances ($2n$) from each other along the x axis in the plane of square $ABCD$. The first point after point D through which the trajectory passes lies on segment PQ (Figure 3-2). The point is chosen using a random number generator generating uniformly distributed numbers between 0 and 1. Let the random number generated be x. The point of passage is chosen through the assignment to the random number x a number L for which the following double inequality is fulfilled:

$$(3\text{-}5) \qquad \frac{\sum_{k=0}^{L-1}\binom{2n}{k}\binom{2N-2n}{N-k}}{\binom{2N}{N}} \prec x \leq \frac{\sum_{k=0}^{L}\binom{2n}{k}\binom{2N-2n}{N-k}}{\binom{2N}{N}}.$$

In this way, the uniformly distributed random numbers $0 \leq x \leq 1$ are transformed into numbers $0 \leq L \leq 2n$ distributed according to the hypergeometric distribution valid for intercept PQ characterized by n. Since the numbers L label the points M_k, the points along the intercept are also chosen according to this distribution. This is a standard procedure for creating random number generators subject to non-uniform distributions.[6]

At the next step, as well as at all steps afterwards, we must continue the trajectory starting from an intermediate point. We therefore have to choose the next point from an intercept positioned similarly to intercept $P'Q'$ (Figure 3-2). For this purpose, we assign to the uniformly distributed randomly chosen number x a number L' for which the following double inequality is fulfilled:

$$(3\text{-}6) \qquad \frac{\sum_{k=0}^{L'-1}\binom{2n}{k}\binom{2N-2nK-2n}{N-nK+R-k}}{\binom{2N-2nK}{N-nK+R}} \prec x \leq \frac{\sum_{k=0}^{L'}\binom{2n}{k}\binom{2N-2nK-2n}{N-nK+R-k}}{\binom{2N-2nK}{N-nK+R}}.$$

This inequality is similar to the one given by Eq. (3-5). However, it is modified accordingly to account for the changed position of the intercept. As explained in the previous subsection, R and K determine the coordinates of the intermediate point realized as a point of passage in the previous step. R and K, together with n, also determine the position of the next intercept. Thus the uniformly distributed random numbers $0 \le x \le 1$ are now transformed into numbers $0 \le L' \le 2n$ distributed according to the hypergeometric distribution valid for the corresponding intercept characterized by n, R, and K.

There exist two special cases which are fully examined in Appendix C.

Thus the construction of a generator of randomly chosen monotonically decreasing series/functions, which reflect the density of such functions in different points of the unit square, is completed. Because the theory of random walk was used for its creation, we call it a random walk generator.

3.4 Comparison of different generators

In Sec. 3.1 we mentioned two different generators of monotonically decreasing series of numbers that should also be considered. The algorithms used in these generators are outlined in this section.

3.4.1 Random number descent (Stavrev *et al.*[1])

In this case, pairs of random numbers are generated determining the x and y coordinates of a set of points in the unit square. However, not all points are recorded, but only these for which the y coordinate has a smaller value than the y coordinate of the previous point and the x coordinate has a value higher than the previous one. Once the values $x = 0.99$ and $y = 0.01$ are reached, the point B (1, 0) is automatically added. Thus a set of points determining a monotonically decreasing function/series is constructed.

3.4.2 Random angle - random step descent

This generator is illustrated in Figure 3-3. A random angle, $\alpha_i \in [0, -\pi/2]$, and a random step r_i are generated at each simulation to determine the next point of the monotonically decreasing series/function. The first point that is generated with coordinates outside of the unit square is automatically replaced with point *B*.

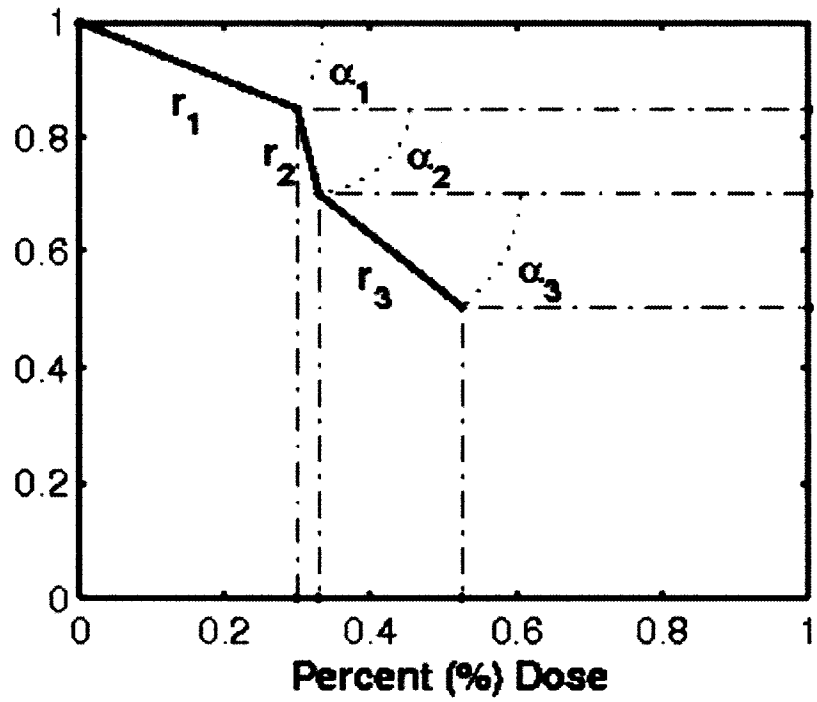

Figure 3-3: Illustration of the random angle - random step descent generator.

In both of the above mentioned random function generators, the point *B* (1, 0) was added artificially. However, since both procedures are intuitive and they are only meant to produce monotonically decreasing series, the artificial addition of point *B* to the generated DVH is of no particular importance.

In the remainder of this section, we investigate the applicability to DVH reverse mapping of these two intuitive generators and compare them to results from our random walk generator.

We used the DVH reverse mapping method in the previous chapter (and in Schinkel *et al.*[2]) to calculate adequate dose-volume constraints for the needs of inverse treatment planning. In that study,[2] an averaged DVH is calculated – for a given organ – from a set of DVHs, which resulted in $NTCP \in [4.5; 5.5]\%$. The NTCP is calculated according to the population based critical volume model[7-10] for each of the generated DVH curves. Subsequently, only DVH curves that result in $NTCP \in [4.5; 5.5]\%$ are selected. The average DVH is obtained as the arithmetic mean of the selected DVHs with respect to the relative volumes (i.e., the y values) of those points of passage that have the same x coordinate (i.e., dose).

In the previous chapter and the work of Schinkel *et al.*,[2] we suggest that the dose-volume constraints be chosen as points from this averaged DVH, because the resultant NTCPs would be in the same interval [4.5; 5.5]%.

To check the applicability of the simpler generators described above to the clinic, we decided to compare the averaged DVHs, produced by them, which result in $NTCP \in [4.5; 5.5]\%$ with the same averaged DVH produced by the random walk generator. Of course, it might also be possible to compare the 2-dimensional distributions of the DVH density produced by the different generators. However, since the dose-volume constraint points are to be chosen from the averaged DVHs, the clinical interest should lie in the generation of such averaged DVH curves. Therefore, a comparison between the generators, based on the averaged DVHs, might be more indicative of the differences and interchangeability of the generators for the clinic. In addition, if all the generators studied in this chapter or any pair of them would produce curves with equal density in the square they would also produce coinciding average curves, since these curves are the average of a subset of curves chosen under the same criterion for all generators. Thus, for this reason it is not necessary to compare 2-dimensional distributions of the DVH density produced by the different generators. It may be that the difference between the average curves (if it exists) depends on the chosen NTCP model and on the parameter values (as Figure 3-4 and Figure 3-5 indicate), but we are only interested in the existence or absence of such a difference indicative of whether or not the generators are interchangeable.

The investigation was carried out for four organs – liver, brain, bladder, and spinal cord and the results are shown in Figure 3-4. The dose is renormalized, that is, translated to absolute dose through multiplying the relative dose by a corresponding maximum dose for each organ. The parameter values for the calculation of the corresponding NTCPs according to the critical volume population NTCP model were

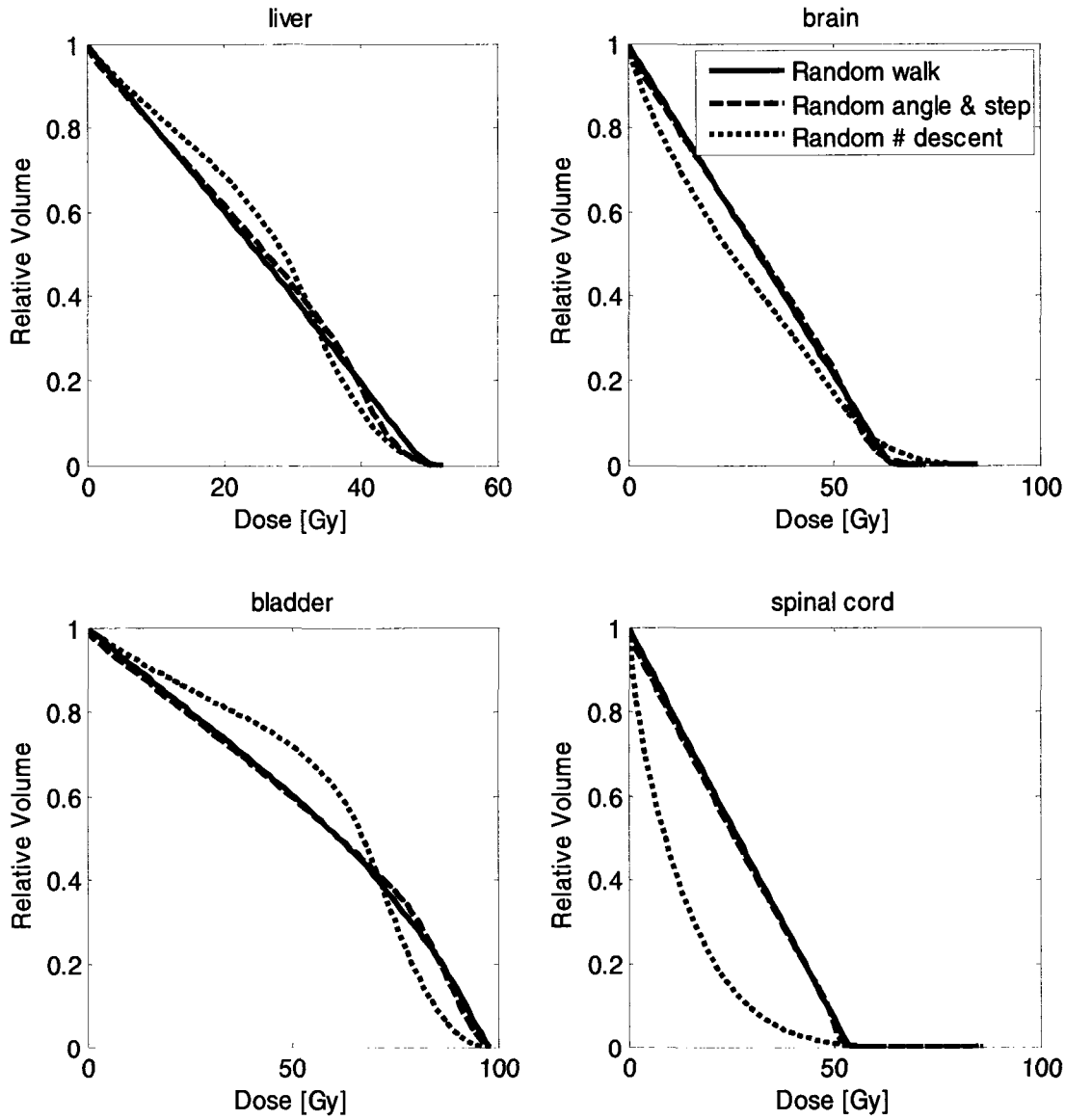

Figure 3-4: Comparison between the three different DVH generators according to the averaged DVH curves resulting in NTCP $\in [4.5; 5.5]\%$ for liver, brain, bladder and spinal cord.

taken from Stavrev *et al.*[11] Based on the graphs shown in Figure 3-4 one may conclude that the random angle generator produces averaged DVHs that are almost identical to the ones produced with the random walk generator. The random number descent generator, however, produces visibly different DVHs than the ones produced by the random walk generator.

In some cases, it may be possible to design a treatment that almost entirely spares part of an organ from irradiation (for example, the DVHs appearing in Coselmon *et al.*[12]). This organ sparing can be represented in a DVH generator by incorporating an initial, random, step downward. In order to include the case of partial organ irradiation, "hybrid" generators were constructed, which are based on the studied generators, in the following way: An initial random jump was used as a starting point to simulate a random part of the organ receiving no radiation and then the corresponding generator was used to complete the DVH generation for the rest of the organ receiving heterogeneous irradiation. A comparison was made of the averaged DVH curves produced by the three hybrid generators, for the same four organs – liver, brain, bladder, and spinal cord – and the results are shown in Figure 3-5. This figure shows that in the case of an initial jump, simulating partial organ irradiation, the averaged DVHs produced via the three generators differ from each other almost always.

The hybrid generators could be used for constraint point calculation in cases where it is possible to spare part of the organ. For cases where partial organ sparing is not possible, the generator could be used as-is, without the incorporation of an initial random step downward.

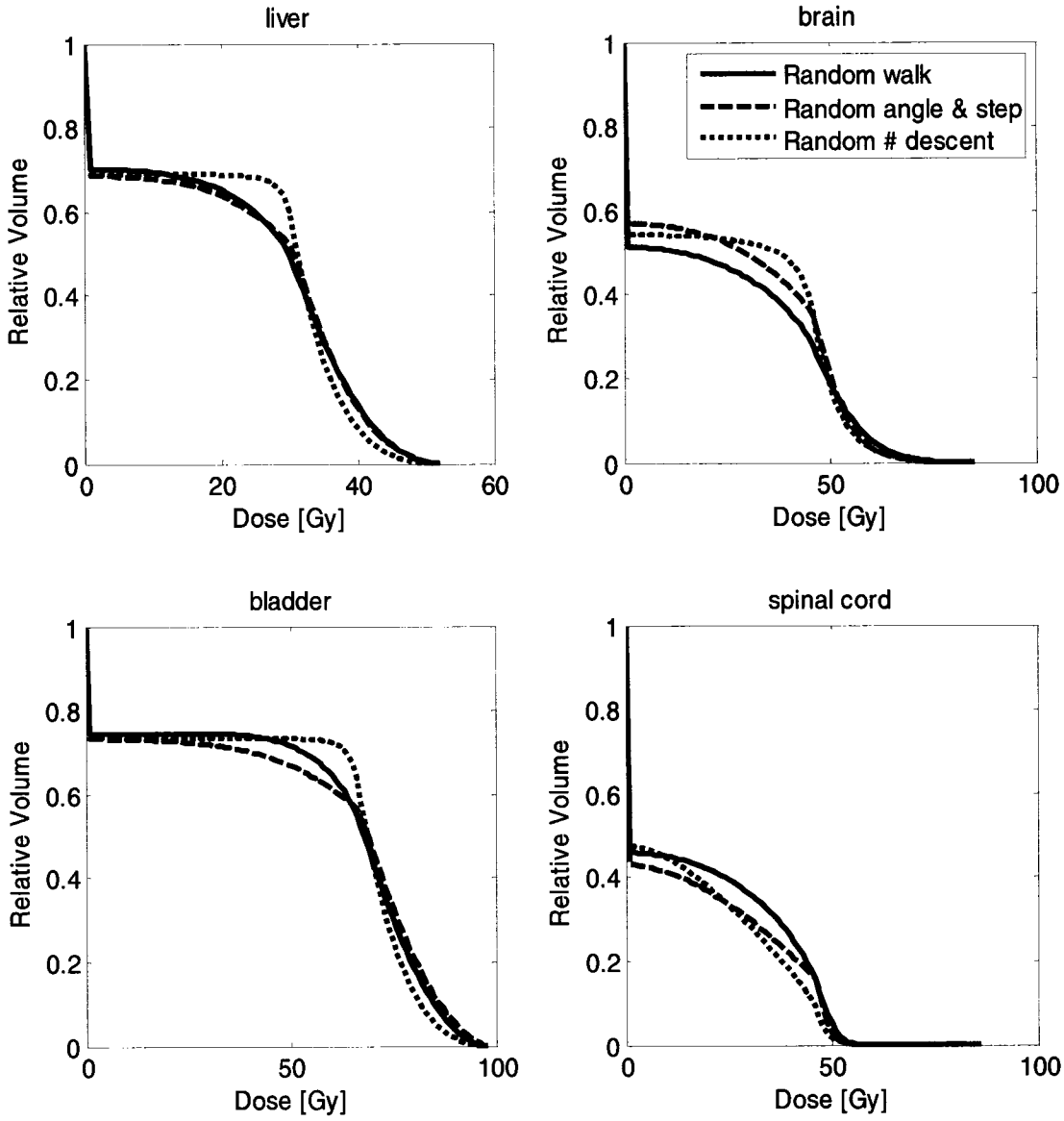

Figure 3-5: Comparison between the three hybrid DVH generators with initial jump simulating partial organ irradiation according to the averaged DVH curves resulting in NTCP $\in [4.5; 5.5]\%$ for liver, brain, bladder, and spinal cord.

3.5 Discussion and conclusions

It was theoretically determined that the distribution of the number of monotonically decreasing finite series passing through a point in the dose volume histogram space follows the hypergeometric distribution.

A generator of random monotonically decreasing series/functions called a random walk generator is constructed. The generator follows the hypergeometric distribution, which was found to describe the probability distribution of the DVHs in the dose-volume space. It is compared with two other intuitive random function generators. The random walk generator is used as a standard in this comparative study since the selection process based on this generator reflects the inherent density of monotonically decreasing functions in the unit square. The comparison is carried out with the purpose of exploring the goodness of the two simpler generators and the potential of using any of them in place of the more complex random walk generator. Based on the results of the comparison between the three random function generators investigated in this chapter, which show that there is a significant difference between the generators (Figure 3-4 and Figure 3-5), it can be concluded that neither of the two simpler generators can replace the random walk generator.

Because we suggest that the averaged DVH curve produced by a random function generator, that results in $\mathrm{NTCP} \in [4.5; 5.5]\%$, is to be used to determine the dose-volume constraints for use in the treatment planning optimization as described in the previous chapter and Schinkel *et al.*,[2] we conclude that it is of high importance to use the correct generator of DVH curves on the basis of which an average DVH resulting in $\mathrm{NTCP} \in [4.5; 5.5]\%$ will be constructed. Therefore, we recommend that the random walk generator be used for the generation of average DVH curves with a subsequent choice of dose-volume constraints.

3.6 References

1. P. Stavrev, N. Stavreva, D. Hristov, and B. G. Fallone, "Reverse mapping of normal tissue complication probabilities onto dose volume histogram space: Problem formulation, illustration, and implications", presented at the Proc. of World Congress on Medical Physics and Biomedical Engineering, Sydney 24 - 29 August, Australia, (2003).

2. C. Schinkel, P. Stavrev, N. Stavreva, and B. G. Fallone, "A theoretical approach to the problem of dose-volume constraint estimation and their impact on the dose-volume histogram selection," Med. Phys. **33**, 3444-3459 (2006).

3. C. Schinkel-Ranger, P. Stavrev, M. Weldon, N. Stavreva, R. Scrimger, and B. G. Fallone, "Reverse NTCP mapping and the problem of physical dose-volume constraint estimation", presented at the Cancer Research Across the Spectrum: National Meeting for Trainees, Mont Tremblant, Canada, (2005).

4. W. Feller, "*An Introduction to Probability Theory and its Applications*", (J. Wiley and Sons, New York, 1970).

5. J. Riordan, "*Combinatorial Identities*", (J. Wiley and Sons, New York, 1968).

6. W. H. Press, B. P. Flannery, S. A. Teukolsky, and W. T. Vetterling, "*Numerical Recipes in C*", (Cambridge University Press, Cambridge, MA, 1988).

7. A. Jackson, G. J. Kutcher, and E. D. Yorke, "Probability of radiation-induced complications for normal tissues with parallel architecture subject to non-uniform irradiation," Med Phys **20**, 613-625 (1993).

8. A. Niemierko and M. Goitein, "Modeling of normal tissue response to radiation: the critical volume model," Int J Radiat Oncol Biol Phys **25**, 135-145 (1993).

9. D. R. Olsen, B. K. Kambestad, and D. T. Kristoffersen, "Calculation of radiation induced complication probabilities for brain, liver and kidney, and the use of a reliability model to estimate critical volume fractions," Br J Radiol **67**, 1218-1225 (1994).

10. P. Stavrev, N. Stavreva, A. Niemierko, and M. Goitein, "Generalization of a model of tissue response to radiation based on the idea of functional subunits and binomial statistics," Phys Med Biol **46**, 1501-1518 (2001).

11. P. Stavrev, N. Stavreva, A. Niemierko, and M. Goitein, "The Application of Biological Models to Clinical Data," *Phys Medica* **XVII**, 71-82 (2001).

12. M. M. Coselmon, J. M. Moran, J. D. Radawski, and B. A. Fraass, "Improving IMRT delivery efficiency using intensity limits during inverse planning," Med Phys **32**, 1234-1245 (2005).

Chapter 4 Analytical investigation of properties of the iso-NTCP envelope

A version of this chapter was published as:

P. Stavrev, C. Schinkel, N. Stavreva, K. Markov, B. G. Fallone, "Analytical investigation of properties of the iso-NTCP envelope," Radiol. Oncol. **41**(1), 41 – 47 (2007)

4.1 Introduction

In Chapter 2 we proposed that the DVH averaged from those resulting in a certain normal tissue complication probability (NTCP) can be used as a source of dose-volume constraints for inverse planning.[1,2] Constraint points were estimated for a number of organs using two NTCP models – the Lyman model[3] with the parameters of Burman *et al.*[4] and the critical volume population model[5] with the parameters of Stavrev *et al.*[6] We also reported an observed property of the integral dose-volume histogram (DVH) space.[1,2] In those reports we constructed a curve, which we called an α-iso-NTCP envelope, by connecting points belonging to step-like integral DVHs. Each of these DVHs corresponded to homogeneous partial organ irradiation of a relative volume v_k to dose D_k such that, for each DVH, the resulting NTCP had a particular value α. We numerically demonstrated that any DVH passing through a point (D_k, v_k) from the α-iso-NTCP envelope, i.e., any DVH that is tangential to or crosses the envelope, will result in $NTCP \geq \alpha$. It should be emphasized that the equality is valid only for the step-like DVH that corresponds to the homogeneous partial organ irradiation of v_k to D_k. In this chapter,

we prove this property of the iso-NTCP envelope analytically for the three most commonly used NTCP models – the Lyman model, the individual critical volume model and the population critical volume model.

4.2 Proof for the Lyman model

For our purposes, a normalized integral DVH is defined as a monotonically decreasing function characterized by the set of points $D_i, v_i : i = 1,...,N$ such that $v_1 = 1$, $v_{N+1} = 0$, $v_{i+1} < v_i$, $D_i < D_{i+1}$.

We begin this proof for the Lyman[3] NTCP model:

$$NTCP = \Phi\left(\frac{EUD - D_{50}}{mD_{50}}\right);$$

$$\Phi(x) = \frac{1}{\sqrt{2\pi}} \int_{-\infty}^{x} \exp\left(\frac{-t^2}{2}\right) dt = \frac{1}{2}\left[1 + erf\left(\frac{x}{\sqrt{2}}\right)\right], \tag{4-1}$$

where m and D_{50} are model parameters, and EUD is the equivalent uniform dose, which will be defined later. It is clear from Eq. (4-1) that NTCP is a monotonically increasing function of EUD. Thus, for two arbitrary EUDs, if $EUD_1 > EUD_2$, then it follows that $NTCP(EUD_1) > NTCP(EUD_2)$.

Consider an arbitrary integral DVH, with points (D_i, v_i: $i = 1, \ldots, N$), that passes through the point (D_k, v_k) on the α-iso-NTCP envelope (Figure 4-1). The EUD of this arbitrary DVH will be referred to as EUD. Now consider a step-like DVH that also passes through the same point. This step-like DVH has an NTCP of α. If we call the EUD of this DVH EUD_α, then we may write that $NTCP(EUD_\alpha) = \alpha$. According to our observation,[2] the NTCP of the arbitrary DVH that passes through a point on the α-iso-NTCP envelope will be greater than α:

$$NTCP(EUD) > NTCP(EUD_\alpha) = \alpha. \tag{4-2}$$

Because of the monotonic nature of NTCP as a function of EUD, this statement is true, if and only if,

$$EUD > EUD_\alpha \ . \tag{4-3}$$

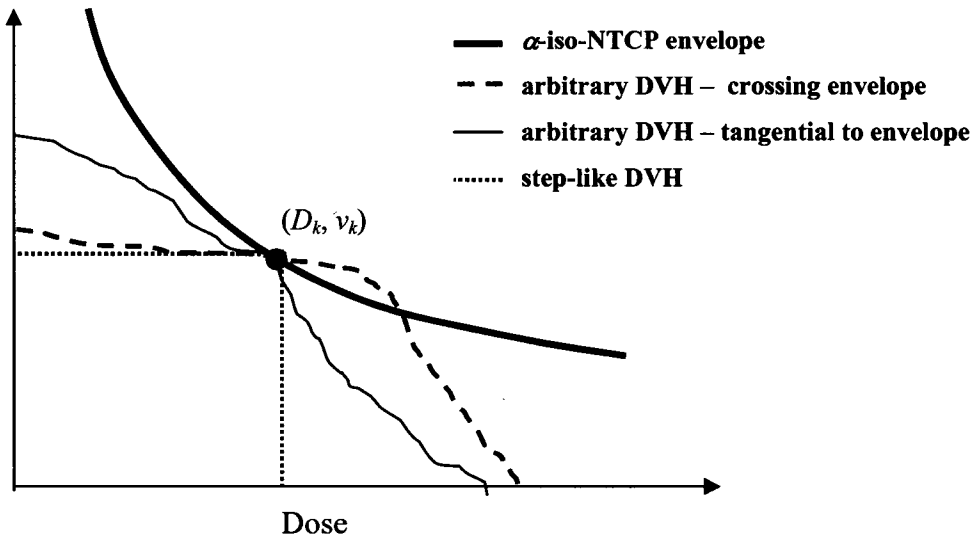

Figure 4-1: Illustration of an α-iso-NTCP envelope and two arbitrary DVH curves – one that crosses the envelope at the point (D_k, v_k) and one that is tangential to the envelope at the same point. Also shown is a step-like DVH passing through (D_k, v_k) that corresponds to homogeneous partial organ irradiation. The NTCP of the step-like DVH should be equal to α, while the NTCP for both arbitrary DVHs should be greater than α.

Therefore, if we can show that $EUD > EUD_\alpha$, then Eq. (4-2) is also true.

To calculate *EUD*, the integral DVHs must be converted into differential DVHs. In the case of homogeneous partial organ irradiation of volume v_k to a dose D_k, the integral and the differential DVHs are determined solely by the pair (v_k, D_k). For any other type of irradiation, the corresponding differential DVH is given by the following set of points: ($v_i - v_{i+1}$, D_i).

One of the commonly accepted forms of *EUD* is the one given by the generalized mean dose (*GMD*):[7-9]

$$EUD = GMD = \left(\sum_i (v_i - v_{i+1}) D_i^{1/a} \right)^a, \tag{4-4}$$

where a is a volume parameter. For the case of partial organ irradiation of the volume v_k to dose D_k, Eq. (4-4) simplifies to:

(4-5) $$EUD_\alpha = \left(v_k D_k^{1/a}\right)^a = v_k{}^a D_k .$$

For the arbitrary DVH passing through point (D_k, v_k), the *EUD* may be written as:

$$EUD = \left(\sum_{i=1}^{N} (v_i - v_{i+1}) D_i^{1/a} \right)^a$$

(4-6) $$= \left(\sum_{i=1}^{k-1} (v_i - v_{i+1}) D_i^{1/a} + (v_k - v_{k+1}) D_k^{1/a} + \sum_{i=k+1}^{N} (v_i - v_{i+1}) D_i^{1/a} \right)^a$$

To prove Eq. (4-3), we have to prove, from Eqs. (4-5) and (4-6), that the following inequality is valid:

$$EUD_\alpha < EUD \Rightarrow$$

(4-7) $$\left(v_k D_k^{1/a}\right)^a < \left(\sum_{i=1}^{k-1} (v_i - v_{i+1}) D_i^{1/a} + (v_k - v_{k+1}) D_k^{1/a} + \sum_{i=k+1}^{N} (v_i - v_{i+1}) D_i^{1/a} \right)^a .$$

Taking each side of Eq. (4-7) to the power of $1/a$, we obtain:

(4-8) $$v_k D_k^{1/a} < \sum_{i=1}^{k-1} (v_i - v_{i+1}) D_i^{1/a} + (v_k - v_{k+1}) D_k^{1/a} + \sum_{i=k+1}^{N} (v_i - v_{i+1}) D_i^{1/a} ,$$

which can then be written as:

(4-9) $$v_{k+1} D_k^{1/a} < \sum_{i=1}^{k-1} (v_i - v_{i+1}) D_i^{1/a} + \sum_{i=k+1}^{N} (v_i - v_{i+1}) D_i^{1/a} .$$

We now proceed by proving that Eq. (4-9) is true.

First, consider the term $v_{k+1} D_k^{1/a}$ in Eq. (4-9). It may be re-written as:

$$v_{k+1} D_k^{1/a} = (v_{k+1} - v_{k+2}) D_k^{1/a} + (v_{k+2} - v_{k+3}) D_k^{1/a} + \ldots + (v_N - v_{N+1}) D_k^{1/a}$$

(4-10) $$= \sum_{i=k+1}^{N} (v_i - v_{i+1}) D_k^{1/a}$$

where, by definition, $v_{N+1} = 0$.

We can expand the second sum in Eq. (4-9):

(4-11) $$\sum_{i=k+1}^{N} (v_i - v_{i+1}) D_i^{1/a} = (v_{k+1} - v_{k+2}) D_{k+1}^{1/a} + (v_{k+2} - v_{k+3}) D_{k+2}^{1/a} + \ldots + (v_N - v_{N+1}) D_N^{1/a} .$$

According to our definition of the integral DVH, $D_i < D_{i+1}$ for all $i = 1 \ldots N$. Therefore, each term of the sum in Eq. (4-10) is less than the corresponding term in Eq. (4-11), and we can write:

$$v_{k+1}D_k^{1/a} < \sum_{i=k+1}^{N}(v_i - v_{i+1})D_i^{1/a} . \quad (4\text{-}12)$$

Because of our definition of an integral DVH, $v_i > v_{i+1}$ for all $i = 1...N$, the first sum in Eq. (4-9) is greater than zero:

$$\sum_{i=1}^{k-1}(v_i - v_{i+1})D_i^{1/a} > 0 . \quad (4\text{-}13)$$

From Eqs. (4-12) and (4-13), the following is true:

$$v_{k+1}D_k^{1/a} < \sum_{i=1}^{k-1}(v_i - v_{i+1})D_i^{1/a} + \sum_{i=k+1}^{N}(v_i - v_{i+1})D_i^{1/a} , \quad (4\text{-}14)$$

which is identical to Eq. (4-9). Thus, we have proven Eq. (4-9), which is equivalent to Eq. (4-7), and thus, Eq. (4-3). Therefore, Eq. (4-2) is also true, and we have thus mathematically proven the property of the envelope for the Lyman model.

4.3 Proof for the critical volume NTCP model

The basic property of the α-iso-NTCP envelope will be proven for the critical volume (CV) NTCP model in this section. The CV model exists in two forms – individual and population models.

The individual CV model is given by:

$$NTCP_{ind} = \Phi\left[\frac{\sqrt{N_{FSU}}(\bar{\mu}_d - \mu_{cr})}{\sigma_{\mu_d}}\right], \quad (4\text{-}15)$$

where N_{FSU} is the total number of functional subunits (FSUs) comprising the organ, $\bar{\mu}_d$ is the mean relative damaged volume, σ_{μ_d} is the variance in $\bar{\mu}_d$, and μ_{cr} is the relative critical volume of the organ.[5,10,11]

The population CV model, under the assumption that only the relative critical volume displays inter-patient variability, is given by:

$$NTCP_{pop} = \Phi\left[\frac{-\ln(-\ln\bar{\mu}_d) + \ln(-\ln\bar{\mu}_{cr})}{-\sigma_{\mu_{cr}}/\bar{\mu}_{cr}\ln\bar{\mu}_{cr}}\right], \quad (4\text{-}16)$$

where $\bar{\mu}_{cr}$ is the population mean relative critical volume and $\sigma_{\mu_{cr}}$ is the variance in $\bar{\mu}_{cr}$.[5]

As can be seen in Eqs. (4-15) and (4-16), both the individual and the population CV models are monotonically increasing functions of the mean relative damaged volume $\overline{\mu}_d$. This quantity is given by the following sum:

(4-17) $$\overline{\mu}_d = \sum_i (v_i - v_{i+1}) P_{FSU}(D_i),$$

where $P_{FSU}(D_i)$ is the probability that a functional subunit is damaged beyond repair. It, in turn is given by:

(4-18) $$P_{FSU}(D_i) = \exp[-N_c \exp(-\alpha_c D_i)],$$

where N_c is the number of cells in an FSU and α_c is the cell radiosensitivity. The quantity $\exp(-\alpha_c D)$ is the probability that a cell survives an irradiation to dose D. Because α_c is a positive quantity, $\exp(-\alpha_c D)$ is a decreasing function of dose. The term $N_c \exp(-\alpha_c D)$ is the mean number of cells that survive dose D and also decreases as D increases. Equation (4-18) is the probability that a functional subunit is damaged beyond repair, which is equivalent to the probability that all cells in the subunit are destroyed. Therefore, $\exp(-N_c e^{-\alpha_c D})$, which is the probability of zero cell survivals, increases with decreasing mean number of cell survivals, $N_c \exp(-\alpha_c D)$, or increasing dose D.

We now compare the mean relative damaged volume caused by an arbitrary DVH that is tangential to or is crossing the α-iso-NTCP envelope at point (D_k, v_k) with the mean relative damaged volume caused by a step-like DVH given by (D_k, v_k). From Eq. (4-17), the mean relative damaged volume for the arbitrary DVH passing through the point (D_k, v_k) on the α-iso-NTCP envelope is:

(4-19)
$$\begin{aligned}\overline{\mu}_d &= \sum_{i=1}^{N} (v_i - v_{i+1}) P_{FSU}(D_i) \\ &= \sum_{i=1}^{k-1} (v_i - v_{i+1}) P_{FSU}(D_i) + (v_k - v_{k+1}) P_{FSU}(D_k) + \sum_{i=k+1}^{N} (v_i - v_{i+1}) P_{FSU}(D_i)\end{aligned}$$

The mean relative damaged volume caused by partial organ homogeneous irradiation of relative volume v_k to dose D_k will be denoted as $\overline{\mu}_{d,\alpha}$ and is given by:

(4-20) $$\overline{\mu}_{d,\alpha} = v_k P_{FSU}(D_k).$$

We now compare $\overline{\mu}_d = \sum_{i=1}^{N}(v_i - v_{i+1})P_{FSU}(D_i)$ [Eq. (4-19)], containing point (D_k, v_k), with $\overline{\mu}_{d,\alpha} = v_k P_{FSU}(D_k)$ [Eq. (4-20)]. Since $P_{FSU}(D)$ is an increasing function of dose, Eqs. (4-19) and (4-20) are similar to the *EUD* form of Eq. (4-4) from the Lyman model. By applying the same process as to the proof of Eq. (4-7) it can be shown that the following inequality is valid:

(4-21) $$\overline{\mu}_d = \sum_{i=1}^{N}(v_i - v_{i+1})P_{FSU}(D_i) > \overline{\mu}_{d,\alpha} = v_k P_{FSU}(D_k).$$

Given that NTCP is an increasing function of the mean relative damaged volume, it follows that $NTCP(\overline{\mu}_d) > NTCP(\overline{\mu}_{d,\alpha}) = \alpha$ for DVHs having a common point with the α-iso-NTCP envelope.

4.4 Discussion and conclusions

Because we have proven that the discussed property of the α-iso-NTCP envelope applies to three of the most commonly used NTCP models – the Lyman model, the critical volume individual model, and the critical volume population model – there is reason to believe that this property may be model-independent.

The α-iso-NTCP envelope divides the dose-volume space in two sub-spaces. For the sub-space above the envelope, we have analytically proven that all DVH curves with at least one point in this region result in NTCP > α. For the sub-space under the envelope, it was numerically demonstrated elsewhere[2] that there exist DVH curves that result in a NTCP < α. However, as it is shown above, there do exist other curves, for example, those that are tangential to the envelope from below, which result in NTCP > α. Nevertheless, because there is a chance that a DVH lying under the α-iso-NTCP envelope will result in a NTCP less than α, one can conclude that it would be preferable in the treatment optimization process to seek solutions for DVHs lying entirely under an iso-NTCP envelope and avoid those that lie even partially above the envelope.

The physical dose-volume constraint points calculated in Chapter 2 and Schinkel *et al.*[2] were found to be dependent on the NTCP model as well as the parameters used for their determination. The iso-NTCP envelope could be used to estimate the impact of a change of NTCP model and/or parameters on the calculated constraint points for a given organ, since the envelope curve is dependent on both of these quantities. Dawson *et al.*[12] observed that the iso-NTCP curve corresponding to their liver parameters for the Lyman[3] model was shifted considerably to the right in DVH space compared to the iso-NTCP curve corresponding to the Burman *et al.*[4] parameters for the same organ. To estimate how the source of dose-volume constraints (the average of DVHs with a certain NTCP) would change with a change of NTCP parameter values, one could calculate the iso-NTCP envelope corresponding to these new parameters. The distance in DVH space between the old and new iso-NTCP curves is approximately the same as the distance between the old and new averaged DVHs. The position of the new dose-volume constraints could then be estimated by shifting them in DVH space by an amount equal to the distance between the two iso-NTCP curves. In this way, one can avoid having to perform an extensive recalculation of the dose-volume constraints.

4.5 References

1. C. Schinkel-Ranger, P. Stavrev, N. Stavreva, M. Weldon, R. Scrimger, and B. G. Fallone, "On the dose-volume constraints based on radiobiological considerations", presented at the AAPM 47th Annual Meeting, Seattle, WA, (2005).

2. C. Schinkel, P. Stavrev, N. Stavreva, and B. G. Fallone, "A theoretical approach to the problem of dose-volume constraint estimation and their impact on the dose-volume histogram selection," Med. Phys. **33**, 3444-3459 (2006).

3. J. T. Lyman, "Complication probability as assessed from dose-volume histograms," Radiat Res Suppl **8**, S13-19 (1985).

4. C. Burman, G. J. Kutcher, B. Emami, and M. Goitein, "Fitting of normal tissue tolerance data to an analytic function," Int J Radiat Oncol Biol Phys **21**, 123-135 (1991).

5. P. Stavrev, N. Stavreva, A. Niemierko, and M. Goitein, "Generalization of a model of tissue response to radiation based on the idea of functional subunits and binomial statistics.," Phys Med Biol **46**, 1501-1518 (2001).

6. P. Stavrev, N. Stavreva, A. Niemierko, and M. Goitein, "The Application of Biological Models to Clinical Data," *Phys Medica* **XVII**, 71-82 (2001).

7. A. Niemierko, "Reporting and analyzing dose distributions: a concept of equivalent uniform dose," Med Phys **24**, 103-110. (1997).

8. A. Niemierko, "A generalized concept of Equivalent Uniform Dose", presented at the 41th AAPM Annual Meeting, Nashville, (1999).

9. P. Stavrev, D. Hristov, and E. Sham, "IMRT Inverse Treatment Planning Optimization Based on Physical Constraints and Biological Objectives", presented at the 47nd Annual General Meeting of the Canadian Organization of Medical Physicists (COMP), Kelowna, BC, Canada, (2001).

10. A. Jackson, G. J. Kutcher, and E. D. Yorke, "Probability of radiation-induced complications for normal tissues with parallel architecture subject to non-uniform irradiation," Med Phys **20**, 613-625 (1993).

11. A. Niemierko and M. Goitein, "Modeling of normal tissue response to radiation: the critical volume model," Int J Radiat Oncol Biol Phys **25**, 135-145 (1993).

12. L. A. Dawson, D. Normolle, J. M. Balter, C. J. McGinn, T. S. Lawrence, and R. K. Ten Haken, "Analysis of radiation-induced liver disease using the Lyman NTCP model," Int J Radiat Oncol Biol Phys **53**, 810-821 (2002).

Chapter 5 Functional form comparison between the population and the individual Poisson based TCP models

A version of this chapter has been accepted for publication:

C. Schinkel, N. Stavreva, P. Stavrev, M. Carlone, B. G. Fallone, "Functional form comparison between the population and the individual Poisson based TCP models," Radiol. Oncol. **41**(2), 90-98 (2007)

5.1 Introduction

In the decades following the introduction of the first individual TCP model by Munro and Gilbert,[1] the distinction between the individual and population response has often been disregarded and individual TCP models have been fit to clinical datasets. The necessity of describing the impact of population heterogeneity on dose-response has led to the development, by a number of authors, of population-based tumour control probability (TCP) models.[2-5]

It has been shown that the presence of population heterogeneity leads to a dose-response curve that is flattened relative to the individual dose-response curve. If an individual TCP model is fit to a population dataset, the biological meaning of the parameter estimates is lost – the radiobiological parameters take on unrealistically low values.[6] Nevertheless, although it is conceptually incorrect, the individual TCP model has been fit to clinical datasets and parameters obtained from these fits have been assumed to have radiobiologically meaningful values.[4,7-10] On the other hand, it has also been shown that these fits are characterized by an acceptable goodness of fit.

It has been expected that the population TCP models would allow for the estimation of biologically meaningful population parameters. Unfortunately, it is impossible to obtain a unique set of parameter values when a population TCP model is fit to clinical data.[6,11] This is due to the fact that different sets of population parameter values produce almost identical TCP curves. Carlone *et al.*[11] analytically demonstrated that when the dominant source of inter-patient heterogeneity is that of tumour radiosensitivity, the population TCP function has only two independent parameters – the dose at 50% TCP, D_{50}, which determines the position of the TCP curve, and the normalized slope of the curve, γ_{50}. These parameters have geometric meaning. Since it is also true that the individual TCP model may be expressed in terms of the same two parameters,[3,12] it is possible that, for a given range of parameter values, both models will exhibit almost identical functional form. In this chapter, we investigate the similarities between these two models expressed in terms of D_{50} and γ_{50} by plotting them for identical values of these geometric parameters.

5.2 Background and method

The general form of the population-based Poisson TCP model has eight parameters. However, it has previously been shown[6,11] that the parameters of such a model are interrelated; many different combinations of parameters lead to one and the same TCP curve. Thus, it may seem difficult to directly compare the functional forms of the individual and population-based TCP models. On the other hand, Carlone *et al.*[6,11] have specified (based on a certain approximation, but a clinically valid one) what these interrelations actually are, and have shown that there are only two independent population model parameters – D_{50} and γ_{50}. Fortunately, the individual Poisson-based TCP model can also be parameterized by these two parameters. This fact makes the comparison of both models an easier task.

5.2.1 The Poisson-based individual TCP model

This common form of the individual TCP model is based on Poisson statistics combined with a simplified description of clonogen repopulation.[4,10,11,13-26] In the case where a tumour undergoes homogeneous irradiation to a total dose D, split into n fractions with equal dose per fraction, d, the individual Poisson TCP model may be written as:[11]

$$TCP_{ind} = e^{-N_S} = \exp\left[-N_0 e^{-(\alpha+\beta d)D+\lambda T}\right] = \exp\left[-N_0 e^{-\left(\alpha+\beta d-\frac{\lambda'}{d}\right)D}\right] = \exp\left[-N_0 e^{-\alpha' D}\right], \tag{5-1}$$

where N_0 is the initial number of clonogens, N_S is the mean number of surviving clonogens following the treatment, α and β are the linear quadratic (LQ) radiosensitivity parameters, λ is the tumour repopulation rate, T is the total treatment time and $\lambda' = \lambda\frac{T}{n}$. Note that as long as an equal dose is given during each fraction of the treatment (as is common clinical practice), the parameters α, β and λ' can be combined into one single parameter:

$$\alpha' = \alpha + \beta d - \frac{\lambda'}{d}. \tag{5-2}$$

The validity of the Poisson TCP model was questioned by Tucker and Travis,[21] and others[27-31] who explored the non-Poisson nature of the TCP in the case where tumour repopulation occurs. Under certain conditions, however, it has been shown[27,32] that the distribution of the number of clonogen cells remaining at the end of a treatment is well-approximated by the Poisson distribution. In view of these results, and also because of the relative complexity of the non-Poissonian TCP models, the individual TCP function presented in Eq. (5-1) is often used.

A form of the individual TCP model[3,12] that is equivalent to Eq. (5-1), but written in terms of the geometric parameters, γ_{50} and D_{50}, is given by:

(5-3) $$TCP_{ind} = 0.5^{\exp\left[\frac{2\gamma_{50}}{\ln 2}\left(1-\frac{D}{D_{50}}\right)\right]}.$$

The notion of normalized slope, γ, was first introduced by Brahme[33] for the purpose of dosimetric precision quantification. Later, Kallman *et al.*[34] used the maximum value of γ at the inflection point of the TCP curve and derived an expression similar to Eq. (5-3), but, as pointed out by Bentzen and Tucker,[35] a slight inconsistency is present in their formula. In general, the Poisson TCP expression given by Eq. (5-1), may be transformed and parameterized in terms of the normalized slope γ_f at any dose point D_f:

(5-4) $$TCP_{ind} = f^{\exp\left[\frac{-\gamma_f}{f\ln f}\left(1-\frac{D}{D_f}\right)\right]}.$$

From Eqs. (5-1) and (5-4), the following relationships between the two different sets of parameters (γ_f, D_f) and (N_0, α') may be derived:

(5-5) $$D_f = \frac{1}{\alpha'}\ln\left(\frac{-N_0}{\ln f}\right)$$

(5-6) $$\gamma_f = -f\ln f\ln\left(\frac{-N_0}{\ln f}\right).$$

and for (γ_{50}, D_{50}) in particular:

(5-7) $$D_{50} = \frac{1}{\alpha'}\ln\left(\frac{N_0}{\ln 2}\right)$$

(5-8) $$\gamma_{50} = \frac{\ln 2}{2}\ln\left(\frac{N_0}{\ln 2}\right).$$

5.2.2 The population-based TCP model

Carlone *et al.*[11] showed that the population TCP model for the case of dominant heterogeneity in radiosensitivity may be written as:

(5-9) $$TCP_{pop} = \frac{1}{2}erfc\left[\sqrt{\pi}\,\gamma_{50}\left(\frac{D_{50}}{D}-1\right)\right].$$

The parameters in Eq. (5-9) – D_{50} and γ_{50} – have the same geometric meaning as the corresponding parameters in Eq. (5-3). The geometric parameters may be expressed in terms of the population-based radiobiological parameters, $\overline{\alpha'}$, σ' and $\overline{\ln N_0}$:[11]

$$D_{50} = \frac{\Gamma + \overline{\ln N_0}}{\overline{\alpha'}} \tag{5-10}$$

$$\gamma_{50} = \frac{\overline{\alpha'}}{\sqrt{2\pi}\sigma'}. \tag{5-11}$$

Here $\overline{\alpha'} = \overline{\alpha} + \overline{\beta}d + \frac{\overline{\lambda'}}{d}$ and $(\sigma')^2 = \sigma_\alpha{}^2 + d^2\sigma_\beta{}^2 + \frac{\sigma_{\lambda'}{}^2}{d^2}$ where $\overline{\alpha}$, $\overline{\beta}$, $\overline{\lambda'}$ and $\overline{\ln N_0}$ are the population averages of the corresponding individual parameters and σ_α, σ_β, $\sigma_{\lambda'}$ and $\sigma_{\ln N_0}$ are their standard deviations. The symbol Γ represents Euler's gamma constant, which has an approximate value of 0.577.

The general form of the Carlone *et al.*[11] population TCP model takes both heterogeneity in radiosensitivity and heterogeneity in clonogen number into account. However, this form of the model has three parameters, and was shown[11] to be almost identical to the one that only takes heterogeneity in radiosensitivity into account. Hence, the latter will be used for this analysis.

5.2.3 Functional form comparison between individual and population-based TCP models

Since both the individual and the population TCP models may be written in terms of the same two parameters, γ_{50} and D_{50}, it seems natural to assume that the two models may display similarity in functional form. In order to explore the functional similarity of these models, Eqs. (5-3) and (5-9) are evaluated for a given range of γ_{50} and D_{50} values. Subsequently, the individual and population TCP curves obtained for equal sets of γ_{50} and D_{50} values are plotted for visual comparison.

The functional closeness of the individual and the population TCP curves may be more rigorously estimated by calculating the normalized difference between the areas under the two TCP curves,

$$\frac{\Delta A}{A_{TCP_{pop}}}(\gamma_{50}) = \frac{\left(A_{TCP_{pop}} - A_{TCP_{ind}}\right)}{A_{TCP_{pop}}}, \tag{5-12}$$

as a function of γ_{50}.

5.3 Results

The individual and the population TCP curves were calculated according to Eqs. (5-3) and (5-9) for values of the parameters γ_{50} and D_{50} reported by Okunieff *et al.*[36] Based on their estimates of γ_{50}, we chose a range of $\gamma_{50} \in [0.5, 6]$. These authors also reported a mean D_{50} for all tumours investigated in their work of 50 Gy, with values ranging from 10 to 90 Gy. We therefore chose a value of D_{50} = 50 Gy for our investigation.

Figure 5-1 shows eight pairs of individual and population TCP curves calculated for the following parameter values: D_{50} = 50 Gy and γ_{50} = [0.5, 1, 1.5, 2, 2.5, 3, 4, 6]. This figure was reproduced for different values of D_{50}, to determine whether this parameter had any influence on functional equivalency. The location of the TCP curves along the dose-axis did not influence their positions relative to each other or the shapes of the curves. Hence, the results shown in Figure 5-1 are transferable to any D_{50} value.

The quantity $\frac{\Delta A}{A_{TCP_{pop}}}(\gamma_{50})$ [Eq. (5-12)] is plotted in Figure 5-2. The largest area difference between the two TCP curves is -17.7% at γ_{50} = 0.5.

Next, we investigated the impact of the slope of the observed clinical dose response on model interpretation. For this purpose, we constructed a comparative table of the biological parameter values for each of the two studied TCP models that correspond to a dose response curve characterized by given geometric parameter values.

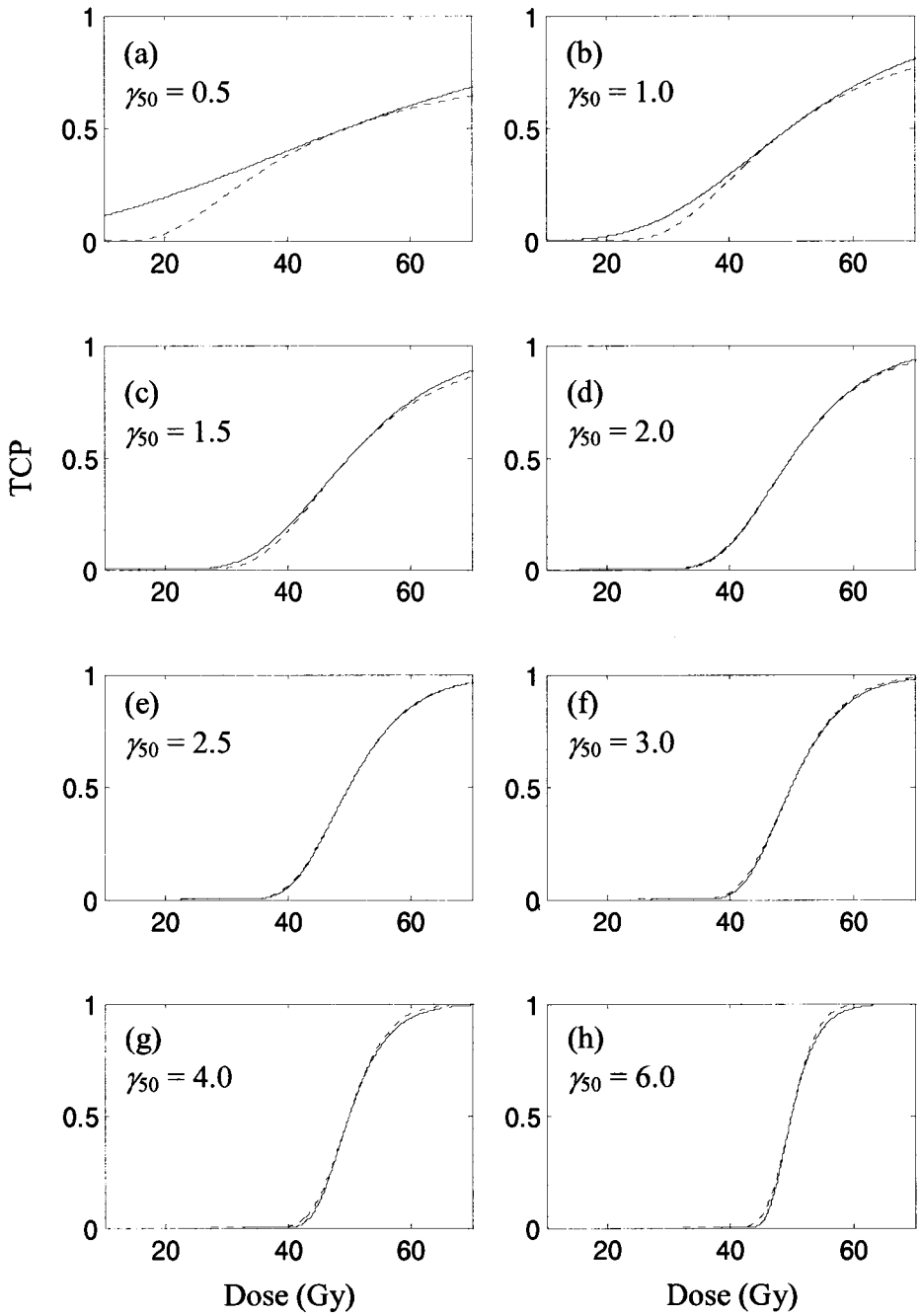

Figure 5-1: Individual (solid) and population-averaged (dotted) TCP curves for D_{50} = 50 Gy and the γ_{50} values shown in each sub-plot.

The individual parameters, α' and N_0, were calculated from Eqs. (5-5) and (5-6) for the D_{50} and γ_{50} values used to generate the graphs in Figure 5-1. We also calculated the values of the population parameters $\overline{\alpha'}$ and σ' for an assumed value of $\overline{N_0}$, using Eqs. (5-10) and (5-11). For this purpose, we chose an average clonogen number of $\overline{N_0} = 10^8$. The results are shown in Table 5-1.

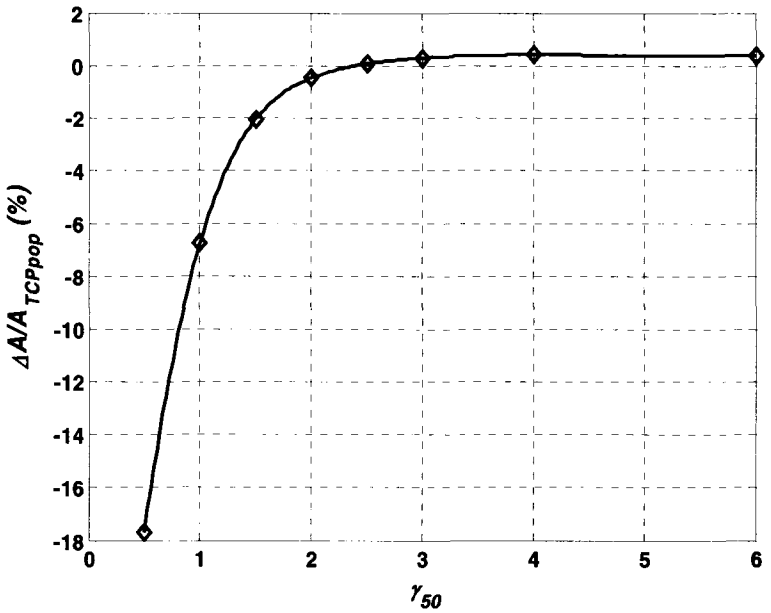

Figure 5-2: The ratio of the area difference, $\Delta A = A_{TCPpop} - A_{TCPind}$, between the two TCP curves, to the total area under the population TCP curve (A_{TCPpop}), plotted for the values of γ_{50} used to generate the curves shown in Figure 5-1.

Table 5-1: Individual parameters (α' and N_0) calculated for the γ_{50} values listed and D_{50} = 50 Gy. A set of population-based parameters ($\overline{\alpha'}$, σ'), calculated for the same values of γ_{50} and D_{50}, is also listed. The population-based parameters were calculated assuming a value of $\overline{N_0} = 10^8$ for the average number of clonogens.

γ_{50}	α' (Gy^{-1})	N_0	$\overline{\alpha'}$ (Gy^{-1})	σ' (Gy^{-1})
0.5	0.029	3	0.380	0.303
1.0	0.058	12	0.380	0.152
1.5	0.087	53	0.380	0.101
2.0	0.115	222	0.380	0.076
2.5	0.144	941	0.380	0.061
3.0	0.173	3.98E+03	0.380	0.051
4.0	0.231	7.13E+04	0.380	0.038
5.0	0.289	1.28E+06	0.380	0.030
6.0	0.346	2.29E+07	0.380	0.025

5.4 Discussion

Based on Figure 5-1(d) – (h) and Figure 5-2, one may conclude that the functional forms of the individual and the population models are almost identical for $\gamma_{50} \in [2,6]$. Indeed, for this range of γ_{50} the index $\left|\Delta A / A_{TCP_{pop}}\right|$ is less than 0.5%. Although $\left|\Delta A / A_{TCP_{pop}}\right|$ is higher ($\Delta A / A_{TCP_{pop}} \in [-0.5, -6.7]\%$) for the interval $\gamma_{50} \in [1,2)$, the plots in Figure 5-1 (b) and (c) indicate that the individual and population TCP curves are still sufficiently close to each other, especially for the clinically-relevant high dose range. The individual and population models differ considerably at γ_{50} = 0.5 ($\left|\Delta A / A_{TCP_{pop}}\right| = 17.7\%$). As can be seen from Figure 5-1, the individual curves overread TCP everywhere except at 50% control when compared with the population-based TCP curves for γ_{50} less than 2.5. For normalized slopes above γ_{50} = 2.5, the individual curves tend to slightly underread the population TCP. The overreading and underreading tendencies are clearly demonstrated by Figure 5-2.

The considerable closeness in functional form of both models explains the observation that the individual TCP model produces a reasonable fit to clinical datasets.[4,10]

In spite of this, the observed equivalence in functional form of the two TCP models should not be regarded as an endorsement to use the individual TCP model to fit clinical data. Indeed, as can be seen from Table 5-1, the variance in α' is relatively small ($\sigma' = 0.025$ Gy^{-1}) only for the case of a very steep response (i.e. $\gamma_{50} = 6$). From this observation, one may deduce that the individuals in a group that displays a steep response are nearly identical. In addition, the values of the individual parameters α' and N_0 (Table 5-1) corresponding to $\gamma_{50} = 6$ are remarkably close to the population mean values of $\overline{N_0}$ and $\overline{\alpha'}$, which confirms the deduction of nearly identical individuals in this case. Therefore, the use of the individual model to describe data corresponding to a very steep response may be justified. Moreover, judging by the parameter values shown in Table 5-1, the biological meaning of the model parameters α' and N_0 in this case is retained, assuming that the population TCP model gives a correct description of tumour control.

However, a very steep dose response is unusual for clinical data sets. Shallower responses are much more typical for populations of patients. As can be seen from Table 5-1, in the cases where γ_{50} is smaller (i.e., shallower responses), σ' is larger. This corresponds to greater differences in the responses of individuals that comprise a given population of patients. Table 5-1 also shows that, as the normalized slope decreases, the values of the individual parameters α' and N_0 start to differ considerably from the population mean values $\overline{N_0}$ and $\overline{\alpha'}$, becoming increasingly inaccurate ($N_0 \leq 222$ and $\alpha' \leq 0.11$ Gy^{-1} for $\gamma_{50} \leq 2$). Thus, a shallow dose response, which is usually observed clinically, can be explained by the presence of considerable inter-patient heterogeneity. Therefore, it would conceptually be more correct to use the population TCP model, which accounts for inter-patient heterogeneity, to fit such data. If, however, the individual TCP model is used, one should take into account that the fitted parameter values have lost any biological meaning and should be interpreted simply as phenomenological coefficients.

As can be seen from Figure 5-1 (a) and (b), both models start to differ in functional form for the clinically observable range of $\gamma_{50} < 1$. In addition, for these values of γ_{50}, the individual model leads to TCP > 0 for $D = 0$. Therefore, fits using the individual model may distort the best-fit estimates of γ_{50} and D_{50}.

We advocate the use of the population model in regards to clinical data. However, the demonstrated equivalence in functional form of the individual and population models can be utilized for the case of heterogeneous tumour irradiation. In this case, the individual TCP model with existing $\{\gamma_{50}, D_{50}\}$ estimates (e.g. Okunieff *et al.*[36]) can be used for the evaluation of TCP[37] according to the following expression:[38]

$$TCP = 0.5^{\sum_i v_i \exp\left[\frac{2\gamma_{50}}{\ln 2}\left(1-\frac{D_i}{D_{50}}\right)\right]} \tag{5-13}$$

Equation (5-13) is a simple, straightforward generalization of Eq. (5-3) for the case of heterogeneous irradiation. However, the generalization of Eq. (5-9) for the case of heterogeneous irradiation, without introducing extra model parameters, presents a complicated mathematical problem, and has not yet been solved.

Strictly speaking, the ability to use Eq. (5-13) as a population TCP descriptor has not yet been proven theoretically. Nevertheless, our experience with the TCP/NTCP estimation module[37] shows that it produces reasonable TCP estimates.

Another approach to the problem of taking dose heterogeneity into account for the population TCP model is to replace the homogeneous dose, D, with the equivalent uniform dose, EUD. It may then be assumed that the EUD is equal to the generalized mean dose (GMD), as is usually done.[39,40] Unfortunately, this approach introduces a third model parameter, and knowledge of its value for each tumour type would then be needed in order to use this model to calculate TCP for a heterogeneously-irradiated tumour. Therefore, until more comprehensive parameter estimates are produced through fits of the population TCP model to clinical data for the case of heterogeneous irradiation, we propose that Eq. (5-13) be used for evaluation of treatment plans in terms of TCP based on the functional form equivalency of both models.

5.5 *Conclusions*

It is thus concluded that:

- The population and the individual TCP responses are almost identical in functional form for γ_{50} belonging to the interval [1, 6]. If each of these models were fit to the same clinical dataset, they would produce statistically indistinguishable values of the parameters D_{50} and γ_{50}.
- It is conceptually incorrect to use the individual TCP model to fit clinical data.
- Until reliable estimates of the population TCP parameters for the case of heterogeneous tumour irradiation are obtained, the individual TCP model [Eq. (5-13)] with existing D_{50} and γ_{50} estimates could be used for TCP evaluations in this situation.
- The case of a shallow dose-response relationship, which is usually observed clinically, can be explained by the presence of significant inter-patient heterogeneity. The population TCP model should be used to fit such data, as it accounts for this heterogeneity. If, however, the individual TCP model is used, the estimated parameter values should be interpreted simply as phenomenological coefficients.
- A steep dose-response relationship can be attributed to the presence of a relatively small inter-patient heterogeneity. Though it is highly improbable to observe such dose-responses clinically, the individual TCP model may be applied to such data for the purpose of estimating biological parameters, as the individual parameters would retain some biological meaning.

5.6 References

1. T. R. Munro and C. W. Gilbert, "The relation between tumour lethal doses and the radiosensitivity of tumour cells," Br J Radiol **34**, 246-251 (1961).

2. J. D. Fenwick, "Predicting the radiation control probability of heterogeneous tumour ensembles: data analysis and parameter estimation using a closed-form expression," Phys Med Biol **43**, 2159-2178 (1998).

3. M. Goitein, A. Niemierko, and P. Okunieff, "The probability of controlling an inhomogeneously irradiated tumour: a strategem for improving tumour control through partial tumour boosting", presented at the 19th L. H. Gray Conference: Quantitative Imaging in Oncology, Newcastle, UK, (1995).

4. S. A. Roberts and J. H. Hendry, "A realistic closed-form radiobiological model of clinical tumor-control data incorporating intertumor heterogeneity," Int J Radiat Oncol Biol Phys **41**, 689-699 (1998).

5. S. Webb and A. E. Nahum, "A model for calculating tumour control probability in radiotherapy including the effects of inhomogeneous distributions of dose and clonogenic cell density," Phys Med Biol **38**, 653-666 (1993).

6. B. Warkentin, P. Stavrev, N. A. Stavreva, and B. G. Fallone, "Limitations of a TCP model incorporating population heterogeneity," Phys Med Biol **50**, 3571-3588 (2005).

7. D. J. Brenner, "Dose, volume, and tumor-control predictions in radiotherapy," Int J Radiat Oncol Biol Phys **26**, 171-179 (1993).

8. W. D. D'Souza, H. D. Thames, and D. A. Kuban, "Dose-volume conundrum for response of prostate cancer to brachytherapy: summary dosimetric measures and their relationship to tumor control probability," Int J Radiat Oncol Biol Phys **58**, 1540-1548 (2004).

9. J. Fowler, R. Chappell, and M. Ritter, "Is alpha/beta for prostate tumors really low?," Int J Radiat Oncol Biol Phys **50**, 1021-1031 (2001).

10. S. A. Roberts and J. H. Hendry, "The delay before onset of accelerated tumour cell repopulation during radiotherapy: a direct maximum-likelihood analysis of a collection of worldwide tumour-control data," Radiother Oncol **29**, 69-74 (1993).

11. M. Carlone, B. Warkentin, P. Stavrev, and B. G. Fallone, "Fundamental form of the population TCP model in the limit of large heterogeneity," Med. Phys. **33**, 1634-1642 (2006).

12. P. Stavrev, N. Stavreva, A. Niemierko, and M. Goitein, "Generalization of a model of tissue response to radiation based on the idea of functional subunits and binomial statistics," Phys Med Biol **46**, 1501-1518 (2001).

13. R. G. Dale, "Radiobiological assessment of permanent implants using tumor repopulation factors in the linear-quadratic model," Br J Radiol **62**, 241-244 (1989).

14. R. G. Dale, "Time-dependent tumour repopulation factors in linear-quadratic equations--implications for treatment strategies," Radiother Oncol **15**, 371-381 (1989).

15. J. F. Fowler, "The linear-quadratic formula and progress in fractionated radiotherapy," British Journal of Radiology **62**, 679-694 (1989).

16. B. Maciejewski, H. R. Withers, J. M. Taylor, and A. Hliniak, "Dose fractionation and regeneration in radiotherapy for cancer of the oral cavity and oropharynx: tumor dose-response and repopulation," Int J Radiat Oncol Biol Phys **16**, 831-843 (1989).

17. B. Maciejewski, H. R. Withers, J. M. Taylor, and A. Hliniak, "Dose fractionation and regeneration in radiotherapy for cancer of the oral cavity and oropharynx. Part 2. Normal tissue responses: acute and late effects," Int J Radiat Oncol Biol Phys **18**, 101-111 (1990).

18. J. M. Taylor, H. R. Withers, and W. M. Mendenhall, "Dose-time considerations of head and neck squamous cell carcinomas treated with irradiation," Radiother Oncol **17**, 95-102 (1990).

19. H. D. Thames, S. M. Bentzen, I. Turesson, M. Overgaard, and W. Van den Bogaert, "Time-dose factors in radiotherapy: a review of the human data," Radiother Oncol **19**, 219-235 (1990).

20. E. L. Travis and S. L. Tucker, "Isoeffect models and fractionated radiation therapy," Int J Radiat Oncol Biol Phys **13**, 283-287 (1987).

21. S. L. Tucker and E. L. Travis, "Comments on a time-dependent version of the linear-quadratic model," Radiother Oncol **18**, 155-163 (1990).

22. J. Van Dyk, K. Mah, and T. J. Keane, "Radiation-induced lung damage: dose-time-fractionation considerations," Radiother Oncol **14**, 55-69 (1989).

23. J. van de Geijn, "Incorporating the time factor into the linear-quadratic model," British Journal of Radiology **62**, 296-298 (1989).

24. T. E. Wheldon and A. E. Amin, "The Linear Quadratic Model," British Journal of Radiology **61**, 700-702 (1988).

25. H. R. Withers, J. M. Taylor, and B. Maciejewski, "The hazard of accelerated tumor clonogen repopulation during radiotherapy," Acta Oncol **27**, 131-146 (1988).

26. R. J. Yaes, "Linear-quadratic model isoeffect relations for proliferating tumor cells for treatment with multiple fractions per day," Int J Radiat Oncol Biol Phys **17**, 901-905 (1989).

27. L. G. Hanin, M. Zaider, and A. Y. Yakovlev, "Distribution of the number of clonogens surviving fractionated radiotherapy: a long-standing problem revisited," Int J Radiat Biol **77**, 205-213 (2001).

28. W. S. Kendal, "A closed-form description of tumour control with fractionated radiotherapy and repopulation," Int J Radiat Biol **73**, 207-210 (1998).

29. A. Yakovlev, "Comments on the distribution of clonogens in irradiated tumors," Radiat Res **134**, 117-122 (1993).

30. M. Zaider and G. N. Minerbo, "Tumour control probability: a formulation applicable to any temporal protocol of dose delivery," Phys Med Biol **45**, 279-293 (2000).

31. M. Zaider, M. J. Zelefsky, L. G. Hanin, A. D. Tsodikov, A. Y. Yakovlev, and S. A. Leibel, "A survival model for fractionated radiotherapy with an application to prostate cancer," Phys Med Biol **46**, 2745-2758 (2001).

32. L. G. Hanin, "A stochastic model of tumor response to fractionated radiation: limit theorems and rate of convergence," Math Biosci **191**, 1-17 (2004).

33. A. Brahme, "Dosimetric precision requirements in radiation therapy," Acta Radiol Oncol **23**, 379-391 (1984).

34. P. Kallman, A. Agren, and A. Brahme, "Tumour and normal tissue responses to fractionated non-uniform dose delivery," Int J Radiat Biol **62**, 249-262 (1992).

35. S. M. Bentzen and S. L. Tucker, "Quantifying the position and steepness of radiation dose-response curves," Int J Radiat Biol **71**, 531-542 (1997).

36. P. Okunieff, D. Morgan, A. Niemierko, and H. D. Suit, "Radiation dose-response of human tumors," Int J Radiat Oncol Biol Phys **32**, 1227-1237 (1995).

37. B. Warkentin, P. Stavrev, N. Stavreva, C. Field, and B. G. Fallone, "A TCP-NTCP estimation module using DVHs and known radiobiological models and parameter sets," J Appl Clin Med Phys **5**, 50-63 (2004).

38. A. Niemierko, "Radiobiological models of tissue response to radiation in treatment planning systems," Tumori **84**, 140-143. (1998).

39. B. Choi and J. O. Deasy, "The generalized equivalent uniform dose function as a basis for intensity-modulated treatment planning," Phys Med Biol **47**, 3579-3589 (2002).

40. Q. Wu, R. Mohan, A. Niemierko, and R. Schmidt-Ullrich, "Optimization of intensity-modulated radiotherapy plans based on the equivalent uniform dose," Int J Radiat Oncol Biol Phys **52**, 224-235 (2002).

Chapter 6 An analytic investigation into the effect of population heterogeneity on parameter ratio estimates

A version of this chapter has been submitted for publication:

C. Schinkel, M. Carlone, B. Warkentin, and B. G. Fallone, "An analytic investigation into the effect of population heterogeneity on parameter ratio estimates," IJROBP, *in press* (2007)

6.1 Introduction

Parameter ratios are clinically important radiobiological quantities. Individual radiobiological parameters such as α, β, and λ of the linear quadratic model have importance in cell survival analysis, but have less clinical significance due to the difficulties involved in accurately determining these parameters. The ratios α/β and λ/α, however, are related to clinically important issues, such as the effect of dose per fraction on biologically effective dose (BED), and the amount of dose per day that is needed to combat tumour growth. The importance of these quantities has been explained in detail.[1]

The accepted paradigm regarding fractionation for most tumour types is that a dose per fraction of about 2 Gy is a good compromise of delivering dose to the tumour sufficiently quickly, while keeping the dose per fraction low enough to avoid excessive normal tissue complications. This is based on the observation that tumours are early responding tissues and typically have an α/β of about 10 Gy, while late responding normal tissues have an α/β of about 3 Gy. One of the most interesting recent innovations in clinical radiobiology was suggested by Brenner and Hall in their landmark paper.[2]

Based on the current understanding of the relationship between the cell cycle and response to fractionation (which is still limited), they suggested that prostate cancer may be atypical of other cancers. Since prostate cancer progresses slowly, they argued that it may respond to fractionation in a similar manner as do late responding normal tissues. If this is indeed the case, then the 2 Gy per fraction paradigm should be revisited for prostate cancer because the differential response to fractionation between tumour and normal tissues would disappear, and so sparing normal tissues by reducing the dose per fraction would become less important, as long as the total dose was adjusted accordingly for larger dose per fraction. As a supporting argument, Brenner and Hall[2] analyzed clinical outcomes from low dose rate ^{125}I brachytherapy treatments along with standard external-beam 2 Gy per fraction treatments to arrive at the now well-known estimate of 1.5 Gy for the α/β ratio of prostate cancer. Subsequently, Fowler *et al.*[3] and others[4-9] have made additional estimates of the α/β ratio for prostate cancer based on clinical tumour control data. To date, numerous clinical trials[10-14] have also been initiated to look at the equivalence of hypofractionation vs. standard fractionation for prostate cancer. If hypofractionation becomes the new standard of care for prostate cancer, it will represent one of the most successful translations of linear quadratic theory into clinical practice.

It should be emphasized that the driving principle behind Brenner and Hall's initial publication, and subsequent publications by Brenner and colleagues, is a biological one. Nonetheless, the ensuing discussion regarding hypofractionation for prostate cancer has centered on estimates of the α/β ratio, and not the underlying biological reasoning. Fitting tumour control models to clinical dose-response data to estimate radiobiological parameters (such as α/β) is a significant departure from conventional methods of estimation based on in-vitro cell survival analysis. Of course, for this new method to yield credible results, the TCP model used must also be credible. However, the most common form of the tumour control probability (TCP) model, which is based on the single clonogen hypothesis and Poisson statistics, may be tenuous at best. For example, it is possible that tumour control may not require that all clonogens be killed by radiation, but only enough so that the immune system can remove the rest. It may also be the case that control depends on the effects of radiation on the tumour vasculature, and not only on the damage to the tumour cells.

Two forms of the common TCP model have been used in parameter ratio estimation: the non-averaged, individual TCP model, and the population averaged TCP model. The individual model assumes that all tumours have identical radiobiological characteristics, i.e. the same radiobiological parameters. The population averaged model is also based on the single clonogen hypothesis; however, it averages the result of a population distribution of radiobiological parameters amongst different tumours.

It is reasonably well accepted[15-18] that neither form of the TCP model can be used to estimate reliable and credible radiobiological parameters. However, it has been assumed that the clinically significant parameter ratios are somewhat insensitive to the type of model used (individual or population), and thus the choice of model is not particularly critical. This argument has been invoked to defend the use of the individual TCP model to estimate radiobiological parameters (Fowler *et al.*[3] and Brenner and Hall[19]).

Recently, Carlone *et al.*[16] published a theoretical development of population TCP modeling. They showed that, in the large heterogeneity limit, the Poisson based population-averaged TCP model expressed in linear quadratic parameters can be exactly reparameterized in terms of the geometric parameters D_{50} and γ_{50}. They also provided an analytic relationship between the linear quadratic and geometric model parameters. Their results could be expressed in both extremes of inter-patient heterogeneity, when the dominant source of heterogeneity is that of tumour radiosensitivity, or when it is due to variation in clonogen number. These population TCP model expressions provide a new framework from which to investigate the impact of population heterogeneity on parameter ratio estimates.

The purpose of this chapter is to use the analytic forms of the individual and population TCP models to generate mapping relationships between parameter ratio estimates obtained from fits using each of these two different types of TCP model. Numerical simulations are then carried out in order to confirm the derived mapping relationships.

6.2 *Background – TCP models*

6.2.1 The individual TCP model

A common form of the individual TCP model is based on Poisson statistics along with a simple description of clonogen repopulation that occurs over the duration of a treatment:[1,16,20-34]

(6-1) $$TCP_{ind} = \exp\left[-N_0 P_S(D) e^{\lambda T}\right],$$

where N_0 is the initial number of clonogens in the tumour, $P_S(D)$ is the probability of cell survival after a uniform dose D, λ is the repopulation constant, and T is the treatment time. If it is assumed that the treatment consists of n fractions of equal dose, d, cell survival probability is given by the linear-quadratic formula, and the repopulation constant, λ, can be scaled by the number of days per fraction, $\lambda' = \lambda T/n$, then the individual TCP model may be written as:[16]

(6-2) $$TCP_{ind} = \exp\left[-N_0 e^{-\left(\alpha+\beta d-\frac{\lambda'}{d}\right)D}\right] = \exp\left[-e^{-(\alpha' D+\ln N_0)}\right],$$

where α and β are the linear quadratic radiosensitivity parameters.

The individual TCP model may be re-written in terms of the dose at 50% control, D_{50}, and the normalized slope at that dose point, γ_{50} ($\gamma_{50} = D_{50}\theta_{50}$, where $\theta_{50} = \left[d(TCP_{ind})/dD\right]_{D_{50}}$). The reparameterized form of this model is: [35]

(6-3) $$TCP_{ind} = \left(\frac{1}{2}\right)^{\exp\left[\frac{2\gamma_{50}}{\ln 2}\left(1-\frac{D}{D_{50}}\right)\right]},$$

where the geometric parameters (D_{50}, γ_{50}) are related to the original radiobiological parameters (α', $\ln N_0$) as follows:

(6-4) $$D_{50} = \frac{1}{\alpha'}\left[\ln N_0 - \ln(\ln 2)\right]$$

(6-5) $$\gamma_{50} = \frac{\ln 2}{2}\left[\ln N_0 - \ln(\ln 2)\right].$$

6.2.2 The population-based TCP model

Recently, Carlone *et al.*[16] derived a fundamental form (equation) of the population TCP model. In the limit of low heterogeneity in clonogen number and no restriction on heterogeneity in radiosensitivity, the fundamental form of the population-based TCP model is:[16]

$$TCP_{pop} = \frac{1}{2} erfc\left[\sqrt{\pi}\,\gamma_{50}\left(\frac{D_{50}}{D} - 1\right)\right]. \tag{6-6}$$

The parameters D_{50} and γ_{50} in Eq. (6-6) are related to the population-based radiobiological parameters:

$$D_{50} = \frac{\Gamma + \overline{\ln N_0}}{\overline{\alpha'}} \tag{6-7}$$

$$\gamma_{50} = \frac{\overline{\alpha'}}{\sqrt{2\pi}\sigma'}, \tag{6-8}$$

where $(\sigma')^2 = \sigma_\alpha{}^2 + d^2\sigma_\beta{}^2 + \frac{\sigma_{\lambda'}{}^2}{d^2}$ and $\overline{\alpha'} = \overline{\alpha} + \overline{\beta}d + \frac{\overline{\lambda'}}{d}$. The quantities $\overline{\alpha}$, $\overline{\beta}$, $\overline{\lambda'}$ and $\overline{\ln N_0}$ are the population averages of the corresponding individual parameters. Heterogeneity in each of these parameters is represented by their standard deviations: σ_α, σ_β, $\sigma_{\lambda'}$ and $\sigma_{\ln N_0}$. Finally, Γ is Euler's gamma constant (approximately equal to 0.577).

In the case where heterogeneity in clonogen number dominates heterogeneity in radiosensitivity, the population TCP model is given by:[16]

$$TCP_{pop} = \frac{1}{2} erfc\left[\sqrt{\pi}\,\gamma_{50}\left(1 - \frac{D}{D_{50}}\right)\right], \tag{6-9}$$

with:

$$D_{50} = \frac{\Gamma + \overline{\ln N_0}}{\overline{\alpha'}} \tag{6-10}$$

$$\gamma_{50} = \frac{\Gamma + \overline{\ln N_0}}{\sqrt{2\pi}\sigma_{\ln N_0}}. \tag{6-11}$$

Based on differing arguments, two publications have arrived at the conclusion that heterogeneity in radiosensitivity is the dominant form in a clinical tumour dose-response dataset.[16,25] Other evidence from studies involving *in-vitro* radiosensitivity parameters and modeling also supports this finding.[36-39] Although it conceivably is possible that other forms of inter-tumour heterogeneity affect the dose-response curve of a clinical dataset, radiosensitivity is often assumed to have the greatest influence.[40] Thus, we suggest that the population TCP model given by Eq. (6-6) is best suited for the analysis of dose-response data.

6.3 Functional similarity of the individual and population TCP models

It is known that the dependence of the shape of the TCP curve on fundamental radiobiological parameters describing radiosensitivity, repopulation and clonogen number is different for the individual and population models. The population model produces a shallower TCP response than the individual one for a given set of radiobiological parameters, due to averaging over the variability in parameter values. From Eq. (6-8) it is clear that the population model predicts that the normalized slope of the TCP dose-response is in fact dictated by the relative heterogeneity, $\overline{\alpha'}/\sigma'$; in contrast, the individual model suggests that clonogen number is the determining factor [Eq. (6-5)]. This discrepancy likely explains why it is commonly found that fits using the individual model require unphysical radiobiological parameters to produce a slope of the dose response that is consistent with population measurements.[17]

A new method of comparing the individual and population models is facilitated by Eqs. (6-3) and (6-6), which show that both TCP models may be written in terms of the same two parameters,[41] γ_{50} and D_{50}. Similarities between the two functions were identified by generating TCP curves for each model, using clinically-relevant D_{50} and γ_{50} values. Clinical parameter values were chosen for this purpose based on the work of Okunieff *et al.*[42] In that work, a phenomenological two-parameter TCP model was fit to a variety of different tumour datasets in order to determine estimates for D_{50} and γ_{50}. It was found that most curves had a shallow slope (i.e. a low γ_{50} value of less than 4), and

that the mean D_{50} for all tumours investigated was 50 Gy, with values falling in the interval [10 Gy, 90 Gy]. Thus, to investigate the functional equivalency of the individual and population TCP models, Eqs. (6-3) and (6-6) were evaluated with D_{50} = 50 Gy and γ_{50} ranging from 1 to 4. These curves are plotted in Figure 6-1(a) – (d). For all γ_{50} values shown, the shapes of the individual (dotted line) and population (solid line) TCP curves are similar, and, for γ_{50} greater than 2, the two functions are essentially identical. Changing the value of D_{50} only influenced the location of these curves along the dose-axis; the position and shape of the population curve relative to the individual curve are independent of this parameter. Though not a rigorous proof, Figure 6-1 shows that the geometric form of Eqs. (6-3) and (6-6) is very nearly equivalent. When the large statistical errors associated with typical clinical dose-response data are taken into account, any difference between the two geometric forms would likely have an insignificant impact on fitting results.

The same procedure was used to compare the individual TCP model with the population model in the limit of dominant heterogeneity in clonogen number [Eqs. (6-3) and (6-9)]. Plots of these functions are shown in Figure 6-1(e) – (h) for D_{50} = 50 Gy and γ_{50} = 1, 1.5, 2 and 4. Again, the geometric forms of the two models are nearly equivalent.

6.4 Mapping relationships between parameter ratios for the individual and population models

6.4.1 Analytic relationship between individual and population radiobiological parameters

Based on the functional similarity[41] that was suggested in the previous section as well as in Chapter 5, the clonogen estimate obtained from the individual model can be expressed in terms of parameters based on the population model using Eqs. (6-5) and (6-8):

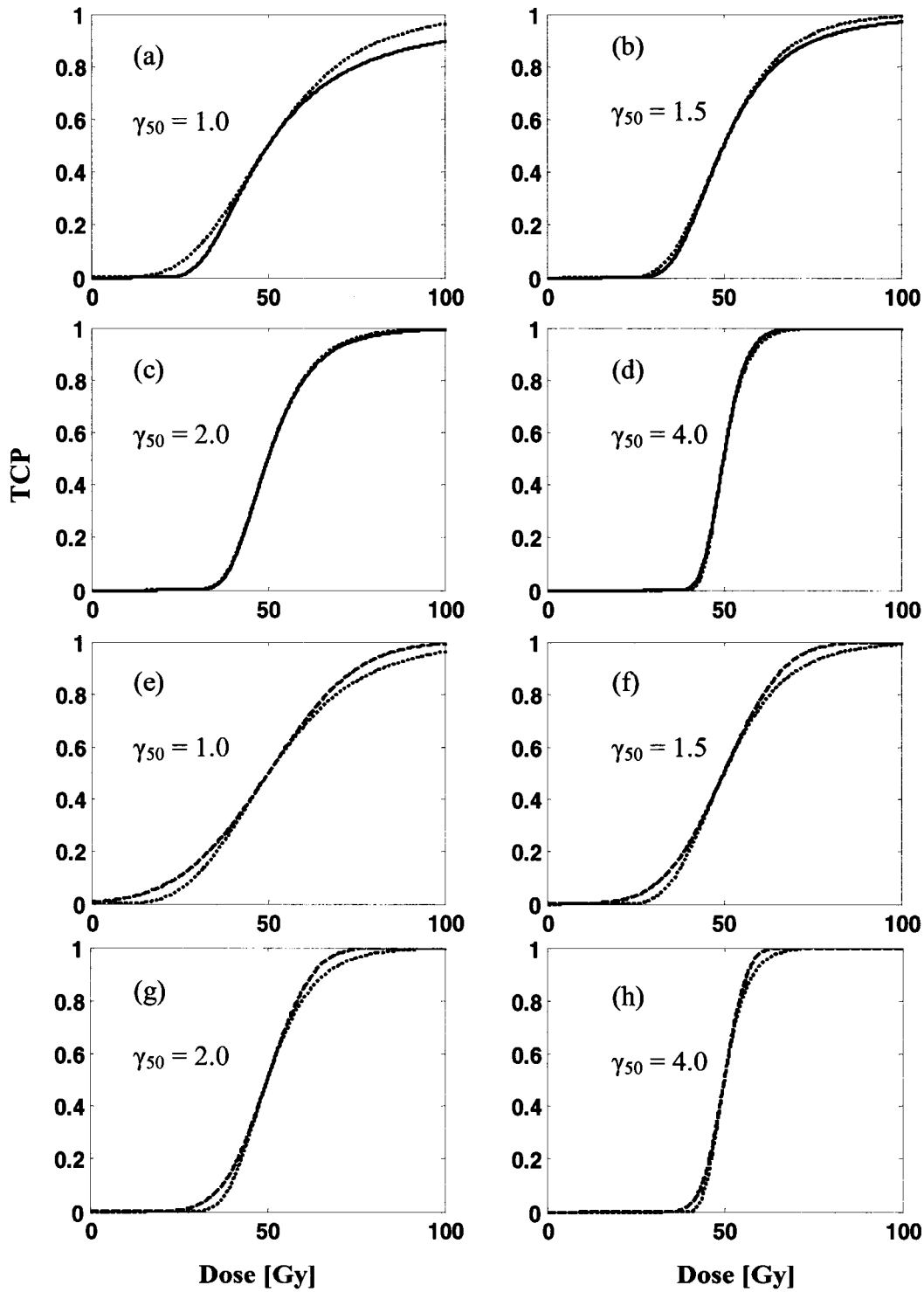

Figure 6-1: **(a) – (d)** Individual TCP curve (dotted) and population TCP curve for the limit of dominant heterogeneity in radiosensitivity (solid) – Eq. (6-6) – with parameter values D_{50} = 50Gy and the γ_{50}'s shown in each sub-plot. **(e) – (h)** Individual TCP curve (dotted) and population TCP curve for the limit of dominant heterogeneity in clonogen number (dashed) – Eq. (6-9) – for the same geometric parameter values as (a) – (d).

$$\gamma_{50} = \frac{\ln 2}{2}\left[\ln N_0 - \ln(\ln 2)\right] = \frac{\overline{\alpha'}}{\sqrt{2\pi}\sigma'}$$

$$\Rightarrow \ln N_0 = \ln(\ln 2) + \frac{2}{\sqrt{2\pi}\ln 2}\frac{\overline{\alpha'}}{\sigma'}. \quad (6\text{-}12)$$

Similarly, the radiosensitivity estimate from the individual model can be expressed by combining Eq. (6-4) with (6-7):

$$D_{50} = \frac{1}{\alpha'}\left[\ln N_0 - \ln(\ln 2)\right] = \frac{\Gamma + \overline{\ln N_0}}{\overline{\alpha'}}$$

$$\Rightarrow \alpha' = \frac{2}{\sqrt{2\pi}\ln 2}\frac{1}{\left(\Gamma + \overline{\ln N_0}\right)}\frac{\left(\overline{\alpha'}\right)^2}{\sigma'}. \quad (6\text{-}13)$$

Equations (6-12) and (6-13) give analytic relationships between the individual and population TCP model parameters that would be obtained in fitting the same dose response data. These equations clearly demonstrate that the parameters acquired by means of an individual TCP model are not equivalent to those obtained from a population TCP model for the same data. Note again that Eq. (6-12) implies that the individual prediction of the clonogen number is unrelated to the corresponding population clonogen parameter, but rather to the level of relative heterogeneity of the dataset, $\overline{\alpha'}/\sigma'$.

6.4.2 Analytic relationship between individual and population α/β in the limit of dominant heterogeneity in radiosensitivity

Although the meaning of the individual TCP model parameter estimates is lost when this model is applied to a clinical dataset,[18] it is often assumed that estimates of parameter *ratios* remain reliable.[3,19] Dubray and Thames[43] investigated the effect of heterogeneity on parameter ratios, and found that they are much less sensitive to the presence of interpatient heterogeneity when compared with single radiobiological parameters, unless the heterogeneity is extremely large, or there exists a significant amount of correlation between total dose delivered and treatment time. This observation was based on numerical simulation experiments in which the amount of heterogeneity in clonogen number was varied. Dubray and Thames also investigated the effect of heterogeneity in radiosensitivity on the ratio $\lambda/(\alpha + \beta d)$. They found that heterogeneity

in radiosensitivity had a more pronounced effect than heterogeneity in clonogen number on $\lambda/(\alpha+\beta d)$ (their Fig. 2). The ratio was found to be insensitive to the presence of heterogeneity in radiosensitivity only when the amount of heterogeneity is small and/or when the total dose and treatment time exhibit little or no correlation.

Equations (6-12) and (6-13) offer the opportunity to improve upon the results of Dubray and Thames. These equations were developed with no assumptions about correlation between total dose and treatment time, and allow a reasonably straightforward investigation of the effect of inter-patient heterogeneity on parameter ratio estimates to be made using analytic methods.

For treatments where the dose rate is low enough for sub-lethal lesions to be repaired before they have a chance to interact (such as treatments involving permanent brachytherapy implants), the beta term of the linear quadratic model can be ignored, and the individual TCP model can be expressed in terms of the parameters α and $\ln N_0$. When fitting the same model to external-beam radiation therapy (EBRT) dose-response data, estimates for $\alpha' = \alpha + \beta d$ and $\ln N_0$ can be determined. From the estimates for α and α', α/β may then be calculated using the following formula:[44]

$$\frac{\alpha}{\beta} = \frac{\alpha d}{\alpha' - \alpha}. \tag{6-14}$$

In deriving Eq. (6-14), it was assumed that clonogen repopulation can be ignored over the duration of a treatment. This is the same assumption that Brenner and Hall made when they estimated α/β for prostate,[2] and is a reasonable one for slowly-proliferating tumours. Equation (6-13) gives an expression for the individual radiosensitivity parameter in terms of population parameters. The heterogeneity parameter, σ', can be written in terms of γ_{50} and the average radiosensitivity parameter, $\overline{\alpha'}$, by means of Eq. (6-8). By combining Eqs. (6-8) and (6-13), one can derive the following relationship between the individual and population radiosensitivity parameters:

$$\alpha' = \frac{2}{\ln 2}\frac{\gamma_{50}}{\left(\Gamma + \overline{\ln N_0}\right)}\overline{\alpha'}. \tag{6-15}$$

Equations (6-14) and (6-15) may then be combined to give an expression for the individual α/β estimate in terms of population α/β estimate:

(6-16) $$\frac{\alpha}{\beta} = \frac{\left(\frac{\overline{\alpha}}{\overline{\beta}}\right)d}{\left(\frac{\gamma_{50,e}}{\gamma_{50,b}}\right)\left(\frac{\Gamma + \overline{\ln N_{0,b}}}{\Gamma + \overline{\ln N_{0,e}}}\right)\left(\frac{\overline{\alpha}}{\overline{\beta}} + d\right) - \frac{\overline{\alpha}}{\overline{\beta}}}$$

where $\overline{\alpha}/\overline{\beta}$ is the ratio of the average radiosensitivity parameters from the population TCP model for the case where heterogeneity in clonogen number may be neglected, $\gamma_{50,e}$ is the normalized slope of the EBRT dataset, $\gamma_{50,b}$ is the normalized slope of the brachytherapy dataset, $\overline{\ln N_{0,e}}$ is the population TCP model average $\ln N_0$ estimate for the EBRT dataset, and $\overline{\ln N_{0,b}}$ is the same parameter for the brachytherapy dataset. Henceforth, the subscript '*e*' will refer to the external-beam dataset and '*b*' will refer to the brachytherapy dataset.

We now assume that the parameter $\overline{\ln N_0}$ is the same for both the EBRT and brachytherapy datasets. This is equivalent to assuming that the tumours used to determine the dose-response points for the brachytherapy dataset are at approximately the same stage (and thus are about the same size) as those used to obtain the EBRT dose-response data. Under this assumption, Eq. (6-16) can be rewritten as:

(6-17) $$\frac{\alpha}{\beta} = \frac{\left(\frac{\overline{\alpha}}{\overline{\beta}}\right)d}{\left(\frac{\gamma_{50,e}}{\gamma_{50,b}}\right)\left(\frac{\overline{\alpha}}{\overline{\beta}} + d\right) - \frac{\overline{\alpha}}{\overline{\beta}}}.$$

The consequence of Eq. (6-17) is that the similarity of the individual and population estimates is a function of the ratio $\gamma_{50,e}/\gamma_{50,b}$, which, from Eq. (6-8), can be seen to depend on the relative amount of radiosensitivity heterogeneity $\left(\overline{\alpha'}/\sigma'\right)$ represented in the two datasets. The α/β estimated by means of the individual TCP model will only be equivalent to the population model estimate for this ratio if γ_{50} is identical for both the external-beam and brachytherapy dose-response curves.

6.4.3 Analytic relationship between individual and population α/β in the limit of dominant heterogeneity in clonogen number

The same process may be used to determine the relationship between the population and individual TCP model estimates of α/β for the case where heterogeneity in clonogen number is dominant [Eqs. (6-9), (6-10) and (6-11)]. Here, we have made the assumption that the individual TCP curve is approximately functionally equivalent to the population TCP curve in the limit of dominant heterogeneity in clonogen number. We verified that this assumption was reasonable [Figure 6-1(e) – (h)]. In this case, the relationship between the α/β ratio estimates from the population and individual models is:

$$\frac{\alpha}{\beta} = \frac{\left(\frac{\overline{\alpha}}{\overline{\beta}}\right)d}{\frac{\sigma_{\ln N_0,b}}{\sigma_{\ln N_0,e}}\left(\frac{\overline{\alpha}}{\overline{\beta}} + d\right) - \frac{\overline{\alpha}}{\overline{\beta}}} = \frac{\overline{\alpha}}{\overline{\beta}} \text{ when } \sigma_{\ln N_0,b} = \sigma_{\ln N_0,e}. \tag{6-18}$$

Assuming that the dose-response data for each of the treatment protocols are based on approximately the same stage of disease, the amount of heterogeneity in clonogen number should be approximately the same for each dataset, and thus the α/β ratio should not be sensitive to heterogeneity in clonogen number.

6.4.4 Results

Figure 6-2 shows the mapping relationship between the individual α/β estimate and the population α/β estimate for a number of different values for the ratio $\gamma_{50,e}/\gamma_{50,b}$, assuming that heterogeneity in radiosensitivity is dominant [Eq. (6-17)]. For the EBRT treatment, the dose per fraction was set equal to the standard value of 2 Gy. As $\gamma_{50,e}/\gamma_{50,b}$ increases, a given value for the population α/β estimate maps to an increasingly smaller individual α/β estimate. Since γ_{50} is not generally expected to be identical for EBRT and low dose rate brachytherapy dose-response curves, the presence of radiosensitivity heterogeneity could potentially have an effect on the α/β estimates. For example, even a moderate difference of 25% in the normalized slope (or equivalently in the relative

heterogeneity, $\overline{\alpha'}/\sigma'$) results in significant differences in the α/β estimates: population values of 10 and 3 would map to individual values of 4 and 1.8, respectively.

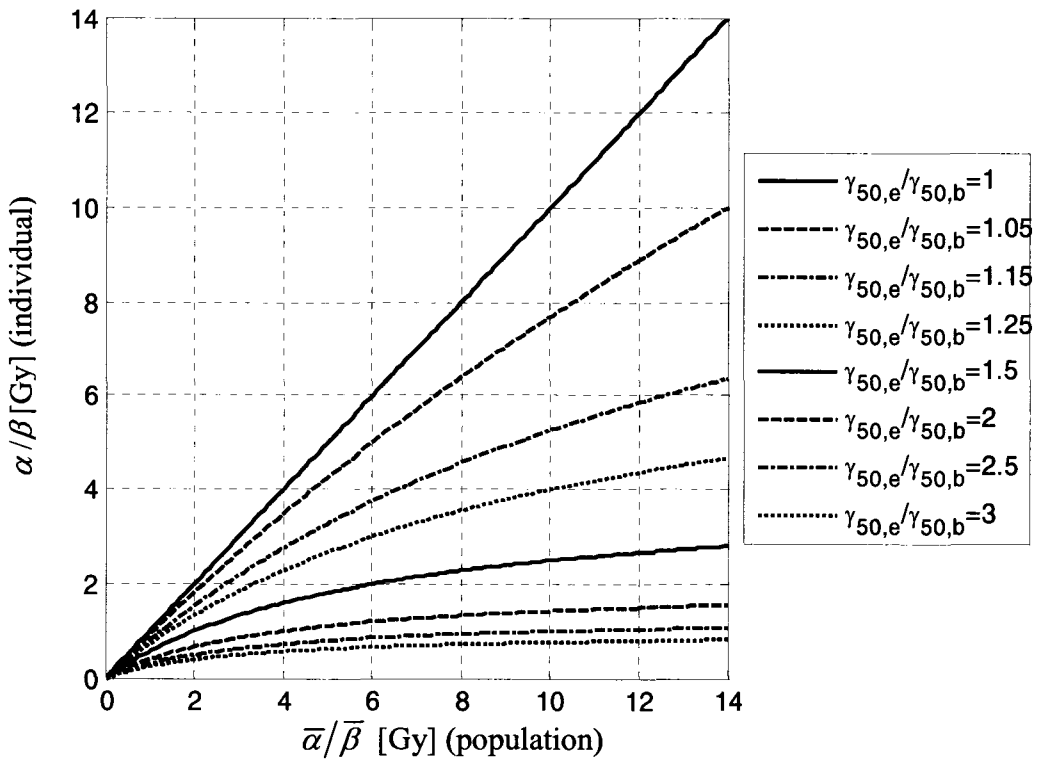

Figure 6-2: The α/β ratio estimated from clinical dose-response data by means of the individual TCP model as a function of the same ratio estimated by means of the population TCP model for the case of dominant heterogeneity in radiosensitivity. Equation (6-17) defines the relationship between the individual and population-based estimates for α/β, and is plotted here for a value of d = 2 Gy/fraction for each of the $\gamma_{50,e}/\gamma_{50,b}$ values shown. For the case of $\gamma_{50,e}/\gamma_{50,b}$ = 1, Eq. (6-17) gives a straight line; that is, the estimate for α/β from the individual model is identical to that from the population model. As $\gamma_{50,e}/\gamma_{50,b}$ increases, a given population α/β maps to a smaller individual α/β.

6.5 Investigation of parameter estimates from the individual and population TCP models

In this section we will use numerical simulations to verify our analytical result that the normalized slopes of the TCP curves affect the mapping of α/β estimates

obtained using the individual or population models. Specifically, we will fit the individual and population models to two different sets of pseudo-data and compare the fit results to our analytical predictions. Using pseudo-data for this purpose has the following advantages. First, pseudo-clinical data may be generated from a TCP curve with a known D_{50} and γ_{50}, so the ability of a TCP model to accurately estimate these parameters from a dataset can be evaluated. In addition, with pseudo-data we are not limited by the quality of the dose-response data; TCP points may be generated over a sufficiently large dose and TCP range such that the quality of the data will not significantly affect the results of the analysis.

6.5.1 Generation of pseudo-data

6.5.1.1 Using assumed radiobiological ($\overline{\alpha}$, $\overline{\ln N_0}$ σ_α) parameters

The first sets of pseudo-data that were generated are based on theoretical dose-response curves representing brachytherapy and EBRT treatments. The theoretical TCP curves were derived by assigning values to the radiobiological parameters of the population TCP model: $\overline{\alpha}$, σ_α, $\overline{\alpha}/\overline{\beta}$, $\sigma_\alpha/\sigma_\beta$, and $\overline{\ln N_0}$. In doing so, we are assuming that the population TCP model gives a correct description of the tumour dose-response relationship. The geometric parameters for the TCP curves, D_{50} and γ_{50}, were calculated from the assumed biological parameters by means of Eqs. (6-7) and (6-8) and then used with Eq. (6-6) to generate pseudo-clinical dose-response points.

To define a theoretical brachytherapy curve, values for the population radiobiological parameters were taken from the literature. Based on the assumptions made by Roberts and Hendry,[25] the average radiosensitivity, $\overline{\alpha}$, was assumed to be equal to 0.3, and the heterogeneity in this parameter, σ_α, was assumed to be equal to 0.14. The dose at 50% control was estimated based on previous fits to clinical brachytherapy dose-response data. Specifically, $D_{50,b}$ was calculated from the data in Appendix C of Carlone *et al.* [44] for the Stock [45] prostate data, which resulted in the value of 84.3 Gy. The parameter $\overline{\ln N_0}$ was then determined by means of Eq. (6-7). Finally, the normalized

slope for this theoretical curve was calculated from the assumed radiobiological parameter values by means of Eq. (6-8), resulting in $\gamma_{50,b} = 0.855$.

Two theoretical EBRT TCP curves were defined – one with an assumed $\overline{\alpha}/\overline{\beta}$ of 3 Gy and one with an $\overline{\alpha}/\overline{\beta}$ of 10 Gy. In each case, the dose per fraction, d, was set equal to the standard value of 2 Gy, and the values for $\overline{\alpha}$, σ_α, and $\overline{\ln N_0}$ that were used to derive the brachytherapy curve were again assumed. To determine an estimate for the heterogeneity in β, it was assumed that $\overline{\alpha}/\overline{\beta} = \sigma_\alpha/\sigma_\beta$. This is the same assumption as was made in Carlone *et al.*[46] For the $\overline{\alpha}/\overline{\beta} = 3$ Gy EBRT curve, the geometric parameters were calculated by means of Eqs. (6-7) and (6-8) – $D_{50,e} = 50.6$ Gy and $\gamma_{50,e} = 1.19$. For the $\overline{\alpha}/\overline{\beta} = 10$ Gy curve, the geometric parameters evaluated to $D_{50,e} = 70.2$ Gy and $\gamma_{50,e} = 1.01$. Using Eq. (6-8), it can be shown that the assumption $\overline{\alpha}/\overline{\beta} = \sigma_\alpha/\sigma_\beta$ leads to

$$\frac{\gamma_{50,e}}{\gamma_{50,b}} = \frac{\left(d + \overline{\alpha}/\overline{\beta}\right)}{\sqrt{d^2 + \left(\overline{\alpha}/\overline{\beta}\right)^2}},$$

in which case the normalized slope of the EBRT curve is always greater than that of the brachytherapy curve. For $\overline{\alpha}/\overline{\beta} = 3$ and 10 Gy, the corresponding $\gamma_{50,e}/\gamma_{50,b}$ ratios are 1.39 and 1.18.

Pseudo-data were generated following the method outlined in Appendix D for the two theoretical EBRT curves and the brachytherapy curve. In each case, 30 points were generated over a dose range of $2D_{50}$. The number of patients per point was chosen to be 50. These statistics were selected in order to produce large enough uncertainties in the generated dose-response points so that the individual and population-based TCP curves defined by the geometric parameters ($D_{50,b}$, $\gamma_{50,b}$) and ($D_{50,e}$, $\gamma_{50,e}$) are equivalent within error. These pseudo-datasets are intended for the purpose of estimating the α/β ratio from each of the two models for the purpose of verifying Eq. (6-17). As this expression was derived based on the assumption that the individual and population curves are equivalent for a given set of geometric parameters, it is essential that this equivalency holds within the precision of the data points. Each pseudo-dataset is shown in Figure 6-3, along with the theoretical TCP curve used for its generation and the individual TCP curve corresponding to the assumed D_{50} and γ_{50} values.

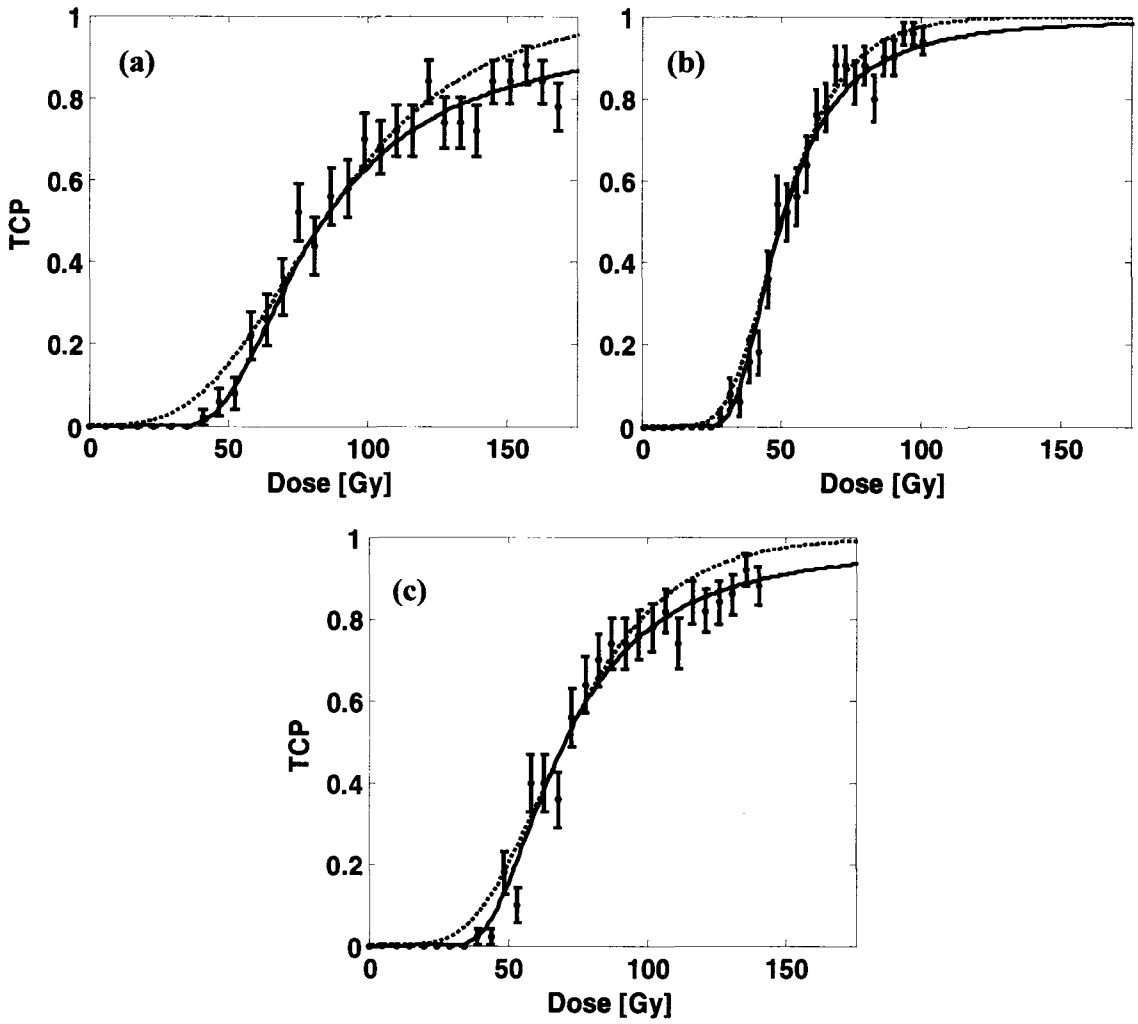

Figure 6-3: Pseudo-data generated from theoretical brachytherapy and EBRT dose-response curves. The theoretical population-based TCP curve from which the points were generated is also shown (solid line), along with the individual TCP curve that corresponds to the same γ_{50} and D_{50} values (dotted line). The value of $\overline{\alpha}$ was assumed to be equal to 0.3, σ_{α} was assumed to be equal to 0.14, and the D_{50} for the brachytherapy curve was taken to be 84.9 Gy. Pseudo-data and the assumed TCP curves for permanent implant brachytherapy are shown in (a), (b) shows the pseudo-data and curves for $\overline{\alpha}/\overline{\beta}$ = 3 Gy, and (c) corresponds to $\overline{\alpha}/\overline{\beta}$ = 10 Gy.

6.5.1.2 Using the geometric (D_{50}, γ_{50}) parameters

A set of TCP pseudo-data was also generated for the purpose of calculating the α/β ratio for different, pre-defined $\gamma_{50,e}/\gamma_{50,b}$ values – 1.05, 1.15 and 1.50. These

particular normalized slope ratios were selected in order to investigate the validity of Eq. (6-17) over a large region of Figure 6-2. For these curves, no assumptions about radiobiological parameter values were made. Instead, values for $D_{50,b}$, $\gamma_{50,b}$, and $D_{50,e}$ were assumed, based on fits to clinical dose-response data for permanent-implant and EBRT treatments for prostate.[44]

A theoretical brachytherapy curve was defined based on the Stock fitting results reported in Carlone *et al.*[44] (γ_{50} and D_{50} were calculated from the data in Table VII of their Appendix C) – $D_{50,b}$ = 84.3 Gy and $\gamma_{50,b}$ = 1.35. For each of the theoretical EBRT curves, $D_{50,e}$ was chosen to be equal to 69.5 Gy (the best-fit value for the Pinover[47] dataset from Carlone *et al.*[44]). The normalized slopes for the EBRT curves were assigned the values of $\gamma_{50,e}$ = 1.42, 1.56, and 2.03, based on the three pre-defined $\gamma_{50,e}/\gamma_{50,b}$ ratios defined above.

Again, for the purpose of generating pseudo-data from each curve, the method in Appendix D was used with a dose range of $2D_{50}$. A total of 30 points were generated from each curve, with the number of patients per point chosen such that the individual and population-based TCP curves could be considered equivalent within error (this time, a value of N = 70 was used for the brachytherapy dataset, and a value of N = 80 was used for each of the EBRT datasets). These datasets are plotted in Figure 6-4, along with the population TCP curves used for their generation, and the individual TCP curves corresponding to identical D_{50} and γ_{50} values.

6.5.2 Method – estimating α/β from the individual and population-based TCP models

To estimate α/β for the pseudo-datasets by means of the individual TCP model, the Poisson form given by Eq. (6-2) was fit to the brachytherapy and EBRT datasets to first determine α and α' (along with $\ln N_{0,b}$ and $\ln N_{0,e}$). Equation (6-14),

$$\frac{\alpha}{\beta} = \frac{\alpha d}{\alpha' - \alpha},$$

was then used to estimate α/β, and the Monte Carlo procedure described in Carlone *et al.*[44] was used to determine confidence intervals.

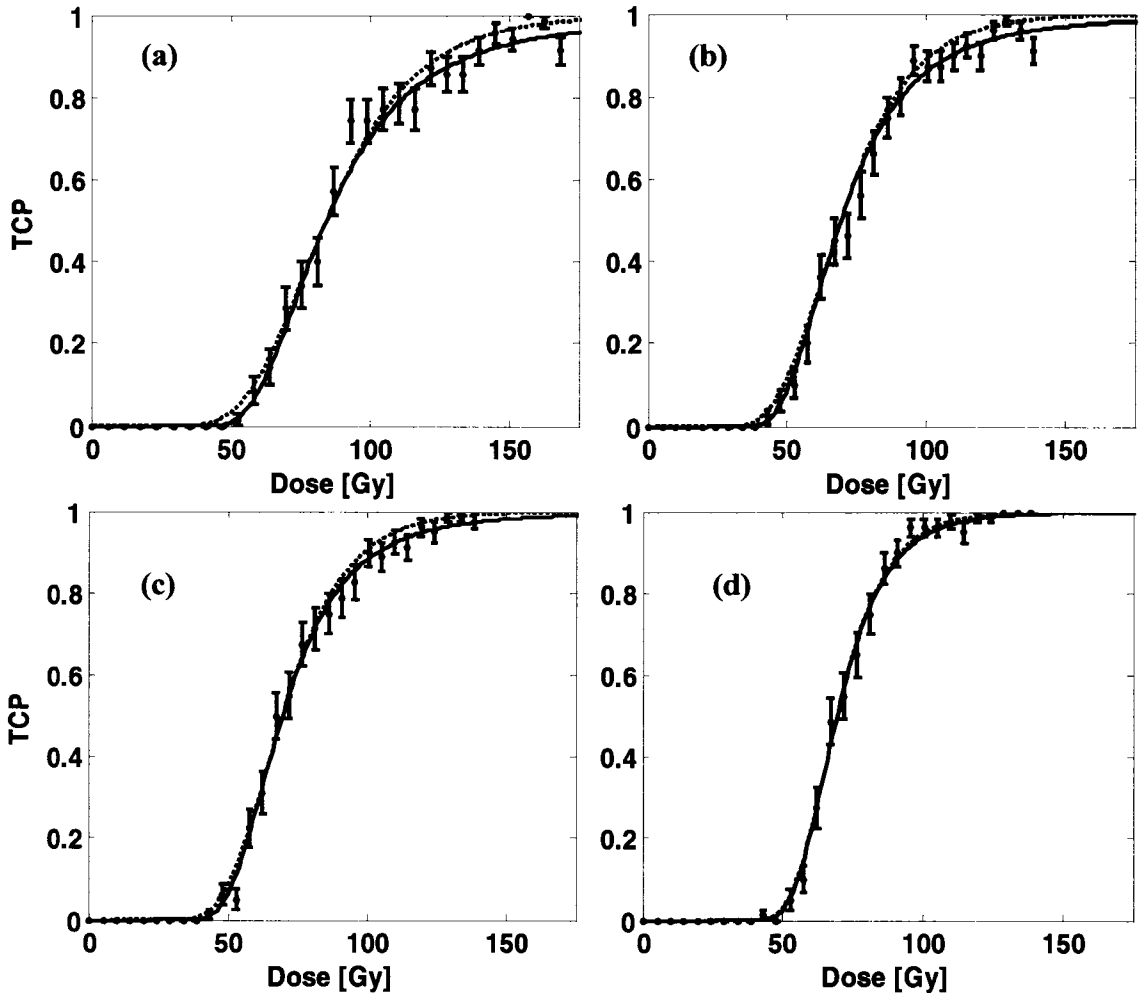

Figure 6-4: Pseudo-data generated from theoretical population TCP curves (solid line). In each case, the individual TCP curve corresponding to the same D_{50} and γ_{50} values is also shown. (a) shows the pseudo-data corresponding to a theoretical brachytherapy curve with $D_{50,b}$ = 84.3 Gy and $\gamma_{50,b}$ = 1.35. (b), (c) and (d) show the pseudo-data corresponding to theoretical EBRT curves with $D_{50,e}$ = 69.5 and $\gamma_{50,e}/\gamma_{50,b}$ ratios of 1.05, 1.15 and 1.50, respectively.

A slightly different approach was taken to estimate $\overline{\alpha}/\overline{\beta}$ by means of the population TCP model. Following Carlone *et al.* [44], an expression that is similar to Eq. (6-14) was used to express the population α/β ratio in terms of average radiosensitivity parameters:

$$\frac{\overline{\alpha}}{\overline{\beta}} = \frac{\overline{\alpha} d}{\overline{\alpha'} - \overline{\alpha}}. \tag{6-19}$$

Equation (6-10) can be used to express average radiosensitivity in terms of D_{50} and $\overline{\ln N_0}$:

$$\overline{\alpha'} = \frac{\Gamma + \overline{\ln N_0}}{D_{50}}. \tag{6-20}$$

If Eq. (6-20) is combined with Eq. (6-19) and we once again assume that $\overline{\ln N_{0,e}} = \overline{\ln N_{0,b}}$, $\overline{\alpha}/\overline{\beta}$ for the population TCP model may be expressed in terms of the D_{50} values for the brachytherapy and EBRT datasets:

$$\frac{\overline{\alpha}}{\overline{\beta}} = \frac{D_{50,e}\, d}{D_{50,b} - D_{50,e}}. \tag{6-21}$$

This approach is equivalent to rewriting Eq. (6-6) in terms of radiobiological parameters and using Eq. (6-19) directly to determine an estimate of $\overline{\alpha}/\overline{\beta}$ for different, fixed, $\overline{\ln N_0}$ values (the latter method is described in Carlone *et al.*[44]). For one of the generated pseudo-datasets, $\overline{\alpha}/\overline{\beta}$ was calculated using both methods, and it was found that parameter estimates were identical. As it is more computationally efficient to use Eqs. (6-6) and (6-21) to estimate $\overline{\alpha}/\overline{\beta}$, we used this approach.

6.5.3 Results

6.5.3.1 Results using assumed radiobiological parameters

For each EBRT-brachytherapy dataset pair generated from curves with assumed radiobiological parameters, the α/β ratio and its 95% confidence interval (CI) were estimated from the individual and population TCP models, as described above. The α/β estimates and 95% CIs are shown in the first two rows of Table 6-1 for the theoretical tumours with assumed $\overline{\alpha}/\overline{\beta}$ values of 3 and 10 Gy. In each case, the individual model α/β ratio is lower than the estimate from the population model. The $\overline{\alpha}/\overline{\beta}$ estimates from the population TCP model agree with the theoretical values within error, while the individual TCP model underestimates the α/β ratio in each case.

Table 6-1: Estimates for the population and individual α/β ratio, along with 95% confidence intervals, from the pseudo-datasets shown in Figure 6-3. Also shown are estimates and 95% CIs for the ratio $\gamma_{50,e}/\gamma_{50,b}$, calculated by means of each TCP model. Finally, Eq. (6-17) was used to calculate an estimate and 95% CI for the individual α/β ratio based on the population estimate for the same parameter. All of these quantities were calculated for the EBRT-brachytherapy dataset pairs that were generated from assumed values for the population radiobiological parameters (Sec. 6.4.1) and the theoretical population α/β ratios shown.

	$(\overline{\alpha}/\overline{\beta})_{th} = 3$ Gy	$(\overline{\alpha}/\overline{\beta})_{th} = 10$ Gy
$\overline{\alpha}/\overline{\beta}$ **estimate from** TCP_{pop}	3.15 [2.76, 3.65]	12.10 [8.85, 19.16]
α/β **estimate from** TCP_{ind}	1.45 [1.17, 1.85]	4.97 [3.30, 8.38]
$\gamma_{50,e}/\gamma_{50,b}$ **from** TCP_{pop}	1.50 [1.30, 1.75]	1.23 [1.05, 1.43]
$\gamma_{50,e}/\gamma_{50,b}$ **from** TCP_{ind}	1.45 [1.27, 1.65]	1.20 [1.05, 1.37]
$(\alpha/\beta)_{ind}$ **from Eq. (6-17)**	1.37 [1.05, 1.77]	4.64 [2.92, 9.10]

For each of the theoretical pseudo-data pairs (EBRT plus brachytherapy), a Monte-Carlo method was used to estimate the $\gamma_{50,e}/\gamma_{50,b}$ ratios from the individual and population model fitting results. The estimates for this quantity are shown in Table 6-1, in the third and fourth rows. In both cases, the individual and population-based ratios agree within error. This result is not surprising, considering the equivalency of the individual and population-based TCP models as described in Section 6.2.

Finally, the individual α/β was calculated from the population $\overline{\alpha}/\overline{\beta}$ estimates for each EBRT-brachytherapy dataset pair by means of Eq. (6-17). These values, along with their 95% confidence intervals, are shown in the fifth row of Table 6-1. In each case, the estimates for α/β obtained directly from the individual TCP model agree with the estimates calculated by means of Eq. (6-17), within error.

The relationship between Eq. (6-17) and the model predictions for the individual and population-based α/β estimates is illustrated for these two theoretical datasets in Figure 6-5(a). In this figure, Eq. (6-17) is plotted for the best-fit population-based $\gamma_{50,e}/\gamma_{50,b}$ ratios from Table 6-1 (the solid line corresponds to the $(\overline{\alpha}/\overline{\beta})_{th} = 3$ Gy data and the dotted line corresponds to the $(\overline{\alpha}/\overline{\beta})_{th} = 10$ Gy data). A point representing the best-fit

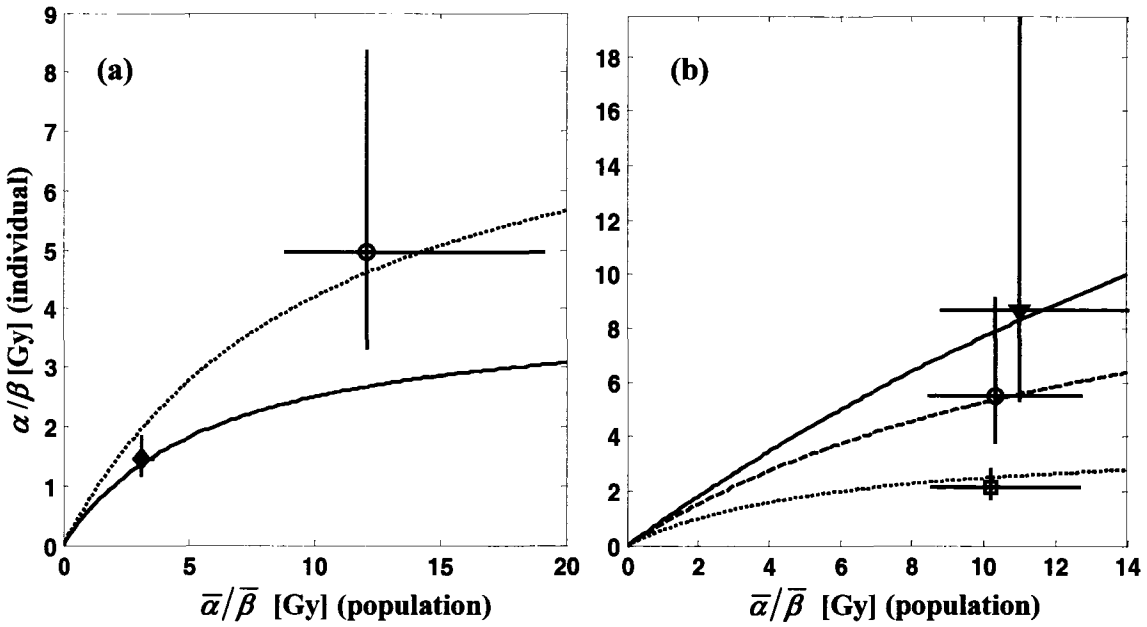

Figure 6-5: **(a)** Plot of the best-fit value of α/β as estimated from the individual TCP model vs. the best-fit value of $\bar{\alpha}/\bar{\beta}$ from the population TCP model for the pseudo-datasets generated from assumed radiobiological population parameters. The diamond point corresponds to the pseudo-data for a theoretical $\bar{\alpha}/\bar{\beta}$ of 3 Gy, and the circular point corresponds to the pseudo-data for a theoretical $\bar{\alpha}/\bar{\beta}$ of 10 Gy (Figure 6-3). The 95% confidence intervals for the individual and population-based α/β ratios are also shown. The solid line represents the relationship given by Eq. (6-17) for the best-fit value of $\gamma_{50,e}/\gamma_{50,b}$ as estimated from the population TCP model for the $(\bar{\alpha}/\bar{\beta})_{th}$ = 3 Gy data – 1.50 (Table 6-1). The dotted line represents Eq. (6-17) for the best-fit normalized slope ratio corresponding to the $(\bar{\alpha}/\bar{\beta})_{th}$ = 10 Gy data ($\gamma_{50,e}/\gamma_{50,b}$ = 1.23, Table 6-1). **(b)** This plot shows the same data as (a), for the pseudo-data generated from theoretical TCP curves with assumed values for the geometric parameters D_{50} and γ_{50}. The solid line represents the relationship given by Eq. (6-17) for $(\gamma_{50,e}/\gamma_{50,b})_{th}$ = 1.05, the dashed line corresponds to $(\gamma_{50,e}/\gamma_{50,b})_{th}$ = 1.15, and the dotted line corresponds to to $(\gamma_{50,e}/\gamma_{50,b})_{th}$ = 1.50. The triangle point represents the best-fit α/β ratios and 95% confidence intervals from the individual and population-based models for the dataset generated assuming $(\gamma_{50,e}/\gamma_{50,b})_{th}$ = 1.05, the circular point corresponds to $(\gamma_{50,e}/\gamma_{50,b})_{th}$ = 1.15, and the square point corresponds to $(\gamma_{50,e}/\gamma_{50,b})_{th}$ = 1.50.

α/β values from the individual and population models is shown for each pseudo-dataset pair, along with the 95% CIs (the diamond point corresponds to $(\bar{\alpha}/\bar{\beta})_{th}$ = 3 Gy and the

circular point corresponds to $(\overline{\alpha}/\overline{\beta})_{th}$ = 10 Gy). In each case, the model estimates for α/β agree with the predictions based on Eq. (6-17).

6.5.3.2 Results using geometric parameters

Table 6-1 was reproduced for the pseudo-data generated from theoretical TCP curves based on assumed D_{50}, γ_{50}, and $\gamma_{50,e}/\gamma_{50,b}$ values. The α/β ratios calculated from the individual and population-based TCP models are shown in the first two rows of Table 6-2 for the theoretical TCP curves with $\gamma_{50,e}/\gamma_{50,b}$ ratios of 1.05, 1.15 and 1.50. Again, the individual estimates are lower than the population estimates. The $\overline{\alpha}/\overline{\beta}$ estimates for each EBRT-brachytherapy data pair agree with one another within error. According to Eq. (6-21), this ratio should depend only on the D_{50} values for the EBRT and brachytherapy curves, along with the dose per fraction. As the same $D_{50,e}$ value was assigned to each theoretical EBRT curve in this case, it is not unexpected that the $\overline{\alpha}/\overline{\beta}$ values agree.

As can be seen in rows 3 and 4 of

Table **6-2**, the estimates for $\gamma_{50,e}/\gamma_{50,b}$ obtained from the individual and population-based TCP models agree within error. In addition, the ratios obtained from fitting the pseudo-data agree with the assumed values of 1.05, 1.15 and 1.50, within error.

Table 6-2: This table shows the same information as for Table 6-1, but for the EBRT-brachytherapy dataset pairs illustrated in Figure 6-4.

	$(\gamma_{50,e}/\gamma_{50,b})_{th}$ = **1.05**	$(\gamma_{50,e}/\gamma_{50,b})_{th}$ = **1.15**	$(\gamma_{50,e}/\gamma_{50,b})_{th}$ = **1.50**
$\overline{\alpha}/\overline{\beta}$ **estimate from** TCP_{pop}	11.00 [8.80, 14.06]	10.30 [8.43, 12.72]	10.20 [8.52, 12.69]
α/β **estimate from** TCP_{ind}	8.67 [5.27, 19.70]	5.49 [3.77, 9.17]	2.17 [1.67, 2.85]
$\gamma_{50,e}/\gamma_{50,b}$ **from** TCP_{pop}	1.03 [0.92, 1.15]	1.13 [1.00, 1.27]	1.54 [1.37, 1.74]
$\gamma_{50,e}/\gamma_{50,b}$ **from** TCP_{ind}	1.04 [0.92, 1.17]	1.14 [1.02, 1.28]	1.62 [1.43, 1.87]
$(\alpha/\beta)_{ind}$ **from Eq. (6-17)**	9.09 [5.46, 23.05]	5.77 [3.95, 10.02]	2.38 [1.86, 3.10]

Row 5 of Table 6-2 shows estimates for the individual α/β ratio calculated by means of Eq. (6-17) from the population $\overline{\alpha}/\overline{\beta}$ estimates. Once again, the estimates for α/β obtained directly from the individual TCP model agree with those calculated directly from Eq. (6-17). The agreement between Eq. (6-17) and the individual and population-based model predictions is also illustrated in Figure 6-5(b) for these three dataset-pairs. Equation (6-17) is plotted for each theoretical $\gamma_{50,e}/\gamma_{50,b}$ ratio (solid – 1.05, dashed – 1.15 and dotted – 1.50). As in Figure 6-5(a) a point representing the best-fit α/β ratios from the individual and population models is also shown, along with the estimated 95% CIs [triangle – $(\gamma_{50,e}/\gamma_{50,b})_{th}$ = 1.05, circle – $(\gamma_{50,e}/\gamma_{50,b})_{th}$ = 1.15, and square – $(\gamma_{50,e}/\gamma_{50,b})_{th}$ = 1.50]. In each case, the model predictions agree with that of Eq. (6-17).

Thus, we have verified the theoretical relationship between the population and individual α/β ratios that was derived in Section 6.3.2 by means of numerical simulations.

6.6 Discussion

Based on the functional similarities between the individual and population-based TCP models for given values of D_{50} and γ_{50}, analytic expressions were derived that relate the α/β ratio that would be obtained from a fit of the individual model to the ratio that would be estimated by the application of the population-based TCP model to the same dataset. These expressions were derived for the population model in the case of dominant heterogeneity in clonogen number [Eq. (6-18)] and in the case of dominant heterogeneity in radiosensitivity [Eq. (6-17)]. For the case where heterogeneity in clonogen number dominates, Eq. (6-18), it was seen that the presence of heterogeneity should not have a large impact on the estimate of the α/β ratio. This result is consistent with Dubray and Thames.[43]

For the case where heterogeneity in radiosensitivity among a population of patients is the dominant form, the mapping relationship between the α/β ratios as determined from the population and individual TCP models, Eq. (6-17), suggests that the

relationship between these parameters is dependent on the ratio of γ_{50} values for each dose-response dataset. Based on Eq. (6-17) and the numerical simulations carried out in the previous section, we expect that the presence of heterogeneity in radiosensitivity will have an effect on the estimated α/β ratio. For example, Figure 6-2 shows that for a $\gamma_{50,e}/\gamma_{50,b}$ ratio of 1.25, a population α/β of 10 Gy, which is typical for early-responding tissues, maps to an individual value of 4 Gy, which is more typical of late-responding tissues. The analytic result represented by Eq. (6-17) is also consistent with the Dubray and Thames paper – their numerical simulations showed that parameter ratios are more sensitive to the presence of heterogeneity in radiosensitivity, particularly for the case where total dose and treatment time are correlated. It should be noted here that the conclusions of Dubray and Thames are based on numerical simulations carried out for the $\lambda/(\alpha+\beta d)$ ratio, as opposed to α/β.

The effect of heterogeneity on the α/β ratio has previously been debated by King and Mayo[6] and Brenner and Hall.[19] King and Mayo postulated that Brenner and Hall's extremely low value of 1.5 Gy for the α/β ratio of prostate may be a result of using a TCP model that neglects the effects of inter-tumour heterogeneity. They estimated the ratio using a population-averaged TCP model in which α and β are correlated, and came up with a value of $\alpha/\beta = 4.5$ Gy. Brenner and Hall[19] re-did King and Mayo's calculation, making use of a TCP model that assumed independent Gaussian distributions for α and β, and arrived at a slightly increased value of $\alpha/\beta = 2.1$ Gy (compared to the original 1.5 Gy estimate). Although Brenner and Hall concluded that the "estimated value of the ratio α/β changed very little,"[19] confidence intervals for this new parameter ratio estimate were not given. This result is consistent with the prediction of Eq. (6-17), even though the increase in α/β observed by Brenner and Hall when they used a population TCP model was small.

Nahum *et al.*[7] calculated the α/β ratio for prostate cancer using a method that incorporates measurements for tumour hypoxia. The incorporation of variations in the level of tumour hypoxia among a patient population corresponds to taking heterogeneity in radiosensitivity into account. Their calculations for α/β yielded a value that was much

closer to the 10 Gy typically assumed for cancers. This result also supports the idea that the presence of heterogeneity in radiosensitivity affects the estimated α/β ratio.

In Figure 6-2 and the numerical simulations based on the pseudo-data described in Section 6.4.1, we only considered cases where γ_{50} for an EBRT dose-response curve is steeper than for a brachytherapy dose-response curve. For the theoretical EBRT and brachytherapy datasets shown in Figure 6-3 and described in Section 6.4.1.1, the normalized slope of the former turned out to be greater than that of the latter. To further show that $\gamma_{50,e} > \gamma_{50,b}$ is a reasonable choice, the clinical datasets for prostate utilized by Brenner and Hall[2] and Carlone *et al.*[44] were fit with the population TCP model [Eq. (6-6)] and γ_{50} was estimated. Two EBRT datasets were fit – Hanks[48] and Pinover,[47] along with one brachytherapy dataset – Stock.[45] Each of the EBRT datasets yielded γ_{50} values that were greater than that of the brachytherapy dataset within a confidence level of 68%. In both cases, however, the 95% CIs were found to overlap, but this is most likely due to the relatively poor quality of the Hanks and Pinover datasets. While the quality of the EBRT prostate datasets prevents us from determining with certainty whether γ_{50} for a brachytherapy dose-response is lower, it is unlikely that γ_{50} would be exactly identical for both datasets, and thus the presence of heterogeneity in radiosensitivity among a patient population will likely have an effect on the estimated α/β ratio.

In this chapter, we used simulated brachytherapy and EBRT datasets to investigate the dependence on the TCP model used to obtain estimates for α/β. The method of using simulated datasets avoids the practical difficulties associated with estimating parameter ratios by combining brachytherapy and external beam datasets. The relative biological effectiveness (RBE) of ^{125}I implants may be greater than 1 due to Auger electrons associated with the relatively low energies of these sources.[49,50] There may also be other problems due to inconsistencies between the two dose-response datasets, and the heterogeneous nature of the brachytherapy dose distribution within the treatment volume.[44] However, the results of this chapter were derived on the basis of theoretical and numerical simulation investigations based on generated data. In doing so, we have effectively assumed that any such difficulties as described above can be ignored, as our synthetic datasets were constructed using well-defined assumptions (which effectively forced a uniform dose distribution and equivalent α parameter for low dose

rate and high dose rate therapy). This allowed us to directly investigate the analytical/numerical process of estimating parameter ratios from TCP models.

Given the difficulties associated with estimating radiobiological parameters from either form of the TCP model,[15-18] it seems that the most reliable way to estimate the α/β ratio from clinical dose-response data is by first finding γ_{50} and D_{50}, and then making use of Eq. (6-21). If the average clonogen number is expected to be different for the EBRT and brachytherapy datasets (that is, if the dose-response data in each case represent tumours at different stages), a modified form of Eq. (6-21) may be used to determine $\overline{\alpha}/\overline{\beta}$:

$$\frac{\overline{\alpha}}{\overline{\beta}} = \frac{d}{\left(\frac{D_{50,b}}{D_{50,e}}\right)\left(\frac{\Gamma + \overline{\ln N_{0,e}}}{\Gamma + \overline{\ln N_{0,b}}}\right) - 1}. \tag{6-22}$$

In this case, the ratio of average log clonogen numbers could conceivably be estimated.

This chapter concerns the precision of α/β estimates that have previously been given based on radiobiological modeling. The original biological argument put forth by Brenner and Hall[2] is still viable and credible. Our center and others are currently engaging in randomized clinical trials to establish the clinical effectiveness of hypofractionated prostate radiotherapy. Only these clinical trials will have the ability to determine the validity of Brenner and Hall's hypothesis. Our results are meant to show that the supporting argument of estimating the prostate α/β ratio by means of a TCP model is problematic. This should only reflect on our ability to accurately determine the absolute value of the α/β ratio for prostate cancer, not to determine if hypofractionation is a suitable therapy for this disease. While early evidence from the hypofractionation trials suggests that prostate cancer responds to fractionation in a manner similar to late responding tissues,[11] the fact that inter-tumour heterogeneity has an effect on parameter ratio estimates may indicate that the value of α/β = 1.5 [0.8, 2.2] Gy as reported by Brenner and Hall is inaccurate. In addition, Carlone *et al.*[44] showed that the individual TCP model may underestimate the 95% confidence interval of the α/β ratio – if the population model is used to estimate this ratio, the confidence intervals increase markedly. Thus, we caution against the creation of treatment protocols that are based on

the assumption of prostate α/β being equal to exactly 1.5 Gy, and thus lower than the α/β ratio of the surrounding normal tissues, as suggested by Fowler *et al.*[51,52]

6.7 Conclusion

Both the individual and population TCP models can be expressed in a form where the parameterization is in terms of D_{50} and γ_{50}. The functional form of these models is very similar. Based on this equivalence of functional form, it was shown that both individual parameters and parameter ratios do not map identically if these are obtained by fitting the models to clinical data. In the case where the low dose rate TCP curve has a shallower slope, the individual model always underestimates the α/β from the population model. This result was also demonstrated numerically. The only exception is the case where the dominant form of heterogeneity is due to clonogen number, and in this case, it was found that parameter ratios do map on a one to one basis if they are estimated using either the individual or population TCP model.

6.8 References

1. J. F. Fowler, "The linear-quadratic formula and progress in fractionated radiotherapy," British Journal of Radiology **62**, 679-694 (1989).

2. D. J. Brenner and E. J. Hall, "Fractionation and protraction for radiotherapy of prostate carcinoma," Int J Radiat Oncol Biol Phys **43**, 1095-1101 (1999).

3. J. Fowler, R. Chappell, and M. Ritter, "Is alpha/beta for prostate tumors really low?," Int J Radiat Oncol Biol Phys **50**, 1021-1031 (2001).

4. H. B. Kal and M. P. Van Gellekom, "How low is the alpha/beta ratio for prostate cancer?," Int J Radiat Oncol Biol Phys **57**, 1116-1121 (2003).

5. C. R. King and J. F. Fowler, "A simple analytic derivation suggests that prostate cancer alpha/beta ratio is low," Int J Radiat Oncol Biol Phys **51**, 213-214 (2001).

6. C. R. King and C. S. Mayo, "Is the prostrate alpha/beta ratio of 1.5 from Brenner & Hall a modeling artifact?," Int J Radiat Oncol Biol Phys **47**, 536-539 (2000).

7. A. E. Nahum, B. Movsas, E. M. Horwitz, C. C. Stobbe, and J. D. Chapman, "Incorporating clinical measurements of hypoxia into tumor local control modeling of prostate cancer: implications for the alpha/beta ratio," Int J Radiat Oncol Biol Phys **57**, 391-401 (2003).

8. J. Z. Wang, M. Guerrero, and X. A. Li, "How low is the alpha/beta ratio for prostate cancer?," Int J Radiat Oncol Biol Phys **55**, 194-203 (2003).

9. J. Z. Wang, X. A. Li, C. X. Yu, and S. J. DiBiase, "The low alpha/beta ratio for prostate cancer: what does the clinical outcome of HDR brachytherapy tell us?," Int J Radiat Oncol Biol Phys **57**, 1101-1108 (2003).

10. G. S. Higgins, D. B. McLaren, G. R. Kerr, T. Elliott, and G. C. Howard, "Outcome analysis of 300 prostate cancer patients treated with neoadjuvant androgen deprivation and hypofractionated radiotherapy," Int J Radiat Oncol Biol Phys **65**, 982-989 (2006).

11. P. A. Kupelian, V. V. Thakkar, D. Khuntia, C. A. Reddy, E. A. Klein, and A. Mahadevan, "Hypofractionated intensity-modulated radiotherapy (70 gy at 2.5 Gy per fraction) for localized prostate cancer: long-term outcomes," Int J Radiat Oncol Biol Phys **63**, 1463-1468 (2005).

12. J. E. Livsey, R. A. Cowan, J. P. Wylie, R. Swindell, G. Read, V. S. Khoo, and J. P. Logue, "Hypofractionated conformal radiotherapy in carcinoma of the prostate: five-year outcome analysis," Int J Radiat Oncol Biol Phys **57**, 1254-1259 (2003).

13. A. Pollack, A. L. Hanlon, E. M. Horwitz, S. J. Feigenberg, A. A. Konski, B. Movsas, R. E. Greenberg, R. G. Uzzo, C. M. Ma, S. W. McNeeley, M. K. Buyyounouski, and R. A. Price, Jr., "Dosimetry and preliminary acute toxicity in the first 100 men treated for prostate cancer on a randomized hypofractionation dose escalation trial," Int J Radiat Oncol Biol Phys **64**, 518-526 (2006).

14. E. E. Yeoh, R. H. Holloway, R. J. Fraser, R. J. Botten, A. C. Di Matteo, J. Butters, S. Weerasinghe, and P. Abeysinghe, "Hypofractionated versus conventionally fractionated radiation therapy for prostate carcinoma: Updated results of a phase III randomized trial," Int J Radiat Oncol Biol Phys **66**, 1072-1083 (2006).

15. D. J. Brenner, "Dose, volume, and tumor-control predictions in radiotherapy," Int J Radiat Oncol Biol Phys **26**, 171-179 (1993).

16. M. Carlone, B. Warkentin, P. Stavrev, and B. G. Fallone, "Fundamental form of the population TCP model in the limit of large heterogeneity," Med. Phys. **33**, 1634-1642 (2006).

17. A. Dasu, I. Toma-Dasu, and J. F. Fowler, "Should single or distributed parameters be used to explain the steepness of tumour control probability curves?," Phys Med Biol **48**, 387-397 (2003).

18. B. Warkentin, P. Stavrev, N. A. Stavreva, and B. G. Fallone, "Limitations of a TCP model incorporating population heterogeneity," Phys Med Biol **50**, 3571-3588 (2005).

19. D. J. Brenner and E. J. Hall, "In response to Drs King and Mayo: Low α/β values for prostate appear to be independent of modeling details," Int J Radiat Biol Oncol Phys **47**, 538-539 (2000).

20. R. G. Dale, "Radiobiological assessment of permanent implants using tumor repopulation factors in the linear-quadratic model," Br J Radiol **62**, 241-244 (1989).

21. R. G. Dale, "Time-dependent tumour repopulation factors in linear-quadratic equations--implications for treatment strategies," Radiother Oncol **15**, 371-381 (1989).

22. B. Maciejewski, H. R. Withers, J. M. Taylor, and A. Hliniak, "Dose fractionation and regeneration in radiotherapy for cancer of the oral cavity and oropharynx: tumor dose-response and repopulation," Int J Radiat Oncol Biol Phys **16**, 831-843 (1989).

23. B. Maciejewski, H. R. Withers, J. M. Taylor, and A. Hliniak, "Dose fractionation and regeneration in radiotherapy for cancer of the oral cavity and oropharynx. Part 2. Normal tissue responses: acute and late effects," Int J Radiat Oncol Biol Phys **18**, 101-111 (1990).

24. S. A. Roberts and J. H. Hendry, "The delay before onset of accelerated tumour cell repopulation during radiotherapy: a direct maximum-likelihood analysis of a collection of worldwide tumour-control data," Radiother Oncol **29**, 69-74 (1993).

25. S. A. Roberts and J. H. Hendry, "A realistic closed-form radiobiological model of clinical tumor-control data incorporating intertumor heterogeneity," Int J Radiat Oncol Biol Phys **41**, 689-699 (1998).

26. J. M. Taylor, H. R. Withers, and W. M. Mendenhall, "Dose-time considerations of head and neck squamous cell carcinomas treated with irradiation," Radiother Oncol **17**, 95-102 (1990).

27. H. D. Thames, S. M. Bentzen, I. Turesson, M. Overgaard, and W. Van den Bogaert, "Time-dose factors in radiotherapy: a review of the human data," Radiother Oncol **19**, 219-235 (1990).

28. E. L. Travis and S. L. Tucker, "Isoeffect models and fractionated radiation therapy," Int J Radiat Oncol Biol Phys **13**, 283-287 (1987).

29. S. L. Tucker and E. L. Travis, "Comments on a time-dependent version of the linear-quadratic model," Radiother Oncol **18**, 155-163 (1990).

30. J. Van Dyk, K. Mah, and T. J. Keane, "Radiation-induced lung damage: dose-time-fractionation considerations," Radiother Oncol **14**, 55-69 (1989).

31. J. van de Geijn, "Incorporating the time factor into the linear-quadratic model," British Journal of Radiology **62**, 296-298 (1989).

32. T. E. Wheldon and A. E. Amin, "The Linear Quadratic Model," British Journal of Radiology **61**, 700-702 (1988).

33. H. R. Withers, J. M. Taylor, and B. Maciejewski, "The hazard of accelerated tumor clonogen repopulation during radiotherapy," Acta Oncol **27**, 131-146 (1988).

34. R. J. Yaes, "Linear-quadratic model isoeffect relations for proliferating tumor cells for treatment with multiple fractions per day," Int J Radiat Oncol Biol Phys **17**, 901-905 (1989).

35. P. Stavrev, N. Stavreva, A. Niemierko, and M. Goitein, "Generalization of a model of tissue response to radiation based on the idea of functional subunits and binomial statistics," Phys Med Biol **46**, 1501-1518 (2001).

36. S. M. Bentzen, "Steepness of the clinical dose-control curve and variation in the in vitro radiosensitivity of head and neck squamous cell carcinoma," Int J Radiat Biol **61**, 417-423 (1992).

37. S. M. Bentzen and H. D. Thames, "Tumor volume and local control probability: clinical data and radiobiological interpretations," Int J Radiat Oncol Biol Phys **36**, 247-251 (1996).

38. S. M. Bentzen, H. D. Thames, and J. Overgaard, "Does variation in the in vitro cellular radiosensitivity explain the shallow clinical dose-control curve for malignant melanoma?," Int J Radiat Biol **57**, 117-126 (1990).

39. A. A. Khalil, S. M. Bentzen, and J. Overgaard, "Steepness of the dose-response curve as a function of volume in an experimental tumor irradiated under ambient or hypoxic conditions," Int J Radiat Oncol Biol Phys **39**, 797-802 (1997).

40. S. M. Bentzen, "Dose-response relationships in radiotherapy", in *Basic Clinical Radiobiology* edited by G. Steel (Hodder Arnold, London (Gr. Britain), 2002), pp. 94-104.

41. C. Schinkel, N. Stavreva, M. Carlone, P. Stavrev, and B. G. Fallone, "On the equivalence of the population and individual TCP models [Abstract]," Med Phys **33**, 2125 (2006).

42. P. Okunieff, D. Morgan, A. Niemierko, and H. D. Suit, "Radiation dose-response of human tumors," Int J Radiat Oncol Biol Phys **32**, 1227-1237 (1995).

43. B. M. Dubray and H. D. Thames, "The clinical significance of ratios of radiobiological parameters," Int J Radiat Oncol Biol Phys **35**, 1099-1111 (1996).

44. M. Carlone, D. Wilkins, B. Nyiri, and P. Raaphorst, "Comparison of alpha/beta estimates from homogeneous (individual) and heterogeneous (population) tumor control models for early stage prostate cancer," Med Phys **30**, 2832-2848 (2003).

45. R. G. Stock, N. N. Stone, A. Tabert, C. Lannuzzi, and J. K. DeWyngaert, "A dose-response study for I-125 prostate implants," Int J Radiat Oncol Biol Phys **41**, 101-108 (1998).

46. M. Carlone, D. Wilkins, B. Nyiri, and P. Raaphorst, "TCP isoeffect analysis using a heterogeneous distribution of radiosensitivity," Med Phys **31**, 1176-1182 (2004).

47. W. H. Pinover, A. L. Hanlon, E. M. Horwitz, and G. E. Hanks, "Defining the appropriate radiation dose for pretreatment PSA < or = 10 ng/mL prostate cancer," Int J Radiat Oncol Biol Phys **47**, 649-654 (2000).

48. G. E. Hanks, T. E. Schultheiss, A. L. Hanlon, M. Hunt, W. R. Lee, B. E. Epstein, and L. R. Coia, "Optimization of conformal radiation treatment of prostate cancer: report of a dose escalation study," Int J Radiat Oncol Biol Phys **37**, 543-550 (1997).

49. R. Taschereau, R. Roy, and J. Pouliot, "Relative biological effectiveness enhancement of a 125I brachytherapy seed with characteristic x rays from its constitutive materials," Med Phys **29**, 1397-1402 (2002).

50. C. S. Wuu and M. Zaider, "A calculation of the relative biological effectiveness of 125I and 103Pd brachytherapy sources using the concept of proximity function," Med Phys **25**, 2186-2189 (1998).

51. J. F. Fowler, R. J. Chappell, and M. A. Ritter, "The prospects for new treatments for prostate cancer," Int J Radiat Oncol Biol Phys **52**, 3-5 (2002).

52. J. F. Fowler, M. A. Ritter, R. J. Chappell, and D. J. Brenner, "What hypofractionated protocols should be tested for prostate cancer?," Int J Radiat Oncol Biol Phys **56**, 1093-1104 (2003).

Chapter 7 Statistical quality of clinical dose-response data required to resolve TCP model parameters

7.1 Introduction

Despite the developments in clinical radiobiology that have occurred over the past few decades, TCP and NTCP models have seen limited clinical use. The main reason for this is the scarcity and limited quality of available clinical dose-response data (e.g. Moiseenko *et al.*[1] and Zaider & Amols[2]).

Many dose-response datasets suffer from relatively poor statistics (e.g., Hanks *et al.*,[3] Choi & Doucette[4]) or, in some instances (e.g., Emami *et al.*[5]), are not even statistical in nature. These datasets also tend to cover a narrow range in dose-TCP/NTCP space (e.g., about 8 – 10 Gy for prostate dose-escalation trials[3,6-8]) because the delivered dose must be at least equal to the current curative standard, and, at the same time, must remain low enough to limit normal tissue complications. For the accurate estimation of model parameters, data points should ideally span the entire dose-response curve. While it is true that older dose-response datasets (e.g., Bedwinek *et al.*[9] and Bataini *et al.*[10]) cover relatively wide dose and response ranges, they may suffer from other uncertainties, such as uncertainty in dose distribution and delivered dose.

The lack of high-quality dose-response data is the main reason for the inherent uncertainty of TCP and NTCP model predictions. This in turn limits the use of these models in the evaluation and ranking of treatment plans, and in the planning process itself. For example, in Chapter 2 it was demonstrated that physical inverse planning optimization excludes a large number of DVHs with acceptable NTCP. However, in spite of this limitation, modern treatment planning systems still utilize physical constraint points, instead of biological ones, for optimization.

The currently-available clinical data are not of a sufficient quality to distinguish between different TCP (or NTCP) models. In Chapter 2, the Lyman and critical volume population models behaved similarly when they were used to estimate physical dose-volume constraint points. In Chapter 5, it was shown that the individual and population-averaged TCP models would produce nearly identical D_{50} and γ_{50} values when fit to a clinical dataset. Even in the case of $\gamma_{50} < 1$, where the two models differ most in functional form, both would fit existing clinical data equally well.

The poor quality of existing clinical data leads to model parameter and ratio estimates with large confidence intervals. For example, the prostate α/β estimates that Carlone *et al.*[11] obtained using a population-averaged TCP model had 95% CIs of ~[2, 40]. Because of this, pseudo-data were used to test the derived mapping relationships for α/β estimates from two different TCP models in Chapter 6.

It is clear that the available dose-response data are, for the most part, insufficient for the purpose of clinical TCP and NTCP modeling. In this chapter, the minimum number of patients per point that must be analyzed during a clinical trial to estimate reasonably accurate model parameters from the collected dose-response data is determined. Pseudo-datasets, with different numbers of patients per point, that conform to current clinical limitations (with regard to dose range and minimum TCP values) are generated from TCP curves with differing $\gamma_{50,th}$ and $D_{50,th}$ values. A TCP curve is then fit to each dataset to obtain parameter estimates. The impact of the quantities $\gamma_{50,th}$, $D_{50,th}$, dose range, number of patients per point (i.e., statistical error), and minimum TCP value on the 95% confidence intervals (CIs) of the fitted parameters is assessed. From these results, the values that would be required to produce a reasonably narrow 95% CI for each of the fitted parameters are estimated.

7.2 *Method*

7.2.1 Generation of pseudo-data

The method used to generate pseudo-data for this numerical experiment is similar to the one described in Appendix D, with one exception. Using the notation of this appendix, D_x is the dose at the specified TCP value, TCP_x. Here, this point is designated as the first in the series of n_p points – they are assigned dose values that are evenly spaced over the interval of $[D_x, D_x + \Delta D]$.

For the purpose of data generation, it was assumed that the population-averaged TCP model for the limit of dominant heterogeneity in radiosensitivity,[12]

$$TCP = \frac{1}{2} erfc\left[\sqrt{\pi}\gamma_{50,th}\left(\frac{D_{50,th}}{D} - 1\right)\right], \tag{7-1}$$

gives a correct description of the tumour dose-response relationship.

A series of datasets were generated to investigate the effect of variations in the following quantities on the model parameter estimates that would be obtained by fitting Eq. (7-1) to the pseudo-data:

(i) the number of patients per point, N,

(ii) the dose range encompassed by the points, ΔD,

(iii) the normalized slope of the theoretical TCP curve, $\gamma_{50,th}$,

(iv) the dose at 50% control of the theoretical TCP curve, $D_{50,th}$, and

(v) the location of the dataset in dose-TCP space, TCP_x.

Each dataset was assumed to consist of a total of $n_p = 5$ points. (Varying n_p between 3 and 7 did not have a significant effect on the accuracy of the estimated parameters). The value for n_p was selected based on the number of points that are typically considered in modern dose escalation trials. The dose range of clinical datasets, which is limited by clinical concerns, is quite small and therefore only covers a narrow portion of the TCP curve. Thus, it is expected that the inclusion of more than 7 points over a typical dose range will likewise not affect the accuracy of the estimated parameters. If, however, it

were possible to collect clinical dose-response data over a larger dose range, more than five points would be required to fully define the dose-response curve.

The values for all quantities associated with the pseudo-datasets are shown in Table 7-1. Each row represents the series of datasets generated to determine the effect of variations in that particular quantity.

The $\gamma_{50,th}$ and $D_{50,th}$ parameters in Table 7-1 were assigned ranges of values that are characteristic of clinical dose-response data, based on the results of Okunieff *et al.*[13] The 'standard' starting TCP level for the generated data was set to $TCP_x = 70\%$, which is about the same as the TCP of the lowest dose point in the EBRT prostate datasets of Hanks *et al.*[3] and Pinover *et al.*[8] The 'standard' value for ΔD of 10 Gy was selected based on these same two datasets.

Table 7-1: Values for all quantities that characterize each of five series of generated pseudo-datasets. The leftmost column gives the main varied quantity of each series, and blue cells represent the specific values chosen for the varied quantity of interest. To assess the impact of a certain quantity on the accuracy of estimated model parameters, each pseudo-dataset in the series was fit with Eq. (7-1), and the corresponding change in the 95% CI width of each parameter was assessed.

Varied quantity	**Assumed values for all quantities**					
	n_p	ΔD (Gy)	N	$\gamma_{50,th}$	$D_{50,th}$ (Gy)	TCP_x (%)
Dose range of data points, ΔD	5	**10, 20, 30**	50, 100, 200, 500, 1000, 2000	1	50	70
Number of patients per point, N	5	10, 20, 30	**50, 100, 200, 500, 1000, 2000**	1, 1.5, 2	30, 50, 70	60, 70, 80
Normalized slope, $\gamma_{50,th}$	5	10, 20, 30	50, 100, 200, 500, 1000, 2000	**1, 1.5, 2**	50	70
Dose at 50% control, $D_{50,th}$	5	10, 20	50, 100, 200, 500, 1000, 2000	1	**30, 50, 70**	70
Location of data in dose-TCP space, TCP_x	5	10	50, 100, 200, 500, 1000, 2000	1	50	**60, 70, 80**

Examples of some pseudo-datasets with different numbers of patients per point, N, are shown in Figure 7-1. They were each generated from a population-averaged TCP curve with theoretical parameter values of $\gamma_{50,th} = 1$ and $D_{50,th} = 50$ Gy, and they all span a dose range of $\Delta D = 10$ Gy. The error bars shown in Figure 7-1 represent the 68% CI for each point, and were calculated assuming binomial statistics,

$$\sigma = \sqrt{\frac{TCP_{th}(D)[1 - TCP_{th}(D)]}{N}}, \tag{7-2}$$

where $TCP_{th}(D)$ is the theoretical TCP value for the point at dose, D, and σ is the standard deviation.

7.2.2 Determination of parameters of best fit and their confidence intervals

The TCP model [Eq. (7-1)] parameters of best fit were obtained for each of the generated dose-response datasets using maximum likelihood estimation, and the confidence intervals were calculated using the Monte Carlo procedure[11,14] described in Appendix E. The relative size of the 95% CI was used to assess the accuracy of model parameters estimated from a given pseudo-dataset. The effect of varying a given quantity on the certainty of the resulting parameter estimates was measured by observing the corresponding change in the width of the 95% CIs. A decrease in the width of the 95% CI means that the estimated parameter may be determined with greater certainty.

7.3 Results

The D_{50} and γ_{50} parameter values of best fit, along with their upper and lower 95% confidence limits, are shown in Appendix F for each of the generated datasets described in Section 7.2.1. Also shown for each dataset is the minimum negative log likelihood value that corresponds to the best-fit parameters, and its 95% CI.

The remainder of this section begins with an overview of the general results for the numerical experiments described in Table 7-1. This is followed by more detailed results for each experiment, complete with figures and tables.

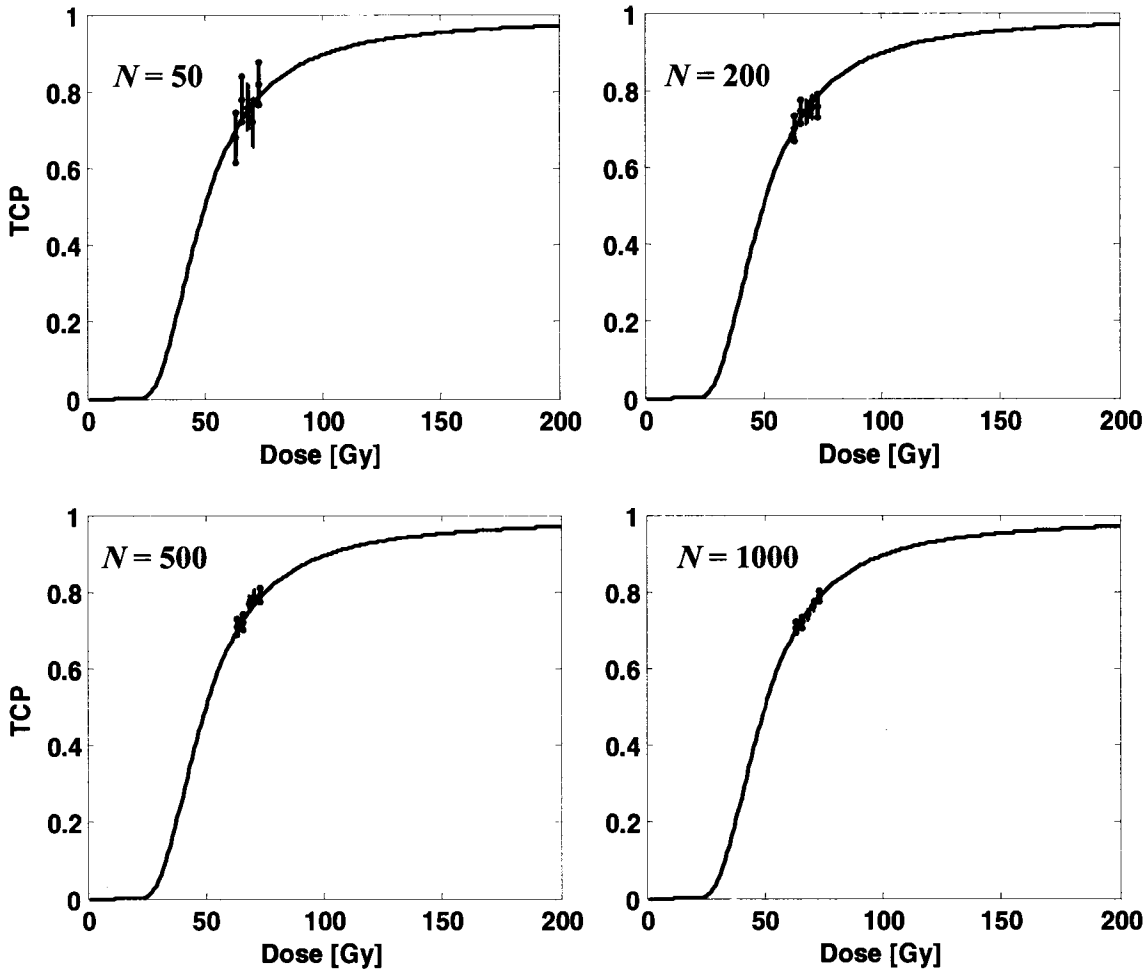

Figure 7-1: Pseudo-datasets with n_p = 5 points over a dose interval of ΔD = 10 Gy generated from a population-averaged TCP curve with $D_{50,th}$ = 50 Gy and $\gamma_{50,th}$ = 1. Each dataset was generated assuming a different number of patients per point (N); the selected values of N are shown in each sub-plot. The error bars represent the 68% CI for each point, and were calculated assuming binomial statistics.

7.3.1 General results

Table 7-2 summarizes the effect of an increase in each of the quantities outlined in Table 7-1 on the width of the 95% CIs of the fitted parameter estimates: D_{50} and γ_{50}.

Improvements in the certainty of the estimated parameters were found to occur with increases in the dose range of the data points (ΔD), the number of patients per point

(N), and the normalized slope of the TCP curve from which the pseudo-data are generated ($\gamma_{50,th}$). The certainty of the estimated parameters became worse with increases in the dose at 50% control of the theoretical TCP curve ($D_{50,th}$) and the TCP level at which the data points are located (TCP_x). One does not generally have control over the properties of the theoretical TCP curve ($D_{50,th}$ and $\gamma_{50,th}$). The dose range is limited by clinical concerns, but the results in Table 7-2 indicate that it is desirable to select as large a dose range as possible for clinical dose-response trials. The location of the data in dose-TCP space tends to be site-specific, and therefore the value of TCP_x cannot be influenced. The quantity that may be controlled to the greatest degree is the number of patients per point, N. For clinical trials, N should be assigned as large a value as possible to reliably estimate TCP model parameters.

Table 7-2: Illustrates the effect of an increase in each quantity in the leftmost column on the width of the 95% CI for parameters obtained from fitting. Up-arrows in the rightmost column indicate an increase in the 95% CI width (and correspondingly, a decrease in the accuracy of the estimated parameters), and down-arrows indicate a decrease in the 95% CI width (i.e., an increase in the accuracy of the parameter estimates).

Varied quantity		Effect on 95% CI width of fitted parameters: D_{50}, γ_{50}
Dose range of data points	$\Delta D \uparrow$	$\downarrow$
Number of patients per point	$N \uparrow$	$\downarrow$
Normalized slope	$\gamma_{50,th} \uparrow$	$\downarrow$
Dose at 50% control	$D_{50,th} \uparrow$	$\uparrow$
Location of data in dose-TCP space	$TCP_x \uparrow$	$\uparrow$

7.3.2 Effect of dose range and statistics per point on 95% CI

The effect of dose range, ΔD, and the number of patients per point, N, on the accuracy of each estimated parameter can be seen in Table 7-3, Figure 7-2 and Figure 7-3. The table shows the absolute width of the 95% CI, $C_u - C_l$, for the fitted parameters

D_{50} and γ_{50}, along with the relative width, $(C_u - C_l)/D_{50,th}$, for each of the pseudo-datasets described in the first row of Table 7-1. Figure 7-2 shows the relative 95% CIs of both fitted parameters as functions of N for each of the three dose intervals, and Figure 7-3 shows the dependence on ΔD alone (for $N = 1000$).

The 95% CI for each fitted parameter narrows as N increases and as ΔD increases. For a dose interval of 10 Gy, at least 1000 patients per point are required to estimate D_{50} with a relative 95% CI of around 25%. According to these simulations, it is not possible to resolve γ_{50} to the same degree of accuracy as D_{50} – for a dose interval of 10 Gy, a dataset with 2000 patients per point will yield an estimate for γ_{50} with a relative 95% CI of around 40%.

The relationship between the relative 95% CI of γ_{50} and the number of patients per point is linear on a log-log scale. This is also generally true for the relative 95% CI of D_{50} as a function of N, although this CI is subject to considerably more statistical variation than that of γ_{50}. In each case, the relative 95% CI is roughly proportional to $\sqrt{N}$ (i.e., on a log-log scale, the relative CI as a function of N is linear with a slope of approximately -0.5).

Table 7-3: 95% confidence intervals (absolute, $C_u - C_l$, and relative, %) for the parameters D_{50} and γ_{50} obtained from fits to pseudo-datasets with $n_p = 5$ and $TCP_x = 70\%$ generated from a TCP curve with $D_{50,th} = 50$ Gy and $\gamma_{50,th} = 1$.

N	$\Delta D \rightarrow$	10 Gy		20 Gy		30 Gy	
		$C_u - C_l$	(%)	$C_u - C_l$	(%)	$C_u - C_l$	(%)
50	D_{50} 95% CI	122.1	244.3%	62.5	125.0%	27.8	55.6%
	γ_{50} 95% CI	2.30	230.1%	1.43	142.9%	1.13	113.3%
200	D_{50} 95% CI	115.8	231.6%	26.4	52.9%	17.7	35.3%
	γ_{50} 95% CI	1.22	121.5%	0.72	71.7%	0.55	55.4%
500	D_{50} 95% CI	16.7	33.4%	15.2	30.5%	8.0	16.0%
	γ_{50} 95% CI	0.86	85.7%	0.45	45.0%	0.33	32.6%
1000	D_{50} 95% CI	12.3	24.5%	6.8	13.7%	5.4	10.8%
	γ_{50} 95% CI	0.57	57.2%	0.31	31.2%	0.24	24.0%
2000	D_{50} 95% CI	6.2	12.3%	5.0	10.0%	4.7	9.4%
	γ_{50} 95% CI	0.40	40.4%	0.23	22.5%	0.16	16.5%

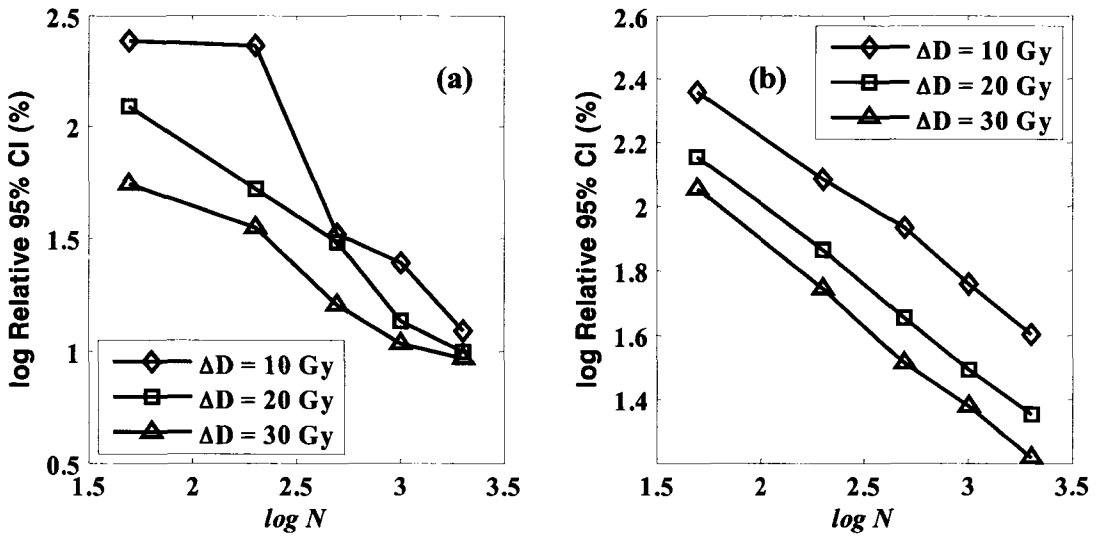

Figure 7-2: The relative 95% CI for D_{50} (a) and γ_{50} (b) from Table 7-3 plotted as a function of the number of patients per point (N) on a log-log scale for the three dose intervals 10, 20 and 30 Gy.

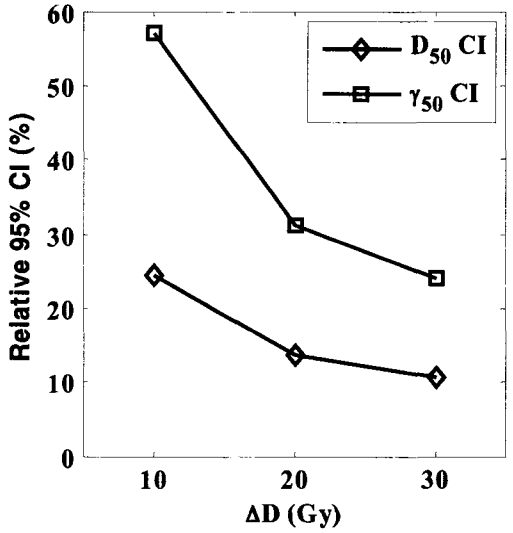

Figure 7-3: The relative 95% CI for D_{50} (◇) and γ_{50} (□) as a function of dose range, ΔD, corresponding to the pseudo-datasets with $TCP_x = 70\%$, $N = 1000$, $D_{50,th} = 50$ Gy and $\gamma_{50,th} = 1$.

7.3.3 Effect of $\gamma_{50,th}$ on 95% CI

Table 7-4 and Table 7-5 show the same information as Table 7-3, but for the datasets that were generated to quantify the effect of varying $\gamma_{50,th}$ on parameter estimates (represented by the third row of Table 7-1). The dependence of the relative 95% CI on normalized slope is illustrated in Figure 7-4 and Figure 7-5.

As before, the 95% CIs for each fitted parameter decrease with increasing N and ΔD. The normalized slope of the TCP curve from which the pseudo-data are generated clearly has an influence on the 95% CIs for the estimated parameters. Figure 7-5 shows that a steeper slope leads to a smaller relative 95% CI, and a correspondingly more accurate parameter estimate. This trend is mostly independent of the number of patients per point in the dataset, as can be seen in Figure 7-4.

Table 7-4: 95% confidence intervals (absolute, $C_u - C_l$, and relative, %) for the parameters D_{50} and γ_{50} obtained from fits to pseudo-datasets with $n_p = 5$ and $TCP_x = 70\%$ generated from a TCP curve with $D_{50,th} = 50$ Gy and $\gamma_{50,th} = 1.5$.

N	$\Delta D \rightarrow$	10 Gy		20 Gy		30 Gy	
		$C_u - C_l$	(%)	$C_u - C_l$	(%)	$C_u - C_l$	(%)
50	D_{50} 95% CI	25.2	50.3%	10.2	20.4%	24.6	49.3%
	γ_{50} 95% CI	2.56	170.5%	1.56	103.8%	1.16	77.3%
200	D_{50} 95% CI	18.8	37.6%	6.8	13.6%	6.2	12.4%
	γ_{50} 95% CI	1.25	83.3%	0.75	49.9%	0.56	37.6%
500	D_{50} 95% CI	8.2	16.4%	6.3	12.6%	4.6	9.2%
	γ_{50} 95% CI	0.80	53.1%	0.45	30.3%	0.35	23.5%
1000	D_{50} 95% CI	5.2	10.4%	3.3	6.7%	3.2	6.3%
	γ_{50} 95% CI	0.55	36.4%	0.34	22.6%	0.24	16.1%
2000	D_{50} 95% CI	3.6	7.2%	2.8	5.7%	2.5	5.1%
	γ_{50} 95% CI	0.39	26.3%	0.24	15.8%	0.18	12.1%

Table 7-5: 95% confidence intervals (absolute, $C_u - C_l$, and relative, %) for the parameters D_{50} and γ_{50} obtained from fits to pseudo-datasets with $n_p = 5$ and $TCP_x = 70\%$ generated from a TCP curve with $D_{50,th} = 50$ Gy and $\gamma_{50,th} = 2$.

N	$\Delta D \rightarrow$	10 Gy		20 Gy		30 Gy	
		$C_u - C_l$	(%)	$C_u - C_l$	(%)	$C_u - C_l$	(%)
50	D_{50} 95% CI	35.3	70.5%	6.2	12.4%	9.3	18.5%
	γ_{50} 95% CI	2.47	123.4%	1.86	92.9%	1.34	67.2%
200	D_{50} 95% CI	9.6	19.1%	6.1	12.3%	4.7	9.5%
	γ_{50} 95% CI	1.24	62.2%	0.77	38.6%	0.74	36.8%
500	D_{50} 95% CI	2.8	5.7%	2.8	5.6%	3.0	5.9%
	γ_{50} 95% CI	0.80	39.8%	0.49	24.7%	0.42	20.8%
1000	D_{50} 95% CI	2.9	5.8%	2.7	5.3%	2.4	4.8%
	γ_{50} 95% CI	0.55	27.7%	0.35	17.6%	0.31	15.5%
2000	D_{50} 95% CI	2.4	4.8%	1.5	3.1%	1.8	3.6%
	γ_{50} 95% CI	0.39	19.6%	0.26	12.8%	0.20	10.0%

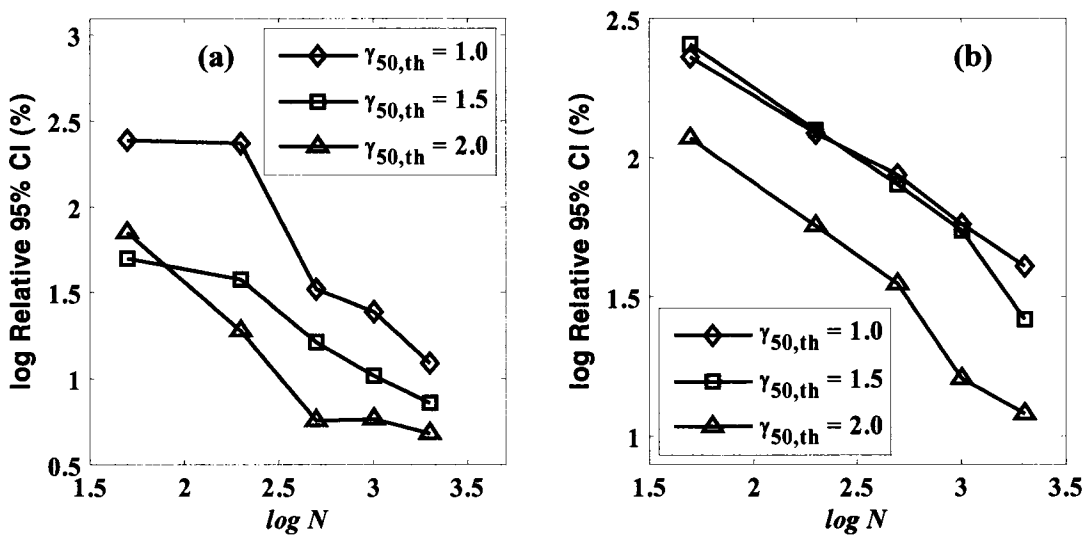

Figure 7-4: The relative 95% CIs for the parameters D_{50} (a) and γ_{50} (b) plotted as a function of the number of patients per point (N) on a log-log scale for three theoretical normalized slope values – $\gamma_{50,th} = 1$, 1.5 and 2. The estimated parameters correspond to datasets where $n_p = 5$, $TCP_x = 70\%$, $\Delta D = 10$ Gy, and $D_{50,th} = 50$ Gy.

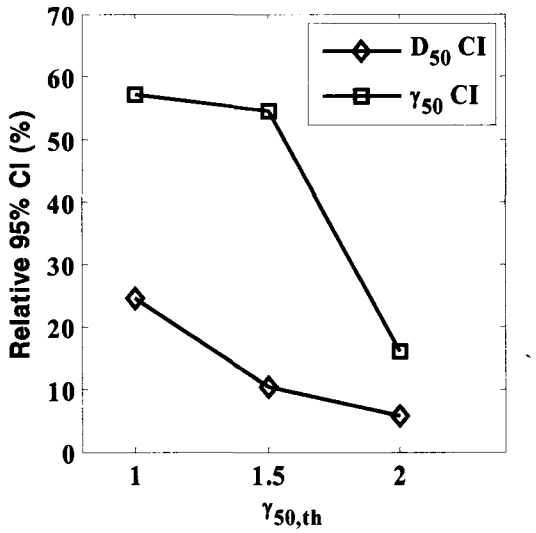

Figure 7-5: The relative 95% CI for D_{50} (◇) and γ_{50} (□) as a function of the assumed normalized slope, $\gamma_{50,th}$, corresponding to the pseudo-datasets with $n_p = 5$, $TCP_x = 70\%$, $N = 1000$, $D_{50,th} = 50$ Gy and $\Delta D = 10$ Gy.

7.3.4 Effect of $D_{50,th}$ on 95% CI

The effect of varying $D_{50,th}$ on the accuracy of estimated TCP model parameters can be seen in Table 7-6, which shows the absolute and relative 95% CIs for the fitted parameters from the datasets corresponding to the fourth row of Table 7-1. Figure 7-6 shows the relative 95% CIs for the fitted parameters as a function of the number of patients per point, for each of three $D_{50,th}$ values – 30, 50 and 70 Gy, and Figure 7-7 shows the relative 95% CI for each fitted parameter as a function of $D_{50,th}$ alone, for datasets with $N = 1000$ and $\Delta D = 10$ Gy.

Generally, the width of the 95% CI increases (i.e., the certainty of the estimated parameters decreases) as the assumed dose at 50% control increases. As before, increasing N also increases the certainty of the parameter estimates.

Table 7-6: 95% confidence intervals (absolute, $C_u - C_l$, and relative, %) for the parameters D_{50} and γ_{50} obtained from fits to pseudo-datasets with $n_p = 5$ and $TCP_x = 70\%$ generated from TCP curves with $D_{50,th} = 30$ and 70 Gy and $\gamma_{50,th} = 1$.

		$D_{50,th}$ = 30 Gy				$D_{50,th}$ = 70 Gy			
N	$\Delta D \rightarrow$	10 Gy		20 Gy		10 Gy		20 Gy	
		$C_u - C_l$	(%)	$C_u - C_l$	(%)	$C_u - C_l$	(%)	$C_u - C_l$	(%)
50	D_{50} 95% CI	55.8	186.0%	17.6	58.8%	248.5	354.9%	170.6	243.7%
	γ_{50} 95% CI	1.64	164.5%	1.10	110.0%	2.75	275.4%	1.75	174.6%
200	D_{50} 95% CI	20.0	66.5%	7.1	23.6%	54.3	77.5%	34.0	48.6%
	γ_{50} 95% CI	0.82	81.6%	0.51	50.8%	1.74	174.4%	1.01	101.3%
500	D_{50} 95% CI	8.1	27.0%	4.6	15.3%	20.0	28.6%	24.2	34.5%
	γ_{50} 95% CI	0.51	50.9%	0.31	31.3%	1.06	106.2%	0.60	60.3%
1000	D_{50} 95% CI	3.8	12.7%	4.4	14.5%	39.3	56.2%	11.5	16.5%
	γ_{50} 95% CI	0.38	38.1%	0.22	22.5%	0.80	80.2%	0.41	40.7%
2000	D_{50} 95% CI	3.2	10.6%	2.4	8.1%	19.3	27.5%	8.8	12.6%
	γ_{50} 95% CI	0.26	26.3%	0.15	14.8%	0.54	53.9%	0.29	29.5%

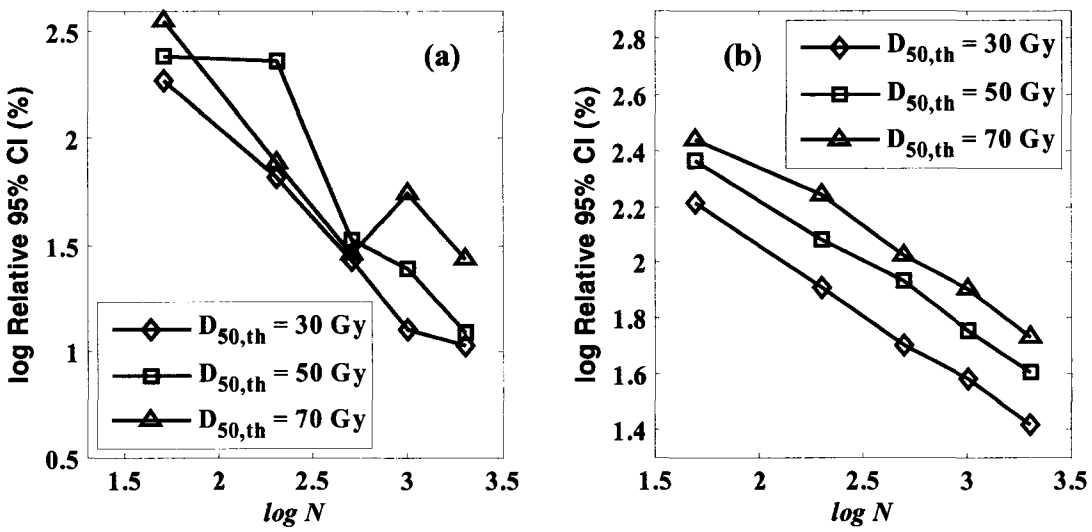

Figure 7-6: The relative 95% CIs for the parameters D_{50} (a) and γ_{50} (b) plotted as a function of the number of patients per point (N) on a log-log scale for three theoretical D_{50} values – $D_{50,th}$ = 30, 50 and 70 Gy. The estimated parameters correspond to datasets where $n_p = 5$, $TCP_x = 70\%$, $\Delta D = 10$ Gy, and $\gamma_{50,th} = 1$.

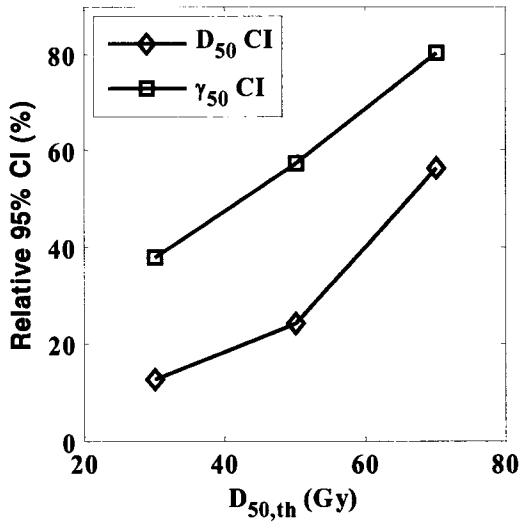

Figure 7-7: The relative 95% CI for D_{50} (◇) and γ_{50} (□) as a function of the assumed dose at 50% control, $D_{50,th}$, corresponding to the pseudo-datasets with TCP_x = 70%, N = 1000, $\gamma_{50,th}$ = 1 and ΔD = 10 Gy.

7.3.5 Effect of data location (TCP_x) on 95% CI

To illustrate the effect of varying TCP_x on the 95% CIs for the fitted parameters, the generated datasets from a TCP curve with $D_{50,th}$ = 50 Gy and $\gamma_{50,th}$ = 1 were examined (fifth row of Table 7-1). The absolute and relative 95% CIs for the fitted parameters of each dataset are shown in Table 7-7. Figure 7-8 illustrates the relationship between the relative 95% CI of each fitted parameter and N for TCP_x values of 60, 70 and 80%. As before, the size of the relative 95% CI decreases with increasing N. The dependence of relative 95% CI on TCP_x is shown in Figure 7-9 for the parameters estimated from fits to the datasets with 1000 patients per point.

An examination of these figures and Table 7-7 reveals that, regardless of the number of patients per point, N, the 95% CI for each fitted parameter increases as TCP_x increases. In all cases, D_{50} may be determined with greater certainty than γ_{50} for a given dataset, as before.

Table 7-7: 95% confidence intervals (absolute, $C_u - C_l$, and relative, %) for the parameters D_{50} and γ_{50} obtained from fits to pseudo-datasets with $n_p = 5$ and $TCP_x = 60\%$ and 80% generated from TCP curves with $D_{50,th} = 50$ Gy and $\gamma_{50,th} = 1$.

N	$TCP_x \rightarrow$	60%		80%	
		$C_u - C_l$	(%)	$C_u - C_l$	(%)
50	D_{50} 95% CI	27.5	54.9%	256.3	512.7%
	γ_{50} 95% CI	2.11	211.3%	2.46	246.2%
200	D_{50} 95% CI	34.8	69.6%	33.3	66.5%
	γ_{50} 95% CI	1.14	114.2%	1.68	167.6%
500	D_{50} 95% CI	18.1	36.3%	28.2	56.3%
	γ_{50} 95% CI	0.70	70.0%	1.03	103.1%
1000	D_{50} 95% CI	6.4	12.9%	18.8	37.6%
	γ_{50} 95% CI	0.49	48.5%	0.77	76.7%
2000	D_{50} 95% CI	4.6	9.3%	15.0	30.0%
	γ_{50} 95% CI	0.35	35.0%	0.53	53.2%

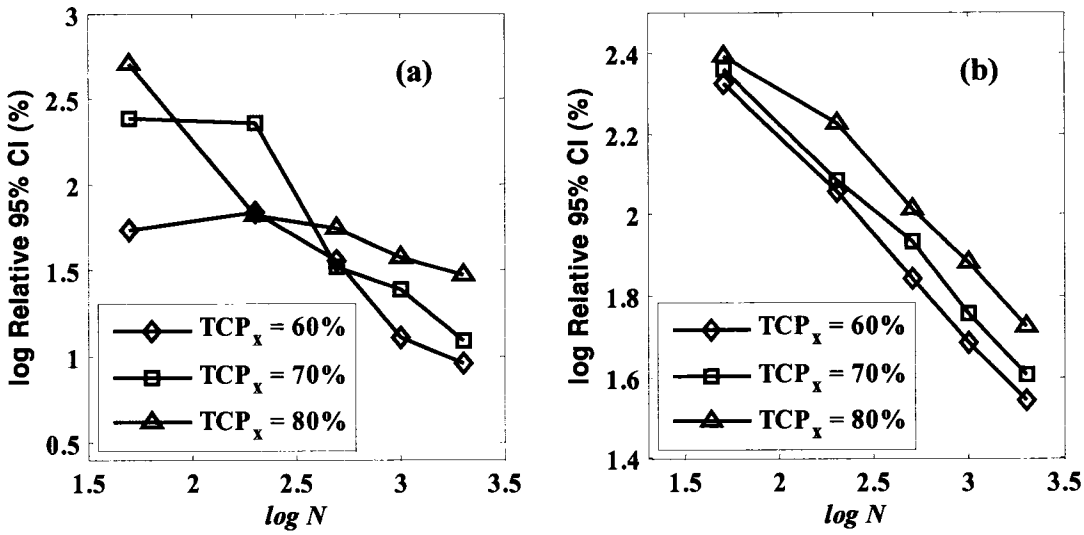

Figure 7-8: The relative 95% CIs for the parameters D_{50} (a) and γ_{50} (b) plotted as a function of the number of patients per point (N) on a log-log scale for three TCP_x values – 60%, 70% and 80%. The estimated parameters correspond to datasets generated from a curve with $D_{50,th} = 50$ Gy and $\gamma_{50,th} = 1$ where $n_p = 5$ and $\Delta D = 10$ Gy.

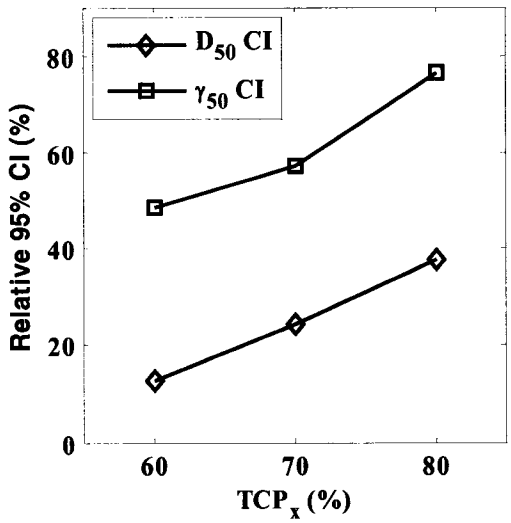

Figure 7-9: The relative 95% CI for D_{50} (◇) and γ_{50} (□) as a function of TCP_x, corresponding to the pseudo-datasets with $D_{50,th}$ = 50 Gy, $\gamma_{50,th}$ = 1, N = 1000, and ΔD = 10 Gy.

7.4 Discussion

The number of patients per point required to estimate parameters with a particular degree of certainty depends on the inherent shape of the dose-response curve that is characteristic of a particular site and treatment regime, i.e., $\gamma_{50,th}$ and $D_{50,th}$. It would be beneficial if one could get a rough estimate for these parameters before designing a clinical trial to collect dose-response data, and this is possible to do if data have previously been published for a given site. Otherwise, the worst-case scenario of a relatively high $D_{50,th}$ and a relatively low $\gamma_{50,th}$ may be assumed to determine a sufficiently large value for N. For example, if it is assumed that $D_{50,th}$ is relatively high (around 70 Gy), the normalized slope is around 1, and the first dose-response point has an expected TCP value of 70%, then for a dose interval of ΔD = 10 Gy, a value of N = 2000 would allow one to estimate D_{50} with an accuracy (i.e., with a relative 95% CI) of around 27.5% and γ_{50} with an accuracy of around 54%.

The dependence of the 95% CIs on $D_{50,th}$ and $\gamma_{50,th}$ arises because both parameters are functions of the non-normalized slope, $\theta_{50} = \gamma_{50}/D_{50}$. A larger $\theta_{50,th}$ means that the

difference between the measured TCP at subsequent dose-response points will be greater, and the fitted parameters will be more accurate. As can be seen in Table 7-8, an increase in $\gamma_{50,th}$ corresponds to an increase in $\theta_{50,th}$, and thus more certain parameter estimates. On the other hand, an increase in $D_{50,th}$ for a fixed $\gamma_{50,th}$ value corresponds to a decreasing $\theta_{50,th}$, and thus the fitted parameters become less certain.

Table 7-8: Non-normalized slope, $\theta_{50,th}$, corresponding to the $D_{50,th}$ and $\gamma_{50,th}$ values listed.

$D_{50,th}$ [Gy]	$\gamma_{50,th}$	$\theta_{50,th}$ [Gy^{-1}]
50	1.0	0.020
50	1.5	0.030
50	2.0	0.040
30	1.0	0.033
70	1.0	0.014

The certainty of estimated model parameters was found to increase with the dose interval, ΔD, spanned by the dose-response points. The maximum dose interval is limited by clinical concerns, such as the tolerance of the surrounding normal tissues to irradiation, but the simulations in this chapter indicate that the largest possible dose interval should be chosen for dose escalation trials.

The effect of varying TCP_x on the accuracy of the estimated parameters is related to the changing slope of the TCP curve with dose. For a given ΔD, a set of dose-response points starting at a TCP_x of 60% lies on a steeper portion of the TCP curve than a set of points starting at TCP_x = 80%. Generally, the expected TCP of the lowest dose point in a clinical trial is known. If this quantity is relatively low, fewer patients per point will be needed to determine parameter estimates to the desired degree of accuracy.

In most of the cases investigated in this chapter, the number of patients per point required to adequately resolve D_{50} and γ_{50} was found to be greater than 1000. In comparison, published clinical datasets from dose escalation trials tend to have fewer than 100 patients per point, and it is often the case that the number of patients is not the same for each point. These statistics are far from sufficient: the dataset with 200 patients

per point that was generated from a TCP curve with theoretical parameter values of $D_{50,th}$ = 50 Gy and $\gamma_{50,th}$ = 1 starting at TCP_x = 70% and spanning a dose interval of 10 Gy resulted in estimated parameters with relative 95% CIs that were greater than 100% (Table 7-3).

The TCP model considered in this chapter [Eq. (7-1)] was derived under the assumption of homogeneous tumour irradiation to dose D. In most cases, especially for IMRT treatments, tumours are irradiated heterogeneously, so a TCP model such as Eq. (5-13) should be used with full tumour DVHs to estimate model parameters. If it is assumed that the results of this chapter are applicable to the heterogeneous case, then the number of patients per point required to estimate parameters with a given degree of accuracy would be equivalent to the total number of clinical tumour DVHs that correspond to different prescription doses in a clinical trial.

This chapter concentrated on estimating parameters for tumours by means of TCP models. A similar type of analysis may be carried out for NTCP models. However, it is often the case that TCP and NTCP information is collected simultaneously from a clinical trial.

7.5 Conclusions

For dose-response datasets subject to clinical restrictions (with respect to starting TCP level, dose range, and number of points), a large number of patients per point must be chosen for fitted parameters to be resolved with reasonable certainty. The required statistics depend on the intrinsic slope of the dose-response curve. For a situation that is typical for prostate dose escalation trials (TCP_x = 70%, n_p = 5 points, ΔD = 10 Gy), the number of patients for each prescription dose (i.e., each dose-response point) must be sufficiently large – between 1000 and 2000 at least. This is a significantly larger number than what is typical of previously-published dose escalation datasets (e.g. Hanks *et al.*,[3] Pinover *et al.*[8]).

If TCP model parameters are ever to be resolved with a reasonable accuracy, a sufficient amount of data must be collected through clinical trials. This will most likely

be achievable only if multiple institutions become involved, and conduct trials according to a strict protocol. The determination of model parameters for both tumours and normal tissues to a reasonable degree of accuracy has the potential to lead to more widespread clinical use of TCP/NTCP models.

7.6 References

1. V. Moiseenko, J. Battista, and J. Van Dyk, "Normal tissue complication probabilities: dependence on choice of biological model and dose-volume histogram reduction scheme," Int J Radiat Oncol Biol Phys **46**, 983-993 (2000).

2. M. Zaider and H. I. Amols, "Practical considerations in using calculated healthy-tissue complication probabilities for treatment-plan optimization," Int J Radiat Oncol Biol Phys **44**, 439-447 (1999).

3. G. E. Hanks, T. E. Schultheiss, A. L. Hanlon, M. Hunt, W. R. Lee, B. E. Epstein, and L. R. Coia, "Optimization of conformal radiation treatment of prostate cancer: report of a dose escalation study," Int J Radiat Oncol Biol Phys **37**, 543-550 (1997).

4. N. C. Choi and J. A. Doucette, "Improved survival of patients with unresectable non-small-cell bronchogenic carcinoma by an innovated high-dose en-bloc radiotherapeutic approach," Cancer **48**, 101-109 (1981).

5. B. Emami, J. Lyman, A. Brown, L. Coia, M. Goitein, J. E. Munzenrider, B. Shank, L. J. Solin, and M. Wesson, "Tolerance of normal tissue to therapeutic irradiation," Int J Radiat Oncol Biol Phys **21**, 109-122 (1991).

6. D. Brabbins, A. Martinez, D. Yan, D. Lockman, M. Wallace, G. Gustafson, P. Chen, F. Vicini, and J. Wong, "A dose-escalation trial with the adaptive radiotherapy process as a delivery system in localized prostate cancer: analysis of chronic toxicity," Int J Radiat Oncol Biol Phys **61**, 400-408 (2005).

7. R. Jacob, A. L. Hanlon, E. M. Horwitz, B. Movsas, R. G. Uzzo, and A. Pollack, "Role of prostate dose escalation in patients with greater than 15% risk of pelvic lymph node involvement," Int J Radiat Oncol Biol Phys **61**, 695-701 (2005).

8. W. H. Pinover, A. L. Hanlon, E. M. Horwitz, and G. E. Hanks, "Defining the appropriate radiation dose for pretreatment PSA < or = 10 ng/mL prostate cancer," Int J Radiat Oncol Biol Phys **47**, 649-654 (2000).

9. J. M. Bedwinek, C. A. Perez, and D. J. Keys, "Analysis of failures after definitive irradiation for epidermoid carcinoma of the nasopharynx," Cancer **45**, 2725-2729 (1980).

10. P. Bataini, J. Brugere, J. Bernier, C. H. Jaulerry, C. Picot, and N. A. Ghossein, "Results of radical radiotherapeutic treatment of carcinoma of the pyriform sinus: experience of the Institut Curie," Int J Radiat Oncol Biol Phys **8**, 1277-1286 (1982).

11. M. Carlone, D. Wilkins, B. Nyiri, and P. Raaphorst, "Comparison of alpha/beta estimates from homogeneous (individual) and heterogeneous (population) tumor control models for early stage prostate cancer," Med Phys **30**, 2832-2848 (2003).

12. M. Carlone, B. Warkentin, P. Stavrev, and B. G. Fallone, "Fundamental form of the population TCP model in the limit of large heterogeneity," Med. Phys. **33**, 1634-1642 (2006).

13. P. Okunieff, D. Morgan, A. Niemierko, and H. D. Suit, "Radiation dose-response of human tumors," Int J Radiat Oncol Biol Phys **32**, 1227-1237 (1995).

14. W. H. Press, B. P. Flannery, S. A. Teukolsky, and W. T. Vetterling, "*Numerical Recipes in C*", (Cambridge University Press, Cambridge, MA, 1988).

Chapter 8 Summary and general discussion

8.1 The incorporation of NTCP models and parameters into inverse planning

In Chapters 2 and 3 of this thesis, a method for calculating physical dose-volume constraints based on existing biological models and datasets was developed. It allows one to incorporate biological information in the physical inverse planning optimization process, which is used almost exclusively in modern treatment planning systems. A number of constraint points were calculated for each of 16 organs, based on the Lyman and critical volume population NTCP models and parameters derived from the Emami *et al.*[1] data.

It was found that the application of two or more of these constraint points for inverse planning optimization can sufficiently restrict NTCP. However, when a single 'raw' Emami dose-volume point is applied as a constraint, all resulting DVH solutions will have an undesirably large NTCP. In Chapter 4, it was shown that this occurs because the Emami points lie on a curve called the iso-NTCP envelope. Thus, the practice of applying 'raw' dose-response data points for the purpose of inverse planning optimization should be avoided.

In Chapter 2 it was observed that the physical dose-volume constraint points calculated for rectum coincide with the average non-bleeder DVH deduced from a previous work[2] for relative volumes less than ~0.4. This is a good indication of their usefulness for inverse planning optimization. On the other hand, it was demonstrated that the application of physical dose-volume constraints excludes a large number of acceptable DVH solutions. Thus, biological or physico-biological optimization is theoretically a better option for inverse planning.

However, biological optimization is currently not being used, mainly because of the uncertainty associated with NTCP models and parameters. Nevertheless, some authors have shown that even the use of the Lyman[3] NTCP model with the Burman *et al.*[4] parameters for physico-biological inverse planning "allows the generation of clinically acceptable plans similar to or better than the ones produced with standard forward or inverse planning techniques. In addition, the use of NTCP-based objective function eliminates the need for numerous dose and dose-volume prescriptions and distributes the integral dose to the various critical organs in a pattern that minimizes the probabilities of radiation-related complications."[5]

Because physical optimization suffers from certain limitations (as shown in Chapter 2), biological optimization should be implemented for the purpose of inverse planning as soon as NTCP models and parameters are reliable enough to be used clinically. The reverse mapping method could potentially be useful as an intermediate inverse planning method until this occurs.

8.2 Functional similarity of the individual and population-based TCP models

In the second part of this thesis, it was demonstrated that the individual (non-averaged) and population-averaged TCP models are functionally similar. Hence, if both models are fit to the same clinical dataset, the D_{50} and γ_{50} parameter estimates should be statistically indistinguishable. For $\gamma_{50} < 1$, the difference between the two models becomes more pronounced.

Despite this functional similarity, it is conceptually incorrect to fit the individual model to clinical data, which represents a population response. In Chapter 5, it was demonstrated that the individual model parameters lose their biological meaning when fit to population data and in Chapter 6, it was analytically shown that the biological parameters obtained from fits of both models to the same dataset do not exhibit a one-to-one relationship. Because the population TCP model explicitly takes the effects of inter-patient heterogeneity into account, it is recommend that this model be used to fit clinical dose-response data.

While the population TCP model is conceptually more accurate than the individual model, it still has its shortcomings. As demonstrated in Carlone *et al.*[6] and Warkentin *et al.*,[7] it is not possible to obtain unique estimates for the radiobiological parameters exclusively from modeling. In addition, the derivation of the population model makes use of several assumptions that may be called into question.[8] It is subject to the same assumptions as the Poisson-based individual model, along with others (e.g., the population distribution functions of individual radiobiological parameters).

Even the assumption that all tumour clonogens must be killed to achieve control may not be completely correct. For example, tumour control may depend on the destruction of the tumour vasculature,[9-13] or it may only be necessary to destroy all but a finite number of clonogens, while the rest are taken care of by the immune system. However, TCP models based on the zero-clonogen assumption and Poisson statistics are expected to adequately describe tumour control in these cases.

Consider the assumption that the immune system is capable of eliminating the final m tumour clonogens, and thus only $N_0 - m$ must be destroyed by irradiation to achieve control. This assumption could easily be incorporated by replacing the Poisson-based individual TCP model with a cumulative binomial distribution. Individual TCP will then be equal to the probability that m or fewer cells survive irradiation to dose, D,

$$TCP_{ind} = \sum_{i=0}^{m} \frac{i!}{N_0!(N_0 - i)!} [P_S(D)]^i [1 - P_S(D)]^{N_0 - i}, \tag{8-1}$$

where $P_S(D)$ is the probability that a single clonogen will survive irradiation to dose D. If $P_S(D)$ is given by the linear quadratic formula, $P_S(D) = \exp(-\alpha' D)$, then Eq. (8-1) will yield a TCP curve with a similar shape as the standard model [Eq. (1-12)].

A disadvantage to using Eq. (8-1) for the individual model is the difficulty in determining analytic expressions for D_{50} and γ_{50} in terms of the radiobiological parameters α', m and N_0. However, this difficulty can be overcome by noting that, under certain conditions ($m >\sim 30$, according to initial simulations), Eq. (8-1) is well-approximated by a cumulative Gaussian curve,

$$TCP_{ind} = \frac{1}{2}\left\{1 + erf\left[\frac{m - N_0 P_S(D)}{\sqrt{2N_0 P_S(D)[1 - P_S(D)]}}\right]\right\}. \tag{8-2}$$

Equation (8-2) is also advantageous because it would not be overly difficult to derive the corresponding population TCP model following the method of Carlone *et al.*[6] Such a model would have an extra set of population-based parameters, $\overline{\ln m}$ and $\sigma_{\ln(m)}$, and the relationships between the radiobiological and geometric (D_{50}, γ_{50}) parameters would be different than Eqs. (1-14) and (1-15). However, the form of this model would likely be similar to that of Carlone *et al.* [Eq. (1-13)]. Therefore, Eq. (1-13) could provide a good description of the clinical dose-response relationship in the case where tumour control is achieved when m or fewer clonogens remain at the end of a treatment.

The destruction of tumour vasculature by radiation fundamentally involves cell killing, and thus the Poisson TCP model should provide a reasonable macroscopic description of this process. The dependency of tumour control on the destruction of vasculature may partially account for the difference between *in vitro* and *in vivo* parameter estimates; the latter could be characteristic of the tumour vasculature, or they may represent an average of tumour and vasculature cells.

The assumption about vasculature destruction could potentially be incorporated into TCP models. One possible way to do so is to include intra-tumour heterogeneity in the model parameters. Alternatively, one may attempt to derive a model that considers the vasculature and the rest of the tumour (i.e., clonogens) as two separate 'structures'. In this case, there would be separate parameters for both cell types, and assumptions would have to be made about the fraction of the tumour that consists of vessels. However, it is

likely that the biological parameters of such a model would exhibit relationships similar to those inherent to the population TCP model,[6,7] which would make it impossible to extract their values from clinical data.

Another disadvantage to the population TCP model used in this thesis is that it neglects the heterogeneous nature of tumour dose distributions. For a model to be useful for purposes such as treatment plan evaluation, it should take this heterogeneous irradiation into account. In Chapter 5, it was suggested that the heterogeneous individual TCP model [Eq. (5-13)] may be used as a phenomenological population TCP model in this case. Another possibility would be to use a modified version of the homogenous population model, with dose D replaced with EUD,

$$TCP_{pop} = \frac{1}{2} erfc\left[\sqrt{\pi}\gamma_{50}\left(\frac{D_{50}}{\left(\sum_{i=1}^{N} v_i D_i^{1/a}\right)^a} - 1\right)\right]. \tag{8-3}$$

8.3 The effect of inter-tumour heterogeneity on parameter ratio estimates

In Chapter 6, it was analytically shown that the individual and population-averaged TCP models do not yield identical α/β estimates when fit to the same dose-response data. Therefore, the assumption that inter-tumour heterogeneity has no effect on parameter ratios is invalid, implying that estimates for the α/β ratio obtained by fitting the individual model to clinical data may not be accurate.

On the other hand, the accuracy of α/β estimates from the population-averaged model is limited by the quality of clinical data used for their extraction.[8] The confidence intervals are typically too large to determine whether α/β is consistent with early or late-responding tissues.

Even if α/β could be estimated from fitting the population TCP model to high-quality clinical data, the obtained value would still be subject to a degree of uncertainty based on the potential inaccuracy of the assumptions invoked in this process. For

example, one assumption is that cell survival curves are accurately described by the LQ model. In a recent paper by Garcia *et al.*,[14] detailed cell survival curves were measured for a number of different cell lines. The LQ model [Eq. (1-1)] was then fit to different dose ranges (low, intermediate, and high doses), yielding estimates for α, β, and α/β for each dose range. It was found that the selected dose range had an impact on the estimated LQ parameters, which implies that this model does not accurately describe cell survival curves. The Garcia *et al.* paper supports the idea that absolute values of the α/β ratio cannot be determined through fitting models to clinical data (as discussed in Chapter 6), even at the *in-vitro* level.

In the low-dose region of cell survival curves, effects such as hypersensitivity and the adaptive response result in deviations from the predictions of LQ theory. Experimental cell survival curves are also characterized by a final slope in the high-dose region, while the LQ model predicts a continuous curve. Ideally, a cell survival model that describes both the low-dose and high-dose effects should be developed and implemented. Unfortunately, this would require the inclusion of additional model parameters, and would likely make it difficult to isolate the α/β ratio.

The results of Chapter 6 indicate that the original estimate for the value of α/β of prostate cancer that was obtained by Brenner and Hall[15] from fits of the individual TCP model to clinical data, α/β = 1.5 [0.8, 2.2], is likely incorrect. However, specific treatment protocols based on the assumption that $(\alpha/\beta)_{prostate}$ = 1.5 Gy and $(\alpha/\beta)_{organs}$ = 3.0 Gy have recently been proposed by Fowler *et al.*[16,17] Because the exact α/β values for both prostate cancer and normal tissues are unknown, the use of these protocols should be avoided, as they may lead to underdosing of the tumour or overdosing of organs at risk. Instead, a conservative approach should be taken when designing hypofractionation trials, and they should not deviate too drastically from the standard 2 Gy/fraction treatment regime.

For prostate cancer, only the clinical hypofractionation trials that are currently underway will reveal whether the α/β ratio for this tumour type is, in fact, low. Early evidence from these trials indicates that this is indeed the case.

8.4 *Quality of available clinical dose-response data*

A significant drawback to existing radiobiological models that is apparent throughout the work in this thesis is the poor quality of the dose-response data on which they are based. In Chapter 7, pseudo-data (subject to clinical limitations) were utilized to determine the number of patients per point that would be required to resolve the TCP model parameters D_{50} and γ_{50} with reasonable certainty. It was found that, in the worst case, at least 1000 – 2000 patients per point would be needed to estimate parameters with relative confidence intervals of ~25% or less for D_{50} and ~40% or less for γ_{50}. This number is much greater than the ~20 – 100 patients per point that constitute typical published clinical dose-response data. As a result, parameters estimated from published clinical datasets generally have unsuitably large 95% CIs, which translates into a corresponding uncertainty in TCP model predictions and parameter ratio (e.g., α/β) estimates.

The collection of a sufficiently large amount of DVH-response data is thus a necessary step which must be taken before TCP (and NTCP) models can be utilized to a greater extent in the clinical setting.

8.5 *References*

1. B. Emami, J. Lyman, A. Brown, L. Coia, M. Goitein, J. E. Munzenrider, B. Shank, L. J. Solin, and M. Wesson, "Tolerance of normal tissue to therapeutic irradiation," Int J Radiat Oncol Biol Phys **21**, 109-122 (1991).

2. A. Jackson, M. W. Skwarchuk, M. J. Zelefsky, D. M. Cowen, E. S. Venkatraman, S. Levegrun, C. M. Burman, G. J. Kutcher, Z. Fuks, S. A. Liebel, and C. C. Ling, "Late rectal bleeding after conformal radiotherapy of prostate cancer. II. Volume effects and dose-volume histograms," Int J Radiat Oncol Biol Phys **49**, 685-698 (2001).

3. J. T. Lyman, "Complication probability as assessed from dose-volume histograms," Radiat Res Suppl **8**, S13-19 (1985).

4. C. Burman, G. J. Kutcher, B. Emami, and M. Goitein, "Fitting of normal tissue tolerance data to an analytic function," Int J Radiat Oncol Biol Phys **21**, 123-135 (1991).

5. P. Stavrev, D. Hristov, B. Warkentin, E. Sham, N. Stavreva, and B. G. Fallone, "Inverse treatment planning by physically constrained minimization of a biological objective function," Med Phys **30**, 2948-2958 (2003).

6. M. Carlone, B. Warkentin, P. Stavrev, and B. G. Fallone, "Fundamental form of the population TCP model in the limit of large heterogeneity," Med. Phys. **33**, 1634-1642 (2006).

7. B. Warkentin, P. Stavrev, N. A. Stavreva, and B. G. Fallone, "Limitations of a TCP model incorporating population heterogeneity," Phys Med Biol **50**, 3571-3588 (2005).

8. M. Carlone, D. Wilkins, B. Nyiri, and P. Raaphorst, "Comparison of alpha/beta estimates from homogeneous (individual) and heterogeneous (population) tumor control models for early stage prostate cancer," Med Phys **30**, 2832-2848 (2003).

9. J. Denekamp, "The current status of targeting tumour vasculature as a means of cancer therapy: an overview," Int J Radiat Biol **60**, 401-408 (1991).

10. J. Denekamp, "Inadequate vasculature in solid tumours: consequences for cancer research strategies," BJR Suppl **24**, 111-117 (1992).

11. J. Denekamp, "Review article: angiogenesis, neovascular proliferation and vascular pathophysiology as targets for cancer therapy," Br J Radiol **66**, 181-196 (1993).

12. J. Denekamp, "The tumour microcirculation as a target in cancer therapy: a clearer perspective," Eur J Clin Invest **29**, 733-736 (1999).

13. J. Denekamp, A. Dasu, and A. Waites, "Vasculature and microenvironmental gradients: the missing links in novel approaches to cancer therapy?," Adv Enzyme Regul **38**, 281-299 (1998).

14. L. M. Garcia, D. E. Wilkins, and G. P. Raaphorst, "Alpha/beta ratio: A dose range dependence study," Int J Radiat Oncol Biol Phys **67**, 587-593 (2007).

15. D. J. Brenner and E. J. Hall, "Fractionation and protraction for radiotherapy of prostate carcinoma," Int J Radiat Oncol Biol Phys **43**, 1095-1101 (1999).

16. J. F. Fowler, R. J. Chappell, and M. A. Ritter, "The prospects for new treatments for prostate cancer," Int J Radiat Oncol Biol Phys **52**, 3-5 (2002).

17. J. F. Fowler, M. A. Ritter, R. J. Chappell, and D. J. Brenner, "What hypofractionated protocols should be tested for prostate cancer?," Int J Radiat Oncol Biol Phys **56**, 1093-1104 (2003).

Chapter 9 Conclusions and future work

9.1 Concluding remarks

Using the method of reverse mapping, physical dose-volume constraints were calculated based on biological models and parameters. It was shown that these constraint points are capable of limiting the radiation dose to organs at risk if they are used for inverse planning optimization. However, direct biological optimization is theoretically a better choice because the application of physical constraint points results in the exclusion of a significant number of DVHs with acceptable NTCP.

It was demonstrated that the individual and population-based TCP models are functionally similar, and thus should produce identical D_{50} and γ_{50} estimates when fit to clinical dose-response datasets. The individual model should be treated as phenomenological when fit to clinical data.

Based on this functional similarity, it was analytically shown that fitting the population model to clinical data yields an α/β ratio that is different from that which would be obtained from fitting the individual model to the same dataset. Thus, the

assumption that inter-tumour heterogeneity has no effect on parameter ratio estimates is invalid. This implies that α/β ratio estimates based on the individual model are most likely incorrect.

A limitation that is apparent throughout the work in this thesis is the relatively poor quality of existing dose-response data. This prevents the widespread use of TCP and NTCP models for treatment planning and parameter estimation. It was demonstrated that the number of patients per dose point in clinical trials should be equal to 1000 or more in order to adequately estimate TCP model parameters. Most current clinical trials are not designed for TCP/NTCP parameter estimation, however. TCP and NTCP models have the potential to become valuable tools in the treatment process, but before this can happen, clinical data of sufficient quality must be collected.

9.2 Future work

The work described in Chapters 2 – 4 was mainly theoretical in nature; the next step in the reverse mapping project would be to apply the idea in the clinic. The calculated constraint points have yet to be tested in an actual treatment planning system, which is an essential step that must be taken before they may be used clinically. This project may thus be extended by using the reverse mapping method of constraint determination to optimize a clinical IMRT plan for a specific site (e.g., prostate) or a number of different sites. The method could be used to calculate constraints for all relevant OARs, subject to a user-specified NTCP range and maximum organ dose. The selection of maximum dose would be based on prescribed dose and the proximity of the OAR to the PTV, or knowledge from previously-optimized IMRT plans. Either the Lyman or critical volume NTCP model could be used, with parameter values based on Emami *et al.*, for the calculation of constraint points. Two or more of these constraints may then be applied to all relevant OARs, and the treatment plan optimized. The DVHs obtained from this process could then be compared with those from IMRT plans with conventional clinical constraints. If the plans based on the reverse mapping constraints consistently produce equivalent or better results than conventional plans, then it may be possible to deliver IMRT treatments optimized using these reverse mapping constraints.

If more clinical dose-response data become available in the future, leading to increased reliability of NTCP models, then the reverse mapping method may be used as a transitional means to bridge the gap between purely physical inverse planning optimization and physico-biological optimization.

One limitation to the population TCP model used in this thesis is the assumption of homogeneous tumour irradiation. Given that the dose distribution of a tumour is not entirely uniform, it is necessary to develop a heterogeneous population TCP model. The best way to do so would be to analytically derive such a model, using a similar process as described in Carlone *et al.*[1] However, this is not easy to do; hence the suggestion of two alternate heterogeneous TCP model forms in Chapter 5. Before either of these simpler heterogeneous models can be implemented, however, their ability to describe population TCP in the case of heterogeneous irradiation should be explored. One way to do this is through pseudo-numerical experiments. First, heterogeneous tumour DVHs can be generated using a mathematical expression that very closely mimics clinical DVHs. The TCP of each DVH can then be calculated using the population TCP expression of Nahum and Webb[2] with assumed parameter values. In this way, a pseudo DVH-response dataset can be obtained. Each of the proposed alternative heterogeneous population TCP models may then be fit to the pseudo-data, and the fits can be compared, along with each model's ability to predict TCP.

The heterogeneous individual model [Eq. (5-13)] has been used previously[3] to evaluate TCP, with D_{50} and γ_{50} estimates[4] from fits to clinical data representing homogeneously-irradiated tumours, with reasonable results. Currently, this appears to be the best (and only) option to evaluate TCP in the case of heterogeneous irradiation. The heterogeneous population TCP model based on the EUD formalism has three parameters: D_{50}, γ_{50}, and a volume parameter, a. If this model proves to more accurately represent heterogeneous irradiation according to the simulations described above, clinical datasets that contain tumour DVH information will be needed to estimate parameters. Thus, before a heterogeneous population TCP model can be used clinically, a sufficient amount of clinical DVH-TCP data must be collected and analyzed.

It is apparent from the work in this thesis that the currently-available clinical dose-response data are not of a sufficient quality to facilitate the regular clinical use of TCP and NTCP models. A significant effort should therefore be made to collect DVH-response data by means of clinical trials. In most cases, it is impractical to conduct clinical trials of the required magnitude within a single institution, and thus multi-institutional trials that are designed to collect a large amount of data should be implemented. A few such organizations, such as the RTOG (Radiation Therapy Oncology Group), have already made efforts in this direction. However, the clinical trials that have been conducted by existing organizations suffer from several limitations. Some of these include limitations on the types and amount of data that may be stored in databases, unclear specifications on volume definition for standard structures of interest (leading to DVH differences), and differences in the characterization of normal tissue complications.[5]

Efforts should be made to overcome these limitations. Specific multi-institutional trials could potentially be designed with clear protocols to ensure that the information collected from such an effort is useful for TCP/NTCP modeling. With an adequate process in place for collecting, storing and accessing DVH-response data, more accurate information could be extracted from radiobiological modeling, and TCP and NTCP modeling may very well be used with increasing frequency in the clinic.

Assuming that a sufficient amount of clinical data can be collected, it is likely that models with geometric parameters, like the TCP models discussed and investigated in this thesis, will be the first used regularly in the clinic. These types of models could be used for biological optimization and treatment plan ranking, and could potentially simplify the process by removing the need to rely on previous clinical knowledge in order to assess the 'goodness' of a dose-distribution.

In Chapter 6 [Eq. (6-21)], it was demonstrated that it may be possible to estimate biological parameter ratios, such as α/β, from geometric parameters (in this case, D_{50}). Assuming appropriate data could be collected for such a calculation, the ability to obtain parameter ratios from clinical datasets could lead to insights as to the optimal fractionation regime to treat different tumour types.

The development and clinical utilization of detailed TCP and NTCP models that incorporate more complicated radiobiology likely cannot be achieved using clinical dose-response data alone. Even the radiobiological parameters of the relatively simple population-averaged TCP model given by Eq. (1-13) are interrelated. Other experimental methods will have to be employed in order to obtain more radiobiological information from TCP and NTCP modeling. Perhaps, in future, this will be accomplished by combining information from animal experiments and/or biological imaging with data from clinical trials. The existing TCP and NTCP models provide a good starting point for this type of research.

It is important to continue the radiobiological modeling work discussed in this thesis because this is the only method that can, in future, be used to determine, with certainty, which treatment methods and protocols are best suited for each site. Once an appropriate amount of clinical data has been collected, TCP and NTCP models have the potential to provide the quantitative justification for the best regimen for modern radiation treatments.

9.3 References

1. M. Carlone, B. Warkentin, P. Stavrev, and B. G. Fallone, "Fundamental form of the population TCP model in the limit of large heterogeneity," Med. Phys. **33**, 1634-1642 (2006).

2. S. Webb and A. E. Nahum, "A model for calculating tumour control probability in radiotherapy including the effects of inhomogeneous distributions of dose and clonogenic cell density," Phys Med Biol **38**, 653-666 (1993).

3. B. Warkentin, P. Stavrev, N. Stavreva, C. Field, and B. G. Fallone, "A TCP-NTCP estimation module using DVHs and known radiobiological models and parameter sets," J Appl Clin Med Phys **5**, 50-63 (2004).

4. P. Okunieff, D. Morgan, A. Niemierko, and H. D. Suit, "Radiation dose-response of human tumors," Int J Radiat Oncol Biol Phys **32**, 1227-1237 (1995).

5. C. Field, "Summary of radiotherapy data collection techniques for clinical trials (WESCAN, Edmonton, AB, Mar. 21 - 24)," Canadian Medical Physics Newsletter **53**, 56-57 (2007).

Appendix A NTCP model parameters

A list of parameters for the NTCP models used in Chapter 2 is presented for each of 16 organs. Both sets of parameters were calculated based on the Emami *et al.*[1] estimates. The Lyman model parameters are those of Burman *et al.*,[2] and the CV population model parameters are from Stavrev *et al.*[3]

	Lyman model parameters			CV population model parameters			
Organ/Endpoint	a	m	D_{50}	μ_{cr}	$\sigma_{\mu cr}$	D_{50}^{FSU}	γ_{50}^{FSU}
lung/pneumonitis	0.87	0.18	24.5	0.0793	0.1162	220.000	0.2720
liver	0.32	0.15	40.0	0.0372	0.1060	180.599	0.4582
brain	0.25	0.15	60.0	0.0763	0.3060	106.001	1.0428
heart/pericarditis	0.35	0.10	48.0	0.1421	0.1701	83.000	0.7992
kidney/nephritis	0.70	0.10	28.0	0.2167	0.1412	59.119	0.4420
esophagus	0.06	0.11	68.0	0.0147	0.3644	96.674	2.4401
stomach	0.15	0.14	65.0	0.0206	0.3761	94.000	2.2117
brachial plexus	0.03	0.12	75.0	0.0148	0.8532	86.501	6.0417
bladder	0.50	0.11	80.0	0.2619	0.1926	108.000	0.8050
mandible	0.07	0.10	72.0	0.0724	0.4725	85.788	3.1533
brain stem	0.16	0.14	65.0	0.1202	0.3302	97.404	1.1484
larynx/necrosis	0.11	0.08	80.0	0.0688	0.2270	108.159	1.9095
small intestine	0.15	0.16	55.0	0.0423	0.2803	96.750	1.1561
colon	0.17	0.11	55.0	0.0329	0.1699	107.731	1.0632
spinal cord	0.05	0.18	66.5	0.0849	0.7529	81.000	2.5664
skin	0.10	0.12	70.0	0.1009	0.4216	92.974	1.7154
rectum	0.12	0.15	80.0	...	...	...	...

A.1 References

1. B. Emami, J. Lyman, A. Brown, L. Coia, M. Goitein, J. E. Munzenrider, B. Shank, L. J. Solin, and M. Wesson, "Tolerance of normal tissue to therapeutic irradiation," Int J Radiat Oncol Biol Phys **21**, 109-122 (1991).

2. C. Burman, G. J. Kutcher, B. Emami, and M. Goitein, "Fitting of normal tissue tolerance data to an analytic function," Int J Radiat Oncol Biol Phys **21**, 123-135 (1991).

3. P. Stavrev, N. Stavreva, A. Niemierko, and M. Goitein, "The Application of Biological Models to Clinical Data," *Phys Medica* **XVII**, 71-82 (2001).

Appendix B Determination of the number of trajectories connecting two points in DVH space

Let the number of steps necessary to reach point E (m, r) from point D (0, 0) be p steps in the forward direction and q steps in the downward direction. Then, the total number of steps is $p+q$. As can be seen, it is also equal to m, the x coordinate of point E, since each step increases the x coordinate with +1. Therefore, we have $E_x = m = p+q$. On the other hand, each step in the forward direction increases the y coordinate with +1 while each step down decreases the ordinate with -1. Therefore, the y coordinate of point E, r, is equal to $E_y = r = p-q$. We can determine p and q from these two relations: $p=(m+r)/2$ and $q=(m-r)/2$.

The number of ways in which p out of a total of $p+q$ steps can be realized in the forward direction is given by the corresponding binomial coefficient:

$$B_{p+q,p} = \binom{p+q}{p} = \binom{m}{(m+r)/2}.$$

Alternatively, the number of ways in which q out of a total of $p+q$ steps can be realized in the downward direction is given by

$$B_{p+q,q} = \binom{p+q}{q} = \binom{m}{(m-r)/2}.$$

Either of these numbers equals the number of trajectories connecting the two points. Therefore, we have proven that

$$N_{m,r} = \binom{m}{(m+r)/2} = \binom{m}{(m-r)/2}.$$

The right-hand equality can also be proven directly.

It can also be seen that point $E_2\,(x_2, y_2)$ can be reached from point $E_1\,(x_1, y_1)$ via a total number of steps equal to $x_2 - x_1$ out of which $p = [\underbrace{(x_2 - x_1)}_{m} + \underbrace{(y_2 - y_1)}_{r}]/2$ are in the forward direction and $q = [(x_2 - x_1) - (y_2 - y_1)]/2$ are in the downward direction. Therefore,

$$N_{E_1(x_1,y_1),E_2(x_2,y_2)} = \begin{pmatrix} x_2 - x_1 \\ [(x_2 - x_1) \pm (y_2 - y_1)]/2 \end{pmatrix} = \begin{pmatrix} m \\ (m \pm r)/2 \end{pmatrix}.$$

Appendix C Special cases for the number of trajectories connecting two points in DVH space

It is possible that in certain cases part of the vertical segment $P'Q'$ protrudes out of square $ABCD$ as shown in Figure C-1. This can happen when the point (T) chosen in the previous step has a y coordinate such that $2R \succ 2N - 2nK - 4n$. Indeed, in this case the y coordinate of point P', $P'_y = 2R + 2n$, is bigger than the y coordinate of point W (the cross point of $P'Q'$ and BC), $W_y = 2N - 2nK - 2n$. As a result segment $P'W$ lies outside $ABCD$ and only curves from T to B passing through WQ' should be counted. Therefore, we should count now the reduced number of curves from T to B according to the following formula:

$$N_{T,B}^{red} = \sum_{k=0}^{k'} \binom{2n}{k} \binom{2N - 2nK - 2n}{N - nK + R - k}, \qquad k' = -nK - R + N,$$

where k' labels the dividing point $P_{k'}$ which coincides with W. Indeed, for $P_{k'} \equiv W$, we have $P_{k',y} = 2R - 2n + 2k' = W_y = 2N - 2nK - 2n \Rightarrow k' = -nK - R + N$. This expression should be substituted in Eq. (3-4),

$$N_{T,B} = \sum_{k'=0}^{2n} N_{T,M'_{k'}} . N_{M'_{k'},B} = \binom{2N - 2nK}{N - nK + R} = \sum_{k'=0}^{2n} \binom{2n}{k'} \binom{2N - 2nK - 2n}{N - nK + R - k'},$$

and used instead of $\binom{2N - 2nK}{N - nK + R}$ for the number of curves from T to B. Also, all cases in the random number generation for which $L \geq k'$ should be disregarded.

The mirror symmetric case when the vertical segment $P''Q''$ protrudes out of square $ABCD$ from beneath is also examined and shown in Figure C-1. Applying the same reasoning as above one finds that the reduced number of curves from point T' to point B, i.e., the number of curves from point T' to point B passing through VP'' is:

$$N_{T',B}^{red} = \sum_{k=k''}^{2n} \binom{2n}{k} \binom{2N-2nK-2n}{N-nK+R-k}, \qquad k'' = nK+R-N+2n\,.$$

This expression should now be substituted in Eq. (3-4) and used for the number of curves from T' to B. Also, all cases in the random number generation for which $L \le k''$ should be disregarded.

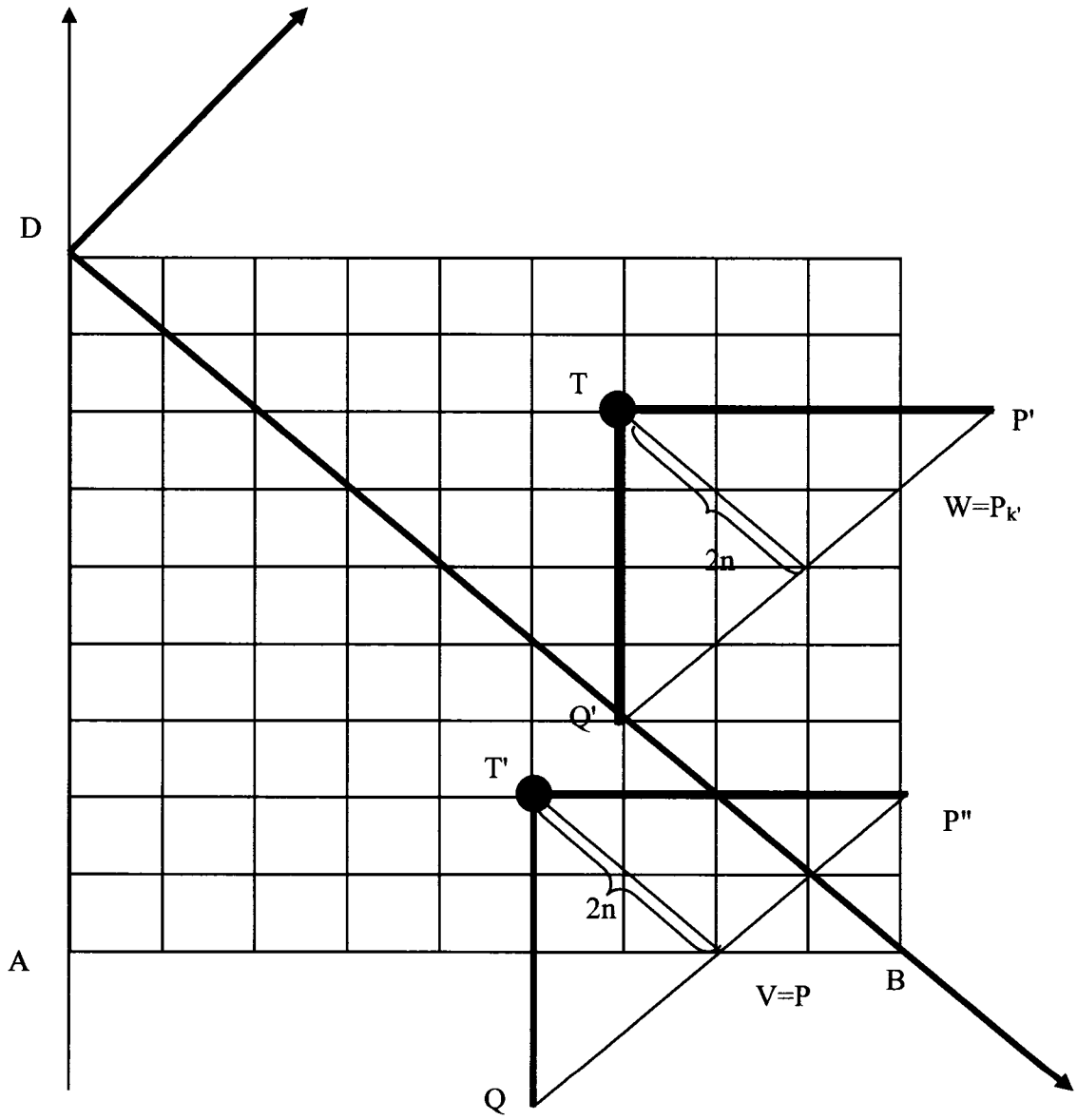

Figure C-1: Consideration of the special cases when the random walk created by the generator may leave the unit square.

Appendix D Generation of pseudo-clinical dose-response data

This section outlines the process used to generate dose response data from a TCP curve with known (or assumed) D_{50} and γ_{50} values.

(i) Specify the TCP curve and parameters from which the dose-response points will be generated. We used the fundamental form of the population model [Eq. (6-6)],

$$TCP_{pop} = \frac{1}{2} erfc\left[\sqrt{\pi}\,\gamma_{50}\left(\frac{D_{50}}{D} - 1\right)\right],$$

for this purpose.

(ii) Let D_x be the dose at TCP = x. Choose a value for D_x that represents the mean delivered dose for the set of dose-response data to be generated. Specifically, select a TCP level, x, and then calculate D_x from the TCP curve in (i).

(iii) Select a dose range, ΔD, that the simulated dose-response points will fall within, and choose the total number of points to be generated, n_p. The minimum dose in the simulated dataset is $D_x - \Delta D/2$ and the maximum is $D_x + \Delta D/2$, and the points are spaced equally between these two limits.

(iv) For each of the n_p dose points, D_i: $i = 1 \ldots n_p$, assign a value for the total number of 'patients', N_i, treated to a dose of D_i. This is done by generating a uniform random value between selected lower and upper limits, N_{low} and N_{high}. Alternatively, one could assign specific values of N_i for each point, based on existing dose-response data.

(v) Generate a value for the number of patients cured, n_i, for each dose point, D_i. The value n_i is randomly sampled from a binomial distribution where n_i is the number of successes (cures), N_i is the number of trials (patients), and the probability of a success is $p_i = TCP(D_i)$:

$$P(n_i) = \frac{N_i!}{n_i!(N_i - n_i)!} p_i^{n_i} [1 - p_i]^{N_i - n_i}. \qquad \text{(E-1)}$$

Specifically:

(a) Generate a random number, r, distributed uniformly in the interval [0, 1].

(b) Find a number, n_i, for which the following identity is satisfied:

$$\sum_{m=0}^{n_i-1} P(m) < r \leq \sum_{m=0}^{n_i} P(m).$$

where P is the binomial distribution. In this way, any uniform random number, $0 \leq r \leq 1$, is transformed into another number, $0 \leq n_i \leq N_i$ that follows a binomial distribution.[1]

D.1 References

1. W. H. Press, B. P. Flannery, S. A. Teukolsky, and W. T. Vetterling, "*Numerical Recipes in C*", (Cambridge University Press, Cambridge, MA, 1988).

Appendix E Determining best-fit TCP parameters and their confidence limits

The following Monte Carlo procedure[1,2] was used in this thesis for the purpose of fitting a TCP model represented by $TCP_{th}(\vec{\pi})$ to a dataset consisting of n_p dose-response points, (D_i, n_i, N_i).

(i) For each clinical data point, generate a random number of cures, $n^j_{gen,i}$, by sampling from a binomial distribution where the number of trials (patients) is N_i, and the probability of a successful outcome on any one trial, p_i, is equal to the measured TCP value: $p_i = \text{TCP}_i(D_i) = n_i/N_i$. To generate a random number of cures for each data point, the same procedure as outlined in step (v) of Appendix D is used.

(ii) Determine the best-fit parameters for the chosen TCP model, TCP_{th}, by minimizing the negative of the log likelihood function (or equivalently, maximizing the log likelihood function):

$$L_j = -\sum_{i=1}^{n_p}\left\{n^j_{gen,i}\ln\left[TCP_{th}(D_i;\vec{\pi}_j)\right]+\left(N_i - n^j_{gen,i}\right)\ln\left[1-TCP_{th}(D_i;\vec{\pi}_j)\right]\right\},$$

where $\vec{\pi}_j$ represents the TCP model parameters of best fit for the j^{th} set of randomly-generated dose-response points.

(iii) Store the parameters of best fit, $\vec{\pi}_j$, for the current iteration, and the minimum of the negative log likelihood function, L_j.

(iv) Repeat the process many times (we used 1000 iterations).

(v) Use the stored values for the best-fit parameters and of the minimum negative log likelihood function to generate distributions for these quantities.

(vi) Determine the 95% and 68% confidence intervals (CIs) for the parameters of best fit, $\vec{\pi}$, along with the minimum of the negative log likelihood function, L, directly from their distributions. This may be accomplished by sorting each quantity in ascending order, and then finding the cutoff value for the lowest and highest 16%

of the values for the 68% CI, and similarly for the lowest and highest 2.5% of the values for the 95% CI.

E.1 References

1. M. Carlone, D. Wilkins, B. Nyiri, and P. Raaphorst, "Comparison of alpha/beta estimates from homogeneous (individual) and heterogeneous (population) tumor control models for early stage prostate cancer," Med Phys **30**, 2832-2848 (2003).

2. W. H. Press, B. P. Flannery, S. A. Teukolsky, and W. T. Vetterling, "*Numerical Recipes in C*", (Cambridge University Press, Cambridge, MA, 1988).

Appendix F Fitted parameter values for pseudo-data

This appendix contains tables of estimated parameter values from fits of the population TCP model [Eq. (7-1)] to each of the pseudo-datasets generated in Chapter 7. The minimum negative log likelihood corresponding to the best-fit parameters is also shown in each case.

Table F-1: Fitted parameter values (D_{50}, γ_{50}) and 95% confidence intervals for the pseudo-datasets generated from a TCP curve with theoretical parameter values of $D_{50,th}$ = 50 Gy and $\gamma_{50,th}$ = 1. The minimum negative log likelihood value is also shown, with its 95% confidence interval, for each fitted pseudo-dataset. Each dataset consisted of a total of n_p = 5 points, with the first point at a dose corresponding to TCP_x = 70%.

N	$\Delta D \rightarrow$	10 Gy	20 Gy	30 Gy
50	D_{50}	50.0 [-61.9, 60.2]	47.9 [-4.3, 58.2]	53.8 [33.7, 61.5]
	γ_{50}	1.03 [0.14, 2.45]	0.98 [0.30, 1.73]	1.15 [0.60, 1.74]
	L_{min}	139 [122, 153]	125 [107, 141]	122 [102, 136]
200	D_{50}	43.0 [-60.6, 55.2]	46.7 [27.8, 54.2]	48.1 [36.9, 54.5]
	γ_{50}	0.70 [0.13, 1.34]	0.85 [0.49, 1.22]	0.97 [0.70, 1.26]
	L_{min}	571 [539, 598]	530 [495, 562]	471 [433, 507]
500	D_{50}	50.6 [38.8, 55.5]	46.5 [36.7, 51.9]	51.5 [46.9, 54.9]
	γ_{50}	1.08 [0.64, 1.50]	0.84 [0.61, 1.06]	1.03 [0.87, 1.20]
	L_{min}	1382 [1330, 1428]	1330 [1276, 1379]	1230 [1177, 1279]
1000	D_{50}	49.4 [41.4, 53.6]	51.1 [46.9, 53.7]	51.5 [48.4, 53.8]
	γ_{50}	0.96 [0.66, 1.24]	1.07 [0.90, 1.22]	1.08 [0.96, 1.20]
	L_{min}	2835 [2774, 2895]	2582 [2499, 2652]	2378 [2302, 2450]
2000	D_{50}	51.8 [48.2, 54.4]	50.3 [47.5, 52.6]	49.5 [47.0, 51.6]
	γ_{50}	1.10 [0.90, 1.30]	1.02 [0.91, 1.13]	0.96 [0.87, 1.04]
	L_{min}	5655 [5558, 5742]	5191 [5088, 5288]	4925 [4817, 5030]

Table F-2: Shows the same information as does Table F-1, but in this case the data were generated from a TCP curve with theoretical parameter values of $D_{50,th}$ = 50 Gy and $\gamma_{50,th}$ = 1.5. Each dataset consisted of a total of n_p = 5 points, with the first point at a dose corresponding to TCP_x = 70%.

N	$\Delta D \rightarrow$	10 Gy	20 Gy	30 Gy
50	D_{50}	52.4 [31.5, 56.6]	55.4 [48.7, 58.9]	47.1 [29.5, 54.1]
	γ_{50}	1.89 [0.62, 3.18]	1.92 [1.22, 2.78]	1.26 [0.71, 1.87]
	L_{min}	129 [1010, 143]	120 [102, 135]	102 [80.0, 118]
200	D_{50}	47.1 [33.5, 52.3]	51.4 [47.4, 54.2]	51.7 [48.1, 54.3]
	γ_{50}	1.32 [0.71, 1.96]	1.67 [1.31, 2.06]	1.63 [1.36, 1.92]
	L_{min}	501 [467, 533]	438.7 [399.1, 474.2]	386 [347, 422]
500	D_{50}	48.8 [43.8, 52.0]	48.4 [44.7, 51.0]	49.7 [47.1, 51.7]
	γ_{50}	1.40 [1.02, 1.82]	1.40 [1.17, 1.62]	1.55 [1.38, 1.73]
	L_{min}	1297 [1244, 1348]	1104 [1042, 1158]	921 [858, 975]
1000	D_{50}	49.4 [46.3, 51.5]	51.1 [49.3, 52.6]	50.1 [48.4, 51.6]
	γ_{50}	1.45 [1.18, 1.73]	1.57 [1.39, 1.73]	1.47 [1.35, 1.59]
	L_{min}	2610 [2534, 2677]	2263 [2183, 2339]	1471 [1353, 1595]
2000	D_{50}	49.6 [47.6, 51.2]	49.2 [47.7, 50.6]	49.0 [47.7, 50.2]
	γ_{50}	1.46 [1.26, 1.65]	1.43 [1.32, 1.55]	1.44 [1.36, 1.54]
	L_{min}	5232 [5126, 5332]	4473 [4362, 4578]	3831 [3707, 3945]

Table F-3: Shows the same information as Table F-1 and Table F-2, but in this case the data were generated from a TCP curve with theoretical parameter values of $D_{50,th}$ = 50 Gy and $\gamma_{50,th}$ = 2. Each dataset consisted of a total of n_p = 5 points, with the first point at a dose corresponding to TCP_x = 70%.

N	$\Delta D \rightarrow$	10 Gy	20 Gy	30 Gy
50	D_{50}	47.4 [17.7, 52.9]	53.6 [49.8, 56.0]	51.3 [45.6, 54.9]
	γ_{50}	1.71 [0.53, 3.00]	2.78 [1.99, 3.85]	2.10 [1.53, 2.88]
	L_{min}	116 [97.0, 131]	89.2 [72.3, 105]	78.9 [61.3, 96.3]
200	D_{50}	48.7 [42.2, 51.8]	49.4 [45.7, 51.9]	51.0 [48.3, 53.0]
	γ_{50}	1.75 [1.14, 2.39]	1.94 [1.57, 2.35]	2.12 [1.79, 2.52]
	L_{min}	489 [456, 520]	372 [334, 407]	303 [266, 336]
500	D_{50}	52.1 [50.4, 53.3]	51.1 [49.5, 52.3]	51.2 [49.6, 52.5]
	γ_{50}	2.46 [2.07, 2.87]	2.11 [1.88, 2.37]	2.05 [1.84, 2.26]
	L_{min}	1203 [1149, 1258]	957 [895, 1009]	802 [746, 857]
1000	D_{50}	50.0 [48.4, 51.2]	49.0 [47.6, 50.2]	49.7 [48.5, 50.9]
	γ_{50}	2.02 [1.73, 2.28]	1.91 [1.74, 2.09]	2.01 [1.85, 2.16]
	L_{min}	2394 [2317, 2472]	1842 [1760, 1920]	1489 [1406, 1567]
2000	D_{50}	49.1 [47.8, 50.1]	50.8 [50.0, 51.5]	48.9 [47.9, 49.7]
	γ_{50}	1.86 [1.67, 2.06]	2.10 [1.97, 2.23]	1.83 [1.74, 1.94]
	L_{min}	4789 [4676, 4896]	3777 [3664, 3889]	3151 [3033, 3261]

Table F-4: Fitted parameters and 95% confidence intervals for datasets generated from TCP curves with $D_{50,th}$ = [30, 70] Gy and $\gamma_{50,th}$ = 1. Each dataset consisted of a total of n_p = 5 points over a dose interval (ΔD) of either 10 or 20 Gy, with the first point at a dose corresponding to TCP_x = 70%.

		$D_{50,th}$ = 30 Gy		$D_{50,th}$ = 70 Gy	
N	$\Delta D \rightarrow$	10 Gy	20 Gy	10 Gy	20 Gy
50	D_{50}	29.9 [-19.9, 35.9]	31.4 [18.6, 36.3]	66.6 [-163.6, 84.9]	67.2 [-86.8, 83.8]
	γ_{50}	0.93 [0.18, 1.82]	1.10 [0.59, 1.69]	0.92 [0.10, 2.85]	0.87 [0.16, 1.90]
	L_{min}	138 [119, 151]	118 [96.4, 132]	142 [125, 154]	139 [122, 152]
200	D_{50}	27.5 [12.6, 32.6]	30.9 [26.7, 33.8]	74.8 [28.5, 82.8]	69.4 [45.0, 79.0]
	γ_{50}	0.81 [0.42, 1.23]	1.13 [0.88, 1.38]	1.20 [0.36, 2.10]	1.03 [0.54, 1.55]
	L_{min}	546 [510, 574]	448 [411, 481]	586 [556, 610]	531 [496, 560]
500	D_{50}	28.8 [23.7, 31.8]	30.7 [28.1, 32.7]	74.4 [60.3, 80.3]	66.6 [50.2, 74.4]
	γ_{50}	0.91 [0.67, 1.18]	1.03 [0.88, 1.19]	1.23 [0.71, 1.77]	0.88 [0.57, 1.17]
	L_{min}	1340 [1286, 1385]	1191 [1132, 1246]	1444 [1400, 1487]	1371 [1318, 1416]
1000	D_{50}	31.3 [29.1, 32.9]	28.5 [26.0, 30.3]	64.5 [34.6, 73.9]	70.8 [63.7, 75.2]
	γ_{50}	1.13 [0.94, 1.33]	0.94 [0.83, 1.06]	0.81 [0.41, 1.21]	1.02 [0.81, 1.22]
	L_{min}	2649 [2571, 2722]	2317 [2235, 2395]	2892 [2829, 2951]	2735 [2663, 2802]
2000	D_{50}	30.3 [28.4, 31.6]	30.0 [28.7, 31.2]	66.5 [53.7, 73.0]	69.7 [64.6, 73.4]
	γ_{50}	1.03 [0.89, 1.15]	1.00 [0.93, 1.08]	0.86 [0.58, 1.12]	0.99 [0.84, 1.14]
	L_{min}	5323 [5225, 5420]	4720 [4607, 4821]	5809 [5720, 5889]	5461 [5363, 5555]

Table F-5: Fitted parameters and 95% confidence intervals for datasets generated from TCP curves with $D_{50,th}$ = 50 Gy and $\gamma_{50,th}$ = 1. Each dataset consisted of a total of n_p = 5 points over a dose range of ΔD = 10 Gy, with the first point at a dose corresponding to TCP_x = 60% in one case and 80% in the other.

N	$TCP_x \rightarrow$	60%	80%
50	D_{50}	53.5 [29.8, 57.3]	41.7 [-188.5, 67.9]
	γ_{50}	1.26 [0.30, 2.41]	0.80 [0.12, 2.58]
	L_{min}	161 [149, 168]	113 [91.7, 130]
200	D_{50}	47.3 [17.9, 52.7]	59.9 [33.6, 66.8]
	γ_{50}	0.81 [0.25, 1.39]	1.52 [0.66, 2.34]
	L_{min}	632 [609, 652]	454 [416, 489]
500	D_{50}	46.0 [32.4, 50.6]	55.4 [34.3, 62.4]
	γ_{50}	0.75 [0.40, 1.10]	1.19 [0.64, 1.67]
	L_{min}	1575 [1541, 1607]	1172 [1114, 1229]
1000	D_{50}	48.7 [44.7, 51.1]	53.6 [41.3, 60.1]
	γ_{50}	0.95 [0.71, 1.20]	1.17 [0.80, 1.57]
	L_{min}	3127 [3076, 3176]	2249 [2163, 2330]
2000	D_{50}	48.5 [45.8, 50.4]	51.5 [42.2, 57.2]
	γ_{50}	0.92 [0.74, 1.09]	1.07 [0.81, 1.34]
	L_{min}	6278 [6210, 6344]	4551 [4430, 4668]

Bibliography

(page numbers in the brackets at the end of each entry identify the locations of each reference in the thesis)

Bataini, P., J. Brugere, J. Bernier, C. H. Jaulerry, C. Picot and N. A. Ghossein (1982). "Results of radical radiotherapeutic treatment of carcinoma of the pyriform sinus: experience of the Institut Curie." Int J Radiat Oncol Biol Phys **8**(8): 1277-86. [p. 150]

Bedford, J. S. and J. B. Mitchell (1973). "Dose-rate effects in synchronous mammalian cells in culture." Radiat Res **54**(2): 316-27. [p. 6]

Bedwinek, J. M., C. A. Perez and D. J. Keys (1980). "Analysis of failures after definitive irradiation for epidermoid carcinoma of the nasopharynx." Cancer **45**(11): 2725-9. [p. 150]

Belderbos, J. S., W. D. Heemsbergen, K. De Jaeger, P. Baas and J. V. Lebesque (2006). "Final results of a Phase I/II dose escalation trial in non-small-cell lung cancer using three-dimensional conformal radiotherapy." Int J Radiat Oncol Biol Phys **66**(1): 126-34. [p. 23]

Bentzen, S. M. (1992). "Steepness of the clinical dose-control curve and variation in the in vitro radiosensitivity of head and neck squamous cell carcinoma." Int J Radiat Biol **61**(3): 417-23. [p. 124]

Bentzen, S. M. (2002). Dose-response relationships in radiotherapy. Basic Clinical Radiobiology. G. Steel. London (Gr. Britain), Hodder Arnold: 94-104. [p. 124]

Bentzen, S. M. and H. D. Thames (1996). "Tumor volume and local control probability: clinical data and radiobiological interpretations." Int J Radiat Oncol Biol Phys **36**(1): 247-51. [p. 124]

Bentzen, S. M., H. D. Thames and J. Overgaard (1990). "Does variation in the in vitro cellular radiosensitivity explain the shallow clinical dose-control curve for malignant melanoma?" Int J Radiat Biol **57**(1): 117-26. [p. 124]

Bentzen, S. M. and S. L. Tucker (1997). "Quantifying the position and steepness of radiation dose-response curves." Int J Radiat Biol **71**(5): 531-42. [p. 106]

Brabbins, D., A. Martinez, D. Yan, D. Lockman, M. Wallace, G. Gustafson, P. Chen, F. Vicini and J. Wong (2005). "A dose-escalation trial with the adaptive radiotherapy process as a delivery system in localized prostate cancer: analysis of chronic toxicity." Int J Radiat Oncol Biol Phys **61**(2): 400-8. [pp. 23, 150]

Bradley, J., M. V. Graham, K. Winter, J. A. Purdy, R. Komaki, W. H. Roa, J. K. Ryu, W. Bosch and B. Emami (2005). "Toxicity and outcome results of RTOG 9311: a phase I-II dose-escalation study using three-dimensional conformal radiotherapy in patients with inoperable non-small-cell lung carcinoma." Int J Radiat Oncol Biol Phys **61**(2): 318-28. [p. 23]

Brahme, A. (1984). "Dosimetric precision requirements in radiation therapy." Acta Radiol Oncol **23**(5): 379-91. [pp. 106]

Brahme, A. (1999). "Optimized radiation therapy based on radiobiological objectives." Semin Radiat Oncol **9**(1): 35-47. [pp. 22, 120, 128, 143, 144]

Brahme, A. (2000). "Development of radiation therapy optimization." Acta Oncol **39**(5): 579-95. [p. 22]

Brahme, A. (2001). "Individualizing cancer treatment: biological optimization models in treatment planning and delivery." Int J Radiat Oncol Biol Phys **49**(2): 327-37. [p. 22]

Brenner, D. J. (1993). "Dose, volume, and tumor-control predictions in radiotherapy." Int J Radiat Oncol Biol Phys **26**(1): 171-9. [pp. 24, 103, 121, 144]

Brenner, D. J. and E. J. Hall (1999). "Fractionation and protraction for radiotherapy of prostate carcinoma." Int J Radiat Oncol Biol Phys **43**(5): 1095-101. [pp. 24, 175]

Brenner, D. J. and E. J. Hall (2000). "In response to Drs King and Mayo: Low a/b values for prostate appear to be independent of modeling details." Int J Radiat Biol Oncol Phys **47**(2): 538-539. [pp. 121, 127, 142]

Burman, C., G. J. Kutcher, B. Emami and M. Goitein (1991). "Fitting of normal tissue tolerance data to an analytic function." Int J Radiat Oncol Biol Phys **21**(1): 123-35. [pp. 40, 43, 94, 101, 171, 184]

Carlone, M., B. Warkentin, P. Stavrev and B. G. Fallone (2006). "Fundamental form of the population TCP model in the limit of large heterogeneity." Med. Phys. **33**(6): 1634-1642. [pp. 13, 14, 104, 105, 106, 107, 121, 122, 123, 124, 144, 152, 172, 173, 174].

Carlone, M., D. Wilkins, B. Nyiri and P. Raaphorst (2003). "Comparison of alpha/beta estimates from homogeneous (individual) and heterogeneous (population) tumor control models for early stage prostate cancer." Med Phys **30**(10): 2832-48. [pp. 25, 26, 128, 132, 135, 136, 137, 143, 144, 150, 154, 172, 173, 174].

Carlone, M., D. Wilkins, B. Nyiri and P. Raaphorst (2004). "TCP isoeffect analysis using a heterogeneous distribution of radiosensitivity." Med Phys **31**(5): 1176-82. [p. 33]

Chadwick, K. H. and H. P. Leenhouts (1973). "A molecular theory of cell survival." Phys Med Biol **18**(1): 78-87. [p. 5]

Chapet, O., E. Thomas, M. L. Kessler, B. A. Fraass and R. K. Ten Haken (2005). "Esophagus sparing with IMRT in lung tumor irradiation: an EUD-based optimization technique." Int J Radiat Oncol Biol Phys **63**(1): 179-87. [p. 22]

Cheng, J. C., J. K. Wu, C. M. Huang, H. S. Liu, D. Y. Huang, S. H. Cheng, S. Y. Tsai, J. J. Jian, Y. M. Lin, T. I. Cheng, C. F. Horng and A. T. Huang (2002). "Radiation-induced liver disease after three-dimensional conformal radiotherapy for patients with hepatocellular carcinoma: dosimetric analysis and implication." Int J Radiat Oncol Biol Phys **54**(1): 156-62. [p. 39]

Cheung, R., S. L. Tucker, A. K. Lee, R. de Crevoisier, L. Dong, A. Kamat, L. Pisters and D. Kuban (2005). "Dose-response characteristics of low- and intermediate-risk prostate cancer treated with external beam radiotherapy." Int J Radiat Oncol Biol Phys **61**(4): 993-1002. [p. 23]

Choi, B. and J. O. Deasy (2002). "The generalized equivalent uniform dose function as a basis for intensity-modulated treatment planning." Phys Med Biol **47**(20): 3579-89. [p. 113]

Choi, N. C. and J. A. Doucette (1981). "Improved survival of patients with unresectable non-small-cell bronchogenic carcinoma by an innovated high-dose en-bloc radiotherapeutic approach." Cancer **48**(1): 101-9. [p. 150]

Cornforth, M. N. and J. S. Bedford (1987). "A quantitative comparison of potentially lethal damage repair and the rejoining of interphase chromosome breaks in low passage normal human fibroblasts." Radiat Res **111**(3): 385-405. [p. 5]

Coselmon, M. M., J. M. Moran, J. D. Radawski and B. A. Fraass (2005). "Improving IMRT delivery efficiency using intensity limits during inverse planning." Med Phys **32**(5): 1234-45. [pp. 64, 89]

Cozzi, L., F. M. Buffa and A. Fogliata (2000). "Comparative analysis of dose volume histogram reduction algorithms for normal tissue complication probability calculations." Acta Oncol **39**(2): 165-71. [p. 39]

D'Souza, W. D., H. D. Thames and D. A. Kuban (2004). "Dose-volume conundrum for response of prostate cancer to brachytherapy: summary dosimetric measures and their relationship to tumor control probability." Int J Radiat Oncol Biol Phys **58**(5): 1540-8. [p. 103]

Dale, R. G. (1989). "Radiobiological assessment of permanent implants using tumor repopulation factors in the linear-quadratic model." Br J Radiol **62**(735): 241-244. [pp. 105, 122]

Dale, R. G. (1989). "Time-dependent tumour repopulation factors in linear-quadratic equations--implications for treatment strategies." Radiother Oncol **15**(4): 371-81. [pp. 105, 122]

Dasu, A., I. Toma-Dasu and J. F. Fowler (2003). "Should single or distributed parameters be used to explain the steepness of tumour control probability curves?" Phys Med Biol **48**(3): 387-97. [pp. 24, 121, 124, 144]

Dawson, L. A., D. Normolle, J. M. Balter, C. J. McGinn, T. S. Lawrence and R. K. Ten Haken (2002). "Analysis of radiation-induced liver disease using the Lyman NTCP model." Int J Radiat Oncol Biol Phys **53**(4): 810-21. [pp. 39, 61, 101]

Dawson, L. A. and R. K. Ten Haken (2005). "Partial volume tolerance of the liver to radiation." Semin Radiat Oncol **15**(4): 279-83. [p. 39]

Dawson, L. A., R. K. Ten Haken and T. S. Lawrence (2001). "Partial irradiation of the liver." Semin Radiat Oncol **11**(3): 240-6. [p. 39]

De Gersem, W. R., S. Derycke, C. O. Colle, C. De Wagter and W. J. De Neve (1999). "Inhomogeneous target-dose distributions: a dimension more for optimization?" Int J Radiat Oncol Biol Phys **44**(2): 461-8. [pp. 22, 39]

De Gersem, W. R., S. Derycke, C. De Wagter and W. C. De Neve (2000). "Optimization of beam weights in conformal radiotherapy planning of stage III non-small cell lung cancer: effects on therapeutic ratio." Int J Radiat Oncol Biol Phys **47**(1): 255-60. [pp. 22, 39]

De Meerleer, G. O., L. A. Vakaet, W. R. De Gersem, C. De Wagter, B. De Naeyer and W. De Neve (2000). "Radiotherapy of prostate cancer with or without intensity modulated beams: a planning comparison." Int J Radiat Oncol Biol Phys **47**(3): 639-48. [pp. 22, 39]

Denekamp, J. (1991). "The current status of targeting tumour vasculature as a means of cancer therapy: an overview." Int J Radiat Biol **60**(1-2): 401-8. [p. 172]

Denekamp, J. (1992). "Inadequate vasculature in solid tumours: consequences for cancer research strategies." BJR Suppl **24**: 111-7. [p. 172]

Denekamp, J. (1993). "Review article: angiogenesis, neovascular proliferation and vascular pathophysiology as targets for cancer therapy." Br J Radiol **66**(783): 181-96. [p 172]

Denekamp, J. (1999). "The tumour microcirculation as a target in cancer therapy: a clearer perspective." Eur J Clin Invest **29**(9): 733-6. [p. 172]

Denekamp, J., A. Dasu and A. Waites (1998). "Vasculature and microenvironmental gradients: the missing links in novel approaches to cancer therapy?" Adv Enzyme Regul **38**: 281-99. [p. 172]

Dritschilo, A., J. T. Chaffey, W. D. Bloomer and A. Marck (1978). "The complication probability factor: a method for selection of radiation treatment plans." Br J Radiol **51**(605): 370-4. [p. 39]

Dubray, B. M. and H. D. Thames (1996). "The clinical significance of ratios of radiobiological parameters." Int J Radiat Oncol Biol Phys **35**(5): 1099-111. [pp. 26, 127, 141]

Eisbruch, A., J. A. Ship, H. M. Kim and R. K. Ten Haken (2001). "Partial irradiation of the parotid gland." Semin Radiat Oncol **11**(3): 234-9. [p. 39]

El Naqa, I., G. Suneja, P. E. Lindsay, A. J. Hope, J. R. Alaly, M. Vicic, J. D. Bradley, A. Apte and J. O. Deasy (2006). "Dose response explorer: an integrated open-source tool for exploring and modelling radiotherapy dose-volume outcome relationships." Phys Med Biol **51**(22): 5719-35. [p. 23]

Emami, B., J. Lyman, A. Brown, L. Coia, M. Goitein, J. E. Munzenrider, B. Shank, L. J. Solin and M. Wesson (1991). "Tolerance of normal tissue to therapeutic irradiation." Int J Radiat Oncol Biol Phys **21**(1): 109-22. [pp. 38, 43, 52, 69, 150, 170, 184]

Feller, W. (1970). An Introduction to Probability Theory and its Applications. New York, J. Wiley and Sons. [p. 80]

Fenwick, J. D., V. S. Khoo, A. E. Nahum, B. Sanchez-Nieto and D. P. Dearnaley (2001). "Correlations between dose-surface histograms and the incidence of long-term rectal bleeding following conformal or conventional radiotherapy treatment of prostate cancer." Int J Radiat Oncol Biol Phys **49**(2): 473-80. [pp. 39, 103]

Field, C. (2007). "Summary of radiotherapy data collection techniques for clinical trials (WESCAN, Edmonton, AB, Mar. 21 - 24)." Canadian Medical Physics Newsletter **53**(2): 56-57. [p. 182]

Fischer, J. J. and J. E. Moulder (1975). "The steepness of the dose-response curve in radiation therapy. Theoretical considerations and experimental results." Radiology **117**(1): 179-84. [p. 4]

Fowler, J., R. Chappell and M. Ritter (2001). "Is alpha/beta for prostate tumors really low?" Int J Radiat Oncol Biol Phys **50**(4): 1021-31. [pp. 25, 103, 120, 127, 121]

Fowler, J. F. (1983). "Dose response curves for organ function or cell survival." Br J Radiol **56**(667): 497-500. [pp. 10, 24]

Fowler, J. F. (1989). "The linear-quadratic formula and progress in fractionated radiotherapy." British Journal of Radiology **62**(740): 679-694. [pp. 105, 119, 122]

Fowler, J. F., R. J. Chappell and M. A. Ritter (2002). "The prospects for new treatments for prostate cancer." Int J Radiat Oncol Biol Phys **52**(1): 3-5. [pp. 145, 175]

Fowler, J. F., M. A. Ritter, R. J. Chappell and D. J. Brenner (2003). "What hypofractionated protocols should be tested for prostate cancer?" Int J Radiat Oncol Biol Phys **56**(4): 1093-104. [pp. 145, 175]

Gagliardi, G., I. Lax and L. E. Rutqvist (2001). "Partial irradiation of the heart." Semin Radiat Oncol **11**(3): 224-33. [p. 39]

Garcia, L. M., D. E. Wilkins and G. P. Raaphorst (2007). "Alpha/beta ratio: A dose range dependence study." Int J Radiat Oncol Biol Phys **67**(2): 587-93. [p. 175]

Gayou, O., D. S. Parda and M. Miften (2007). "EUCLID: an outcome analysis tool for high-dimensional clinical studies." Phys Med Biol **52**(6): 1705-19. [p. 23]

Goitein, M., A. Niemierko and P. Okunieff (1995). The probability of controlling an inhomogeneously irradiated tumour: a strategem for improving tumour control through partial tumour boosting. 19th L. H. Gray Conference: Quantitative Imaging in Oncology, Newcastle, UK. [pp. 103, 104, 105]

Hanin, L. G. (2004). "A stochastic model of tumor response to fractionated radiation: limit theorems and rate of convergence." Math Biosci **191**(1): 1-17. [pp. 13, 105]

Hanin, L. G., M. Zaider and A. Y. Yakovlev (2001). "Distribution of the number of clonogens surviving fractionated radiotherapy: a long-standing problem revisited." Int J Radiat Biol **77**(2): 205-13. [pp. 13, 105]

Hanks, G. E., T. E. Schultheiss, A. L. Hanlon, M. Hunt, W. R. Lee, B. E. Epstein and L. R. Coia (1997). "Optimization of conformal radiation treatment of prostate cancer: report of a dose escalation study." Int J Radiat Oncol Biol Phys **37**(3): 543-50. [pp. 25, 26, 64, 143, 150, 167, 153]

Hartford, A. C., A. Niemierko, J. A. Adams, M. M. Urie and W. U. Shipley (1996). "Conformal irradiation of the prostate: estimating long-term rectal bleeding risk using dose-volume histograms." Int J Radiat Oncol Biol Phys **36**(3): 721-30. [pp. 65, 66, 67, 70]

Higgins, G. S., D. B. McLaren, G. R. Kerr, T. Elliott and G. C. Howard (2006). "Outcome analysis of 300 prostate cancer patients treated with neoadjuvant androgen deprivation and hypofractionated radiotherapy." Int J Radiat Oncol Biol Phys **65**(4): 982-9. [pp. 25, 120]

Horton, J. K., J. S. Halle, S. X. Chang and C. I. Sartor (2006). "Comparison of three concomitant boost techniques for early-stage breast cancer." Int J Radiat Oncol Biol Phys **64**(1): 168-75. [p. 64]

Hristov, D., P. Stavrev, E. Sham and B. G. Fallone (2002). "On the implementation of dose-volume objectives in gradient algorithms for inverse treatment planning." Med Phys **29**(5): 848-56. [p. 40]

Huang, E. H., A. Pollack, L. Levy, G. Starkschall, L. Dong, I. Rosen and D. A. Kuban (2002). "Late rectal toxicity: dose-volume effects of conformal radiotherapy for prostate cancer." Int J Radiat Oncol Biol Phys **54**(5): 1314-21. [p. 65]

Jackson, A. (2001). "Partial irradiation of the rectum." Semin Radiat Oncol **11**(3): 215-23. [p. 39]

Jackson, A., G. J. Kutcher and E. D. Yorke (1993). "Probability of radiation-induced complications for normal tissues with parallel architecture subject to non-uniform irradiation." Med Phys **20**(3): 613-25. [pp. 17, 40, 42, 60, 87, 98]

Jackson, A., M. W. Skwarchuk, M. J. Zelefsky, D. M. Cowen, E. S. Venkatraman, S. Levegrun, C. M. Burman, G. J. Kutcher, Z. Fuks, S. A. Liebel and C. C. Ling (2001). "Late rectal bleeding after conformal radiotherapy of prostate cancer. II. Volume effects and dose-volume histograms." Int J Radiat Oncol Biol Phys **49**(3): 685-98. [pp. 65, 66, 67, 171]

Jackson, A., R. K. Ten Haken, J. M. Robertson, M. L. Kessler, G. J. Kutcher and T. S. Lawrence (1995). "Analysis of clinical complication data for radiation hepatitis using a parallel architecture model." Int J Radiat Oncol Biol Phys **31**(4): 883-91. [p. 42]

Jacob, R., A. L. Hanlon, E. M. Horwitz, B. Movsas, R. G. Uzzo and A. Pollack (2005). "Role of prostate dose escalation in patients with greater than 15% risk of pelvic lymph node involvement." Int J Radiat Oncol Biol Phys **61**(3): 695-701. [pp. 23, 150]

Kal, H. B. and M. P. Van Gellekom (2003). "How low is the alpha/beta ratio for prostate cancer?" Int J Radiat Oncol Biol Phys **57**(4): 1116-21. [pp. 25, 120]

Kallman, P., A. Agren and A. Brahme (1992). "Tumour and normal tissue responses to fractionated non-uniform dose delivery." Int J Radiat Biol **62**(2): 249-62. [pp. 22, 120]

Kellerer, A. M. and H. H. Rossi (1972). "The theory of dual radiation action." Current Topics in Radiation Research Quarterly **8**: 85-158. [p. 7]

Kendal, W. S. (1998). "A closed-form description of tumour control with fractionated radiotherapy and repopulation." Int J Radiat Biol **73**(2): 207-10. [pp. 13, 105]

Khalil, A. A., S. M. Bentzen and J. Overgaard (1997). "Steepness of the dose-response curve as a function of volume in an experimental tumor irradiated under ambient or hypoxic conditions." Int J Radiat Oncol Biol Phys **39**(4): 797-802. [p. 124]

King, C. R. and J. F. Fowler (2001). "A simple analytic derivation suggests that prostate cancer alpha/beta ratio is low." Int J Radiat Oncol Biol Phys **51**(1): 213-4. [pp. 25, 120]

King, C. R. and C. S. Mayo (2000). "Is the prostrate alpha/beta ratio of 1.5 from Brenner & Hall a modeling artifact?" Int J Radiat Oncol Biol Phys **47**(2): 536-9. [pp. 25, 120, 142]

Kupelian, P. A., V. V. Thakkar, D. Khuntia, C. A. Reddy, E. A. Klein and A. Mahadevan (2005). "Hypofractionated intensity-modulated radiotherapy (70 gy at 2.5 Gy per fraction) for localized prostate cancer: long-term outcomes." Int J Radiat Oncol Biol Phys **63**(5): 1463-8. [pp. 25, 120, 144]

Kwa, S. L., J. V. Lebesque, J. C. Theuws, L. B. Marks, M. T. Munley, G. Bentel, D. Oetzel, U. Spahn, M. V. Graham, R. E. Drzymala, J. A. Purdy, A. S. Lichter, M. K. Martel and R. K. Ten Haken (1998). "Radiation pneumonitis as a function of mean lung dose: an analysis of pooled data of 540 patients." Int J Radiat Oncol Biol Phys **42**(1): 1-9. [p. 39]

Lea, D. E. (1946). "Actions of Radiations on Living Cells." University Press, Cambridge. [pp. 6, 7]

Lebesque, J. V., A. M. Bruce, A. P. Kroes, A. Touw, R. T. Shouman and M. van Herk (1995). "Variation in volumes, dose-volume histograms, and estimated normal tissue complication probabilities of rectum and bladder during conformal radiotherapy of T3 prostate cancer." Int J Radiat Oncol Biol Phys **33**(5): 1109-19. [p. 39]

Levegrun, S., L. Ton and J. Debus (2001). "Partial irradiation of the brain." Semin Radiat Oncol **11**(3): 259-67. [p. 39]

Livsey, J. E., R. A. Cowan, J. P. Wylie, R. Swindell, G. Read, V. S. Khoo and J. P. Logue (2003). "Hypofractionated conformal radiotherapy in carcinoma of the prostate: five-year outcome analysis." Int J Radiat Oncol Biol Phys **57**(5): 1254-9. [pp. 25, 120]

Lof, J., B. K. Lind and A. Brahme (1998). "An adaptive control algorithm for optimization of intensity modulated radiotherapy considering uncertainties in beam profiles, patient set-up and internal organ motion." Phys Med Biol **43**(6): 1605-28. [p. 22]

Lyman, J. T. (1985). "Complication probability as assessed from dose-volume histograms." Radiat Res Suppl **8**(9): S13-9. [pp. 16, 40, 41, 60, 94, 95, 101, 171]

Maciejewski, B., H. R. Withers, J. M. Taylor and A. Hliniak (1989). "Dose fractionation and regeneration in radiotherapy for cancer of the oral cavity and oropharynx: tumor dose-response and repopulation." Int J Radiat Oncol Biol Phys **16**(3): 831-43. [pp. 105, 122]

Maciejewski, B., H. R. Withers, J. M. Taylor and A. Hliniak (1990). "Dose fractionation and regeneration in radiotherapy for cancer of the oral cavity and oropharynx. Part 2. Normal tissue responses: acute and late effects." Int J Radiat Oncol Biol Phys **18**(1): 101-11. [pp. 105, 122]

Mackie, T. R., J. Balog, K. Ruchala, D. Shepard, S. Aldridge, E. Fitchard, P. Reckwerdt, G. Olivera, T. McNutt and M. Mehta (1999). "Tomotherapy." Semin Radiat Oncol **9**(1): 108-17. [p. 63]

Mackie, T. R., T. Holmes, S. Swerdloff, P. Reckwerdt, J. O. Deasy, J. Yang, B. Paliwal and T. Kinsella (1993). "Tomotherapy: a new concept for the delivery of dynamic conformal radiotherapy." Med Phys **20**(6): 1709-19. [p. 63]

Markov, K., C. Schinkel, P. Stavrev, N. Stavreva, M. Weldon and B. G. Fallone (2006). "Reverse mapping of normal tissue complication probabilities onto dose volume histogram space: the problem of randomness of the dose volume histogram sampling." Med. Phys. **33**(9): 3435-3443. [pp. 28, 40, 44, 63]

Martel, M. K., W. M. Sahijdak, R. K. Ten Haken, M. L. Kessler and A. T. Turrisi (1998). "Fraction size and dose parameters related to the incidence of pericardial effusions." Int J Radiat Oncol Biol Phys **40**(1): 155-61. [p. 39]

Memorial Sloan-Kettering Cancer Center (2003). A Practical Guide to Intensity-Modulated Radiation Therapy. Madison, Wisconsin, Medical Physics Publishing. [pp. 20, 21]

Moiseenko, V., J. Battista and J. Van Dyk (2000). "Normal tissue complication probabilities: dependence on choice of biological model and dose-volume histogram reduction scheme." Int J Radiat Oncol Biol Phys **46**(4): 983-93. [pp. 23, 39, 150]

Moiseenko, V., T. Craig, A. Bezjak and J. Van Dyk (2003). "Dose-volume analysis of lung complications in the radiation treatment of malignant thymoma: a retrospective review." Radiother Oncol **67**(3): 265-74. [p. 39]

Munro, T. R. and C. W. Gilbert (1961). "The relation between tumour lethal doses and the radiosensitivity of tumour cells." Br J Radiol **34**: 246-51. [pp. 12, 103]

Nahum, A. E., B. Movsas, E. M. Horwitz, C. C. Stobbe and J. D. Chapman (2003). "Incorporating clinical measurements of hypoxia into tumor local control modeling of prostate cancer: implications for the alpha/beta ratio." Int J Radiat Oncol Biol Phys **57**(2): 391-401. [pp. 25, 120, 142]

Niemierko, A. (1992). "Random search algorithm (RONSC) for optimization of radiation therapy with both physical and biological end points and constraints." Int J Radiat Oncol Biol Phys **23**(1): 89-98. [p. 22]

Niemierko, A. (1997). "Reporting and analyzing dose distributions: a concept of equivalent uniform dose." Med Phys **24**(1): 103-10. [pp. 16, 22, 42, 96]

Niemierko, A. (1998). "Radiobiological models of tissue response to radiation in treatment planning systems." Tumori **84**(2): 140-3. [p. 113]

Niemierko, A. (1999). A generalized concept of Equivalent Uniform Dose. 41th AAPM Annual Meeting, Nashville. [pp. 16, 22, 42, 96]

Niemierko, A. and M. Goitein (1991). "Calculation of normal tissue complication probability and dose-volume histogram reduction schemes for tissues with a critical element architecture." Radiother Oncol **20**(3): 166-76. [pp. 16, 42]

Niemierko, A. and M. Goitein (1993). "Modeling of normal tissue response to radiation: the critical volume model." Int J Radiat Oncol Biol Phys **25**(1): 135-45. [pp. 17, 40, 60, 42, 87]

Niemierko, A., M. Urie and M. Goitein (1992). "Optimization of 3D radiation therapy with both physical and biological end points and constraints." Int J Radiat Oncol Biol Phys **23**(1): 99-108. [p. 39]

Okunieff, P., D. Morgan, A. Niemierko and H. D. Suit (1995). "Radiation dose-response of human tumors." Int J Radiat Oncol Biol Phys **32**(4): 1227-37. [pp. 108, 113, 153, 181]

Olafsson, A., R. Jeraj and S. J. Wright (2005). "Optimization of intensity-modulated radiation therapy with biological objectives." Phys Med Biol **50**(22): 5357-79. [p. 22]

Olsen, D. R. (1990). The tissue volume effect: a reliability model. Proc. 9th Annual ESTRO Meeting. [pp. 40, 60]

Olsen, D. R., B. K. Kambestad and D. T. Kristoffersen (1994). "Calculation of radiation induced complication probabilities for brain, liver and kidney, and the use of a reliability model to estimate critical volume fractions." Br J Radiol **67**(804): 1218-25. [pp. 40, 42, 87]

Pinover, W. H., A. L. Hanlon, E. M. Horwitz and G. E. Hanks (2000). "Defining the appropriate radiation dose for pretreatment PSA < or = 10 ng/mL prostate cancer." Int J Radiat Oncol Biol Phys **47**(3): 649-54. [pp. 26, 135, 143, 150, 167, 153]

Pollack, A., A. L. Hanlon, E. M. Horwitz, S. J. Feigenberg, A. A. Konski, B. Movsas, R. E. Greenberg, R. G. Uzzo, C. M. Ma, S. W. McNeeley, M. K. Buyyounouski and R. A. Price, Jr. (2006). "Dosimetry and preliminary acute toxicity in the first 100

men treated for prostate cancer on a randomized hypofractionation dose escalation trial." Int J Radiat Oncol Biol Phys **64**(2): 518-26. [pp. 25, 120]

Pollack, A., G. K. Zagars and V. S. Kavadi (1994). "Prostate specific antigen doubling time and disease relapse after radiotherapy for prostate cancer." Cancer **74**(2): 670-8. [p. 65]

Press, W. H., B. P. Flannery, S. A. Teukolsky and W. T. Vetterling (1988). Numerical Recipes in C. Cambridge, MA, Cambridge University Press. [pp. 84, 154, 191, 192]

Riordan, J. (1968). Combinatorial Identities. New York, J. Wiley and Sons. [p. 82]

Roberts, S. A. and J. H. Hendry (1993). "The delay before onset of accelerated tumour cell repopulation during radiotherapy: a direct maximum-likelihood analysis of a collection of worldwide tumour-control data." Radiother Oncol **29**(1): 69-74. [pp. 103, 105, 112, 122]

Roberts, S. A. and J. H. Hendry (1998). "A realistic closed-form radiobiological model of clinical tumor-control data incorporating intertumor heterogeneity." Int J Radiat Oncol Biol Phys **41**(3): 689-99. [pp. 103, 105, 112, 122, 124, 132]

Sanchez-Nieto, B. and A. E. Nahum (2000). "BIOPLAN: software for the biological evaluation of radiotherapy treatment plans." Med Dosim **25**(2): 71-6. [p. 23]

Schinkel-Ranger, C., P. Stavrev, N. Stavreva, M. Weldon, R. Scrimger and B. G. Fallone (2005). On the dose-volume constraints based on radiobiological considerations. AAPM 47th Annual Meeting, Seattle, WA. [p. 94]

Schinkel-Ranger, C., P. Stavrev, M. Weldon, N. Stavreva, R. Scrimger and B. G. Fallone (2005). Reverse NTCP mapping and the problem of physical dose-volume constraint estimation. Cancer Research Across the Spectrum: National Meeting for Trainees, Mont Tremblant, Canada. [p. 77]

Schinkel, C., M. Carlone, B. Warkentin and B. G. Fallone (2007). "An analytic investigation into the effect of population heterogeneity on parameter ratio estimates." Int J Radiat Oncol Biol Phys **in press**. [p. 29]

Schinkel, C., P. Stavrev, N. Stavreva and B. G. Fallone (2006). "A theoretical approach to the problem of dose-volume constraint estimation and their impact on the dose-volume histogram selection." Med. Phys. **33**(9): 3444-3459. [pp. 28, 77, 87, 91, 94, 95, 100, 101]

Schinkel, C., N. Stavreva, M. Carlone, P. Stavrev and B. G. Fallone (2006). "On the equivalence of the population and individual TCP models (AAPM 48th Annual Meeting, Orlando, FL, July 30 - Aug 3)." Med Phys **33**: 2125. [pp. 28, 124, 125]

Schinkel, C., N. Stavreva, P. Stavrev, M. Carlone and B. G. Fallone (2007). "Functional form comparison between the population and the individual Poisson based TCP models." Radiol Oncol **41**(2): 90-98. [p. 28]

Schultheiss, T. E. (2001). "The controversies and pitfalls in modeling normal tissue radiation injury/damage." Semin Radiat Oncol **11**(3): 210-4. [p. 39]

Seppenwoolde, Y. and J. V. Lebesque (2001). "Partial irradiation of the lung." Semin Radiat Oncol **11**(3): 247-58. [p. 39]

Seppenwoolde, Y., J. V. Lebesque, K. de Jaeger, J. S. Belderbos, L. J. Boersma, C. Schilstra, G. T. Henning, J. A. Hayman, M. K. Martel and R. K. Ten Haken (2003). "Comparing different NTCP models that predict the incidence of radiation

pneumonitis. Normal tissue complication probability." Int J Radiat Oncol Biol Phys **55**(3): 724-35. [p. 39]

Stanescu, T., J. Hans-Sonke, P. Stavrev and B. G. Fallone (2006). "3T MR-based treatment planning for radiotherapy of brain lesions." Radiol Oncol **40**(2): 125-132. [p. 23]

Stavrev, P., D. Hristov and E. Sham (2001). IMRT Inverse Treatment Planning Optimization Based on Physical Constraints and Biological Objectives. 47th Annual General Meeting of the Canadian Organization of Medical Physicists (COMP), Kelowna, BC, Canada. [pp. 16, 42, 96]

Stavrev, P., D. Hristov, B. Warkentin, E. Sham, N. Stavreva and B. G. Fallone (2003). "Inverse treatment planning by physically constrained minimization of a biological objective function." Med Phys **30**(11): 2948-58. [pp. 22, 39, 68, 69, 171]

Stavrev, P., C. Schinkel, N. Stavreva, K. Markov and B. G. Fallone (2006). "SU-FF-T-370: Properties of the Iso-NTCP Envelope (AAPM 48th Annual Meeting, Orlando, FL, July 30 - Aug 3)." Med Phys **33**: 2131. [p. 28]

Stavrev, P., C. Schinkel, N. Stavreva, K. Markov and B. G. Fallone (2007). "Analytical investigation of properties of the iso-NTCP envelope." Radiol Oncol **41**(1): 41-47. [p. 28]

Stavrev, P., N. Stavreva, D. Hristov and B. G. Fallone (2003). Reverse mapping of normal tissue complication probabilities onto dose volume histogram space: Problem formulation, illustration, and implications. Proc. of World Congress on Medical Physics and Biomedical Engineering, Sydney 24 - 29 August, Australia. [pp. 76, 77, 85]

Stavrev, P., N. Stavreva, A. Niemierko and M. Goitein (2001). "The Application of Biological Models to Clinical Data." *Phys Medica* **XVII**(2): 71-82. [pp. 40, 42, 43, 61, 66, 89, 94, 184]

Stavrev, P., N. Stavreva, A. Niemierko and M. Goitein (2001). "Generalization of a model of tissue response to radiation based on the idea of functional subunits and binomial statistics." Phys Med Biol **46**(5): 1501-18. [pp. 17, 40, 42, 60, 87, 94, 98, 104, 105, 122]

Stavrev, P., M. Weldon, B. Warkentin, N. Stavreva and B. G. Fallone (2005). "Radiation damage, repopulation and cell recovery analysis of in vitro tumour cell megacolony culture data using a non-Poissonian cell repopulation TCP model." Phys Med Biol **50**(13): 3053-61. [pp. 12, 23]

Stavreva, N., P. Stavrev, B. Warkentin and B. G. Fallone (2002). "Derivation of the expressions for gamma50 and D50 for different individual TCP and NTCP models." Phys Med Biol **47**(20): 3591-604. [pp. 39, 40]

Stavreva, N., P. Stavrev, B. Warkentin and B. G. Fallone (2003). "Investigating the effect of cell repopulation on the tumor response to fractionated external radiotherapy." Med Phys **30**(5): 735-42. [pp. 4, 23, 40]

Stavreva, N. A., B. Warkentin, P. V. Stavrev and B. G. Fallone (2005). "Investigating the effect of clonogen resensitization on the tumor response to fractionated external radiotherapy." Med Phys **32**(3): 720-5. [p. 23]

Stock, R. G., N. N. Stone, A. Tabert, C. Lannuzzi and J. K. DeWyngaert (1998). "A dose-response study for I-125 prostate implants." Int J Radiat Oncol Biol Phys **41**(1): 101-8. [pp. 25, 26, 132, 143]

Taschereau, R., R. Roy and J. Pouliot (2002). "Relative biological effectiveness enhancement of a 125I brachytherapy seed with characteristic x rays from its constitutive materials." Med Phys **29**(7): 1397-402. [p. 143]

Taylor, J. M., H. R. Withers and W. M. Mendenhall (1990). "Dose-time considerations of head and neck squamous cell carcinomas treated with irradiation." Radiother Oncol **17**(2): 95-102. [pp. 105, 122]

Thames, H. D., S. M. Bentzen, I. Turesson, M. Overgaard and W. Van den Bogaert (1990). "Time-dose factors in radiotherapy: a review of the human data." Radiother Oncol **19**(3): 219-35. [pp. 105, 122]

Thames, H. D., Jr., L. J. Peters, H. R. Withers and G. H. Fletcher (1983). "Accelerated fractionation vs hyperfractionation: rationales for several treatments per day." Int J Radiat Oncol Biol Phys **9**(2): 127-38. [p. 10]

Thames, H. D., Jr., H. R. Withers, L. J. Peters and G. H. Fletcher (1982). "Changes in early and late radiation responses with altered dose fractionation: implications for dose-survival relationships." Int J Radiat Oncol Biol Phys **8**(2): 219-26. [p. 10]

Ting, J. Y., X. Wu, J. A. Fiedler, C. Yang, M. L. Watzich and A. Markoe (1997). "Dose-volume histograms for bladder and rectum." Int J Radiat Oncol Biol Phys **38**(5): 1105-11. [p. 39]

Travis, E. L. (2001). "Organizational response of normal tissues to irradiation." Semin Radiat Oncol **11**(3): 184-96. [p. 39]

Travis, E. L. and S. L. Tucker (1987). "Isoeffect models and fractionated radiation therapy." Int J Radiat Oncol Biol Phys **13**(2): 283-7. [pp. 105, 122]

Tsougos, I., P. Mavroidis, J. Rajala, K. Theodorou, R. Jarvenpaa, M. A. Pitkanen, K. Holli, A. T. Ojala, B. K. Lind, S. Hyodynmaa and C. Kappas (2005). "Evaluation of dose-response models and parameters predicting radiation induced pneumonitis using clinical data from breast cancer radiotherapy." Phys Med Biol **50**(15): 3535-54. [p. 39, 65, 60]

Tucker, S. L. and E. L. Travis (1990). "Comments on a time-dependent version of the linear-quadratic model." Radiother Oncol **18**(2): 155-63. [pp. 14, 105, 122]

van de Geijn, J. (1989). "Incorporating the time factor into the linear-quadratic model." British Journal of Radiology **62**(735): 296-298. [pp. 105, 122]

Van Dyk, J., K. Mah and T. J. Keane (1989). "Radiation-induced lung damage: dose-time-fractionation considerations." Radiother Oncol **14**(1): 55-69. [pp. 105, 122]

Vargas, C., D. Yan, L. L. Kestin, D. Krauss, D. M. Lockman, D. S. Brabbins and A. A. Martinez (2005). "Phase II dose escalation study of image-guided adaptive radiotherapy for prostate cancer: use of dose-volume constraints to achieve rectal isotoxicity." Int J Radiat Oncol Biol Phys **63**(1): 141-9. [p. 23]

Wang, J. Z., M. Guerrero and X. A. Li (2003). "How low is the alpha/beta ratio for prostate cancer?" Int J Radiat Oncol Biol Phys **55**(1): 194-203. [pp. 25, 120]

Wang, J. Z., X. A. Li, C. X. Yu and S. J. DiBiase (2003). "The low alpha/beta ratio for prostate cancer: what does the clinical outcome of HDR brachytherapy tell us?" Int J Radiat Oncol Biol Phys **57**(4): 1101-8. [pp. 25, 120]

Wang, X., X. Zhang, L. Dong, H. Liu, Q. Wu and R. Mohan (2004). "Development of methods for beam angle optimization for IMRT using an accelerated exhaustive search strategy." Int J Radiat Oncol Biol Phys **60**(4): 1325-37. [p. 64]

Wang, X. H., R. Mohan, A. Jackson, S. A. Leibel, Z. Fuks and C. C. Ling (1995). "Optimization of intensity-modulated 3D conformal treatment plans based on biological indices." Radiother Oncol **37**(2): 140-52. [p. 22]

Warkentin, B., P. Stavrev, N. Stavreva, C. Field and B. G. Fallone (2004). "A TCP-NTCP estimation module using DVHs and known radiobiological models and parameter sets." J Appl Clin Med Phys **5**(1): 50-63. [pp. 23, 113, 181]

Warkentin, B., P. Stavrev, N. A. Stavreva and B. G. Fallone (2005). "Limitations of a TCP model incorporating population heterogeneity." Phys Med Biol **50**(15): 3571-88. [pp. 103, 121, 127, 144, 172, 174]

Webb, S. and A. E. Nahum (1993). "A model for calculating tumour control probability in radiotherapy including the effects of inhomogeneous distributions of dose and clonogenic cell density." Phys Med Biol **38**(6): 653-66. [pp. 103, 181]

Wheldon, T. E. and A. E. Amin (1988). "The Linear Quadratic Model." British Journal of Radiology **61**(728): 700-702. [pp. 105, 122]

Withers, H. R., J. M. Taylor and B. Maciejewski (1988). "The hazard of accelerated tumor clonogen repopulation during radiotherapy." Acta Oncol **27**(2): 131-46. [pp. 60, 105, 122]

Withers, H. R., J. M. Taylor and B. Maciejewski (1988). "Treatment volume and tissue tolerance." Int J Radiat Oncol Biol Phys **14**(4): 751-9. [p. 17]

Wolbarst, A. B., E. S. Sternick, B. H. Curran and A. Dritschilo (1980). "Optimized radiotherapy treatment planning using the complication probability factor (CPF)." Int J Radiat Oncol Biol Phys **6**(6): 723-8. [p. 39]

Wu, Q., D. Djajaputra, Y. Wu, J. Zhou, H. H. Liu and R. Mohan (2003). "Intensity-modulated radiotherapy optimization with gEUD-guided dose-volume objectives." Phys Med Biol **48**(3): 279-91. [p. 22]

Wu, Q., R. Mohan, A. Niemierko and R. Schmidt-Ullrich (2002). "Optimization of intensity-modulated radiotherapy plans based on the equivalent uniform dose." Int J Radiat Oncol Biol Phys **52**(1): 224-35. [p. 113]

Wuu, C. S. and M. Zaider (1998). "A calculation of the relative biological effectiveness of 125I and 103Pd brachytherapy sources using the concept of proximity function." Med Phys **25**(11): 2186-9. [p. 143]

Yaes, R. J. (1989). "Linear-quadratic model isoeffect relations for proliferating tumor cells for treatment with multiple fractions per day." Int J Radiat Oncol Biol Phys **17**(4): 901-5. [pp. 105, 122]

Yakovlev, A. (1993). "Comments on the distribution of clonogens in irradiated tumors." Radiat Res **134**(1): 117-22. [pp. 13, 105]

Yeoh, E. E., R. H. Holloway, R. J. Fraser, R. J. Botten, A. C. Di Matteo, J. Butters, S. Weerasinghe and P. Abeysinghe (2006). "Hypofractionated versus conventionally fractionated radiation therapy for prostate carcinoma: Updated results of a phase III randomized trial." Int J Radiat Oncol Biol Phys **66**(4): 1072-83. [pp. 25, 120]

Yorke, E. D. (2001). "Modeling the effects of inhomogeneous dose distributions in normal tissues." Semin Radiat Oncol **11**(3): 197-209. [p. 39]

Yorke, E. D., A. Jackson, K. E. Rosenzweig, L. Braban, S. A. Leibel and C. C. Ling (2005). "Correlation of dosimetric factors and radiation pneumonitis for non-small-cell lung cancer patients in a recently completed dose escalation study." Int J Radiat Oncol Biol Phys **63**(3): 672-82. [p. 55]

Zaider, M. and H. I. Amols (1999). "Practical considerations in using calculated healthy-tissue complication probabilities for treatment-plan optimization." Int J Radiat Oncol Biol Phys **44**(2): 439-47. [pp. 23, 39, 150]

Zaider, M. and G. N. Minerbo (2000). "Tumour control probability: a formulation applicable to any temporal protocol of dose delivery." Phys Med Biol **45**(2): 279-93. [pp. 4, 13, 105]

Zaider, M., M. J. Zelefsky, L. G. Hanin, A. D. Tsodikov, A. Y. Yakovlev and S. A. Leibel (2001). "A survival model for fractionated radiotherapy with an application to prostate cancer." Phys Med Biol **46**(10): 2745-58. [pp. 13, 105]

Zelefsky, M. J., D. A. Kuban, L. B. Levy, L. Potters, D. C. Beyer, J. C. Blasko, B. J. Moran, J. P. Ciezki, A. L. Zietman, T. M. Pisansky, M. Elshaikh and E. M. Horwitz (2007). "Multi-institutional analysis of long-term outcome for stages T1-T2 prostate cancer treated with permanent seed implantation." Int J Radiat Oncol Biol Phys **67**(2): 327-33. [p. 23]

Zhang, X., H. Liu, X. Wang, L. Dong, Q. Wu and R. Mohan (2004). "Speed and convergence properties of gradient algorithms for optimization of IMRT." Med Phys **31**(5): 1141-52. [p. 22]